PML Nuclear Bodies and the Spatial Analysis of Interphase Mammalian Cell Nuclear Architecture

Elizabeth Batty

Imperial College London
Division of Molecular Biosciences
Macromolecular Structure and Function Research Group

Submitted for the degree of Doctor of Philosophy of Imperial College London

October 2009

Abstract

Promyelocytic leukaemia nuclear bodies (PML NBs) are found within the nucleus of mammalian cells. Numbering between 10 and 30 per nucleus, they are an obvious feature of the nuclear landscape, yet their functions have still to be unambiguously defined. In the mammalian nucleus, compartmentalization of functions is apparent, as reflected in the wide-range of other nuclear compartments that can be identified. Quantification of relationships between PML NBs and other nuclear functional compartments is essential for a complete understanding of PML NB function. Initially, PML size, number, distance relationships, and spatial organisation in relation to each other, and the nuclear boundary and centroid, under the spatial point pattern theory hypothesis of Complete Spatial Randomness (CSR), were investigated in both normal and SV40 transformed MRC5 and WI38 human foetal lung fibroblasts. This was also completed in normal MRC5 cells treated with heat shock, and interferon β (both of which alter PML NB morphometrics), and also serum starvation. PML NBs appeared to locate according to CSR with respect to each other, and inter – PML distances were dependent upon median PML NB number per nucleus. PML NBs did not tend to associate with the nuclear centroid, and were repelled from the nuclear boundary in all cell lines and conditions. The distance and spatial organisation relationships between PML NBs and eleven different nuclear compartments were also compared and contrasted in the cell lines and conditions mentioned previously. PML NBs were shown to share strong distance and spatial organisation relationships with the 11S immunoproteasome regulator, SC35 domains, and transcriptional compartments in normal asynchronous nuclei, and with telomeres in transformed cells, highlighting likely functions for the bodies. Lastly, the three dimensional spatial preference of functional compartments in the nucleus was determined using an aggregate map, which provided a novel means to visualise the nuclear location of functional compartments in relation to each other, and under different cellular conditions. Spatial preference fell into four categories: 1) diffuse, 2) annular, 3) core, and 4) polar. Nucleoli and RNA polymerase maintained their spatial preference across cell lines and conditions, whereas other compartments showed altered spatial preferences. Interestingly, viral transformation led to global disorganisation of the nucleus, where most compartments (including PML NBs) reverted to a diffuse spatial preference.

Acknowledgements

When I began this project I had just graduated and was full of the mysteries of what PML nuclear bodies might actually do. Over the last four years I estimate that I have spent about five hundred hours sitting in the dark on my own on the microscope and that presented me with quite some time for contemplation. Unsurprisingly I never managed to solve the puzzle of PML nuclear bodies, but I hope to have contributed towards our understanding of where they are found in the cell nucleus, and why they are found there.

Firstly, I would like to thank my supervisor Paul Freemont for taking me on as an MSci student five years ago, and again as a PhD student a year later, and for all of his advice and the enthusiasm he shows for the field of nuclear architecture. Also, for his belief in my scientific and written abilities, and that I would eventually complete this project. To my second supervisor Niall Adams: I have appreciated your good humour and tolerance with regard to my naïve questions about all things statistical. Thank you to Kirsten Jensen for sharing with me her experiences (in both the lab and life), and for being a trusty advisor in all things experiment-related. Many thanks to Carol Shiels for teaching me the basics during my MSci year in the MSF lab. To Vincent Rouilly and James Chappell – thank you for making the last year more bearable by being someone cheerful to talk to! To Richard Russell – thank you for all your help with the data management, analyses and chats about results, in addition to your friendship. To the other members of the MSF lab, past and present: Alex, Andreas, Athena, Caroline, Chris, Ciaran, Dan, Frank, Haji, Heidi, Ingrid, Jolanta, Liz, Louise, Mat, Pascale, Patrik, Suhail, Tama, Tillmann, Val, Xiaodong, and Yilmaz – I've enjoyed working with you, and might even have learnt a little about crystallography and EM along the way.

To my old Durrels House flatmates Pallavi Bhatta, Francesco Coletti and Benjamin Shaw – we had so many fun times and I'm glad that we all took a chance and moved in together when we started out as PhD students. To my good friends from my undergraduate Biochemistry studies: Saiko Hoshino, Caroline Sands and Amy Crouch, and my school friends: Zara Walker and Katherine Shing – thank you for taking an interest in how everything was going and being there to chat when respite was needed!

To my wonderful friend Naomi Tsai – thank you for being a leaky tap (amongst other things!).

I spent the last two years of my PhD studies as a Subwarden, and so to my friends at Tizard Hall, Southside: Alex Lamaison, Dominik Weiss, Hugo Doyle, Tim Arnold, Trish Doyle and Verity Leeson – I'd like to thank you all for being such great people to work with, and for knowing not to ask about how the thesis was going!

To my extended family in Yorkshire, and to the Farrells – thank you all for looking interested when I tried to explain my PhD to you! To my parents John and Mara – I hope that you are proud of my achievement. You have both been such an inspiration to me in life and with respect to my studies. Whenever I felt like giving up I especially thought of you Mamma, and of how much you would have appreciated the chance to complete something like this.

And lastly, to Daniel – thank you for your endless encouragement, optimism and positivity, and for being a perfect example of someone who enjoys being alive and immersing himself in the subject that he loves, for making me laugh and cry (often together), and for helping me to realise that there is far more to life than I could ever imagine.

Elizabeth Celia Batty
London, October 2009.

The work in this thesis was supported by a BBSRC postgraduate studentship.

Contents

Abstract **2**

Acknowledgements **3**

Abbreviations **19**

1 Introduction **23**

1.1 Structure and function in the nucleus **23**

1.1.1 The mammalian nucleus and functional compartmentalization 23

1.1.2 Spatial organization of the nucleus – possible driving mechanisms 24

1.2 PML nuclear bodies **25**

1.2.1 Introduction 25

1.2.2 PML nuclear body structure and function 25

1.2.2.1 PML nuclear body composition 26

1.2.2.2 *PML* gene locus and PML isoforms 26

1.2.2.3 PML NB formation 29

1.2.2.4 Functions of PML NBs 30

1.3 Types of spatial relationships and association in the nucleus **31**

1.3.1 Introduction 31

1.3.2 Examples of known compartment relationships with PML NBs 32

1.3.2.1 Complete co-localization with PML NBs 32

1.3.2.1.1 Sp100 33

1.3.2.1.2 CBP 33

1.3.2.1.3 SATB1 (MAR-binding protein) 34

1.3.2.1.4 eIF4E 34

1.3.2.1.5 PLZF 35

1.3.2.2 Partial co-localization with PML NBs 35

1.3.2.2.1 Cajal bodies 35

1.3.2.2.2 Active transcriptional domains 36

1.3.2.2.3 Proteasomal protein degradation 37

1.3.2.2.4 Telomeres 38

1.3.2.3 Adjacent localization 39

1.3.2.3.1 Middle-late S-phase replication domains 39

1.3.2.3.2 PLC-γ1 40
1.3.2.3.3 Chromosome territories 40
1.3.2.3.4 Splicing speckles 40
1.3.2.4 Induced relationships with PML NBs 41
1.3.2.4.1 DNA damage 41
1.3.2.4.1.1 Single strand DNA damage 41
1.3.2.4.1.2 Double strand DNA damage 41
1.3.2.4.2 Viral infection and response to foreign DNA 42
1.3.2.4.2.1 Viral infection 42
1.3.2.4.2.2 Foreign DNA 42
1.3.2.4.3 The Interferon Response 43
1.3.2.4.3.1 NDH II 43
1.3.2.4.3.2 PA28 and the immunoproteasome 44
1.3.2.4.4 Stress: effects upon PML NBs 44
1.3.2.4.4.1 Stress and nucleoli 44
1.3.2.4.4.2 Proteasomal inhibition and centromeres 45
1.3.2.5 Associations with PML NBs to a varying degree 45
1.3.2.5.1 MHC gene cluster 45
1.4 What affects PML NB spatial organisation in the nucleus? 46
1.4.1 Introduction 46
1.4.2 Cell-line specific factors and disease states 46
1.4.3 PML cell cycle dynamics – protein expression, NB number and size 48
1.4.4 PML NB movement and dynamics 49
1.4.5 PML isoforms 50
1.5 Research aims and objectives 51
1.5.1 Overview and systems biology approach 51
1.5.2 Study scope: functional groupings of nuclear compartments, and cell perturbations 52
1.5.3 Hypotheses for the relationships between PML NBs and functional compartments in the nucleus 53
1.6 How can we measure PML NB-nuclear compartment relationships? 54
1.6.1 Using spatial statistics to learn about nuclear organisation 55
1.6.2 Spatial point patterns and nuclear organisation 56
1.6.3 Complete Spatial Randomness 56
1.7 In-depth project aims 57
2 Methods 59

2.1 Project approach 59
2.2 Reagents and solutions 60
2.2.1 Reagents and sources 60
2.2.2 Solutions 61
2.2.2.1 Tissue culture solutions 61
2.2.2.2 Fixing and permeabilisation solutions 61
2.2.2.3 Immunofluorescence and slide mounting 61
2.3 Cell culture 62
2.3.1 Cell lines 62
2.3.2 Cell revival 62
2.3.3 Subculture and plating 62
2.3.4 Maintenance of cell line stocks in liquid nitrogen 64
2.3.5 Fixing and permeabilisation 64
2.3.6 Nucleotide incorporations 64
2.3.6.1 Bromouridine (BU) 65
2.3.6.2 Bromodeoxyuridine (BrdU) 65
2.3.7 Treatments used to perturb PML NBs in normal MRC5 fibroblasts 66
2.3.7.1 Heat shock 66
2.3.7.2 IFNβ 66
2.3.7.3 Serum starvation 66
2.4 Immunofluorescence detections 66
2.4.1 Theory of Immunofluorescence 66
2.4.2 Immunofluorescence staining methods 67
2.4.2.1 Antibodies used 68
2.4.2.2 Markers of cell cycle phase 72
2.4.2.3 Blocking 73
2.4.2.4 Slide preparation 73
2.5 Confocal microscopy 74
2.5.1 Theory of Confocal microscopy 74
2.5.2 Confocal microscopy methods 74
2.6 Western Blotting 78
2.6.1 Total cell protein extracts 78
2.6.2 Nuclear and cytoplasmic protein extracts 78

2.6.3 SDS polyacrylamide gel electrophoresis (SDS-PAGE), Western blotting and chemiluminescent detection of proteins 79
2.7 Data processing and statistical analyses 80
2.7.1 File conversion 80
2.7.2 SCT algorithm 81
2.7.3 Distance analysis (NNDs) 82
2.7.4 Spatial analysis (CSR) 83
2.7.5 Aggregate Mapping 84
2.8 List of companies and academic groups 86
2.8.1 Companies 86
2.8.2 Academic groups and facilities 86
3 PML nuclear bodies and their spatial relationships 88
3.1 Introduction 88
3.2 Defining the nucleus 88
3.2.1 Introduction 88
3.2.2 Characterisation of the nuclear boundary and DNA within the nucleus 89
3.2.3 Nuclear volume estimation 89
3.2.3.1 Nuclear volumes of MRC5 ASYNC, HS, IFN, SS and VA cells 90
3.2.3.2 Nuclear volumes of MRC5 subsets: G1, G0 and S 92
3.2.3.3 Nuclear volumes of WI38 ASYNC and VA nuclei 93
3.2.4 Summary 93
3.3 PML NB morphometrics 94
3.3.1 Introduction 94
3.3.2 Data sets collected: MRC5 ASYNC, HS, IFN, SS, VA, and WI38 94
3.3.3 Immunofluorescence detections: PML nuclear body/protein localisations 95
3.3.3.1 PML NBs in MRC5 ASYNC, HS, IFN, SS and VA nuclei 97
3.3.3.2 PML NBs in WI38 ASYNC and VA nuclei 98
3.3.3.3 Other PML morphologies 98
3.3.3.3.1 PML rings 98
3.3.3.3.2 Cytoplasmic bodies 98
3.3.3.3.3 MAPPs 98
3.3.3.3.4 Nucleoplasmic PML protein 99
3.3.4 PML NB Number 99
3.3.4.1 PML NB number in MRC5 ASYNC, HS, IFN, SS and VA nuclei 99

3.3.4.2 PML NB number in Subsets of MRC5 (G1, G0 and S) 100
3.3.4.3 PML NB number in WI38 ASYNC and VA nuclei 101
3.3.5 PML NB size (volume) 103
3.3.5.1 PML NB size in MRC5 ASYNC, HS, IFN, SS, VA nuclei 103
3.3.5.2 PML NB size in MRC5 subsets (G1, G0, S) 104
3.3.5.3 PML NB size in WI38 ASYNC and VA nuclei 105
3.3.5.4 PML NB size (volume) and number in MRC5 105
3.3.5.5 Summary of mean PML NB size and number for MRC5 and WI38 datasets. 107
3.3.6 ECDF of PML NB volume in MRC5 and WI38 nuclei 110
3.3.7 PML volume 112
3.3.7.1 PML volume in MRC5 ASYNC, HS, IFN, SS and VA nuclei 112
3.3.8 Summary 114
3.4 PML NB distance relationships – NND analysis 116
3.4.1 Introduction 116
3.4.2 Inter – PML NB-PML NB total minimum NNDs 116
3.4.2.1 Inter – PML NB total minimum NNDs MRC5 ASYNC, HS, IFN, SS and MRC5VA nuclei 116
3.4.2.2 Inter – PML NB total minimum NNDs MRC5 G1, G0 and S subsets 117
3.4.2.3 Inter PML NB total minimum NNDs in WI38 ASYNC and VA nuclei 117
3.4.3 PML NB-nuclear boundary total minimum NNDs 119
3.4.3.1 PML NB – boundary total minimum NNDs in MRC5 ASYNC, HS, IFN, SS and VA nuclei 119
3.4.3.2 PML NB – boundary total minimum NNDs in MRC5 subsets 119
3.4.3.3 PML NB – boundary total minimum NNDs in WI38 ASYNC and VA 119
3.4.4 PML NB- nuclear centroid total minimum NNDs 120
3.4.5 Summary 123
3.5 PML NB spatial organisation – CSR analysis 125
3.5.1 Introduction 125
3.5.2 Inter – PML NB spatial organisation 125
3.5.2.1 Inter – PML NB CSR analysis for MRC5 ASYNC, HS, IFN, SS and VA nuclei…. 127
3.5.2.2 Inter – PML NB CSR analysis for WI38 ASYNC and VA nuclei 128
3.5.3 PML NB-nuclear boundary spatial organisation 128

3.5.3.1 PML NB – boundary CSR analysis for MRC5 ASYNC, HS, IFN, SS and VA nuclei…. 130
3.5.3.2 PML NB – boundary CSR analysis for WI38 ASYNC and VA nuclei 131
3.5.4 PML NB-nuclear centroid spatial organisation 132
3.5.4.1 PML NB – nuclear centroid CSR analysis for MRC5 ASYNC, HS, IFN, SS and VA nuclei 132
3.5.4.2 PML NB – boundary CSR analysis for WI38 ASYNC and VA nuclei 134
3.5.5 Summary 134
3.6 Chapter summary 136
4 PML NBs and Nuclear Compartments 138
4.1 Introduction 138
4.2 Immunofluorescence of nuclear compartments in different cell lines and conditions 139
4.2.1 Introduction 139
4.2.2 Chromosomal topology compartments 139
4.2.2.1 Chromosomes (ACA) 139
4.2.2.2 Telomeres (TELO) 141
4.2.3 Transcriptional compartments 141
4.2.3.1 Acetylated histones (ACHIS) 141
4.2.3.2 Methylated histones (MEHIS) 142
4.2.3.3 Nascent RNA (RNA) 142
4.2.3.4 RNA polymerase II_O (RNAPII) 143
4.2.3.5 Nucleoli (B23) 143
4.2.4 Post-transcription compartments 145
4.2.4.1 Splicing speckles (SC35) 145
4.2.4.2 Cajal bodies (CB) 145
4.2.5 Proteolysis compartments 145
4.2.5.1 19S core proteasome regulator (19S) 145
4.2.5.2 11S immunoproteasome regulator (11S) 146
4.2.6 Summary 146
4.3 Average voxels of functional compartments per nucleus 148
4.3.1 Introduction 148
4.3.2 Average voxels of functional compartments in MRC5 and WI38 nuclei 148
4.3.2.1 Chromosome topology 148

4.3.2.2 Transcriptional compartments....152
4.3.2.3 Post-transcription compartments....154
4.3.2.4 Proteolysis....155
4.3.3 Summary....156
4.4 PML NB – functional compartment NNDs....156
4.4.1 Introduction....156
4.4.2 PML NB – functional compartment total minimum NNDs in MRC5 and WI38……....157
4.4.2.1 Chromosomal topology....157
4.4.2.2 Transcription compartments....158
4.4.2.3 Post-transcriptional compartments....162
4.4.2.4 Proteolysis compartments....162
4.4.3 Distance hierarchies for all compartments from PML NBs....163
4.4.3.1 MRC-5....165
4.4.3.2 WI-38....166
4.4.4 Summary....170
4.5 PML NB – functional compartment CSR analysis for MRC5 and WI38....171
4.5.1 Introduction....171
4.5.2 PML NB – functional compartment CSR analysis....171
4.5.2.1 Centromeres (ACA)....171
4.5.2.2 Telomeres (TELO)....183
4.5.2.3 Acetylated histones (ACHIS)....185
4.5.2.4 Methylated histones (MEHIS)....186
4.5.2.5 Nascent RNA (RNA)....187
4.5.2.6 RNA polymerase II_O (RNAPII)....188
4.5.2.7 Nucleoli (B23)....190
4.5.2.8 Splicing speckles (SC35)....191
4.5.2.9 Cajal bodies (CB)....192
4.5.2.10 19S core proteasome regulator (19S)....192
4.5.2.11 11S immunoproteasome regulator (11S)....194
4.5.2.12 General trends for PML NB – functional compartment CSR analysis....195
4.5.3 Summary....196
4.6 Chapter Summary....200

5 Aggregate Maps of Nuclear Compartments....201

5.1 Introduction – Making the Aggregate Maps 201
5.2 Mean Nucleus shape 202
5.2.1 Mean nucleus shape for MRC5 nuclei 202
5.2.2 Summary 203
5.3 Aggregate maps 204
5.3.1 Aggregate map pattern description 204
5.3.1.1 Diffuse 204
5.3.1.2 Core 204
5.3.1.3 Annular 205
5.3.1.4 Polar 205
5.3.2 AMs for PML NBs and functional compartments in MRC5 and WI38 nuclei 205
5.3.2.1 Summary of AM classification for the data set 222
5.3.2.2 Overall AM trends 222
5.3.2.3 Spatial preference trends for functional compartments in MRC5 and WI38 223
5.3.2.3.1 Spatial preference trends of PML NB in MRC5 and WI38 223
5.3.2.3.2 Chromosome topology markers 223
5.3.2.3.3 Spatial preference trends for transcriptional compartments 224
5.3.2.3.4 Spatial preference trends for post-transcriptional compartments 225
5.3.2.3.5 Spatial preference trends for proteolysis compartments 225
5.3.3 Summary 225
5.3.4 Functional compartment trends for cell lines and condition in MRC5 & WI38 226
5.3.4.1 Spatial preference trends for compartments in ASYNC nuclei 226
5.3.4.2 Spatial preference trends for compartments in HS nuclei 226
5.3.4.3 Spatial preference trends for compartments in IFN nuclei 227
5.3.4.4 Spatial preference trends for compartments in SS nuclei 227
5.3.4.5 Spatial preference trends for compartments in VA nuclei 227
5.4 Chapter summary 228
6 Discussion and conclusions 230
6.1 Introduction 230
6.2 PML NBs – organisation and function in the nucleus 230
6.2.1 Discussion of nuclear volume and PML NB findings in asynchronous normal and virally transformed fibroblasts 230
6.2.2 Discussion of nuclear volume and PML NB findings in normal fibroblasts treated with heat shock, interferon β, and serum starvation 238

6.2.3 PML NBs in MRC5 cell-cycle subsets 245
6.2.4 PML NB functional insights 246
6.2.5 PML NB organisational insights 250
6.3 Technical limitations: Problems and resolution 253
6.3.1 Biological issues - can these influence PML spatial relationships? 253
6.3.1.1 Choice of experimental time points 253
6.3.1.2 Effects of stress and handling of cells upon PML NBs 253
6.3.2 Methods related factors – can these influence PML spatial relationships? 254
6.3.2.1 Fixation, permeabilization and immunofluorescence 254
6.3.2.2 Blocking 255
6.3.2.3 Reliability of using cell cycle markers to determine PML NB spatial organisation in subset of MRC5 nuclei 255
6.3.2.4 Labelling 256
6.3.3 Imaging methods 256
6.3.3.1 Data collection 256
6.3.3.2 Automatic Thresholding 257
6.3.3.2.1 Main sources of thresholding problems 257
6.3.3.2.1.1 Red channel 257
6.3.3.2.1.2 Green channel 257
6.3.3.2.1.3 Blue channel 258
6.3.3.3 Inter – PML NB and PML NB – functional compartment distance measurements 258
6.3.4 Statistical methodology issues 259
6.3.4.1 Sample size 259
6.3.4.2 CSR analysis 260
6.3.4.2.1 Object number and size 260
6.3.4.2.2 CSR: a useful model for PML NB organisation in the nucleus? 260
6.3.4.3 AM limitations 262
6.4 Conclusions 262
7 Appendix 264
7.1 Total sample sizes 264
7.2 WB: PML and Ki67 protein levels in normal, treated and virally transformed MRC5 and WI38 cells 264
References 268

List of figures

Figure 1 Functional compartments in the nucleus 24
Figure 2 PML nuclear bodies in an MRC5 cell nucleus projection 26
Figure 3 Gene structure, structural domains, and post-translational modifications of PML. 28
Figure 4 PML NB formation 29
Figure 5 Schematic diagram of 26S proteasome 38
Figure 6 Types of Spatial Point Pattern 57
Figure 7 Overview of the Systems Biology approach to the project 59
Figure 8 Indirect immunofluorescence staining of antigens 68
Figure 9 Diagram of light path in confocal microscope 76
Figure 10 Intensity profile for an example image 77
Figure 11 Image segmentation schematic 82
Figure 12 Example CSR results montage 85
Figure 13 What is a boxplot? 90
Figure 14 Nuclear volumes for all cell lines and conditions 91
Figure 15 MRC5 and WI38 median nuclear volumes arranged by size 94
Figure 16 PML in various human fibroblast cells 96
Figure 17 PML NB number in MRC5 and WI38 fibroblasts 102
Figure 18 Mean PML NB number in MRC5 and WI38 fibroblasts 103
Figure 19 PML NB size in MRC5 and WI38 fibroblasts 106
Figure 20 Mean PML NB size and number in MRC5 and WI38 108
Figure 21 Mean PML NB size and number in MRC5 subsets 109
Figure 22 MRC5 EDCF of PML NB sizes 111
Figure 23 WI38 ECDF of PML NB sizes 111
Figure 24 Average PML voxels per nucleus for MRC5 and WI38 fibroblasts 112
Figure 25 PML NB size arranged by median 115
Figure 26 Inter - PML NB NNDs for MRC5 and WI38 118
Figure 27 PML NB - nuclear boundary NNDs in MRC5 and WI38 121
Figure 28 PML NB - nuclear centroid NNDs for MRC5 and WI38 122
Figure 29 Inter PML NB NND hierarchy 123
Figure 30 PML NB - nuclear boundary NND hierarchy 124
Figure 31 PML NB - nuclear centroid NND hierarchy 125

Figure 32 Inter PML NB spatial organisation under CSR..... 126
Figure 33 PML NB - nuclear boundary spatial organisation under CSR..... 129
Figure 34 PML NB - nuclear centroid spatial organisation under CSR..... 133
Figure 35 Centromeres, telomeres, acetylated histone, and methylated histone in MRC5 normal and treated fibroblasts, WI38 normal fibroblasts, and the SV40-transformed cell lines MRC5 VA and WI38 VA 140
Figure 36 Nascent RNA, RNA polymerase II (elongation) and nucleoli in MRC5 normal and treated fibroblasts, WI38 normal fibroblasts, and the SV40-transformed cell lines MRC5 VA and WI38 VA..... 144
Figure 37 SC35 domains (splicing speckles), Cajal bodies, 19S core proteasome regulator, and 11S immunoproteasome regulator in MRC5 normal and treated fibroblasts, WI38 normal fibroblasts, and the SV40-transformed cell lines MRC5 VA and WI38 VA..... 147
Figure 38 Average voxels of ACA, TELO, ACHIS, MEHIS and RNA per nucleus 149
Figure 39 Average voxels of RNAPII, B23, SC35, CB, 19S and 11S per nucleus.. 150
Figure 40 Boxplot of PML NB - chromosome topology compartments total minimum NNDs in MRC5 and WI38 158
Figure 41 Boxplot of PML NB - transcriptional compartments total minimum NNDs in MRC5..... 160
Figure 42 Boxplot of PML NB - transcriptional compartments total minimum NNDs in WI38 161
Figure 43 Boxplot of PML NB - post-transcriptional compartments total minimum NNDs in MRC5 and WI38 163
Figure 44 Boxplot of PML NB - proteolysis compartments total minimum NNDs in MRC5 and WI38 164
Figure 45 Boxplot of PML NB - functional compartment total minimum NNDs in MRC5 ASYNC, HS and IFN..... 167
Figure 46 Boxplot of PML NB - functional compartment total minimum NNDs in MRC5 SS and VA..... 168
Figure 47 Boxplot of PML NB - functional compartment total minimum NNDs in WI38 ASYNC and VA 169

Figure 48 Summary of the median PML NB distance hierarchy from the PML NB to nearest functional compartment in MRC5 ASYNC, HS, IFN, SS, VA and WI38 ASYNC and VA nuclei 170
Figure 49 PML NB - centromeres spatial organisation under CSR 172
Figure 50 PML NB - telomeres spatial organisation under CSR..... 173
Figure 51 PML NB - nucleoli spatial organisation under CSR..... 174
Figure 52 PML NB - acetylated histone spatial organisation under CSR..... 175
Figure 53 PML NB - methylated histone spatial organisation under CSR 176
Figure 54 PML NB - nascent RNA spatial organisation under CSR 177
Figure 55 PML NB - RNA polymerase II spatial organisation under CSR 178
Figure 56 PML NB - SC35 domains spatial organisation under CSR 179
Figure 57 PML NB - Cajal bodies spatial organisation under CSR 180
Figure 58 PML NB - 19S spatial organisation under CSR.....181
Figure 59 PML NB - 11S spatial organisation under CSR 182
Figure 60 Mean nucleus shape for MRC5 and WI38 fibroblasts 203
Figure 61 Aggregate map of PML NB spatial preference in MRC5..... 206
Figure 62 Aggregate map of centromere spatial preference in MRC5 207
Figure 63 Aggregate map of telomere spatial preference in MRC5..... 208
Figure 64 Aggregate map of acetylated histone spatial preference in MRC5..... 209
Figure 65 Aggregate map of methylated histone spatial preference in MRC5.... 210
Figure 66 Aggregate map of nascent RNA spatial preference in MRC5.....211
Figure 67 Aggregate map of RNA polymerase II spatial preference in MRC5... 212
Figure 68 Aggregate map of nucleolus spatial preference in MRC5 213
Figure 69 Aggregate map of SC35 domain spatial preference in MRC5 214
Figure 70 Aggregate map of 19S proteasome regulator spatial preference in MRC5 215
Figure 71 Aggregate map of 11S immunoproteasome regulator spatial preference in MRC5 216
Figure 72 Aggregate map of PML NB, centromere, and telomere spatial preference in WI38 217
Figure 73 Aggregate map of acetylated and methylated histone spatial preference in WI38 218
Figure 74 Aggregate map of nascent RNA, RNA polymerase II, and nucleolus spatial preference in WI38 219

Figure 75 Aggregate map of SC35 domain spatial preference in WI38, and Cajal body spatial preference in MRC5 VA and WI38 VA..... 220
Figure 76 Aggregate map of 19S and 11S proteasome regulator spatial preference in WI38 221
Figure 77 Summary of aggregate map patterns of spatial preference 228
Figure 78 Measurement of inter-PML NB and PML NB - compartment distances 259
Figure 79 PML and actin blot for MRC5 ASYNC, IFN, HS and VA, and WI38 ASYNC and VA fibroblast total cell extracts 267
Figure 80 PML, Ki67, and actin blot for MRC5 ASYNC and SS cytoplasmic and nuclear extracts 267

List of tables

Table 1 Functional groups of nuclear compartments under investigation..... 52
Table 2 Cellular conditions investigated..... 53
Table 3 Hypothesised relationships between PML NBs and functional compartments under study..... 54
Table 4 Reagents and their sources..... 60
Table 5 Tissue culture solutions..... 61
Table 6 Fixing and permeabilisation solutions..... 61
Table 7 Immunofluorescence and slide mounting solutions..... 61
Table 8 Cell lines and karyotypes..... 63
Table 9 Primary antibodies used in immunofluorescence..... 69
Table 10 Secondary antibodies used in immunofluorescence..... 72
Table 11 Data sets collected - cell lines, conditions and sample size..... 95
Table 12 Summary of data sets and compartments for which the PML NB - compartment relationship is described..... 138
Table 13 Maximum intensities for each aggregate map..... 222
Table 14 Summary of aggregate map classifications for functional compartments in the nucleus..... 222
Table 15 Success rates of SCT algorithm segmentation..... 264

Abbreviations

11S	11S immunoproteasome regulator; IF marker
19S	19S core proteasome regulator; IF marker
2D	Two-dimensional, two dimensions
3D	Three-dimensional, three dimensions
ACA	Anti Centromere Antibody; IF marker
ACHIS	Acetylated Histone; IF marker
ALT	Alternative lengthening of telomeres
APB	ALT-associated PML NB
APL	Acute Promyelocytic Leukaemia
ASYNC	Asynchronous cell population
ATCC	American Type Culture Collection
B23	Nucleophosmin, a nucleolar protein; IF marker
BrdU	Bromodeoxyuridine
BrUTP	Bromouridine Triphosphate
BU	Bromouridine
CBP	CREB Binding Protein
CSR	Complete Spatial Randomness
CTD	C-terminal Domain
DAPI	4',6-diamino-2-phenylindole
DNA	Deoxyribonucleic Acid
DSB	Double Strand Break
dsDNA	double stranded DNA
dsRNA	double stranded RNA
ECACC	European Collection of Cell Cultures
ECDF	Empirical Cumulative Distribution Function
ECL	Enhanced Chemiluminescence
EDTA	Ethylenediaminetetraacetic Acid
FISH	Fluorescence In Situ Hybridisation
FITC	Fluorescein Isothiocyanate
G0	Gap 0, resting (phase of the cell cycle)
G1	Gap 1 (phase of the cell cycle)

G2	Gap 2 (phase of the cell cycle)
HS	Heat Shocked cell population
ICD	Inter-chromatin domain
IF	Immunofluorescence
IFN	IFN β-treated cell population
IFN β	Interferon beta
Ig	Immunoglobulin
IQR	Inter-Quartile Range
IR	Ionizing Radiation
IU	International Units
K	Lysine
M	Mitosis
MAPP	Mitotic Accumulations of PML Protein
MEHIS	Methylated Histone; IF marker
MRC5	MRC-5 human male foetal lung fibroblast cell line
NEAA	Non essential amino acids
NA	Numerical Aperture
ND10	Nuclear Domain 10
NDH II	Nuclear DNA helicase II
NLS	Nuclear Localising Signal
NND	Nearest Neighbour Distance
NOR	Nucleolar organising region
PBS	1 x Phosphate Buffered Saline
PF	Paraformaldehyde
PML	Promyelocytic Leukaemia
PML NB	Promyelocytic Leukaemia Nuclear Body
PNA	Peptide nucleic acid
POD	PML Oncogenic Domain
RAR α	Retinoic Acid Receptor alpha
RBCC/TRIM	RING-finger B-box α-helical Coiled-Coil domain/Tripartite Motif
rDNA	ribosomal DNA
RGB	Red Green Blue
RING	Really Interesting New Gene

RNA	Ribonucleic Acid, nascent RNA; IF marker when BU labelled
RNase	Ribonuclease
RNAP I	RNA Polymerase I
RNAPII	RNA Polymerase II (elongation complex); IF marker
RNAP II_A	RNA Polymerase II – initiation complex
RNAP II_O	RNA Polymerase II – elongation complex
RNF4	RING finger protein 4
rRNA	ribosomal RNA
RT	Room Temperature
S	Serine
S	Synthesis (phase of cell cycle)
SC35	Splicing speckle component; IF marker
SDS-PAGE	SDS polyacrylamide gel electrophoresis
SPP	Spatial Point Pattern
SS	Serum Starvation, Serum Starved cell population
SUMO-1	Small Ubiquitin-like Modifier 1
SV-40	Simian Virus 40
T	Threonine
T Ag	(SV-40) Large T antigen
TELO	Telomeres; IF marker
TRF1	human telomeric-repeat binding factor
VA	Denotes SV-40 virus transformed cell line
VRC	Vanadyl ribosyl complex
WI38	WI-38 human female fetal lung fibroblast cell line
WB	Western Blot

Throughout the text the following abbreviations are used to refer to the nuclei imaged from the cell lines, treatments and functional compartments described in this thesis.

Abbreviation	Meaning
MRC5	MRC-5 normal human foetal lung fibroblast cell line.
WI38	WI-38 normal human foetal lung fibroblast cell line.
ASYNC	Asynchronous MRC-5 cell population.
HS	Heat shocked (42°c for 30 mins) asynchronous MRC-5 cell population.
IFN	IFNβ-treated (1000 units/ml overnight) asynchronous MRC-5 cell population.
SS	Serum starved (plated in 10% FCS for 24 h, followed by 8 days in 0.1% FCS) MRC-5 cell population; G_0 synchronised.
VA	SV40 virus transformed MRC-5 cell line.
G0	G_0/quiescent cells selected from asynchronous MRC-5 cell population by negative IF staining for Ki67 cycling cell marker.
G1	G_1 cells selected from asynchronous MRC-5 cell population by positive IF staining for Ki67 G_1 pattern.
S	S phase cells selected from asynchronous MRC-5 cell population by positive BrdU incorporation.
ACA	Centromeres (unspecified centromeric proteins)
TELO	Telomeres (TRF-1)
ACHIS	Acetylated histones (H4 K12)
MEHIS	Methyated histones (H3 K9, K27)
RNA	Nascent RNA, labelled via BU incorporation.
RNAPII	RNA polymerase II_O, active elongation form.
B23	Nucleoli (nucleophosmin/B23 marker)
SC35	SC35 domains (splicing speckles)
CB	Cajal bodies (coilin)
19S	19S core proteasome regulator
11S	11S immunoproteasome regulator

1

Introduction[1]

1.1 Structure and function in the nucleus

1.1.1 The mammalian nucleus and functional compartmentalization

In the mammalian cell nucleus a number of substructures serve to compartmentalise the various functional activities (Figure 1). Nuclear architecture is complex, with many interactions described between functionally active compartments. Such substructures include the nucleoli, active sites of transcription (including nascent RNA and RNA polymerase II), Cajal bodies, splicing speckles, chromatin, chromosome topological markers such as centromeres and telomeres, the nuclear boundary, the nucleoplasm and promyelocytic leukaemia nuclear bodies (PML NBs). Unlike the nucleus itself, nuclear compartments are non-membrane bound and their formation is not fully understood. It is important to consider whether nuclear organization arises as a result of function, or vice-versa. At present little is known about the 3D spatial and temporal organization of nuclear processes, in comparison to their molecular basis.

Investigation of the spatial organization of the mammalian nucleus has thus far been dependent almost entirely upon observational studies using fluorescence microscopy methods to detect endogenous proteins and over-expressed exogenous proteins. Such studies are observer-subjective, and thus subject to observer biases. An alternative approach is to perform association studies, based upon the premise that when objects

[1] Parts of this introduction have previously been published online in a review I wrote entitled: "PML nuclear bodies and their spatial relationships in the mammalian cell nucleus" for the FBS journal PML special edition issue (Batty, E., K. Jensen, and P. Freemont. 2009. PML nuclear bodies and their spatial relationships in the mammalian cell nucleus. *Front Biosci.* 14:1182-96.). They appear here in revised form.

share a function they will show a closer association than is expected to occur stochastically. This is a more rigorous extension of observational studies.

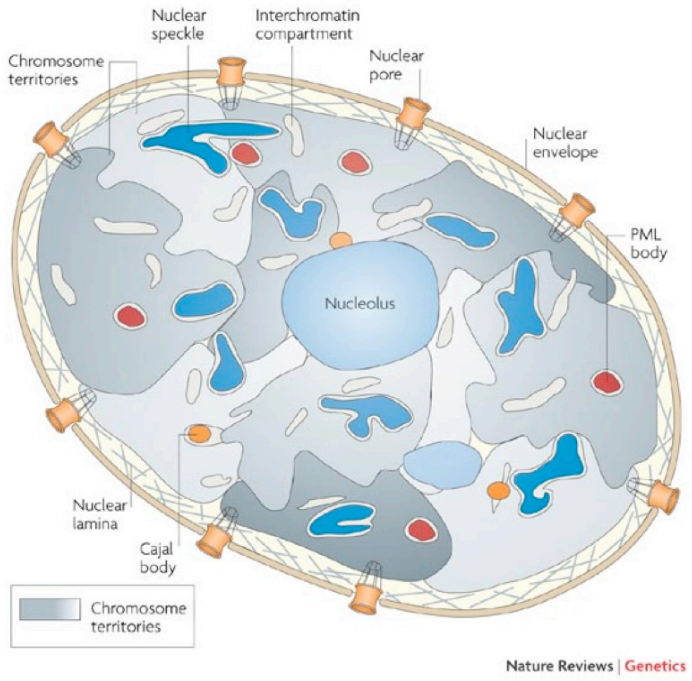


Figure 1 Functional compartments in the nucleus

The mammalian cell nucleus shows functional compartmentalisation. Examples of such compartments are PML nuclear bodies (PML NBs), nucleoli, Cajal bodies, splicing speckles and chromosome territories. A network of channels known as the inter-chromatin domain (ICD) runs between the chromosome territories where certain compartments such as PML NBs and Cajal bodies are typically found. The nucleus is bounded by the nuclear lamina filament network, in which nuclear pores reside and provide entry and exit routes to and from the nucleus. Figure adapted from (Lanctot et al., 2007).

1.1.2 Spatial organization of the nucleus – possible driving mechanisms

The mammalian nucleus is essentially a 3D volume and therefore understanding the mechanisms that drive its organization, and whether these are purely structural or functional, is essential for understanding nuclear function.

There are two main concepts that potentially could drive the organization of the nucleus; a scaffold-based nuclear architecture, or self-organization (Parada et al., 2004). In a scaffold based nuclear architecture structure must direct function – the nucleus has been "designed" to allow functions to be carried out efficiently, and organization is directed by a nuclear matrix structure. However, with self-organization the structure of the nucleus is determined by its functional status (Misteli, 2001). Function is thus directing structure,

incorporating the dynamism of a nucleus adapting to the conditions it finds itself presented with. Self-organization is paramount to the establishment and maintenance of nuclear organization (Dundr and Misteli, 2001). Apparently stable structures are actually the result of highly dynamic components – maintenance of the flux at steady-state equilibrium provides the illusion of stable complexes (Dundr and Misteli, 2001; Misteli, 2001). Stability and flexibility are combined, and both are essential for responsive nuclear functioning.

It is likely that macromolecular crowding, due to high concentrations of macromolecules in the nucleus, may also contribute to the assembly of nuclear compartments, which is in agreement with a self-organization model for nuclear organisation. Such crowding forces can increase association constants between molecules, and may separate different macromolecules into discrete phases (Hancock, 2004).

1.2 PML nuclear bodies

1.2.1 Introduction

We are particularly interested in PML NBs and their spatial relationships with other functional compartments in the nucleus, due to their implication in many different nuclear processes. This study was designed to help reveal the role(s) of PML NBs using spatial information gathered about the bodies in conjunction with neighbouring compartments and nuclear landmarks.

Presented below is a summary of current knowledge pertaining to PML NB structure and function.

1.2.2 PML nuclear body structure and function

PML NBs are a particularly interesting nuclear compartment due to their prominence in the nuclear landscape, which contrasts with their incomplete functional definition (Figure 2).

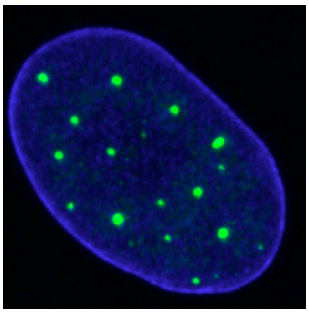


Figure 2 PML nuclear bodies in an MRC5 cell nucleus projection

PML nuclear bodies (green) are spherical bodies found with the nucleus of mammalian cells. They are composed principally of PML protein and typically number between 1 and 10 per nucleus, however this (as well as their size) is cell line and treatment dependent.

1.2.2.1 PML nuclear body composition

PML nuclear bodies (PML NBs), also known as ND10, PODs and Kremer bodies, number between 10 and 30 per cell, but this shows some variation across cell lines and according to cell cycle phase (Dellaire et al., 2006b). Their principle protein component is PML (promyelocytic leukaemia) protein (as shown through the use of Pml knockout mice and cells (Wang et al., 1998)), which along with Sp100 makes up the two proteins that are constituently present at the bodies. In PML -/- cells typical PML NB proteins, such as Sp100, CBP, Daxx and SUMO-1, fail to localize within NBs (Zhong et al., 2000a). This is rectified by transfecting PML into PML -/- cells.

1.2.2.2 *PML* gene locus and PML isoforms

The PML genomic locus is about 35 kb long and consists of nine exons, from which a number of transcripts are produced via alternative splicing (Figure 3a). This leads to the production of various PML isoforms and splice variants ranging from 48 to 97 kDa. There are seven isoforms of PML, PML I to VII, all of which share the N-terminal RBCC (RING-finger B-box, Coiled-coil)/TRIM (Tripartite motif) motif, but show C-terminal differences (Jensen et al., 2001). Exons 2 and 3 contain the RBCC motif and exon 6 contains a nuclear localization signal (NLS). All isoforms except for PML VIIb contain the NLS and thus show a nuclear localization. A nuclear export sequence (NES) in exon 9 is retained in PML I, conferring upon it the ability to shuttle between the nucleus and cytoplasm (Condemine et al., 2006). Therefore there is also a cytoplasmic population of PML protein, which may be implicated in the TGF-β signalling pathway

(Salomoni and Bellodi, 2007). Figure 3b shows the post-translational modification sites of PML. At up to three lysines, (amino acid positions 65, 160 and 490), PML protein may be SUMO-1 (Small Ubiquitin-like Modifier-1) modified (Duprez et al., 1999; Kamitani et al., 1998) (termed SUMOylation). These sites are found within the RING-finger, first B-box and the NLS respectively. There is also a SUMO interaction motif (SIM) (Shen et al., 2006), found at amino acid positions 556-559 within exon 7 (Bernardi and Pandolfi, 2007).

Phosphorylation of PML has been observed at various threonine and serine residues and is associated with PML function in its own enhanced SUMOylation, DNA damage response, and tumour supression (Nichol et al., 2009). Phosphorylation occurs at T28, S36, S38, and S40 (located before the RING-finger domain) by ERK2 in response to arsenic trioxide (Hayakawa and Privalsky, 2004), at S117 (found between the RING-finger and the first B-box) by Chk2 in response to gamma radiation (Yang et al., 2002), and at S517 (found after the NLS) by CK2 (Scaglioni et al., 2006), with respect to the three functions mentioned above.

Recently acetylation has been shown to occur at two lysine residues in PML - K487 within the NLS (and in close proximity to the K490 SUMOylation site), and at K515 (Hayakawa et al., 2008). Acetylated PML has been implicated in trichostatin A (TSA; a histone deacetylase inhibitor) mediated apoptosis, and treatment with TSA led to an increase in PML acetylation, and SUMOylation (Hayakawa et al., 2008).

Lastly, the addition of poly-SUMO chains at K65, K160, and K490 have been shown to trigger the modification of PML (possibly at K401) with poly-Ubiquitin chains (discussed in Section 1.3.2.3) (Lallemand-Breitenbach et al., 2008).

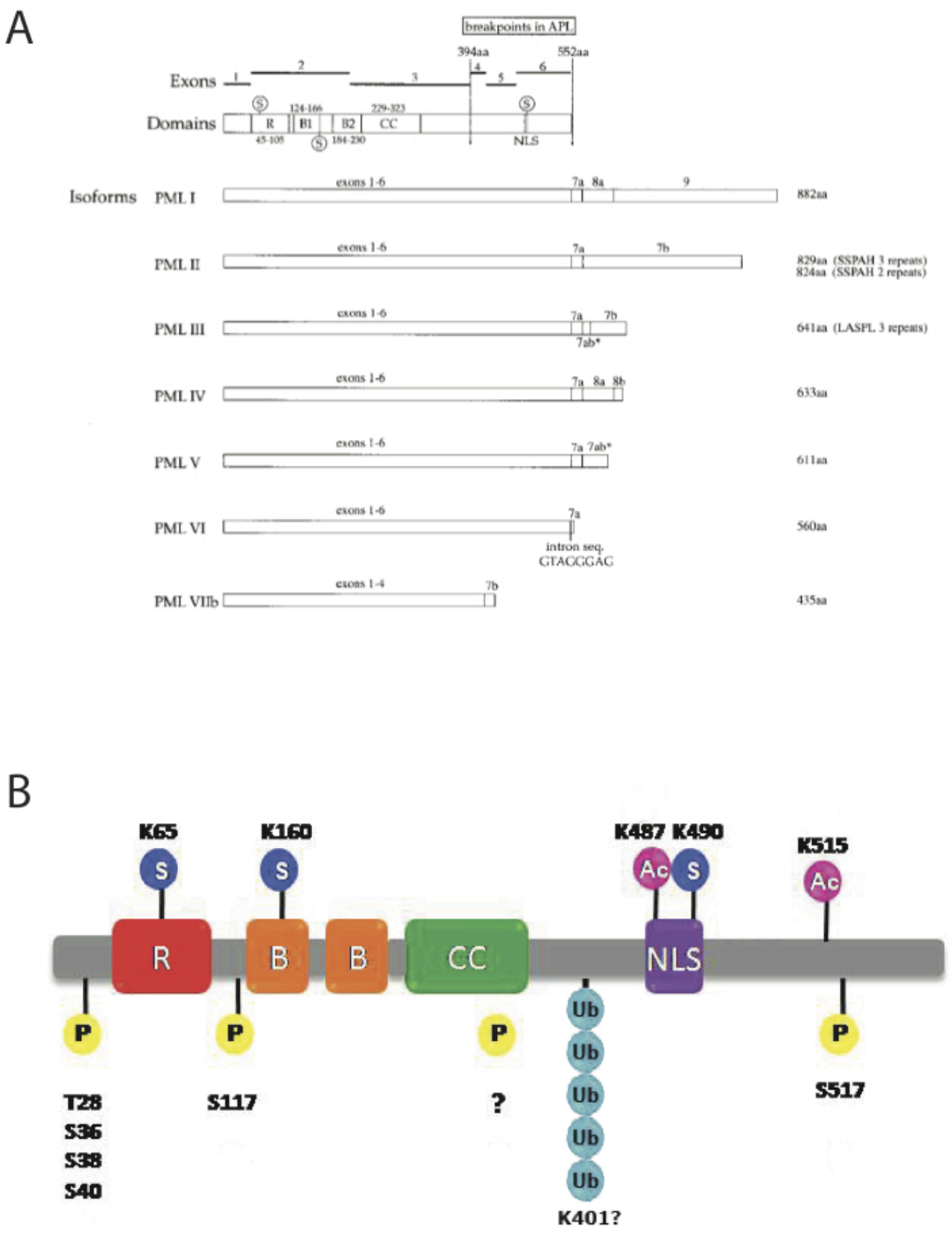


Figure 3 Gene structure, structural domains, and post-translational modifications of PML.

A. Exon assembly and structural domains of the PML isoforms. Adapted from (Jensen et al., 2001). All PML isoforms share the N-terminal region containing the RBCC motif. The seven different C-termini are generated by alternative usage of 3' exons, resulting in PML isoforms of varying sizes (total length of each isoform is given on the right). SUMOylation sites (S) at amino acid positions 65, 160 and 490 are indicated (Duprez et al., 1999; Kamitani et al., 1998). * refers to a retained intron. Exon 7 contains a SUMO interaction motif (SIM) (Shen et al., 2006).

B. Structural domains and post-translational modification sites of PML. Adapted from (Nichol et al., 2009). PML protein is subject to three types of post-translational modification - SUMOylation,

phosphorylation, and acetylation. SUMOylation occurs at three lysine residues (65, 160, and 490) (Duprez et al., 1999; Kamitani et al., 1998). Phosphorylation occurs at various threonine and serine residues - T28, S36, S38 and S40 found before the RING-finger domain, S117 located between the RING-finger and the first B-box, and S517 found after the NLS (Hayakawa and Privalsky, 2004; Scaglioni et al., 2006; Yang et al., 2002). There is also a possible phosphorylation site within the coiled-coil domain. Acetylation has been shown to occur at two lysine residues - K487 within the NLS (and in close proximity to the K490 SUMOylation site), and K515 (Hayakawa et al., 2008). In addition, in response to poly-SUMOylation of PML, RNF4 modifies PML with a polyubiquitin chain (possibly at lysine 401), which leads to PML degradation (Lallemand-Breitenbach et al., 2008; Tatham et al., 2008).

1.2.2.3 PML NB formation

PML protein found diffuse within the nucleoplasm lacks SUMO-1 modification (Muller et al., 1998). Homo-dimerization of PML protein via the coiled-coil moiety of the RBCC/TRIM leads to aggregation of primary PML bodies, which still lack sumolation (Lallemand-Breitenbach et al., 2001) and differ in structure from the mature bodies. Upon covalent attachment of SUMO-1 to PML protein PML NBs mature into structures consisting of an outer PML protein shell that surrounds an inner core of other NB protein components (Lallemand-Breitenbach et al., 2001; LaMorte et al., 1998). There is a need for PML to be sumoylated for PML NB formation (Ishov et al., 1999; Zhong et al., 2000a). The other NB constituent protein Sp100 is also covalently modified by SUMO-1 (Sternsdorf et al., 1997). PML protein mutated so that SUMO-1 can no longer covalently bind to any of the three lysine residues at which SUMO-1 modification occurs forms aberrant nuclear aggregates and typical NB protein components such as Daxx, Sp100 and SUMO-1 are not recruited to these aggregates (Zhong et al., 2000a). PML forms a scaffold facilitating the accumulation of the other PML NB component proteins (Zhong et al., 2000a) (Figure 4).

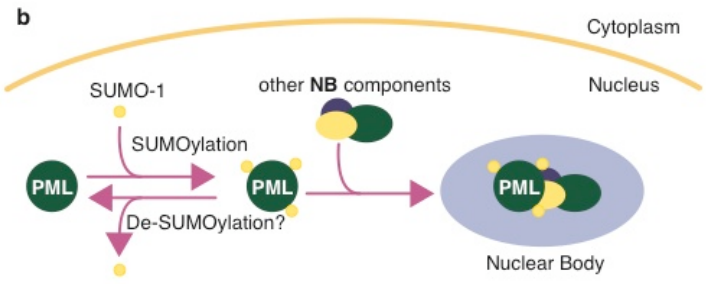


Figure 4 PML NB formation

Adapted from (Zhong et al., 2000b).

The SIM present in PML protein allows it to bind SUMO non-covalently. This is also a requisite for PML NB formation – following PML protein aggregation and sumoylation PML NB formation proceeds with the binding of PML to sumoylated PML through the SIM, along with the recruitment of other SIM-containing or sumoylated NB component proteins (Shen et al., 2006). These inherent biochemical properties of both PML and SUMO provide the molecular basis for PML aggregation and PML NB formation.

Recently, the E3 ubiquitin ligase RNF4 was shown to play a role in the targeting of PML protein for degradation by the proteasome (Lallemand-Breitenbach et al., 2008; Tatham et al., 2008). This process involves the SUMOylation of PML protein at various lyseine residues with SUMO-2 and SUMO-3, which can form polymeric chains (unlike SUMO-1 which cannot, except as the cap on a poly-SUMO chain). Whilst also occurring under normal cellular conditions, this is increased as a consequence of treatment with arsenic trioxide, which encourages SUMO-2/-3 chains to form on PML (Weisshaar et al., 2008). RNF4 is able to bind such poly-SUMO chains, but not the mono-SUMO moieties, and subsequently modifies PML protein with a polyubiquitin chain (Lallemand-Breitenbach et al., 2008; Tatham et al., 2008). The polyubiquitin chain then serves as a marker for proteasomal degradation.

In the disease acute promyelocytic leukaemia (APL) the typical PML NB pattern is disrupted, and PML is found in a granular distribution throughout the nucleus (Dyck et al., 1994; Koken et al., 1994; Weis et al., 1994). This is due to a reciprocal chromosomal translocation at t(15;17) q(22;21), resulting in the formation of a PML-retinoic acid receptor α (RARα) fusion protein, which is able to hetero-dimerize with wild-type PML and disrupt PML NB formation (de The et al., 1991; Goddard et al., 1991; Kakizuka et al., 1991; Pandolfi et al., 1991). Treatment with retinoic acid (RA) leads to reformation of PML NBs (Koken et al., 1994; Weis et al., 1994). In non-APL cells where PML-RARα has been transfected in, the disrupted PML NB organization can also be restored to the endogenous PML NB pattern by RA (Dyck et al., 1994).

1.2.2.4 Functions of PML NBs

There are implications for PML NB function in wide-ranging nuclear activities (Borden, 2002) including tumour suppression (Salomoni and Pandolfi, 2002), apoptosis

(Takahashi et al., 2004), DNA replication and repair (Dellaire and Bazett-Jones, 2004), gene regulation and transcription (Zhong et al., 2000b), and viral infection response (Everett and Chelbi-Alix, 2007). Further insight is provided by PML -/- mice, which although are viable, are more prone to tumours and viral infection (Wang et al., 1998). Since many of the proteins that co-localize with PML NBs do not interact in common pathways, it has therefore also been suggested that PML NBs act as protein storage depots (Negorev and Maul, 2001).

1.3 Types of spatial relationships and association in the nucleus

1.3.1 Introduction

The interplay between structure and function in the mammalian nucleus is manifested in its spatial organization. There are a number of types of spatial relationships between nuclear compartments that can be described. Examples of each can be found between PML NBs and other nuclear compartments.

Many different associations have been found to exist between PML NBs and various other nuclear substructures, mainly from qualitative observational studies using immunofluorescence detection or fluorescent protein fusions of marker proteins to define nuclear compartments. Complete co-localization is where a compartment is found to completely co-localize with all PML NBs in a cell nucleus. It may be the case that the compartment with which PML NBs are being compared is found at other locations within the nucleus in addition to PML NBs, such as diffuse or speckled throughout the nucleoplasm. An example of this is CREB binding protein (CBP), which is found at hundreds of discrete foci throughout the nucleus in addition to showing enrichment at the PML NBs (McManus and Hendzel, 2001). This indicates that there may be functional subsets of the other nuclear compartment, which adds complexity to the analysis of shared functional relationships with PML NBs.

Partial co-localization, where PML NBs and another nuclear compartment only partially overlap, may occur at all or only some PML NBs. This association also includes

compartments that completely co-localize with only a subset of PML NBs, suggesting that PML NBs also may belong to subgroups that have different roles in the nucleus. This could explain the seemingly heterogeneous functions of PML NBs, or tie in with the different isoforms of PML (with their different C-termini) having different roles in the cell. Compartments may also be found adjacent to PML NBs, where there is no co-localization between the two. There may be a visible association between PML NBs and the compartment to varying degrees, but which again involves no co-localization. Such relationships can be quantified using distance-based approaches. Cell cycle phase specific associations, or induced associations between compartments and PML NBs caused by effectors of stress or viral infection may also occur, and thus are not seen all of the time.

Sometimes there are no obvious associations by eye, but they can be shown to occur more often than expected to stochastically – in cases where the compartment pattern is too complex to compute by visual inspection. Lastly, there may be no association above that which occurs by chance, likely showing that there is no relationship between the functions of PML NBs and the compartment with which they are being compared. Such associations are not functionally relevant, yet may still occur because ultimately the nuclear volume can offer only limited locations for compartments to exist at. At the qualitative observational level these associations may easily give false positives with regard to potential PML NB functions, and as such should be reinforced with biochemical and, or, statistical data.

1.3.2 Examples of known compartment relationships with PML NBs

1.3.2.1 Complete co-localization with PML NBs

Classification of co-localization relationships tends to derive from observational studies. By far the most obvious spatial associations between PML NBs and other nuclear components are those that localize to the nuclear bodies themselves. Therefore, for complete co-localization full overlap between compartment and PML NB is a requirement at a site of co-localization.

Proteins may either transiently or covalently associate with the bodies. Those which localize to PML NBs include Sp100 (Szostecki et al., 1990), the other constituent protein of PML NBs, involved in transcriptional regulation, SUMO (Boddy et al., 1996), CBP (Boisvert et al., 2001), BLM (Ishov et al., 1999), Daxx (a transcriptional repressor) (Ishov et al., 1999; Li et al., 2000), p53 (Fogal et al., 2000) (a transcriptional activator) and pRB (Alcalay et al., 1998). Due to the large number of proteins that potentially interact with the PML NB it is difficult to tell whether the bodies play a functional role when they associate, or if they are simply acting as a store. Below we describe some of the proteins that share complete co-localization with PML NBs.

1.3.2.1.1 Sp100

Sp100 was first seen as a nuclear body component protein prior to PML (Szostecki et al., 1987). Together they make up the constituent proteins of PML NBs. Both PML and Sp100 are modified by SUMO-1 (Sternsdorf et al., 1997), and dissociate in mitosis, where they are no longer modified by SUMO-1 (Everett et al., 1999b; Sternsdorf et al., 1997). Sumoylation of Sp100 is not necessary for its targeting to PML NBs (Sternsdorf et al., 1999).

Sp100, and its splice variant Sp100-HMG (or Sp100b) have been shown to bind members of the heterochromatin 1 (HP1) family, and upon overexpression of Sp100, levels of endogenous HP1 have been shown to increase at PML NBs (Seeler et al., 1998). This indicates a potential role for PML NBs within the control of heterochromatin architecture, and also in transcriptional repression as Sp100 may potentially act in a repression complex with HP1 and Sp100-HMG (Lehming et al., 1998; Seeler et al., 1998).

1.3.2.1.2 CBP

PML protein and CREB binding protein (CBP) are found to co-localize within the nucleus at the PML NB (LaMorte et al., 1998). CBP is a transcriptional coactivator and a histone acetyl transferase (McManus and Hendzel, 2001), and is found throughout the nuclear body, whereas PML protein is only found in the outer shell (LaMorte et al.,

1998). CBP is also seen in a finely speckled nucleoplasmic pattern in addition to being at the NBs (LaMorte et al., 1998). Accumulation of CBP at PML NBs is cell-type specific, and as demonstrated with Fluorescence Recovery After Photobleaching (FRAP), CBP moves rapidly between PML NBs and the nucleoplasm, whereas PML is comparatively stable (Boisvert et al., 2001). Compartmentalization of CBP at PML NBs indicates that PML NBs may play a role in transcriptional regulation at the level of histone modification, perhaps providing an environment for this to occur in.

1.3.2.1.3 SATB1 (MAR-binding protein)

The matrix attachment region (MAR)-binding protein special AT-rich sequence binding protein 1 (SATB1) directly interacts with PML protein, and is seen to show complete co-localization in HeLa and normal human WI38 fibroblasts (Kumar et al., 2007). This interaction is required for the organization of the MHC class I locus into chromatin loop-structures, thus linking PML NB function to higher order chromatin organization, and possibly the nuclear matrix.

1.3.2.1.4 eIF4E

eIF4E (eukaryotic translation initiation factor 4E) is involved in nucleo-cytoplasmic messenger RNA (mRNA) transport, and its overexpression leads to increased cyclin D1 levels, cellular transformation and blocking of apoptosis in serum-starved cells (unlike PML which is a negative regulator of growth) (Strudwick and Borden, 2002). Endogenous eIF4E and PML co-localize at PML NBs. Dissimilar to PML protein, eIF4E has a discrete biochemical activity, and directly binds the 7-methyl guanosine 5' cap of mRNA (Lazaris-Karatzas et al., 1990). PML is able to repress eIF4E-dependent cyclin D1 mRNA transport (Cohen et al., 2001), and mutation of the W73 amino acid residue in eIF4E abolishes its interaction with PML. Interaction of the PML RING domain with eIF4E causes a conformational change around the cap-binding site, inhibiting its ability to transport RNA. PML is also able to abrogate eIF4E-mediated transformation through its effects on eIF4E cap-binding (Cohen et al., 2001). Thus, PML function can be directly linked with suppression of transformation.

Interestingly there is also a subset of eIF4E bodies in the nucleus that do not co-localize with PML NBs, and so although eIF4E is present at all PML NBs, not all eIF4E is associated with PML (Culjkovic et al., 2005).

1.3.2.1.5 PLZF

Promyelocytic leukaemia zinc-finger (PLZF) protein localizes to around 14 0.3-0.5 μm nuclear domains in the KG1 myeloid cell line (Ruthardt et al., 1998). These bodies appear similar to PML NBs, and about 30% of PLZF bodies co-localize with PML NBs. However, despite their apparent full co-localization at such sites, closer inspection of confocal microscopy data indicates that PLZF bodies and PML NBs may in fact be discrete structures, with variable degrees of overlap at their surfaces (Ruthardt et al., 1998). Unlike PML NBs, PLZF bodies are not disrupted by E4 ORF3, and do not respond to treatment with IFN (Ruthardt et al., 1998) (yet interestingly such treatment does result in the recruitment of PLZF to PML NBs without an increase in PLZF expression (Koken et al., 1997)). Therefore it is likely that PLZF bodies and PML NBs are functionally distinct, despite the PLZF/RARα fusion protein also being implicated in a rare form of APL (Ruthardt et al., 1998).

1.3.2.2 Partial co-localization with PML NBs

Some nuclear proteins form compartments and bodies that only partially co-localize with PML NBs. This means that a proportion of the compartments overlap to some degree with some or all PML NBs in a nucleus. However, as previously mentioned, partial co-localization also includes the complete co-localization of a compartment, but with only a subset of PML NBs. This indicates that not all PML NBs are equal, and some may behave differently to others.

1.3.2.2.1 Cajal bodies

Cajal, or coiled, bodies (CBs) are small spherical bodies composed of a large number of protein and RNA components including spliceosomal snRNPs (small nuclear ribonucleoproteins, various snoRNAs (small nucleolar RNAs), and the transcription

factors TFIIF and TFIIH. Occasionally CBs can be found within the nucleolus, but they are generally located within the nucleoplasm. They are involved in the transport and maturation of snRNPs and snoRNPs, and associate with specific chromosomal loci, such as the tandemly repeated genes encoding U1 to U4, and U11 to U12 snoRNAs in mammalian interphase nuclei. PML NBs and CBs have been shown to partially co-localize (Berciano et al., 2007; Grande et al., 1996; Sun et al., 2005), where typically at least one PML NB in a nucleus has an associated CB. A CB and its associated PML NB may localize to the same U2 small nucleolar RNA (snRNA) gene locus, where the CB appears positioned between the PML NB and the snRNA locus (Sun et al., 2005). Biochemical interactions between coilin (a CB marker protein) and PIASy (a PML NB component protein) could partially account for this co-localization. However, PML NBs do not contain U2-snRNP itself, which is found in Cajal bodies (Grande et al., 1996; Stuurman et al., 1992). The function of this partial co-localization is so far unknown but may relate to PML NB functions in translational regulation.

1.3.2.2.2 Active transcriptional domains

Subpopulations of PML NBs show associations with sites of active transcription (Kiesslich et al., 2002). By looking at fluorouridine (Fl-U) incorporation into nascent RNA, it has been shown that there are three types of interactions between PML NBs and active transcription sites as observed by indirect immunofluorescence; no overlap (but potentially adjacent localizations of the two foci), a partial overlap, and complete overlap, which was unrelated to the length of exposure to Fl-U. The majority of PML NBs (69%) show no overlap, with 28% showing partial overlap and 3% showing complete overlap; meaning that in unsynchronised cells over 30% of PML NBs show spatial association with transcription sites also demonstrated to contain (transcriptionally) active hyperphosphorylated RNA polymerase II. Cells in G1 phase, or treated with IFN show a spatial association of 70% and 80% respectively between PML NBs and sites of active transcription (Kiesslich et al., 2002). Other studies have also provided evidence for the presence of nascent RNA or RNA polymerase II within PML NBs (LaMorte et al., 1998; von Mikecz et al., 2000). Collectively these strongly point to a role for PML NBs as an environment conducive to transcription.

However, there is some debate surrounding PML NBs' role as a site of active transcription. Using electron microscopy in HeLa cells PML NBs have instead been seen to be surrounded by RNA polymerase II or nascent RNA at distances greater than 25nm, with these not actually being found within the bodies themselves (Xie and Pombo, 2006) confirming others' previous studies (Boisvert et al., 2000) (Grande et al., 1996) (Wang et al., 2004). To account for discrepancies in proximity one might consider that such observational differences may potentially be the result of alternative methodological approaches (discussed further in Section 6.3.2). Despite differences in opinion over the degree of association between PML NBs and nascent RNA transcripts, all of these studies are able to support a functional role for PML NBs at transcriptional compartments. On the other hand, in spite of their nearness to such compartments, it does not necessarily follow that PML NBs actively function in transcription. Indeed, PML NB immediacy to the transcriptional apparatus and nascent transcripts without co-localization may alternatively suggest a post-transcriptional function for the bodies.

1.3.2.2.3 Proteasomal protein degradation

Proteasomes are found in both the nucleus and cytoplasm, and proteasomal protein degradation foci have been demonstrated in the nucleus using immunofluorescence (Rockel et al., 2005). Such foci partially overlap with a number of nuclear compartments, including PML NBs as shown by microinjection of DQ-ovalbumin, which becomes brightly fluorescent upon hydrolysis by proteases (Rockel et al., 2005). The nuclear ubiquitin-proteasome system revolves around the 26S proteasome, which consists of the 20S "core" flanked by two 19S complexes that play a role in the regulation of substrate specificity (Murata et al., 2009; von Mikecz, 2006) (Figure 5). The immunoproteasome, which consists of the 11S complex (replacing the 19S complex at either or both ends of the proteasome) plus the 20S core, is induced by IFNγ, and aids in the proteolysis of peptides prior to their presentation to the MHC. The co-localisation of the 11S proteasome with PML NBs suggests that PML bodies may act as sites of active protein degradation, which may represent an underpinning biochemical function for PML bodies (Lallemand-Breitenbach et al., 2001). The immunoproteasome's inducible association with PML NBs is discussed further in Section 1.4.2.4.3.2.

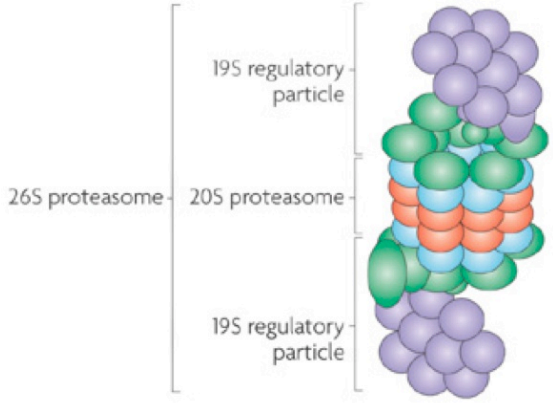


Figure 5 Schematic diagram of 26S proteasome

Adapted from (Murata et al., 2009). In the immunoproteasome either one or both of the 19S regulatory particles are replaced by an 11S particle.

1.3.2.2.4 Telomeres

A further example of partial co-localization between a nuclear substructure and PML NBs is that of telomeres. These subcellular structures consist of TTAGGG repeats bound by a protein complex that prevents chromosome ends from fusing or degrading (Blasco, 2007; Gilson and Geli, 2007). The process of DNA replication results in gradual telomeric shortening, which in turn leads to cellular senescence. To overcome this problem, certain immortalized cell lines are able to maintain, or even extend, telomeres via a homologous recombination (Bryan et al., 1997; Dunham et al., 2000) that does not require telomerase. Alternative lengthening of telomeres (ALT) associated PML NBs (APBs), a subset of PML NBs, co-localize with telomeres in such cells (Blasco, 2007; Henson et al., 2002; Yeager et al., 1999). APBs contain telomeric DNA, telomere-binding proteins TRF1 and 2, and various DNA recombination and replication proteins (Yeager et al., 1999). The role of PML NBs in ALT mechanisms remains unclear but it has been suggested that they may promote the association or stability of recombination complexes, create a suitable chromatin environment for recombination (Bernardi and Pandolfi, 2007), or even be a platform for the sumoylation of telomeric proteins in ALT cells (Bernardi and Pandolfi, 2007; Potts and Yu, 2007).

Previously it was thought, (partially due to their large size in comparison to normal PML NBs), that APBs may just associate with extra-chromosomal telomeric DNA repeats that are found within the nuclei of ALT positive cells (and play a role in the recombination

process), as opposed to true telomeres. However, APBs have now been shown to associate with clusters of between two and five telomeres, which also contain proteins involved in recombination, and their enlargement is due to their containment of multiple telomeres (Draskovic et al., 2009). Recently, *de novo* formation of PML NBs at telomeric DNA during interphase was seen in live cells previously treated with the DNA methylating agent MMS, which causes PML NBs to dissemble (Brouwer et al., 2009). Contrary to previous reports, PML NBs did not necessarily reform at the same positions within the nucleus, and at least a subset formed at telomeric DNA sequences in both ALT postive and non-ALT cells (Brouwer et al., 2009; Eskiw et al., 2003). Such PML NBs did not inevitably remain associated with telomeres, which might account for why PML NB associations with telomeres in non-ALT cells have not been reported before.

1.3.2.3 Adjacent localization

Adjacent localization includes relationships between nuclear substructures and PML NBs that include the two compartments being next to each other, or even touching, but not showing any co-localization. Here we discuss some of the nuclear compartments shown to share this relationship with PML NBs.

1.3.2.3.1 Middle-late S-phase replication domains

There are four different patterns of BrdU (bromodeoxyuridine, a thymidine analogue) incorporation that are found as DNA replication progresses – early (with many small domains), middle (with replication sites at the nuclear periphery and around nucleoli), middle-late (chain like structures of replication sites) and late (fewer large replication domains) (Grande et al., 1996). Whilst being excluded from such domains, PML NBs are often found next to a DNA replication domain in middle-late S-phase (Grande et al., 1996), with 50-80% of PML NBs in middle-late S-phase T24 bladder carcinoma cell nuclei directly adjacent to a replication domain, which may in part reflect the high proliferation rate of these cells. Since PML NB number is known to increase during S-phase it is possible that this is a response to chromatin organization changes, suggesting a role for PML NBs in DNA synthesis (Dellaire et al., 2006b).

1.3.2.3.2 PLC-γ1

The gamma 1 phospholipase C (PLC-γ1) isoform, which is a phosphoinositide hydrolyzing enzyme, was found as an associated protein of PML NBs using mass spectrometry of PML co-precipitates derived from HCT116 human colon carcinoma cells (Ferguson et al., 2007). Phosphoinositides may play a role in nuclear signalling pathways and gene expression. Immunofluorescence reveals that PLC -γ1 puncta are often found adjacent to PML NBs in HCT116 cells. However in normal diploid fibroblasts the staining is cytoplasmic and vesicular suggesting that the observed association may be specific to transformed cells (Ferguson et al., 2007). PML NBs may thus also have a role in phosphoinositide nuclear signalling pathways.

1.3.2.3.3 Chromosome territories

PML NBs, (as well as Cajal bodies) co-localize with NLS-vimentin filaments indicating that they co-exist in an interconnecting nuclear compartment, from which chromosomes are excluded (Bridger et al., 1998), also known as the inter-chromosomal domain compartment (ICD). Therefore PML NBs are likely to be found adjacent to chromatin compartments known as chromosome territories (CTs), which consist of both heterochromatin and euchromatin. However, by scoring individual gene loci (covering a range of locations on chromosomes 1, 6 and 9) for their position either peripheral, internal or external to their corresponding CT, and also whether or not they were touching a PML NB, Wang et al have shown that a locus' association with a PML NB is not dependent upon its position relative to its CT (supplementary data from (Wang et al., 2004)). Also, the PML NB – locus association is not dependent upon the CT to which the locus belongs. Therefore it is likely that PML NBs can also exist within CTs, as well as being peripheral and external to them.

1.3.2.3.4 Splicing speckles

Splicing speckles are dynamic nuclear compartments numbering between 25 and 50 per cell, and are rich in pre-messenger RNA (mRNA) splicing machinery such as snRNPs, spliceosomal subunits and other splicing factors (Lamond and Spector, 2003). PML NBs often appear to be associated with the edges of splicing speckles, as defined by the SC35

spliceosome assembly factor (Ishov et al., 1997; Russell et al., 2009). Their spatial location within interchromatin regions could account for their close association with PML NBs, and since they are storage sites for splicing factors, this could infer a similar nuclear function for PML NBs.

1.3.2.4 Induced relationships with PML NBs

Relationships between PML NBs and other nuclear compartments that are not normally seen can be induced under certain circumstances. Such events include DNA damage, viral infection, interferon (IFN) response and other cellular stresses. Proteins may either be recruited to PML NBs, or PML NBs are themselves recruited to other parts of the nucleus. The latter probably involves the fission products of PML NBs and not *de novo* formation of bodies (Dellaire et al., 2006b). Such associations highlight the potential dynamic nature of the PML NB in response to cellular events.

1.3.2.4.1 DNA damage

1.3.2.4.1.1 Single strand DNA damage

In response to exogenous DNA damage, resulting from UV irradiation for example, PML NBs are able to co-localize with (Carbone et al., 2002) and recruit single-stranded DNA (ssDNA) molecules (Boe et al., 2006). Imaging of live cells expressing YFP-PML shows that ssDNA foci form within existing PML NBs, and formation is inhibited in cells treated with siRNA directed against PML. Therefore ssDNA foci are either recruited into PML NBs (making it possible that PML NBs are DNA damage repair sites), or that PML NBs contain regions of chromosomal DNA that are processed into ssDNA upon DNA damage (Boe et al., 2006).

1.3.2.4.1.2 Double strand DNA damage

γ-H2AX, (histone H2AX phosphorylated on serine 139) localizes to large chromatin domains at sites of radiation-induced sites of double strand breaks (DSBs). Within hours of treatment with ionizing radiation PML NBs and DSBs co-localize (Carbone et al.,

2002; Dellaire et al., 2006a; Varadaraj et al., 2007). Eight to twelve hours subsequent to treatment, PML NBs partially or completely associate with hMre11 ionizing radiation-induced foci (IRIF), and later with p53 (Carbone et al., 2002) in a stable association. Thus PML NBs are involved in DNA damage response and repair pathways, as both PML and DNA repair proteins are recruited to sites of DNA damage.

1.3.2.4.2 Viral infection and response to foreign DNA

1.3.2.4.2.1 Viral infection

Associations between PML NBs and the parental genomes of DNA viruses and early replication compartments have been shown to exist (Everett, 2006; Ishov and Maul, 1996; Maul et al., 1996). Interestingly, PML NBs become disrupted upon infection with adenovirus, where the adenovirus type 5 (Ad 5) early region 4 open reading frame (E4 ORF3) product reorganizes the bodies into thread-like structures within the nucleus (Carvalho et al., 1995; Doucas et al., 1996). The targeting of PML NBs by a variety of viruses suggests that disabling of PML NB function could be an important part of viral viability. In response to IFN, PML NBs may play a role in the antiviral activity of IFN, and thus viruses try to block IFN-meditated actions through the disruption of PML NBs as part of efforts to remove proteins that affect or interfere with efficient viral replication.

1.3.2.4.2.2 Foreign DNA

PML NBs may also help in preventing the expression of foreign DNA (Bishop et al., 2006). Mouse polyomavirus-like particles (VLPs) are able to deliver transgenes into cell nuclei via pathways used by viruses but do not contain factors necessary for initiation and regulation of transcription. Such transgenes are positioned near centromeric heterochromatin to enable silencing. Upon transcriptional activation they are relocated to euchromatin and associate with PML NBs. Despite not playing a role in regulation of transgene expression, PML protein is required to enable interferon α (IFNα) inhibition of transgene expression, suggesting that PML is involved in type I IFN response in the prevention of foreign DNA expression (Bishop et al., 2006).

PML NBs appear to associate with foreign DNA and its protein products, as seen above with viral infection, and also through integration of artificial constructs. In a system developed to directly visualize a gene and its protein product in living cells using the lac operator / repressor system, it was found that the integrated locus became surrounded by a PML NB in a transcription (of the locus) independent association (Tsukamoto et al., 2000). *In vivo* binding of enhanced yellow fluorescent protein (EYFP) / *lac* repressor and tetracycline receptor / VP16 transactivator to the locus was required, showing that the co-localization related to the high concentration of the expressed protein (EYFP / *lac* repressor or tetracycline receptor / VP16 transactivator) needed to associate at the gene locus for the assay, rather than the locus itself. The authors propose that in this case PML NBs may be acting as "sensors" of local accumulations of foreign proteins or DNA in the cell.

1.3.2.4.3 The Interferon Response

IFNs are secreted proteins that meditate a number of cellular responses including antiviral and antiproliferative activities (Regad and Chelbi-Alix, 2001). Treatment with IFN induces an increase in both PML mRNA and protein expression levels, as shown by a greater number and intensity of PML NBs in the nucleus (Lavau et al., 1995). In response to IFN, a significant number of proteins are recruited to PML NBs.

1.3.2.4.3.1 NDH II

Nuclear DNA helicase II (NDH II) is a transient component of PML NBs (Fuchsova et al., 2002), and links CBP to RNA polymerase II. It co-localizes with a small subset of PML NBs under normal conditions, but upon interferon α (IFNα) addition it co-localizes with almost all PML NBs in a transcriptionally dependent association, indicated by the presence of nascent RNA transcripts that are also found at PML NBs to which NDH II is recruited. Therefore PML NBs are implicated in the regulation of transcription of IFNα-inducible genes (Fuchsova et al., 2002).

1.3.2.4.3.2 PA28 and the immunoproteasome

The interferon γ (IFNγ) inducible proteasome activator PA28 (also known as the 11S complex), which is involved in major histocompatibility (MHC) class I antigen presentation, can be found at PML NBs under basal conditions, but IFNγ treatment increases the number and size of PA28-containing PML NBs (Fabunmi et al., 2001). The 20S core proteasome, which is the target of PA28, is not typically found at PML NBs under basal conditions, but upon IFNγ addition "immunoproteasomes" (consisting of the 20S core plus the 11S complex) are recruited to the bodies. Thus, PA28, a normal PML NB component, is able to help establish immunoproteasomes, which are then found at PML NBs under IFNγ conditions. This co-localization suggests that PML NBs play some role in antigen presentation to the MHC, perhaps by providing an environment that is favourable to protein degradation. Alternatively, since PML NBs are targets for viral infection (see Section 1.4.2.4.2), IFN produced in response to viral infection induces immunoproteasome formation and localization to PML NBs in an effort to degrade viral peptides for presentation to the MHC class I at the intranuclear site where they are most likely to be found. It is interesting to note that PML knock-out mice, despite being viable, are more prone to viral infection (Bonilla et al., 2002), suggesting that this process is less efficient in *pml* $^{-/-}$ mice.

1.3.2.4.4 Stress: effects upon PML NBs

1.3.2.4.4.1 Stress and nucleoli

UV-C or IR-γ, and various types of stress such as chemical inhibition of transcription or DNA synthesis, and proteasome inhibition causes endogenous PML protein (specifically the PML I isoform with its C-terminal nucleolar targeting domain) to redistribute to nucleolar caps that eventually surround nucleolar components (Condemine et al., 2007). Whilst there is little evidence to support an association between PML NBs and nucleoli in normal primary cells, in cells with DNA damage PML protein has been shown to sequester Mdm2 (a p53 ubiquitin-ligase) to the nucleolus, and therefore aids p53 stability (Bernardi et al., 2004). In human mesenchymal stem cells novel PML compartments have been observed in association with nucleoli (Janderova-Rossmeislova et al., 2007).

1.3.2.4.4.2 Proteasomal inhibition and centromeres

An association between PML NBs and centromeres may exist as revealed in a significant number of G2 Hep2 cells that had been treated with the proteasome inhibitor MG132 (Everett et al., 1999a). Initially Vmw100 (Herpes simplex virus type 1 regulatory protein) was observed to induce the proteolysis of both PML and Sp100 in a proteasome-dependent manner, in addition to that of CENP-C (a protein found at the centromere). This infers a dynamic link between PML NBs and centromeres in G2, which is only stabilized upon proteasomal inhibition. Thus a cell cycle-dependent link between PML NBs and centromeres can be suggested (Everett et al., 1999a). However, as centromeres are primarily heterochromatin structures this indicates that PML NBs may also be involved in the repression of gene expression (in a cell cycle specific manner), as well as in transcription.

1.3.2.5 Associations with PML NBs to a varying degree

Lastly, associations between PML NBs and other nuclear substructures may not involve direct physical associations, and instead must be measured using a distance-based approach, considering the degree of association and its relevance to shared functionality. This approach requires a strong statistical underpinning, and can also be used in the study of complex nuclear compartment interrelationships in which association cannot be decided by eye alone.

1.3.2.5.1 MHC gene cluster

A highly non-random association between PML NBs and the major histocompatibility complex (MHC) gene cluster on chromosome 6 (specifically the centromeric end extending over 1.6 megabases) has been shown to exist (Shiels et al., 2001). When this region was integrated into chromosome 18 the association with PML NBs remained suggesting that genomic determinants for PML NB association were specific. Association was compared between PML NBs, and two gene-rich regions (MHC on chromosome 6 and epidermal differentiation complex (EDC) on chromosome 1), and the gene-poor 6p24 region on chromosome 6. From observations alone it would seem that PML NBs could be seen to associate closely or overlap with either the MHC or

EDC, both at the same time, or neither region. This highlights the need for more than just observations when showing that associations between nuclear compartments do or do not exist. To address this Shiels et al (Shiels et al., 2001) developed a minimal distance nearest neighbour method to allow probabilities to be calculated for association or non-association showing for the first time that PML NBs associate specifically with particular gene rich regions of the genome.

These quantitative studies were extended by Wang et al (Wang et al., 2004) who found that the distance between a locus and its nearest PML NB correlates with both transcriptional activity and gene density around that specific locus. PML NBs were shown to associate with genomic regions of high transcription activity rather than highly transcribed individual genes. The association of PML NBs with transcriptionally active regions is further shown by the finding that genes on the active X chromosome are more significantly associated with PML NBs than their silenced counterparts, and that the histone-encoding gene cluster, transcribed only in S-phase is more strongly associated with PML NBs in S-phase than in G0/G1 (Wang et al., 2004).

1.4 What affects PML NB spatial organisation in the nucleus?

1.4.1 Introduction

PML NB spatial organisation and their spatial relationships with other nuclear functional compartments and substructures are affected by both internal and external influences on the cell, including cell cycle related changes. These may influence the characterisation of associations to some degree by affecting PML NB morphology or spatial locations, or that of the nuclear compartments being studied in conjunction with PML NBs.

1.4.2 Cell-line specific factors and disease states

PML NB number is known to show variation across cell lines (Dellaire et al., 2006b). Variations in PML NB number, morphology and diameter across cell lines will result in differential PML NB – nuclear compartment relationships depending upon the choice of

cell line of the researcher, which is important to consider when comparing studies between labs.

In certain cells it is possible to observe PML NB relationships with nuclear compartments that do not occur in others. For example, survival of motor neurons (SMN) protein, loss of which causes spinal muscular atrophy, co-localizes with most Cajal bodies. However interestingly in some transformed cell lines and primary foetal tissues SMN localizes to nuclear structures known as Gems, which are commonly found adjacent to Cajal bodies. In cells in which Gems are absent, it would thus be impossible to measure their interrelationships with PML NBs.

Primary cells and tumour cell lines often differ in expression levels of certain proteins, which may in turn alter nuclear organization or morphology, to the point of affecting the presence or absence of particular nuclear compartments. In tumour cells that are positive for telomerase, it is unlikely that they would need to employ ALT mechanisms to maintain telomere length, and thus PML NBs are not likely to show association with telomeres. Some proteins are not present at all in some cells, a good example of which are *pml* $^{-/-}$ cells. For obvious reasons it is not possible to measure relationships between endogenous PML NBs and other nuclear compartments in these cells.

A disease state may also influence the localization of proteins within a cell, as is evident in the PML-implicated disease acute promyelocytic leukaemia (APL). In APL cells the typical PML NB pattern is disrupted, with PML protein unable to form nuclear bodies, instead showing a microspeckled localization throughout the nucleus (Dyck et al., 1994; Koken et al., 1994; Weis et al., 1994), due to wild-type PML and PML-RARα fusion proteins hetero-dimerizing. In such cells normal spatial relationships are obviously disrupted as a consequence of PML protein delocalization from PML NBs. The pathology of APL is characterised by a block in promyelocyte differentiation, which becomes released with all-*trans* retinoic acid (ATRA) treatment (Huang et al., 1988), and a typical PML NB pattern returns to cell nuclei (Daniel et al., 1993).

PML protein is found within giant bodies also containing heterochromatin HP1 proteins over the 1qh and 16qh juxta-centromeric heterochromatins in G2 cells of immunodeficiency, centromeric instability and facial dysmorphy (ICF) syndrome patients

(Luciani et al., 2006). Such bodies also contain satellite DNA unlike normal PML NBs, and may be related to remodelling of heterochromatin in these specific disease cells. They are also likely to share different relationships with nuclear compartments than PML NBs, due to their differences in morphology.

1.4.3 PML cell cycle dynamics – protein expression, NB number and size

The cell cycle can be divided into two main stages: interphase and mitosis. Mitosis encompasses the segregation of the cell's duplicated DNA between daughter cells prior to cytokinesis. This takes up a small proportion of the cell cycle. The rest of the cycle is termed interphase and is subdivided into gap 1 (G_1), synthesis (S) and gap 2 (G_2) phases. G_0 cells are described as quiescent or "resting" – they are not actively taking part in the cell cycle and so are not growing or replicating their DNA, having exited the cycle at G_1. Most of the cells within tissues of the human body will be in this state.

G_1 and G_0 cells contain 2n DNA complement – that is, they possess a normal diploid DNA content. S phase cells contain somewhere between 2n and 4n since this is the phase in which DNA replication takes place. Cells in G_2, during which the cell prepares for division, have a 4n complement of DNA.

PML NB number is known to vary according to cell cycle phase (Dellaire et al., 2006b) and endogenous PML expression levels do differ within a cell population (Koken et al., 1995).

In late G_1 cells, PML NBs are strongly labelled in around 15 bodies (Koken et al., 1995). In S phase cells there are also smaller bodies plus a diffuse nuclear fraction of PML protein, and the number of bodies increase two-fold from G_1 (Dellaire et al., 2006b). This increase is due in part to loss of PML NB structural stability, with fission and fusion events occurring. PML protein is redistributed as opposed to being synthesized *de novo* (Dellaire et al., 2006b). Since the fission products are associated with chromatin, PML NBs probably respond to changes in chromatin organization and topology (Dellaire et al., 2006b). Throughout G_2 PML NB number decreases until a few large PML aggregates (known as mitotic accumulations of PML protein (MAPPs) are found in

mitotic cells, (Dellaire et al., 2006c; Koken et al., 1995). Mitotic PML protein is de-conjugated from SUMO-1 (Everett et al., 1999b). MAPPs also do not contain traditional PML NB component proteins such as Sp100 or Daxx, and contribute to reformation of PML NBs in G_1 (Dellaire et al., 2006c).

Senescence-associated nuclear bodies (SANB) are large PML NBs associated with spontaneous senescence, and include nucleolar proteins in addition to PML protein (Condemine et al., 2007). Changes in PML NB number and morphology related to cell cycle progression or senescence are likely to result in differential PML NB – nuclear compartment relationships as a function of time or age of a cell. Therefore there is also a temporal aspect to studying nuclear compartment interrelationships and in particular when considering PML NB associations.

1.4.4 PML NB movement and dynamics

The spatial location of PML NBs within the mammalian nucleus is fairly restricted by the local chromatin environment that surrounds them. PML NBs exclude chromatin and thus it is likely that they reside in the channels and lacunae of the interchromatin space, whilst migrating though chromatin within a corral (Gorisch et al., 2004). Investigation of nuclear body movement using biologically inert Mx1-YFP expression bodies reveals that bodies diffuse within such a chromatin "corral", which is itself translocated within the nucleus as a result of chromatin diffusion (Gorisch et al., 2004). Therefore nuclear body mobility is a reflection of the accessibility and dynamics of the surrounding chromatin environment. Expression of NLS-Vimentin, a protein that forms filaments in the nucleus, can be used to map the interchromatin "free space" within the nucleus in which PML NBs are able to move (Bridger et al., 1998), providing an idea of the limitations placed upon PML NBs in determining their nuclear locations.

PML NBs can be distinguished into three classes based upon their dynamic properties (Muratani et al., 2002). Using EYFP fused to human Sp100, PML NB dynamics were studied *in vivo* over a 12 min period. PML NBs were divided into those which were positionally stable, (around a quarter of total PML NBs, and which was not size related as stationary bodies ranged in diameter from 0.2 to 1.4 μm), those with limited localized movement (which formed the majority of PML NBs), and finally those which showed

rapid nuclear movements (starting and stopping several times during the 12 mins), roughly numbering 1-2 PML NBs per nucleus. Some nuclei contained over 10 of these fast moving PML NBs, and over half of nuclei studied contained at least one fast moving PML NB. Rapidly moving PML NBs were predominantly smaller bodies, and travelled at an average velocity of 4.0-7.2 μm min^{-1}, with a maximum of 18 μm min^{-1}. Note that whilst being seen in primary mouse embryonic fibroblasts and mouse embryonic stem cells, fast moving PML NBs were not seen in HeLa cells. Their movement is a metabolic-energy dependent mechanism as rapid longer movements ceased during ATP depletion (Muratani et al., 2002).

Other studies have also shown that a population of PML NBs are stable in position and structure over extended periods of interphase (Dellaire et al., 2006b; Eskiw et al., 2003). Stresses including heat shock, heavy metal exposure and expression of adenovirus type 5 E1A protein, result in the fission of small PML-containing microstructures from the parental bodies, which lack in SUMO-1 and Sp100 (Eskiw et al., 2003). There are two subsets of microstructures, the first likely to be trapped within chromatin pockets and therefore sharing diffusion constants with that of mobile chromatin domains, and being able to move 50-70 nm per sec. The second group occupy large, chromatin-free channels allowing diffusion constants much greater than the first subset. Hence, such microstructures show movement of up to 0.5 μm in 1 second and such movement is energy-independent. During recovery microstructures fuse with each other and also with the positionally stable PML NBs (Eskiw et al., 2003).

So whilst PML NB locations are fairly stable over time, PML protein itself is dynamic meaning that a subset of more mobile PML NBs may indeed possess much more variable associations with other nuclear compartments. Use of live cell imaging will be extremely useful in the investigation of such relationships.

1.4.5 PML isoforms

All PML isoforms have been found to co-localize at PML NBs. Although some PML NB – compartment relationships invoke specific PML isoforms, the whole PML NB would still be implicated. However it is interesting to note that when individually expressed in a *Pml*-null background, the different isoforms of PML show varying nuclear

body morphologies (Condemine et al., 2006), such as PML II's thread-like distribution, and PML V's large and dense bodies. Since specific isoform expression is not exclusive to certain cell lines or types (Condemine et al., 2006), this should not bias PML NB relationships noted in particular cell lines or types. There are however differences between levels of particular isoform expression, with the major isoforms being PML I and II (Condemine et al., 2006). Therefore PML NB relationships characterised overall may possibly be more of a reflection of the roles of these isoforms in the nucleus.

1.5 Research aims and objectives

1.5.1 Overview and systems biology approach

This study is a survey of the distance relationships between PML NBs and other functional compartments within the nucleus. Typically in the past the elucidation of spatial relationships between nuclear compartments has been a qualitative process. Our aim is to describe nuclear compartment interrelationships quantitatively, and using a systems biology approach. In this vein, the statistical theory of spatial point patterns has been used to inform parts of the analysis. Such an approach will allow us to reveal functional information about PML NBs. Ultimately, we wish to use the information gathered to create a "virtual" map of the nuclear organisation of functional compartments within a normal human fibroblast, and this will be used to help reveal if nuclear organisation alters in reflection of the cell state.

The following questions regarding PML NBs and the spatial analysis of nuclear organisation directed our research aims.

1. Where are PML NBs located in relation to other functional compartments in the nucleus?
    - Does this change upon transformation of a cell?
    - Does this change upon treatment of the cell under certain conditions?
2. What are the implications of these spatial relationships for PML NB function?

1.5.2 Study scope: functional groupings of nuclear compartments, and cell perturbations

From our knowledge of nuclear compartments and their relationships with PML NBs, the following compartments and conditions were chosen for study, allowing us to garner the relationships held between different functional groups and PML NBs using a quantitative approach.

The compartments chosen to study in association with PML NBs fell into several categories (Table 1). PML NB functions have been shown to fall within all four categories.

Table 1 Functional groups of nuclear compartments under investigation

Function	Nuclear compartment to investigate
Chromosome topology	Centromeres
	Telomeres
Transcription	Acetylated histones
	Methylated histones
	Nascent RNA
	RNA polymerase II_O (active)
	Nucleoli
Post-transcription	Splicing speckles
	Cajal bodies
Proteolysis	19S core proteasome regulator
	11S immunoproteasome regulator

PML NB morphometrics and spatial organisation are sensitive to certain cellular perturbations. The effects of heat shock and IFNβ upon cells and PML NBs specifically are well defined. Viral transformation (leading to immortalisation) leads to a downregulation of PML protein. Since PML NBs are thought to provide environments conducive to transcription, the effects of serum starvation (leading to a decrease in overall global transcription levels) were also investigated. Since a majority of cells in the body are in such a quiescent state, this may be an interesting model for the study of PML NBs. Table 2 lists the five cellular conditions investigated in this study.

Table 2 Cellular conditions investigated

Condition	Treatment/cell line	Expected effect on cells and PML NBs
Normal fibroblasts	None	Asynchronous cells; normal PML NBs
Heat Shock	Cells heated to 42˚c for 30 mins prior to fixing	Asynchronous cells; response to heat stress is fission of small PML fragments from PML NBs resulting in increase in PML NB number, but a decrease in mean NB size. (Eskiw et al., 2003)
Interferon β	Cells treated with 1000U/ml of IFNβ overnight	Asynchronous cells, initiates viral infection response; PML NBs are sensitive – there is PML protein upregulation leading to larger and/or a greater number of PML NBs (Lavau et al., 1995)
Serum starvation	Cells plated in 10% FCS medium for 24h to allow reattachment. Followed by 8d in 0.1% FCS medium.	Synchronised quiescent cells (G_0); unestablished effects upon PML NBs.
SV40 transformation	Fibroblast cell line previously transformed to become immortal by SV40 virus.	A transformed cell line "paired" to the normal fibroblast line; PML expression (down-regulation) and PML NB morphology altered.

1.5.3 Hypotheses for the relationships between PML NBs and functional compartments in the nucleus

PML NB organisation was investigated in various cell populations. The majority of work was completed in MRC5 male normal foetal human lung fibroblasts: in the nuclei of asynchronous, serum starved, IFNβ-treated, or heat shocked cells, and their SV40 transformed counterparts MRC5VA. Other work was completed in WI38 female normal foetal human lung fibroblasts and their SV40 transformed counterparts WI38VA to allow for a comparison of PML NB – functional compartment relationships in a similar cell line.

Based upon current literature there are some simple hypotheses that can be stated in relation to the PML NB – functional compartment relationships studied. These are listed in Table 3.

Table 3 Hypothesised relationships between PML NBs and functional compartments under study

Nuclear compartment	Hypothesised relationship with PML NBs
Centromeres	• PML NBs are not associated with centromeres.
Telomeres	• PML NBs are not associated with telomeres in normal cells. • PML NBs show association with telomeric DNA in SV40 transformed fibroblasts.
Acetylated histones	• PML NBs are associated with acetylated histones.
Methylated histones	• PML NBs are not associated with methylated histones.
Nascent RNA	• PML NBs are associated with nascent RNA foci.
RNA polymerase II_O	• PML NBs are associated with RNA polymerase II_O foci.
Nucleoli	• PML NBs are excluded from nucleoli in normal asynchronous cells. • PML NBs are not excluded from nucleoli in SV40 transformed fibroblasts.
Splicing speckles	• PML NBs are associated with SC35 domains (and the minimum NND is further in serum starved cells).
Cajal bodies	• PML NBs are associated with Cajal bodies in SV40 transformed fibroblasts.
19S proteasome regulator	• PML NBs are associated with 19S proteasome regulator.
11S proteasome regulator	• PML NBs are associated with 11S proteasome regulator, and the minimum NND is shorter in IFNβ treated cells.

1.6 How can we measure PML NB-nuclear compartment relationships?

To investigate the PML NB – functional compartment relationships listed above in a quantitive way a distance based approach was taken. Our colleagues Mr. Richard Russell and Dr. Niall Adams in the Department of Mathematics, Imperial College London, have developed an image segmentation tool known as the SCT algorithm (Russell et al., 2009) to provide automatic thresholding of confocal microscopy images, and measure distance and volume related information relating to fluorescently labelled nuclear compartments.

1.6.1 Using spatial statistics to learn about nuclear organisation

When using an immunofluorescence approach to study nuclear compartment relationships, simple co-localization studies have disadvantages. They cannot discern with any significance if co-localization is due to functional homology, stochastic mechanisms, or a previously undetermined interaction with another nuclear compartment. For compartments showing complex localizations throughout the nucleus it is not always possible to identify trends through observations alone, and therefore a quantitative approach is required.

In order to measure the relationships between nuclear compartments quantitative distance-based studies become the obvious choice for the extrapolation of co-localization studies. Statistical methodologies should be employed to compare distance-based experimental data to simulated data generated using suitable hypotheses. Such studies are made more difficult by the fact that the nucleus is a three-dimensional space, as this poses problems for data modelling. It can then be determined if compartments associate more often than expected due to chance – in which case it is likely that an association exists. It is then prudent to reinforce such data using a biochemical approach, such as seeing if marker proteins from both compartments co-precipitate together. Proteins may directly associate with PML protein (either transiently or covalently), or with PML NB associated proteins, and then be dragged in to the bodies. However, if for example the relationship does not involve complete or partial co-localization, this may not be seen in the biochemical data. Also the wrong marker protein might be chosen, therefore revealing no relationship in the IP, when in fact one exists.

It is relatively simple to observe relationships between PML NBs and other nuclear compartments, but much more difficult to translate such observations into meaningful conclusions, especially in relation to PML NB function. Through use of statistical methodologies to process association measurements it is possible to further investigate and confirm PML NB nuclear compartment interrelationships.

1.6.2 Spatial point patterns and nuclear organisation

IF produces distinct patterns for each nuclear substructure based upon their spatial location within the nucleus that can be described qualitatively. However, visual inspection of the more complex patterns is not always suitable to describe trends and so quantitative approaches should be employed.

Such patterns can be described mathematically as a spatial point pattern (SPP). In collaboration with our colleagues in the Department of Mathematics, novel statistical methods incorporating the theory of SPPs have been developed to test the organisation of compartments within the nucleus and quantify the complex 3D interrelationships. Point like compartments can be described as points within the nuclear volume via a centroid position, located at their centre of gravity.

The arrangement of PML NBs, or any other foci of interest within the nucleus, can be described as an SPP. Compartments are referred to as object types, and individual foci are objects or events (Diggle, 1983).

Statistical tools are used to model the location of objects according to different point processes. Actual patterns obtained from confocal microscopy image data are then compared with the models, possibly leading to inference concerning the underlying processes that drive the objects' spatial organisation.

Most SPP theory deals with two dimensional data and so our data which presents in three dimensions adds a layer of complexity to the analysis.

1.6.3 Complete Spatial Randomness

SPPs are data in the form of a set of points, and the three categories form noticeably different configurations (Diggle, 1983). They are known as complete spatial randomness (CSR), and regular and clustered spacing (Figure 6).

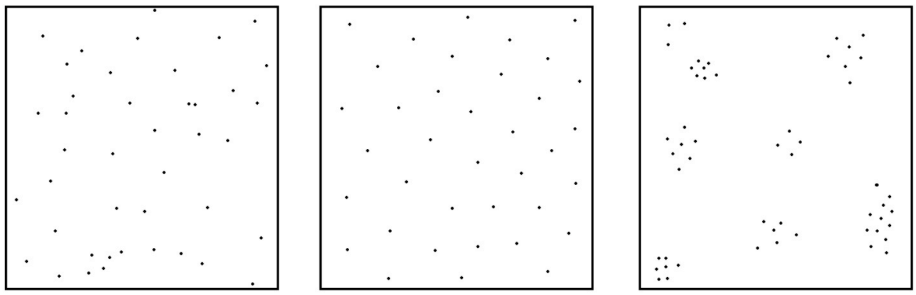


Figure 6 Types of Spatial Point Pattern

There are three classes of spatial point pattern: (from left to right) 1) complete spatial randomness (CSR), 2) regular, and 3) aggregated or clustered. Under CSR points are arranged according to a stochastic mechanism, and there is a complete absence of pattern. In a regular SPP points are arranged uniformly, and under an aggregated CSR points are closer together than expected under the previous two models. This results in patches with increased concentration of events. Adapted from (Diggle, 1983).

Clustered (or aggregated) patterns may arise via a clustering mechanism, or some environmental variation that leads to patches of high concentration of events. Regular spacing describes patterns where points are arranged in a uniform way. CSR is the null model (the complete absence of pattern), and is known as a "straw man" hypothesis – set up so as to be easily refuted. The CSR point process generates foci that are independent and equally likely to occupy any part of the nucleus. Therefore the aim is to establish whether or not an SPP shows CSR. If CSR is rejected then we must also account for the locations of objects within the pattern and infer some biologically relevant explanation. If we consider PML NBs to be events in a 3D SPP, that is they are points in a cell nucleus, it is possible to define the spatial relationships of PML NBs in terms of their consistency with the CSR hypothesis.

1.7 In-depth project aims

The in-depth aims of this study are as follows.

1. To survey the following morphometric information pertaining to PML NBs in two paired normal asynchronous (ASYNC) and SV40-transformed (VA) fibroblast cell lines MRC5 and WI38, and in heat shocked (HS), IFNβ-treated (IFN), and serum starved (SS) MRC5 asynchronous fibroblasts, so as to understand the changes (if any) that these conditions induce.

- Volume of nuclear PML protein
- Size of PML NBs
- Number of PML NBs

2. To understand the inter – PML NB organisation in the cell lines and conditions listed above in terms of:

- Distance relationships (Nearest Neighbour Distance (NND) analysis)
- Spatial organisation (Complete Spatial Randomness (CSR) analysis)

3. To survey PML NB – nuclear compartment relationships (from the point of view of PML NBs) in the cell lines and conditions listed above for nuclear compartments in the functional groups of chromosome topology, transcription, post-transcription and proteolysis, using the following analysis:

- Volume of nuclear compartments
- Distance relationships (Nearest Neighbour Distance (NND) analysis)
- Spatial organisation (Complete Spatial Randomness (CSR) analysis)

4. To visualise the organisation of functional compartments in the nucleus in 3D, and how it varies across different cell lines and conditions, using novel image registration methods.

5. To understand how inter – PML NB and PML NB – compartment relationships contribute to the organisation of the nucleus, and relate to PML NB function.

2

Methods

2.1 Project approach

This project employs a systems biology approach where there is a dialogue between the data collection (Molecular Biosciences) and data processing and analysis (Mathematics) groups to ensure that they are both appropriate, and so that results can be fed back into experimental design. The flow of data is summarised in the chart below (Figure 7).

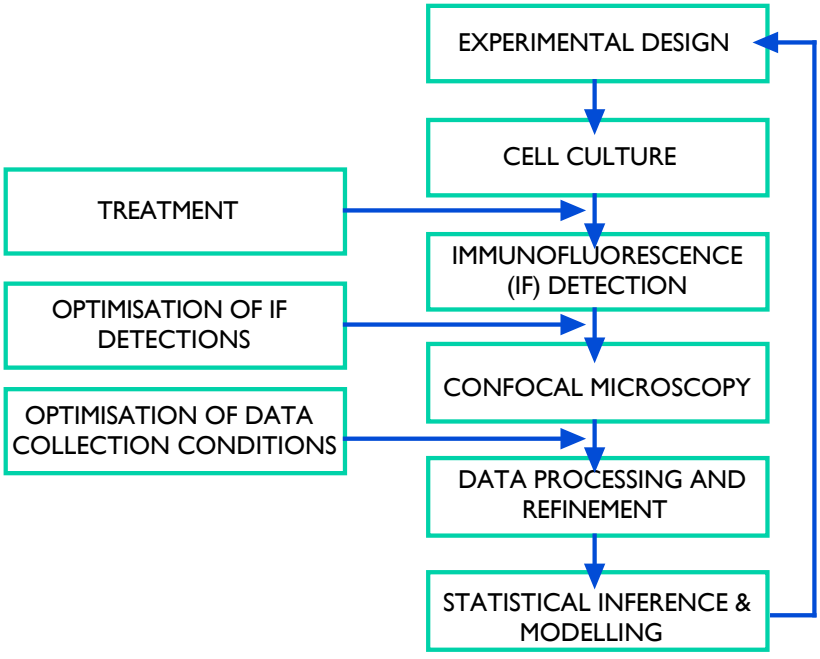


Figure 7 Overview of the Systems Biology approach to the project

There were three main aspects to this project: 1) experimental work (comprising cell biology and sample production), 2) confocal imaging and image processing, and 3) statistical analyses. This required collaboration with colleagues in the Department of Mathematics. The ideal outcome resulted in a feedback loop from the statistical analyses back into the experimental design.

The methods described in detail in this chapter relate to the wet lab data collection. In silico and statistical methods are discussed in less detail to provide an overview of the data analysis methods employed.

2.2 Reagents and solutions

2.2.1 Reagents and sources

Table 4 Reagents and their sources

Reagent	Source
L-glutamine 200mM 100X	Gibco
Foetal Bovine Serum (FBS)	Gibco
Penstrep 50 IU/ml penicillin, 50μg/ml streptomycin	Invitrogen
Trypsin-EDTA (0.5% trypsin, 1mM EDTA)	Gibco
10x phosphate buffered saline	Gibco
Non-essential amino acids (NEAA)	Gibco
Sodium pyruvate	Invitrogen
DMEM	Gibco
DMSO	Merck
MEM with Earles' Salts	Invitrogen
RPMI 1640	Invitrogen
DAPI	Sigma
RNase A	Sigma
Tween 20	Sigma
Triton X-100	Sigma
Formaldehyde (methanol-free)	TAAB Laboratories
Citifluor glycerol mountant including antifade (AF1)	Cityfluor Ltd.
Fluorescein Isothiocyanate (FITC)-conjugated mouse anti-human monoclonal antibody set	BD Biosciences, 556026
VRC	Sigma

2.2.2 Solutions

2.2.2.1 Tissue culture solutions

Table 5 Tissue culture solutions

1 x PBS (PBS)	10 x PBS diluted ten fold in MilliQ water and autoclaved.
DMEM	supplemented with 10% FBS, 2mM L-glutamine and Penstrep (50 IU/ml penicillin and 50μg/ml streptomycin).
MEM with Earles' Salts	supplemented with 10% FBS, 2mM L-glutamine, Penstrep (50 IU/ml penicillin and 50μg/ml streptomycin), 1% NEAA, and sodium pyruvate.
RPMI 1640	supplemented with 10% FBS, 2mM L-glutamine, and Penstrep (50 IU/ml penicillin and 50μg/ml streptomycin).

2.2.2.2 Fixing and permeabilisation solutions

Table 6 Fixing and permeabilisation solutions

Paraformaldehyde (PF) fixing solution	4% (v/v) formaldehyde (methanol-free) in 1x PBS
PBS/Triton-X 100 permeabilisation buffer	0.5% (v/v) Triton X-100 in 1 x PBS.

2.2.2.3 Immunofluorescence and slide mounting

Table 7 Immunofluorescence and slide mounting solutions

PBS/Tween wash solution	1 x PBS with 1ml Polysorbate 20 (Tween 20) per litre of PBS (0.1% v/v).
DAPI	0.25μg/ml or 0.25μg/ml in Citifluor AF1 mountant.

2.3 Cell culture

2.3.1 Cell lines

Cell lines used were as follows (summarised in Table 8). These included both primary and transformed cell lines allowing us to investigate differences in nuclear architecture arising as a result of immortalization. For this the MRC-5 human foetal lung fibroblast line was used, along with an SV-40 transformed immortal MRC-5 cell line (known as MRC-5 VA, or MRC-5 SV2).

2.3.2 Cell revival

Cells, previously stored in liquid nitrogen (either from stocks belonging to the MSF group, or obtained from the ATCC or ECACC) were revived via rapid thawing in a 37°c waterbath, and resuspended in medium appropriate for the cell line. Cells were then either spun down at 1000rpm for 5min and the pellet resuspended in fresh medium, or the initial resuspension was left to attach to a flask for 24h, followed by medium renewal. This was to ensure that all traces of DMSO (used in the freezing process) were removed from the cells.

2.3.3 Subculture and plating

Cells were grown as a monolayer until about 80% confluent prior to passaging, in either T25 or T75 tissue culture treated polycarbonate flasks, in a humid incubator maintained at 37°c and 5% CO_2. They were then washed in 1 x PBS and trypsinised for 5 mins in trypsin-EDTA at 37°c to allow cells to detach from the flasks. Medium containing FBS was added to halt the trypsin reaction and cells were displaced from the flask via pipetting of the solution repeatedly, also ensuring that all cells were single. Cells were then subcultured as follows (summarised in Table 8) to maintain a living stock. The primary cell lines MRC5 and WI38 could not be maintained indefinitely, and were not used beyond certain passages where growth could be clearly seen to have slowed. To avoid mutations accumulating in the transformed cell lines, MRC5VA and WI38VA were not subcultured for longer than four weeks before a fresh population was revived.

Table 8 Cell lines and karyotypes

Cell line	Source and Reference	Morphology and Karyotype	Immortal	Media	Incubator Conditions	Flask size	Subculturing	
							Flask	Coverslip
MRC5	ATCC	Human Caucasian male foetal lung fibroblast. Adherent. Normal diploid human cell line with 2n = 46, XY karyotype. Modal chromosome number = 46, in 70% of cells.	×	• RPMI 1640 (Invitrogen) • 10% FCS (Invitrogen) • 2mM L-glutamine (Invitrogen) • Penstrep (50IU/ml penicillin, 50µg/ml streptomycin, Invitrogen)	37˚c 5% CO_2	T75	1:3	1:9 of a T25
MRC5VA (MRC5 SV2)	ICRF	SV40-transformed MRC5 cells. Fibroblast morphology. Modal number = 60-80, hyperdiploid	✓	• DMEM (Invitrogen) • 10% FCS (Invitrogen) • 2mM L-glutamine (Invitrogen) • Penstrep (50IU/ml penicillin, 50µg/ml streptomycin, Invitrogen)	37˚c 5% CO_2	T25	1:10	1:20
WI38	ECACC	Human Caucasian female foetal lung fibroblast. Adherent. Karyotype 2n = 46 except at high passage number.	×	• MEM with Earles' Salts (Invitrogen) • 10% FCS (Invitrogen) • 2mM L-glutamine (Invitrogen) • 1% NEAA (Invitrogen) • Sodium pyruvate (Invitrogen) • Penstrep (50IU/ml penicillin, 50µg/ml streptomycin, Invitrogen)	37˚c 5% CO_2	T75	1:5	1:15
WI38VA 13 Subline 2RA	ECACC	SV40-transformed WI38. Epithelial morphology. Adherent. Loss of contact inhibition, presence of SV40 antigens. Modal number = 73-78, hyperdiploid.	✓	• MEM with Earles' Salts (Invitrogen) • 10% FCS (Invitrogen) • 2mM L-glutamine (Invitrogen) • 1% NEAA (Invitrogen) • Sodium pyruvate (Invitrogen) • Penstrep (50IU/ml penicillin, 50µg/ml streptomycin, Invitrogen)	37˚c 5% CO_2	T25	1:8	1:16

For use in immunofluorescence experiments where data were collected, cells were plated onto 22mm^2 glass coverslips of 0.17mm thickness, held in six-well plates and incubated at 37˚c for 48h. For control IF detections cell were typically plated onto small round coverslips. For flow cytometry and WB, cells were plated into small or large dishes (6cm or 10cm diameter).

2.3.4 Maintenance of cell line stocks in liquid nitrogen

To maintain a permanent frozen stock from which new populations could be revived, cells were frozen down as 1ml volumes in cryotubes. Flasks were treated with trypsin-EDTA to detach cells, media added and then spun down for 5 mins at 1000rpm. The pellet was resuspended in 90% media / 10% DMSO, and divided into 4 x 1ml volumes. Tubes were then wrapped in multiple thick layers of insulating materials (paper towels and bubble wrap), and placed into the -80˚c freezer for a few days to allow slow cooling. They were then transferred to liquid nitrogen (-196˚c) for long-term storage.

2.3.5 Fixing and permeabilisation

The media was removed from cells growing on coverslips, and then they were rinsed in 1 x PBS, then fixed for 10 mins with orbital shaking in 4% paraformaldehyde (PF) fixing solution at room temperature (RT). This was removed and the cells were washed in 1 x PBS and permeabilised in 0.5% Triton X 100 / 1 x PBS for 20 mins, with shaking at RT. The used PF fixing solution was disposed of appropriately. They were then washed three times for 5 mins in 1 x PBS, and stored in 1 x PBS at 4˚c until required. Fixed cells were stained on the day of fixing, and their nuclei imaged within a few days.

2.3.6 Nucleotide incorporations

In order to visualise regions of RNA and DNA synthesis it was necessary to incorporate labelled nucleotides into the nucleic acids. This was done via BU incorporation for nascent RNA, and BrdU for sites of DNA synthesis prior to fixing and permeabilsation. An antibody which recognises both the BU and BrdU incorporations was used to immunofluorescently detect the incorporations.

2.3.6.1 Bromouridine (BU)

Bromouridine is incorporated into nascent RNA transcripts as a uridine analogue. BU was stored on ice and covered with foil until needed. Prior to fixing, cells grown on coverslips in a six well plate were incubated with BU for 10 mins. The media was removed from the well and 1ml left behind to which the BU was added. Incubation took place at 37°c. In order to label nascent RNA in serum starved cells BU incubation was lengthened to 15 mins, as this was long enough to get foci with a detectable signal. After incubation the media was removed and the cells were washed in PBS. All subsequent steps were performed in the dark. For later antibody incubations VRC (an RNase inhibitor) was added to incubation steps at 37°c to avoid degradation of RNA transcripts. Coverslips with BU incorporation were immunofluorescently stained immediately after fixing and permeabilisation so as to ensure that signal was not lost through degradation of RNA during storage of coverslips.

For heat shock treated cells, BU incorporation took place in the last ten minutes of the heat shock incubation at 42°c in the water bath. The six well plate was covered with foil to prevent degradation of BU during the incubation. After the incubation period finished the media was removed, the cells were washed in PBS, and the method was continued as for cells without treatment (and in the dark).

2.3.6.2 Bromodeoxyuridine (BrdU)

BrdU is incorporated into replicating DNA, and thus is a useful marker of cells at S phase of the cell cycle. There are three main patterns of incorporation each representing a stage of replication: early, mid and late. Different genes are known to replicate at different times during S phase. PML is thought to associate with S phase replication domains (Dellaire et al., 2006b; Wang et al., 2004). 10µl of 100µM (0.1mM) BrdU were added to 1ml of media and cells were incubated in the dark for 1h. After fixing and permeabilising BrdU treated cells were treated with 1ml of 0.1M HCl for 1h at RT (to open the DNA structure so that the incorporated BrdU could be accessed by the antibody), and then washed in 1 x PBS.

2.3.7 Treatments used to perturb PML NBs in normal MRC5 fibroblasts

2.3.7.1 Heat shock

MRC5 cells were plated onto coverslips in six-well plates as performed in section x. The waterbath was warmed to 42˚c. The six-well plate was removed from the incubator and some of the media in each well was removed, leaving 1ml remaining. The plate was sealed with parafilm and then placed floating in the waterbath, and the timer started. The plate was removed from the waterbath after 30min, the media removed and replaced with PBS, and the cells immediately fixed and permeabilised as detailed in Section 2.3.5.

2.3.7.2 IFNβ

IFNβ is a Type I IFN. A stock was maintained at 1000 U/μl at -80˚c. MRC5 cells were plated onto coverslips as in Section 2.3.3, and left to grow for 48h. The evening prior to fixing the cells were treated with IFNβ (added to 2ml of media at a concentration of 1000 U/ml), and left overnight (for 16h).

2.3.7.3 Serum starvation

For serum starvation MRC5 cells were plated as in Section 2.3.3, but 24 hours post-plating medium was changed to RPMI supplemented with 0.1% fetal bovine serum and 2mM L-glutamine only. Cells were left for 8 days and then fixed.

2.4 Immunofluorescence detections

2.4.1 Theory of Immunofluorescence

Immunofluorescence is a technique for the labelling of specific antigens within a cell with primary antibodies raised against the antigen in an animal such as a rabbit, mouse or

goat (Figure 8). Secondary antibodies raised against the primary species and type of immunoglobulin (Ig) in an alternative species, such as donkey, and conjugated with fluors can then be applied to differentially label the primary antibodies according to their species of origin. Each antigen in the sample must be labelled with a primary antibody originating in a separate species to each of the other antigens, and also with a different secondary fluor. The number of different antigens that can be labelled concurrently is dependent upon the availability of primary antibodies originating from separate species, so as to avoid cross-reactions. Ultimately, different antigens can be labelled with different coloured fluors and then detected using fluorescence microscopy.

Typically the antibodies produced in rabbits and goats are polyclonal, which means that they are likely to consist of a collection of antibodies with different binding efficiencies raised at slightly different targets target on the antigen. However, in mice it is possible to produce monoclonal antibodies, which are clonal and therefore have the same affinity for the target. These are produced by the fusion of a mouse lymphocyte from the spleen of a mouse injected with the antigen, and a myeloma cell (a cancerous cell which is immortal). Antibodies produced in this way can then be selected for their binding efficiencies, and propagated.

2.4.2 Immunofluorescence staining methods

Fixed and permeabilised cells grown on coverslips were incubated with primary antibodies diluted to the appropriate titre in PBS at 37˚c for 30 mins. Each coverslip was washed in a separate well of a six-well plate for 3 x 5 mins in 1% Tween-20/PBS, and then incubated at 37˚c for 30 mins with secondary antibodies, conjugated to specific fluorophores, and raised against the species the primary was raised in, diluted in PBS to the appropriate titre.

The majority of stainings were three colour and thus required primary antibodies raised in three different species. Each immunofluorescence experiment included a stain of PML protein (to label PML NBs), and either lamin B or DAPI (to intercalate with DNA) to delineate the nucleus. The third component to be stained was a marker for particular nuclear functional compartments.

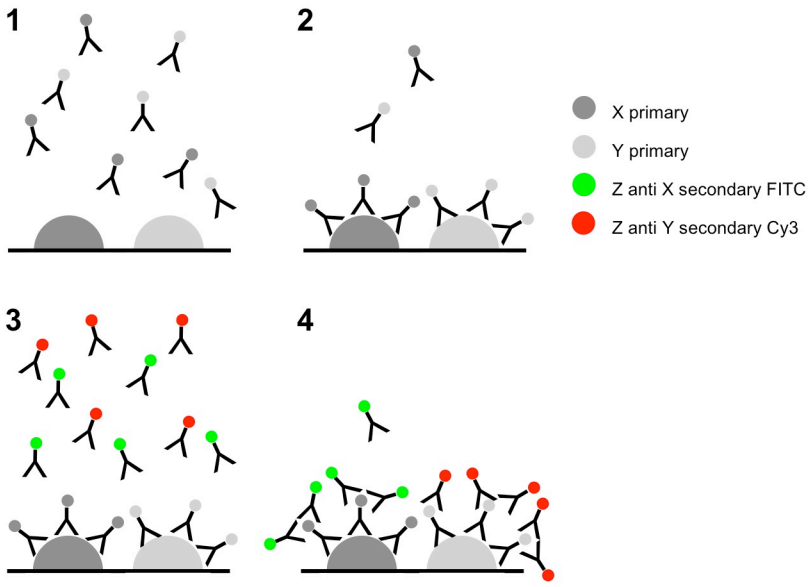


Figure 8 Indirect immunofluorescence staining of antigens

2.4.2.1 Antibodies used

A list of primary antibodies, their species and Ig types, specificities, concentrations (if known), immunogen used, source, and dilutions used for immunofluorescence staining are found in Table 9 below. Table 10, which follows, is a summary of similar information for the secondary antibodies used.

Table 9 Primary antibodies used in immunofluorescence

Antibody target compartment	Specificity/concentration of ab	Epitope/immunogen	Species/Ig type	Titre (IF)	Source/product code
PML nuclear body	• All isoforms of human PML protein. Affinity purified against a synthetic peptide corresponding to residues 228-267 of PML protein (Borden *et al* 1995)		Rabbit Polyclonal	1/200	• Pure bleedout rabbit serum
	• All isoforms of human PML • 200µg/ml	Residues 37-51 of the N-terminal epitope of human PML	Mouse Monoclonal IgG1	1/100	• Santa Cruz Biotechnology. Inc. • PML (PG-M3): sc-966
	• All isoforms of mouse, rat and human PML • 200µg/ml	N-terminal peptide of human PML	Goat Polyclonal IgG	1/200	• Santa Cruz Biotechnology. Inc. • PML (N-19): sc-9862
Nucleolus	• Nucleophosmin (B23) C-terminus of B23 in human, mouse and rat • 0.5µg/µl	B23 purified from rat hepatoma	Mouse Monoclonal IgG1	1/50	• Zymed Laboratories Inc. • 32-5200
Centromere	• Human centromeric proteins	Human centromeric proteins	Human	1/1000	• Human autoantibody positive serum • The Binding Site Ltd. • BP121
Telomere	• Human telomeric repeat binding factor 1 (TRF1)	Human TRF1 protein produced in baculovirus	Mouse Monoclonal IgG1	1/200	• Abcam Ltd. • ab10579 [clone TRF-78]
Histone	• Human, Cow and Indian Muntjac Di-methylated histone H3 (at K9 and K27). Also tri-methylated K27.	Synthetic peptide: KAARK$_{Me2}$SAPATGG-C conjugated to KLH, corresponding to AA 23-34 of human histone H3 (K27)	Rabbit Polyclonal IgG	1/2000	• Abcam Ltd. • ab7312
	Acetylated histone H4 K12 in mammals, amphibia, *Drosophila*, yeast and some plants	Ovalbumin-conjugated peptide: NGKGLGK$_{Ac}$GGAKCc	Rabbit Polyclonal	1/1000	• Serotec • AHP416

Proteasome (antigen processing)	• 11S proteasome regulator subunit (PA28 α) in human, mouse and rat	Synthetic peptide corresponding to residues 5-19 of murine PA28α conjugated to keyhole limpet haemocyanin.	Rabbit Polyclonal	1/500	• Biomol International Lp • PW 8185
	• 19S regulator ATPase subunit Rpt3p (Yta2) in yeast	His_6-tagged recombinant protein corresponding to N terminal 100 AA of YTA2. YTA2 is the yeast homologue of human proteasomal subunit TBP-7 which is a constituent of the human 26S proteasome.	Rabbit Polyclonal	1/1000	• Biomol International Lp • PW 8250
Cajal bodies	• Human and mouse coilin	Recombinant fragment (C-terminus of Human coilin, 389 amino acids) epiptope located between amino acids 363 and 481 of human coilin.	Mouse Monoclonal IgG1	1/125	• Abcam Ltd. • ab11822 [clone Pdelta]
Nascent RNA transcript / replicating DNA	• BrU RNA / BrdU DNA. Binds bromodeoxyuridine, and cross-reacts with iodouridine (and bromouridine).	Bromodeoxy-uridine-bovine serum albumin conjugate.	Mouse Monoclonal IgG1	5/100	• Roche • 1170376
Proliferation marker	• Human and mouse Ki67 • 0.4mg/ml	Synthetic peptide of human Ki67.	Rabbit Polyclonal IgG	1/250	• Abcam Ltd. • ab15580
Active sites of transcription	• RNA polymerase II $_O$ (elongation complex)	Phosphorylated RNA polymerase II	Mouse Monoclonal	1/500	• BAbCo • MMS-129R (H5)

	Phospho-serine 2 version of Pol II • 2-3mg/ml	(phosphorylated at serine 2 in the heptapeptide repeat YSPTSPS at the C terminus) extracted from a transformed cell line	IgM		
Nuclear lamina	• Lamin B of mouse, rat and human • 0.2µg/µl	Peptide from C-terminus of Lamin B of mouse origin	Goat Polyclonal IgG	1/100	• Santa Cruz Biotechnology Inc. • Lamin B (M-20): sc-6217
Splicing speckles	• SC35, splicing factor SC-35 Phospho-epitope of the non-snRNP factor SC-35 in human, rat, newt, frog and *Drosophila*.	Partially purified mammalian spliceosomes.	Mouse Monoclonal IgG1	1/500	• Sigma • Product # S4045 (clone SC-35)

Table 10 Secondary antibodies used in immunofluorescence

Species	Specificity/concentration of ab	Fluor conjugate	Source	Titre (IF)
Donkey	• Rabbit IgG • 1.5mg/ml	FITC	Jackson ImmunoResearch Laboratories, Inc.	1 in 200
Donkey	• Rabbit IgG • 1.5mg/ml	Cy3	Jackson ImmunoResearch Laboratories, Inc.	1 in 200
Donkey	• Rabbit IgG • 1.5mg/ml	Cy5	Jackson ImmunoResearch Laboratories, Inc.	1 in 200
Donkey	• Mouse IgG • 1.5mg/ml	FITC	Jackson ImmunoResearch Laboratories, Inc.	1 in 200
Donkey	• Mouse IgG • 1.4mg/ml	Cy3	Jackson ImmunoResearch Laboratories, Inc.	1 in 200
Donkey	• Mouse IgM (μ chain) • 1.5mg/ml	Cy3	Jackson ImmunoResearch Laboratories, Inc.	1 in 200
Donkey	• Human IgG • 1.5mg/ml	Cy3	Jackson ImmunoResearch Laboratories, Inc.	1 in 200
Donkey	• Goat IgG • 1.5mg/ml	Cy5	Jackson ImmunoResearch Laboratories, Inc.	1 in 200

2.4.2.2 Markers of cell cycle phase

It is possible to employ certain antibody markers against nuclear proteins to help estimate the cell cycle status of cells using immunofluoresence detection. However due to antibody species restrictions and also the total number of fluors that could be imaged at once using confocal microscopy, it was not possible to stain such markers concurrently with PML NBs, the nuclear lamina, and other functional compartments. Instead we aimed to define a classification scheme for PML NBs in MRC5 nuclei at certain cell cycle phases, given that there appears to be a defined progression of PML NB morphology especially between S phase and G_2 (Dellaire et al., 2006b). If successful we could then return to the asynchronous datasets and classify each nucleus as a particular phase according to its PML spatial organisation.

The scheme was as follows. The Ki67 proliferation marker is found in all cycling cells. Therefore quiescent cells (G_0) are negative for Ki67 staining and can be selected using fluorescence microscopy. The pattern of Ki67 staining in G1 cells allowed such nuclei to be selected for imaging (however this can be confused with late G2 staining). Lastly, S phase cells showed BrdU incorporation at DNA replication foci. This allowed us to collect datasets of 50 nuclei in the following phases; G_1 (G1), G_0 (G0) and S (S) from an asynchronous MRC5 population. Within nuclei classified as S phase it was actually possible to subclassify them further as the BrdU marker showed different patterns according to early, mid or late DNA replication. However, the G1, G0 and S MRC5 subsets were already small in comparison to the amounts of data collected for ASYNC, HS, IFN, SS, and VA cells, and therefore may not have been large enough to reveal any trends.

2.4.2.3 Blocking

The immunofluorescence protocol followed in the MSF lab did not incorporate a blocking step, as this was found to be unnecessary to achieve highly specific staining with the antibodies used. However, a blocking control was carried out where coverslips were incubated with 5% (w/v) skimmed milk powder in PBS for 1 hr at 37˚c prior to incubation with antibodies (for PML, B23 and lamin B). Antibody solutions were made up in 1% (w/v) skimmed milk powder in PBS.

It was apparent that the images collected of unblocked and blocked samples under the same conditions appeared similar, with regards to background staining levels within the nucleus. When looking at the PML staining there were some instances where small "bodies" were observed within nucleoli in the blocked samples, and this observation had also been made previously in the lab. Since PML NBs are not typically found with nucleoli (except where PML and nucleolar proteins colocalise in a ring structure under conditions of DNA damage or stress (Bernardi et al., 2004; Condemine et al., 2007), this could be attributable to use of the blocking agent. Therefore we did not include blocking steps due to these artefacts and clean staining within the nucleus.

2.4.2.4 Slide preparation

For ordinary staining where it was only required to delineate nuclei, DAPI was used in the following amounts: 0.25μg/ml of mountant, protected from light and stored at 4˚c. For staining which required DAPI to be used to delineate the nucleus to allow z stack collection (and not fade before the end), a concentration of 0.5μg/ml was used.

Coverslips were mounted on slides, mounted in 8μl of DAPI in glycerol/PBS and Citifluor AF1 antifade, and stored at 4˚c until imaged. Coverslips were typically imaged within a maximum of three days of fixing and IF staining.

2.5 Confocal microscopy

2.5.1 Theory of Confocal microscopy

Confocal microscopy is a type of light microscopy that exploits immunofluorescent labelling of samples. Unlike conventional light microscopy, confocal microscopy allows imaging of cells in 3D by sweeping the focal plane through the sample. A laser is used to excite fluors, which are bound to specific antigens in the sample via indirect immunofluorescence techniques. Since point illumination is used (as opposed to flooding the sample with light), the sample must be scanned sequentially with the laser. Emitted light is only collected from the sample at the focal plane via use of an adjustable pinhole, thereby eliminating the out of focus light that accompanies widefield fluorescence images, and resulting in sharp images that need little or no deconvolution. A beamsplitter directs light towards various filters, of which there are several types, are used to alter the path of light within the microscope and towards the photomultiplier tube (PMT) for detection of different colours of light in different channels. The bandpass filter transmits a defined region or band of wavelengths, but not those shorter or longer than in the band. The longpass filter (also known as highpass) transmits longer wavelengths, and removes those above the one it is set for. The shortpass filter (also known as lowpass) transmits shorter wavelengths (usually UV and visible light) and removes longer wavelengths than that it is set for (olympusconfocal.com, 2009). The PMT converts light into an electrical signal by collecting and amplifying photon signals, which are then transmitted to the processing circuit. It does not form an image (unlike a charge-coupled device) and therefore is not a camera (olympusconfocal.com, 2009).

2.5.2 Confocal microscopy methods

Confocal microscopy data were collected on two confocal microscopes, both Zeiss LSM 510 (Figure 9), with a Zeiss Plan Apochromat x 63 oil immersion objective, numerical aperture (NA) = 1.4. NA is a measure of the range of angles over which the system can accept, or emit, light and provides an indication of the resolving power of a lens, (a higher NA means that finer details can be resolved).

The first was based in the Biochemistry Building, Imperial College London, and the second belonged to the Facility for Imaging with Light Microscopy (FILM) based in the SAF building, Imperial College London. The second microscope only became available half way through the course of this project. It has a fourth laser which is a UV line, and thus has the capability to image DAPI. Both microscopes have the laser lines to image FITC (488nm Argon laser), Cy3 (543nm HeNe laser) and Cy5 (633nm HeNe laser).

Excitation of FITC, Cy3 and Cy5 dyes was achieved as follows. FITC was excited using the 488-nm line of an Argon laser, and Cy3 and Cy5 were excited by the 543-nm and 633-nm lines, respectively, of an HeNe laser. A 405-nm UV laser was used to excite DAPI. The emission fluorescence was first split using an NFT635 VIS dichroic mirror. For FITC and Cy3 detection, the resulting fluorescence of wavelengths <635nm was split with a NFT 545, and then a 505–530 bandpass filter used to collect FITC, and a bandpass 585–615 filter used to collect Cy3, with detection by a photomultiplier tube (PMT). For Cy5 detection, the resulting fluorescence (>635 nm) was passed through a plate followed by a longpass 650 filter before collection by a PMT. PMT voltages (detector gains) were adjusted so that images showed no saturation using the range indicator. Detector gains used for each fluor/compartment combination were varied as little as possible, based upon previous data collection testing, and were chosen to give as close as possible a representation of the image seen down the fluorescence microscope without image saturation.

Data were collected in the form of image stacks which span the nuclei in the x, y and z planes. Image stacks consisted of about 20 sequential slices of either 300 x 300 or 250 x 250 pixels (where 1 μm is equal to 12 pixels), taken at 0.4 μm intervals along the z plane. The pixel resolution was 0.283 μm/pixel, with a digital zoom of 3.4 being used to achieve a resolution of 0.083 μm/pixel. Voxels were interpreted as cuboid, and measured from their middle (in z). Therefore a voxel was 4.8 μm deep (and 1/12 μm by 1/12 μm in XY), and was measured from its centre, which was at 2.4 μm. There was also an overlap of 50% in z.

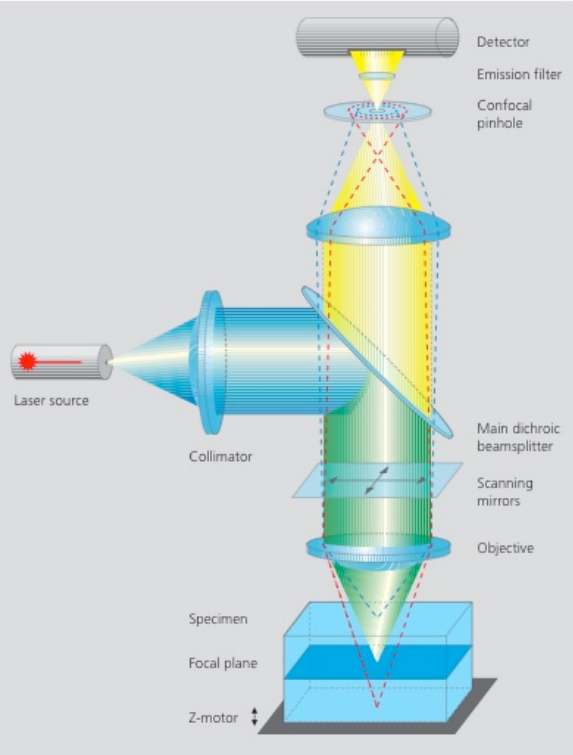


Figure 9 Diagram of light path in confocal microscope

(zeiss.de, 2009)

Cell nuclei to be imaged were chosen at random. However, cells with nuclei that did not fit the field-of view (FOV), a region of interest covering an area of 250 x 250 pixels, were excluded. To ensure that both the upper and lower boundaries of the nucleus were not excluded from the imaging, the fluorescence-free regions directly above and below the nucleus were included in the z stack. The region of interest was delineated, and the z stack boundaries were defined, using the Zeiss acquisition software.

Data sets typically consisted of 50 cell nuclei, immunofluorescently labelled and imaged in 3D. Each stack was also saved as a projection image consisting of all the flattened image slices superimposed at maximum transparency, which was used as a reference image in data processing.

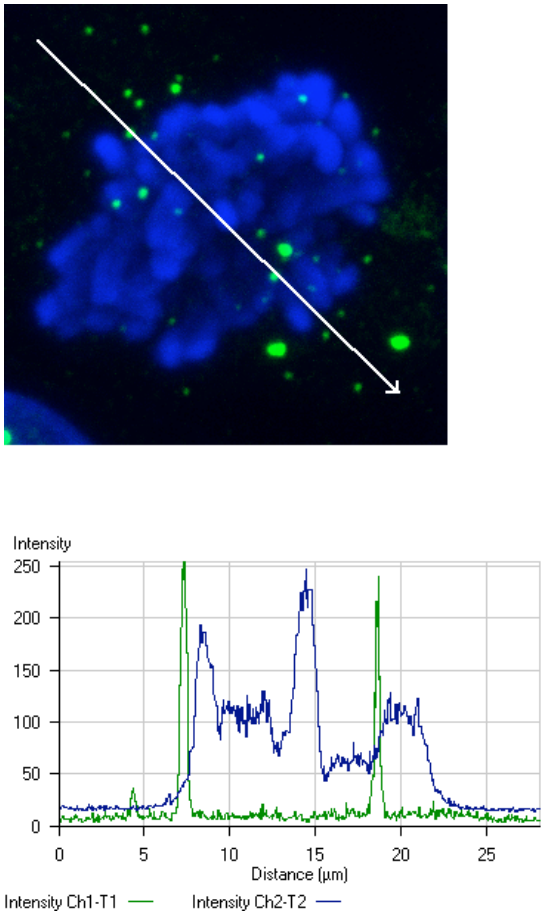


Figure 10 Intensity profile for an example image

Figure 10 shows the intensity profile for the arrow crossing the image of condensed chromosomes in a mitotic cell. As mentioned previously, intensity is measured on a scale of 0 to 255. DNA (blue) and PML (green) are stained. The two peaks in the green channel intensity at 7.5 and 18.5µm are two MAPPs. The background level of green signal is extremely low compared to the true signal (5-10 as opposed to 255), however the intensity of the DNA staining is slightly more variable across the profile, due to the variation in condensation of DNA.

2.6 Western Blotting

2.6.1 Total cell protein extracts

Cells were plated into a small 6cm dish and grown until 70% confluent. The media was removed and the cells were washed in PBS. The plate was then trypsinised in 1 ml trypsin-EDTA and left for 5 min at 37°c to allow the cells to detach. The trypsinisation was halted with 4ml of media containing 10% FBS, and the solution was pipetted up and down to ensure good separation of cells. It was moved to a 15 ml blue cap tube, and then spun down for 5 min at 1000 rpm. The media was removed from the cell pellet with a pipette, and the pellet was then washed in 5ml of 1 x PBS. Whilst the rest of the cells were spun down again for 5 min at 1000 rpm, a sample of the cells was counted using a haemocytometer. The PBS was then carefully removed from the washed cell pellet with a 5 ml pipette, and the tube was placed on ice. If any PBS remained the tube was re-spun and the PBS removed using a Gilson pipette and 200µl tip.

Lysis buffer, containing benzonaze (an endonuclease), was then added directly on top of the cell pellet in the tube. Lysis buffer and benzonaze were used in the following amounts: for a small 6 cm dish with a cell count of 100000 cells per ml, 100 µl lysis buffer with 0.5 µl benzonaze were added. Since the benzonaze concentration needs to be at least 250 U/µl to remove all DNA from the sample it was used at about 1250 U/ml. The tube was flicked to mix well, and also run up and down a rack to aid mixing. It was left on ice for 5 min, and during this time the hot plate was adjusted to 95°c. The sample was then transferred to an Eppendorf tube and boiled at 95°c for 5 min. The tube was cooled on ice, spun down in a desktop centrifuge for 5 min at maximum speed (13.4 rpm) to remove debris, and finally placed on ice and transferred to the -20°c freezer for storage.

2.6.2 Nuclear and cytoplasmic protein extracts

To study the localisation of PML protein in the cell (nuclear and or cytoplasmic), and possible differences in modifications (such as SUMO), between asynchronous and serum

starved populations of MRC5 normal human fibroblasts, the proteins from the cells were fractionated.

A Nuclear/Cytosol Extraction Kit (BioVision Research Products) was used to separate the nuclear extract from the cytoplasmic fraction of mammalian cells. The manufacturer's protocol was followed. Firstly protease inhibitor cocktail and DTT were added to both the Nuclear Extraction Buffer (NEB) and Cytosol Extraction Buffer A (CEB-A), to make NEB Mix and CEB-A Mix respectively, and both were kept on ice. Cells, either asynchronous (control) or serum starved in 0.1% FBS for 8 d, grown in a 6 cm dish were trypsinised in 1ml trypsin-EDTA for 5 min, and the reaction halted with 4 ml of 10% FBS medium. Cells were counted, and the following procedure was carried out on 1 x 10^6 cells. Cells were then centrifuged at 1000 rpm for 5 min. They were then washed in 1 x PBS, and pelleted at 1000 rpm for 5 min. The PBS was removed and 0.1ml of CEB-A Mix was added to the sample. The sample was transferred to an eppendorf tube. The tube was vortexed to fully resuspend the pellet and incubated on ice for 10 min. 5.5 µl of ice-cold Cytosol Extraction Buffer B (CEB-B) was added to the tube, which was then vortexed for 5 s, followed by incubation on ice for 1 min. The tube was again vortexed for 5 s and then centrifuged for 5 min at maximum speed in a microcentrifuge. The supernatent was then transferred straight away to a new tube and placed on ice (the cytoplasmic extract). The pellet, now containing the nuclei, was resuspended in 50 µl of ice cold NEB Mix, vortexed for 15 s and replaced on ice. This was repeated every 10 min for 40 min. The tube was then centrifuged for 10 min in a microcentrifuge, and the supernatent (the nuclear extract) immediately transferred to a new tube, and placed on ice. Both extracts were stored at -80°c, and later used for Western blotting.

The concentration of the nuclear extract prepared according to the manufacturer's protocol is of ~ 1 mg/ml.

2.6.3 SDS polyacrylamide gel electrophoresis (SDS-PAGE), Western blotting and chemiluminescent detection of proteins

Preparation of total cellular and nuclear and cytoplasmic protein extracts was carried out as above. SDS-polyacrylamide electrophoresis was carried out according to standard

protocols. Gels used were commercially available. Samples were lysed in SDS-gel reducing buffer, boiled and loaded onto an appropriate percentage Tris-Glycine polyacrylamide gel. Proteins were then transferred to Hybond ECL nitrocellulose membrane (GE Healthcare Life Sciences) using the Hoefer Semiphor semi-dry transfer procedure and then blocked overnight in 5% (w/v) skimmed milk powder in distilled water.

Blocked membranes were probed with rabbit anti-PML antibody, diluted 1/1000 in blocking solution, and mouse anti-actin antibody (c-2, sc 8432 Santa Cruz Biotechnology Inc.) diluted in blocking solution. Membranes were washed twice in PBS/Tween washing solution followed by once in PBS. Membranes were then incubated with horseradish peroxidase conjugate goat IgG anti-rabbit (Dako) diluted in blocking solution. Membranes were again washed twice in PBS/Tween and once with PBS. Binding of secondary antibodies was detected using ECL solution (GE Healthcare Life Sciences). Membranes containing the nuclear and cytoplasmic protein extracts were stripped of antibodies and reprobed with rabbit anti-Ki67 antibody at a concentration of 1μg/ml and incubated with horseradish peroxidase conjugate goat IgG anti-rabbit diluted in blocking solution.

2.7 Data processing and statistical analyses

2.7.1 File conversion

Microscope data were collected in the form of image stacks (Figure 11) (tif format, consisting of colour images made up of a red, green and blue (RGB) colour value) as described in Section 2.5.2. These stacks were then converted to an input file (inp format), and finally to a format that was accessible to the processing algorithm, termed pis. To create the pis file the RGB 24 bit image, (which has 2^{24} possible values that can be split into three greyscale channels which describe the RGB components), is turned into an 8 bit greyscale image with a value of between 0 and 255. (There are now 2^8 (256) possibilities of value = {0, 1, …, 255} that any voxel can take).

2.7.2 SCT algorithm

There are a range of open source and commercially available software programs that allow segmentation of confocal microscopy data. However, there is an absence of programs that are able to automatically and accurately determine an appropriate threshold, for which user-defined thresholding is the gold standard (Russell et al., 2009). Unfortunately thresholding is often user-subjective, and time consuming. With high throughput microscopy techniques coming to the fore, accurate automatic thresholding methods, able to perform as well as manual thresholding become increasingly important (Russell et al., 2009).

We have worked closely with our colleagues Richard Russell and Dr. Niall Adams in the Department of Mathematics, Imperial College London, to help them develop an in-house thresholding algorithm, known as the stable count thresholding (SCT) algorithm (Russell et al., 2009), which is executed in R script (R). This novel thresholding method automatically determines threshold levels for confocal microscopy z stacks. It principally aims to establish when the voxel count becomes stable in T (a threshold).

The SCT algorithm performs comparably to manual thresholding and is time-efficient (Russell et al., 2009), and also had a high success rate for the correct segmentation of image stacks collected for this project (see Appendix). However, some data sets with particular qualities did prove to be challenging, and the SCT algorithm was unable to correctly segment a high proportion of the voxels found within certain nuclei. This occurred in data sets where there were populations of foci with different intensities, such as the PML NBs found in heat shock (HS) treated cells, or nascent RNA foci. During HS treatment smaller PML NB fragments form as normal PML NBs undergo fission. Since these smaller fragments have a low intensity they cannot be segmented as the automatic global threshold set for the nucleus was set at a level too high, due to the additional presence of the population of larger, and more intensely stained PML NBs.

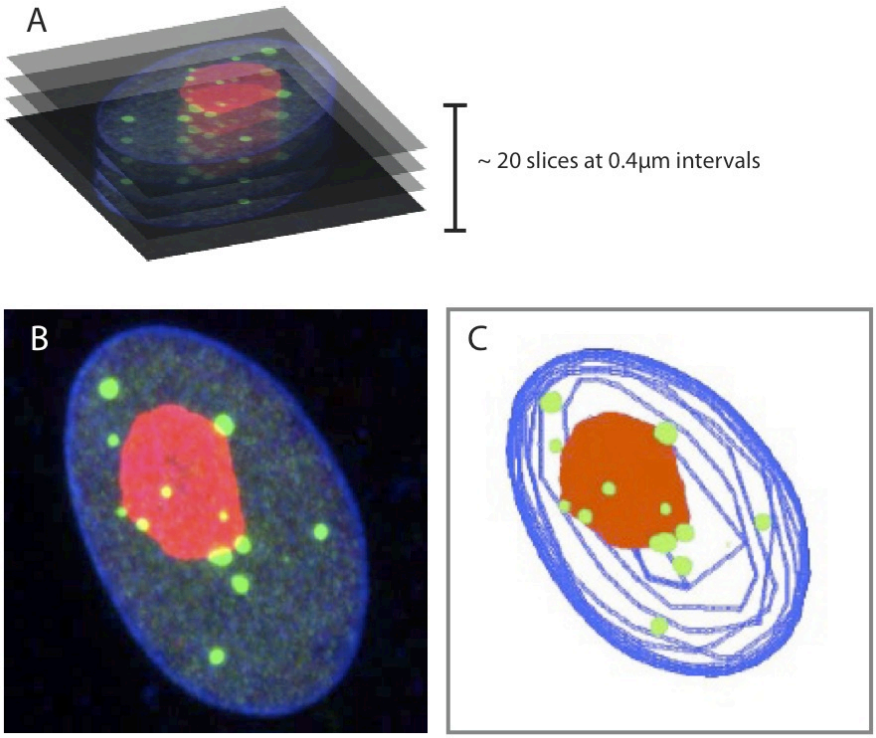


Figure 11 Image segmentation schematic

A) shows an exampled image stack of about 20 slices taken sequentially at 0.4µm intervals throughout a nucleus. B) shows a projection image of all the slices of the nucleus, and C) shows the 3D reconstruction after image segmentation using the SCT algorithm (Russell et al., 2009).

2.7.3 Distance analysis (NNDs)

After image segmentation the *xyz* coordinates of every PML NB centroid in each nucleus of a dataset were known. This allowed the distance between the centroids of every unique pair of PML NBs within a nucleus to be calculated. From these distances, the distance between a PML NB and its closest neighbouring PML NB was recorded, and this was termed the nearest neighbour distance (NND). This could also be applied to measuring the NND between a PML NB and an object of interest that was closest to it. Where the object was a functional compartment the NND was calculated between the PML NB centroid, and the nearest segmented voxel of object. An object could be one of the following: PML NB, nuclear boundary, nuclear centroid, or a functional compartment.

There were two groups of NNDs that were useful for characterising PML NB distance relationships. Both were groups of minimum NNDs. The first comprised of the minimum PML NB – object NND for each PML NB in every nucleus in a dataset, and

was termed the total minimum NNDs. The number of distance observations in this group was upwards of 500. For example, each nucleus contains around 10 PML NBs, and there are 50 nuclei in the PML – object dataset, meaning that there are a total of 500 minimum PML – object NNDs to record. This group of measurements was used to describe the PML NB to PML NB, nuclear boundary and nuclear centroid distances because we wished to understand the range of minimum PML NB – object distances that characterised each dataset.

The second group, termed the minimum NNDs, consisted of the shortest minimum PML NB – object NND for each of the nuclei within a dataset. The number of distance observations in the group was around 50. For example, the shortest PML NB – object NND for each of 50 nuclei in a dataset is recorded. This resulted in the shortest PML NB – object minimum NND representing the entire PML NB – object minimum NNDs for the nucleus from which it came. This group of measurements was used to describe the PML NB to functional compartment distances because we were most interested in the smallest minimum distances between PML NBs and functional compartment as a measure of the most closely positioned PML NB and compartment in each nucleus studied.

2.7.4 Spatial analysis (CSR)

In addition to the *xyz* coordinates of the PML NB centroid, image segmentation also allowed the size of each PML NB to be recorded. This was employed in the spatial analysis of PML NBs, and was done on a cell-by-cell basis. The minimum PML NB – object NND for each PML NB in a nucleus was recorded. This was then compared with 999 Monte Carlo simulations of the same PML NBs (in terms of their size) in the same nuclear volume, and where the object voxels were fixed. Such PML NBs are located at random within the nuclear volume and therefore represent an SPP of complete spatial randomness (CSR). To reflect the true biological situation, in the simulation PML NBs were treated as volumes (as opposed to points) so that superimposition of points was not allowed. The minimum PML NB – object NNDs for the simulated PML NBs were recorded and the upper and lower limits of the simulation envelope was plotted, upon which the empirical distribution function (EDF) of the observed minimum PML NB – object NND for each of the PML NBs within the nucleus was also plotted (Figure 12).

If the observed EDF was not completely contained within the simulation envelope there was evidence to reject the null hypothesis of CSR. Therefore the observed could either be closer to or further from the PML NB than expected under CSR. Finally, the CSR status for every nucleus in a dataset was scored, and converted to a total percentage of nuclei in which the object was closer to or further from PML NBs than expected under CSR.

2.7.5 Aggregate Mapping

Aggregate maps are kernal smoothed intensity plots of all the voxels of the registered objects in their 3D mean shaped nucleus, and are viewed as 2D projections. The aggregate maps apply the Kernel Smoothed Intensity of Point Pattern method to the density function in R. This computes a kernel smoothed intensity function from a point pattern.

They were generated as follows. The outer boundary and centroid was taken for each nucleus in the sample of cells. For each nucleus the maximum ellipse was aligned along the x plane. Using the centroid, 64 polar landmarks that fall around the boundary were found and used to construct the mean shape of the sample (for n nuclear centroids). This mean shape was typically ovoid. This process was extended for the yz and xz planes.

Using a non-rigid registration process the segmented image for each nucleus was transformed onto the 3D mean shape, resulting in an intensity plot. No structure was visible in the aggregate for entire data sets ($n \leq 40$), (as pixels are either displayed as empty or filled, but not assigned an intensity), until smoothing was employed. This revealed patterns of regions in the nuclear where the segmented voxels were found. At present it is not possible to view the patterns according to significance level.

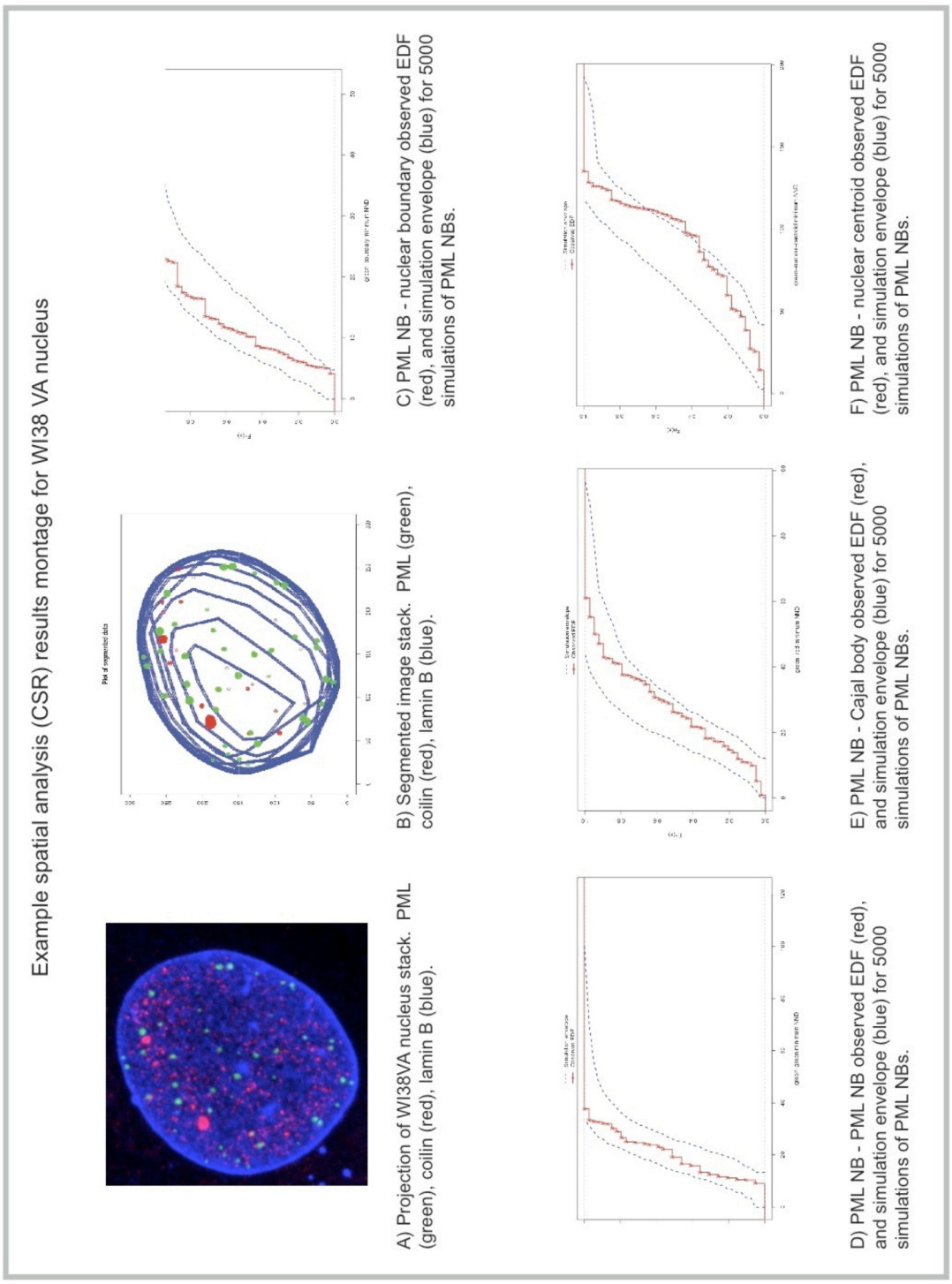


Figure 12 Example CSR results montage

2.8 List of companies and academic groups

2.8.1 Companies

- Abcam Plc., Cambridge, CB4 0FL.
- ATCC, LCG Standards (UK distributor), Teddington, TW11 0LY.
- BAbCo (now part of Covance), Princeton, NJ., USA.
- BD Biosciences, Oxford, OX4 4DQ.
- Biomol International Lp (now Enzo Life Sciences), Exeter, EX2 8NL.
- Biovision Research Products, Cambridge BioScience Ltd (UK distributor), Cambridge, CB5 8LA.
- Citifluor Ltd., London, N1 6LD.
- Dako UK Ltd., Ely, Cambridgeshire, CB7 4EX.
- ECACC, Health Protection Agency Culture Collections, Salisbury, SP4 0JG.
- GE Healthcare Life Sciences, Buckinghamshire, HP7 9NA.
- Invitrogen, Paisley, PA4 9RF.
- Jackson ImmunoResearch, Stratech (UK distributor), Suffolk, CB8 7SY.
- Roche, Hertfordshire, AL7 1TW.
- Santa Cruz Biotechnology Inc., CA. 95060, USA.
- Serotec (now AbD Serotec), Oxford, OX5 1GF.
- Sigma-Aldrich, Dorset, SP8 4XT.
- TAAB Laboratories, Berkshire, RG7 8NA.
- The Binding Site Ltd., Birmingham, B14 4ZB.
- Zymed Laboratories Inc., CA., 94080.

2.8.2 Academic groups and facilities

- Macromolecular Structure and Function Group (MSF), Division of Molecular Biosciences, Faculty of Natural Sciences, Imperial College London, SW7 2AZ.
- Facility for Imaging with Light Microscopy (FILM), Sir Alexander Fleming Building, Faculty of Natural Sciences, Imperial College London, SW7 2AZ.

- Department of Mathematics, Faculty of Natural Sciences, Imperial College London, SW7 2AZ.

3

PML nuclear bodies and their spatial relationships

3.1 Introduction

The primary aim of this project was to quantitatively investigate PML NB morphometrics, their distance interrelationships, and spatial organisation in normal, treated and virally transformed fibroblast cell lines. Treatments were chosen that were thought to influence PML NB morphology. The data gathered pertaining to PML NBs alone are presented in this chapter. This approach was then extended to the relationships that exist between PML NBs and other nuclear compartments (which is presented in Chapter 4). Compartments were chosen that fell into groups according to nuclear functions in which PML NBs are also thought to play some role. The segmentation methods employed here also allowed some quantification of functional compartment volume (approximated using voxel counts).

3.2 Defining the nucleus

3.2.1 Introduction

Initially it was necessary to establish a method for defining immunofluorescence staining as being of nuclear origin. It was decided that the nuclear lamina would suffice as a marker of the nuclear boundary. At a later stage, when alternative imaging equipment became available, DAPI staining of DNA within the nucleus was also used to define the nuclear volume.

3.2.2 Characterisation of the nuclear boundary and DNA within the nucleus

To allow accurate segmentation of the nuclear volume, in each IF detection either the nuclear lamina or the DNA was stained (with DAPI). This served to delineate the nuclear boundary. Figure 16 shows example projection images of both lamin B immunofluorescent staining (MRC5 async nucleus (blue)), and DAPI staining of DNA (PML structure MRC5 cytoplasmic bodies nucleus (blue)). Whereas DNA was stained throughout the nucleus, lamin B was mostly found within the lamin network that exists under the nuclear membrane. However, it was also occasionally found in internal spots within the nuclear volume in G1.

3.2.3 Nuclear volume estimation

Nuclear volumes can be estimated by counting the voxels that fall within the nucleus, as delineated by immunofluorescence staining of lamin B, or DAPI staining of DNA. This was used to derive information that described the volumes of nuclei in the cell lines studied.

However, these measurements are only approximations as they were based upon the selection of cells chosen for each dataset (to a maximum sample size of 500), and do not likely cover extremes (for example very small or very large nuclei), which were not included due to the sampling process. Cells were chosen whose nucleus fitted within the ROI, although there was no preference taken according to stack depth in the z axis.

It should be noted that it is possible for a cell nucleus to have a smaller volume than another that shares its diameter. Hence a smaller volume does not necessarily mean that a cell nucleus has a smaller footprint. Therefore it will be interesting to compare the nuclear volume estimates with the mean cell shape derived by a different process (Section 5.2).

3.2.3.1 Nuclear volumes of MRC5 ASYNC, HS, IFN, SS and VA cells

Boxplots are a useful way to display continuous data such as nuclear volumes of cells within a population. They provide an idea of the spread of the data and present the median data value as a horizontal line through the box, which represents the 50% of the data found between the lower and upper quartiles. Figure 13 summarises how the data should be read from such plots.

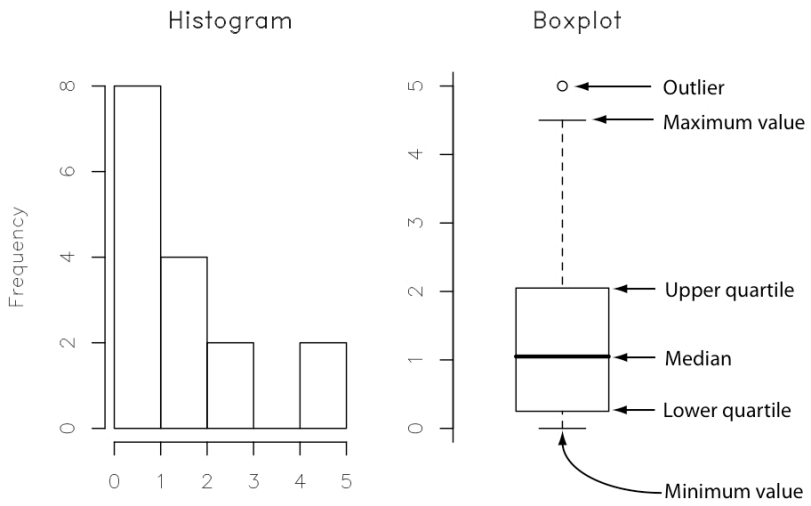


Figure 13 What is a boxplot?

A boxplot is a convenient way of graphically representing the median, spread, skew and outliers of a dataset. Multiple boxplots can be drawn together to easily inspect differences between multiple datasets.

Figure 14 shows boxplots of nuclear volume for MRC5 cells. The boxplots for ASYNC, HS and IFN were fairly similar with medians at around 3 x 10^5 voxels, and lower and upper quartiles that spanned a range of 2 x 10^5 to 4 x 10^5 voxels. The range between the smallest and largest non-outlier observations was greatest for ASYNC (spanning just below 1 x 10^5 to about 6 x 10^5 voxels). There were a few outliers associated with all three, which extended beyond 7 x 10^5 voxels. Since the ASYNC, HS and IFN data sets were not treated in a way that should influence nuclear volume, they were expected to fall within the same limits as they were collected using the same sampling method.

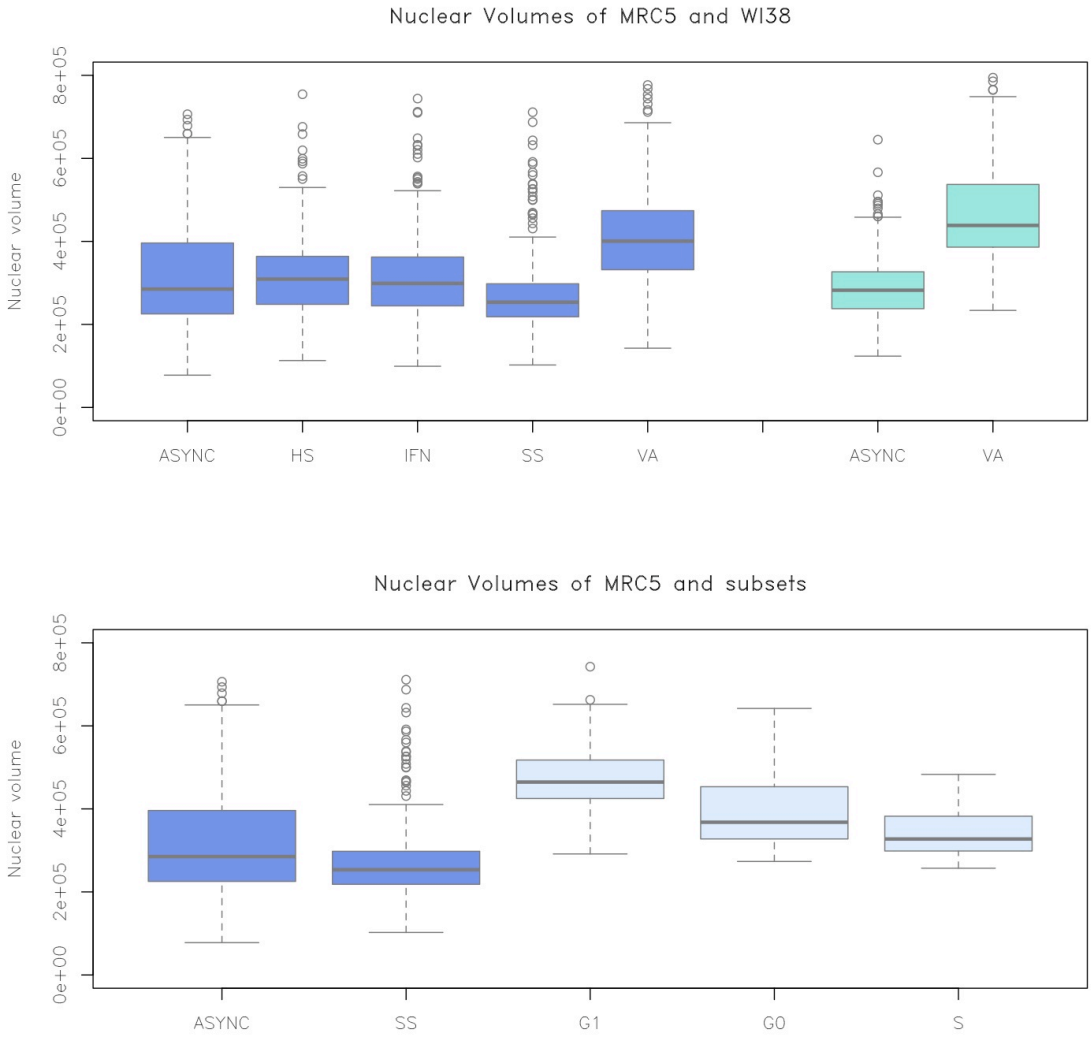


Figure 14 Nuclear volumes for all cell lines and conditions

For SS nuclei the median nuclear volume was slightly lower than that of ASYNC at around 2.5 x 10^5 voxels, and the lower and upper quartiles spanned 2 x 10^5 to 3 x 10^5 voxels, with the smallest and largest non-outlier observations lying at just over 1 x 10^5 and 4 x 10^5 voxels respectively. Therefore the SS cell nuclei had the smallest volume of those investigated. Since this dataset was serum starved it makes sense that the range of the data is smaller as the cells should be synchronised in G_0 phase. However there were a large number of outliers, which extended up to 7 x 10^5 voxels.

In VA nuclei the median nuclear volume was much greater than that of ASYNC, at about 4 x 10^5 voxels. The lower and upper quartiles spanned 3 x 10^5 to just over 4.5 x 10^5 voxels, with the smallest and largest non-outlier observations lying at 0.5 x 10^5 and 7

x 10^5 voxels respectively. Therefore the nuclear volume of MRC5 VA cells was much greater than that of ASYNC. From the image segmentation we saw that MRC5 VA nuclei appear to be more spherical than ASYNC (verified in Section 5.2), which tended to show a more flattened "fibroblast-like" morphology. Therefore the increase in nucleus volume in the VA (whilst not being associated with a larger area) can likely be attributed to their viral transformation.

3.2.3.2 Nuclear volumes of MRC5 subsets: G1, G0 and S

Figure 14 (lower) shows boxplots of nuclear volume for MRC5 G1, G0 and S subsets. The G0 dataset (which was only based only upon 50 cells, compared to up to 500 for the MRC5 ASYNC, HS, IFN, SS and VA) had a median nuclear volume of just under 4 x 10^5 voxels, lower and upper quartiles that fell between 3 x 10^5 and 4.5 x 10^5 voxels, and smallest and largest non-outlier observations for nuclear volumes that fell at just under 3 x 10^5 and 6.5 x 10^5 voxels respectively. There were no outliers. This dataset surprisingly shared no commonality with the SS dataset, as it possessed a greater nuclear volume than both ASYNC and SS nuclei. As both G0 and SS should represent cells which are in a quiescent state, it is likely that there may actually be differences between the nuclei of "resting state" cells which are driven into G0 by serum-starvation, and those which have entered naturally (and were selected using their lack of positive staining for the Ki67 proliferation marker). However as the sample sizes are not comparable this should be repeated in a larger sample of G0 nuclei to confirm this finding.

The G1 nuclear volumes (also based upon a sample of 50 cells) surprisingly showed the greatest nuclear volumes; the median was at 4.5 x 10^5 voxels, with the lower and upper quartiles falling between 4 x 10^5 and just over 5 x 10^5 voxels, and the smallest and largest non-outlier observations for nuclear volumes fell at 3 x 10^5 and 6.5 x 10^5 voxels respectively. Although this falls within the range of ASYNC (which would naturally include cells in G1 phase), it was unexpected because most cells in ASYNC are typically found in G1 (and therefore we might expect similar median values for the two datasets). However, the classification method used to select G1 cells using Ki67 positive staining was not as robust as for G0 cells, making it possible that the G1 sample included non-G1 cells, which may have affected the results.

The S phase nuclear volumes (based upon 50 cell nuclei) showed a smaller median volume than G1 cells, at 3.5 x 10^5 voxels, and lower and upper quartiles that spanned just over 3 x 10^5 to 4 x 10^5 voxels. The smallest and largest non-outlier observations for nuclear volumes lay at 2.5 x 10^5 and just over 4.5 x 10^5 voxels respectively. This was less than for the G1 cells, whereas we expected the converse (as during S phase DNA replication has begun and therefore nuclear volume should begin to increase).

3.2.3.3 Nuclear volumes of WI38 ASYNC and VA nuclei

Figure 14 (upper) shows boxplots of nuclear volume for WI38 ASYNC and VA cells. The WI38 ASYNC dataset had a median nuclear volume of 3 x 10^5 voxels, which was almost identical to that of MRC5 ASYNC. The lower and upper quartiles spanned 2.5 x 10^5 to just over 3 x 10^5 voxels. The smallest and largest non-outlier observations for nuclear volumes were 1.5 x 10^5 and 4.5 x 10^5 voxels respectively. There were a few outliers reaching to 6.5 x 10^5. Therefore the MRC5 and WI38 ASYNC nuclear volumes were similar.

3.2.4 Summary

Nuclear volumes

The nucleus was delineated using an antibody against lamin B, or with DAPI, a dye that intercalates with DNA. This allowed the nuclear volume to be segmented, and defined the boundary of the study region for each cell. Boxplots were plotted to show the spread of nuclear volumes for each of the five MRC5 data sets (ASYNC, HS, IFN, SS, VA), the three MRC5 subsets (G0, G1, S), and the two WI38 data sets (ASYNC, VA). When arranged by median nuclear volume MRC5 SS was smallest, and WI38 VA was largest. The order of median nuclear volumes from smallest to largest is summarised in Figure (Figure 15) for all the cell lines and treatments. As expected all of the asynchronous MRC5 data sets (ASYNC, HS and IFN) shared similar nuclear volumes. SV40 transformed MRC5 (MRC5 VA) was greater in volume than MRC5 ASYNC, and the same was true of WI38 VA and ASYNC. The nuclear volume of the MRC5 subset G0 was much greater than that of MRC5 SS, which is interesting since they should both represent equivalent (quiescent) cell populations.



Figure 15 MRC5 and WI38 median nuclear volumes arranged by size

3.3 PML NB morphometrics

3.3.1 Introduction

Upon successful delineation and segmentation of the nucleus, immunofluorescence staining that fell within the nuclear volume could then be segmented. PML protein, as stained with one of three comparable anti-PML antibodies, was always imaged in the green channel, allowing us to quantitatively characterise various aspects of PML NB morphology and spatial organisation. The human foetal lung fibroblast cell line MRC5 was chosen for the study of PML NBs to determine their morphology and organisation in asynchronous normal cells. Qualitative inspection of an SV40 transformed MRC5 cell line MRC5VA revealed a differing PML morphology, and so PML NBs were also imaged in these as a "paired cell line". We also wanted to understand if the results obtained from the MRC5 and MRC5VA cell lines were cell line specific, or applicable to other normal and transformed fibroblast cell lines. Therefore we also studied PML NBs in the WI38 normal foetal human lung fibroblast cell line, for which there was also an SV40 transformed line, WI38VA. Lastly, the effects of three treatments (heat shock, IFNβ, and serum starvation) thought to alter PML NB morphometrics and spatial organisation were quantified in the MRC5 cell line.

3.3.2 Data sets collected: MRC5 ASYNC, HS, IFN, SS, VA, and WI38

The PML NB data in this chapter was pooled across various datasets where PML NBs were stained in conjunction with a functional compartment of the nucleus. They therefore consist of information gathered from the segmentation of between 300-500 nuclei for each of the normal, treated and virally transformed fibroblast cell lines (Table

11). The MRC5 subsets G1, G0 and S consisted of smaller samples of about 50 nuclei each that were stained for PML, and Ki67 or BrdU. A postive Ki67 G1 pattern was used to determine the G_1 subset, a negative stain for Ki67 revealed G_0 cells, and BrdU incorporation was positive for S phase cells.

Table 11 Data sets collected - cell lines, conditions and sample size

Cell line and perturbation		Nuclear Compartment	Number of nuclei per sample
		PML	
MRC5	ASYNC	✓	435
	HS	✓	438
	IFN	✓	378
	SS	✓	409
	VA	✓	409
	G1	✓	45
	G0	✓	46
	S	✓	48
WI38	ASYNC	✓	421
	VA	✓	376

3.3.3 Immunofluorescence detections: PML nuclear body/protein localisations

Initially PML NB morphology and spatial organisation was qualitatively characterised from the immunofluorescence pattern of the antibodies used as markers for PML protein. Immunofluorescence was carried out as described in Chapter 2.

Across the cell lines and conditions studied there was clearly variation in PML NB number and size, with no obvious reason as to why. However, in different tissues the level of PML expression is known to be variable meaning that PML may be required at greater levels in some cell lines more than others. However it was only possible to describe any differences in PML NB spatial organisation non-quantitatively from simple observation of the IF patterns.

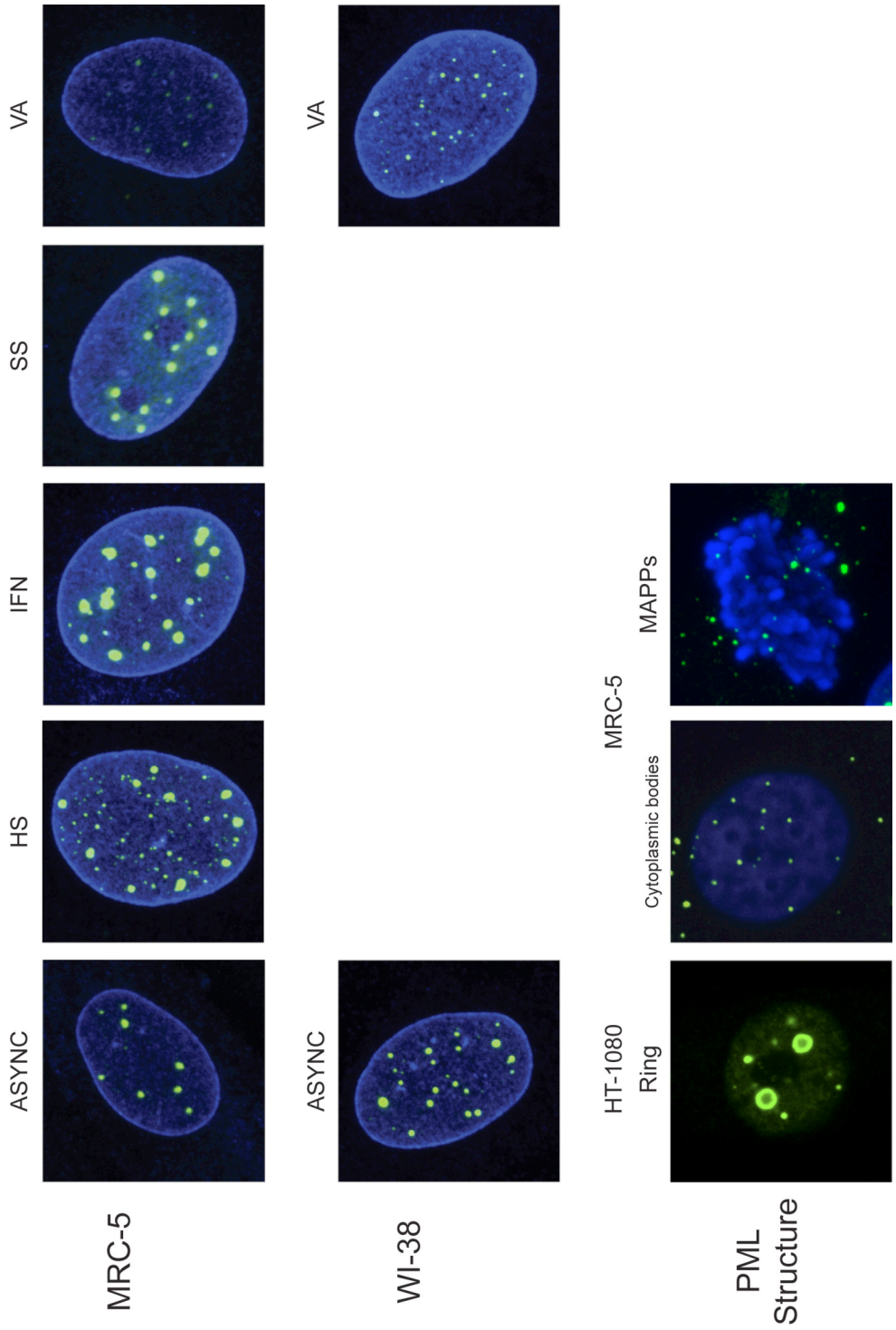


Figure 16 PML in various human fibroblast cells

Projection images of PML NBs (green) in MRC5 normal and treated fibroblasts, WI38 normal fibroblasts, and the SV40-transformed cell lines MRC5 VA and WI38 VA. Examples of other PML structures (green): rings (shown here in the HT-1080 human fibrosarcoma cell line. Rings with similar morphology are also found in the MRC5 and WI38 cell lines.), cytoplasmic bodies, and mitotic accumulations of PML protein (MAPPs). The nuclear envelope (lamin B, Rows 1 and 2) or DNA content of the nucleus (DAPI staining, Row 3, panels 2 (cytoplasmic bodies) and 3 (MAPPs) is indicated in blue.

3.3.3.1 PML NBs in MRC5 ASYNC, HS, IFN, SS and VA nuclei

Figure 16 shows PML NBs in MRC5 nuclei. In MRC5 ASYNC cells the PML NBs were fairly large, and appeared to show a random distribution within the nucleus, except that they were not often found within the nucleolus. There were typically about 10 bodies per nucleus. There was also a slight diffuse PML stain in the nucleoplasm of many of the cells studied.

In MRC5 HS, the typical pattern of 10 or so large PML NBs seen in MRC5 ASYNC remained. However in addition there were also multiple smaller PML foci (numbering up to one hundred), which formed in response to the heat shock treatment. It has been shown that these smaller PML NB foci are not SUMOylated (Eskiw et al., 2003) unlike the larger bodies. All of the PML NBs (large and small) appeared to be randomly organised thoughout the nucleus, with the smaller bodies found to locate within the nucleolus quite often. The diffuse nucleoplasmic PML component was slightly higher than in MRC5 ASYNC cells.

In MRC5 IFN (asynchronous MRC5 cells treated with IFNβ overnight), the size and/or number of PML NBs was increased in comparison to those in MRC5 ASYNC. The increase in body number seemed less likely to occur than the increase in size (as IFN PML NBs were nearly always larger than those in ASYNC).

In MRC5 SS, the size and number of PML NBs appeared to be slightly greater than in MRC5 ASYNC. There were also more occurrences of PML NBs being found within the nucleolus, and they more often appeared to cluster towards the centre of the nucleus than in ASYNC nuclei. The level of diffuse PML within the nucleoplasm was noticeably higher in some SS cells.

The MRC5 VA cell line appeared to contain a similar number of PML NBs to MRC5 ASYNC, but which were much smaller in size. There was barely a detectable PML diffuse nucleoplasmic signal. They appeared to be randomly located within the nucleus.

3.3.3.2 PML NBs in WI38 ASYNC and VA nuclei

Figure 16 shows PML NBs in WI38 nuclei. WI38 ASYNC PML NBs were of similar size and number to those found in MRC5 ASYNC nuclei. They also appeared to be randomly arranged within the nucleolus except for their exclusion from nucleoli.

The WI38 VA cell line contained PML NBs that were often very small (in comparison to those in WI38 ASYNC) than those in MRC5 VA, but were typically greater in number. They appeared to be randomly located.

3.3.3.3 Other PML morphologies

Occasionally other PML structures were detected in the nucleus of all of the cell lines and conditions studied within this thesis. Examples can be found in Figure 16.

3.3.3.3.1 PML rings

These structures were typically larger than the PML NBs of the cell they were found in, and to which B23 (nucleophosmin) was also found to colocalise (not shown). They were most often found within the transformed VA cell lines, but were sometimes seen in ASYNC cell lines too, particularly at later passages. They are likely to be enlarged PML NBs produced as a result of stress (Condemine et al., 2007). Nuclei that contained such structures were not included in the analysis.

3.3.3.3.2 Cytoplasmic bodies

There were also PML structures in the cytoplasm, found most commonly in the virally transformed cell lines. Cytoplasmic PML is implicated in TGFβ signalling (Lin et al., 2004). Due to the nature of the SCT algorithm, any extra-nuclear staining in the image stack was discarded from the analysis.

3.3.3.3.3 MAPPs

Mitotic Accumulations of PML Protein (MAPPs) are the PML structures formed upon

breakdown of the nuclear envelope and entry of the cell into mitosis. They are irregular in shape, and typically larger than normal PML NBs. They are not SUMOylated, but are modified by phosphorylation (Dellaire et al., 2006c). However, mitotic cells were not included in the analysis.

3.3.3.3.4 Nucleoplasmic PML protein

PML protein was also present as a diffuse nucleoplasmic component. This is thought to consist of unsumolyated PML protein, which is therefore unable to dimerise (the first step in PML NB formation) (Zhong et al., 2000a). The level of background was variable, and may relate to cell cycle phase. This diffuse staining cannot be removed via use of blocking reagents during the IF protocol. However it typically remained unsegmented by the SCT algorithm.

3.3.4 PML NB Number

After image stack segmentation accurate quantification of PML NB morphometric data could be achieved for all the cell lines and conditions imaged. The data obtained included the number, size and distance relationships of PML NBs. Boxplots of PML NB number in MRC5 and WI38 are plotted in Figure 17. The mean number of PML NBs per cell was plotted as a barplot in Figure 18, but varied little from the median values and is therefore not discussed here.

3.3.4.1 PML NB number in MRC5 ASYNC, HS, IFN, SS and VA nuclei

Figure 17 shows that in ASYNC the median number of NBs was 10, with the lower and upper quartiles covering 8-12 bodies, and the smallest and largest non-outlier observations for body number being 2 and 18 bodies respectively. However, in HS the median number increased dramatically to about 60 bodies, and the lower and upper quartiles spanned 40-78 bodies. The smallest and largest non-outlier observations for number of bodies were 10 and 128 respectively. There were also a few outliers including one where the number of bodies in the nucleus exceeded 150. The number of PML NBs in HS cell nuclei was therefore much higher than in ASYNC, and there was also much greater variation in the number of bodies in nuclei of HS cells than in ASYNC nuclei.

However, most of these bodies were small though in comparison to typical MRC5 ASYNC PML NBs.

The median number of PML NBs in IFN (IFN-β treated) nuclei was greater than in ASYNC, at 18. The lower and upper quartiles spanned 14 to 24 bodies, and the smallest and largest non-outlier observations for PML NB numbers were 8 and 38 bodies respectively. Therefore IFN-β treatment increases the number of PML NBs, which was as expected. In SS nuclei the median number of NBs was 16, with the lower and upper quartiles spanning 13 to 22 bodies, and the smallest and largest non-outlier observations for bodies spanning between 6 and 32 bodies. This showed that the SS and IFN datasets were quite similar in terms of PML NB number, with almost identical medians. Since stresses on the cell (such as heat shock and interferon treatment) obviously lead to an increase in the number of PML NBs within the nucleus, it is possible that serum-starvation also acts as a stress on cells.

The VA median number of PML NBs was about 8, with the lower and upper quartiles spanning 6 to 10 bodies, and the smallest and largest non-outlier observations for body numbers being 2 and 16 respectively. This is extremely similar to that of ASYNC, but with a slightly lower median body number. Therefore transformation does not appear to have affected body number in MRC5 VA. However later we will see that there are differences in PML NB size between ASYNC and VA.

3.3.4.2 PML NB number in Subsets of MRC5 (G1, G0 and S)

Figure 17 shows PML NB number for the MRC5 subsets. In G0 the median number of bodies was 10, with the lower and upper quartiles ranging from 8 to 13 bodies. The smallest and largest non-outlier observations for body number were 6 and 21 respectively. This is fairly similar to the ASYNC result and is not the same as seen in the SS data set, and despite the two samples' sizes being very different (500 versus 50 nuclei) one still might expect them to share a trend. However, this reinforces the idea that whilst driving a cell into G_0, serum-starvation also acts as a stress and thus alters PML NB morphometrics in a stress-related manner, resulting in increased body number. Therefore PML NBs in quiescent cells (G0) may not be comparable with those found in the MRC5 SS dataset.

In the G1 data set the median number of PML NBs was 9, and the lower and upper quartiles ranged from 8 to 12, with the smallest and largest non-outlier observations for body number being 3 and 18 respectively. This was again similar to that seen in the ASYNC data set, and close to that in G0 (but not in SS). Since cells enter G_0 directly from G_1 it seems logical that these two datasets share a similarity in terms of PML NB number. However, when they are driven into G_0 by serum-starvation this also triggers a stress response that increases the number of PML NBs. However, as we cannot be sure that all cells in the G1 dataset are indeed in G_1 phase (see Section 2.4.2.2), we can only assume homogeneity of the G1 subset.

In the S dataset the median was at about 7 bodies per nucleus, with the lower and upper quartiles ranging from 6 to 10 PML NBs. The smallest and largest non-outlier observations for PML NB body values were 2 and 14 respectively. Interestingly this does not concur with published data that suggests that the number of PML NBs increases during S phase (Dellaire et al., 2006b). It could be that the nuclei collected were mostly in early S phase (although unlikely to be true as ascertained by visual study of the pattern of BrdU incorporation). However since the sample size was fairly small (50 nuclei only), it would be beneficial to image a larger dataset of S phase nuclei to clarify this further.

3.3.4.3 PML NB number in WI38 ASYNC and VA nuclei

In WI38 ASYNC (Figure 17) the median PML NB number per cell was 10, the lower and upper quartiles spanned 6 to 11 bodies, and the smallest and largest non-outlier observations for PML NB number per cell were 2 and 18 respectively. This is a very similar distribution to that of the MRC5 ASYNC dataset. Therefore the number of PML NBs is similar in these two human fetal lung fibroblast cell lines. However in WI38 VA the median body number was 26, with the lower and upper quartiles spanned 18 to 34 PML NBs, and smallest and largest non-outlier observations for PML NB number were 4 and 53 bodies per cell respectively. This is a much greater number of bodies than in both WI38 ASYNC and MRC5 VA cell nuclei. Therefore viral transformation in WI38 VA has resulted in a large increase in the number of PML NBs. Interestingly transformation with SV40 has not resulted in the same changes in different cell lines. It is likely that this is connected to WI38 VA morphology being "epithelial-like," whereas

MRC5 ASYNC, MRC5 VA and WI38 ASYNC are all either fibroblasts or show "fibroblast-like" morphology.

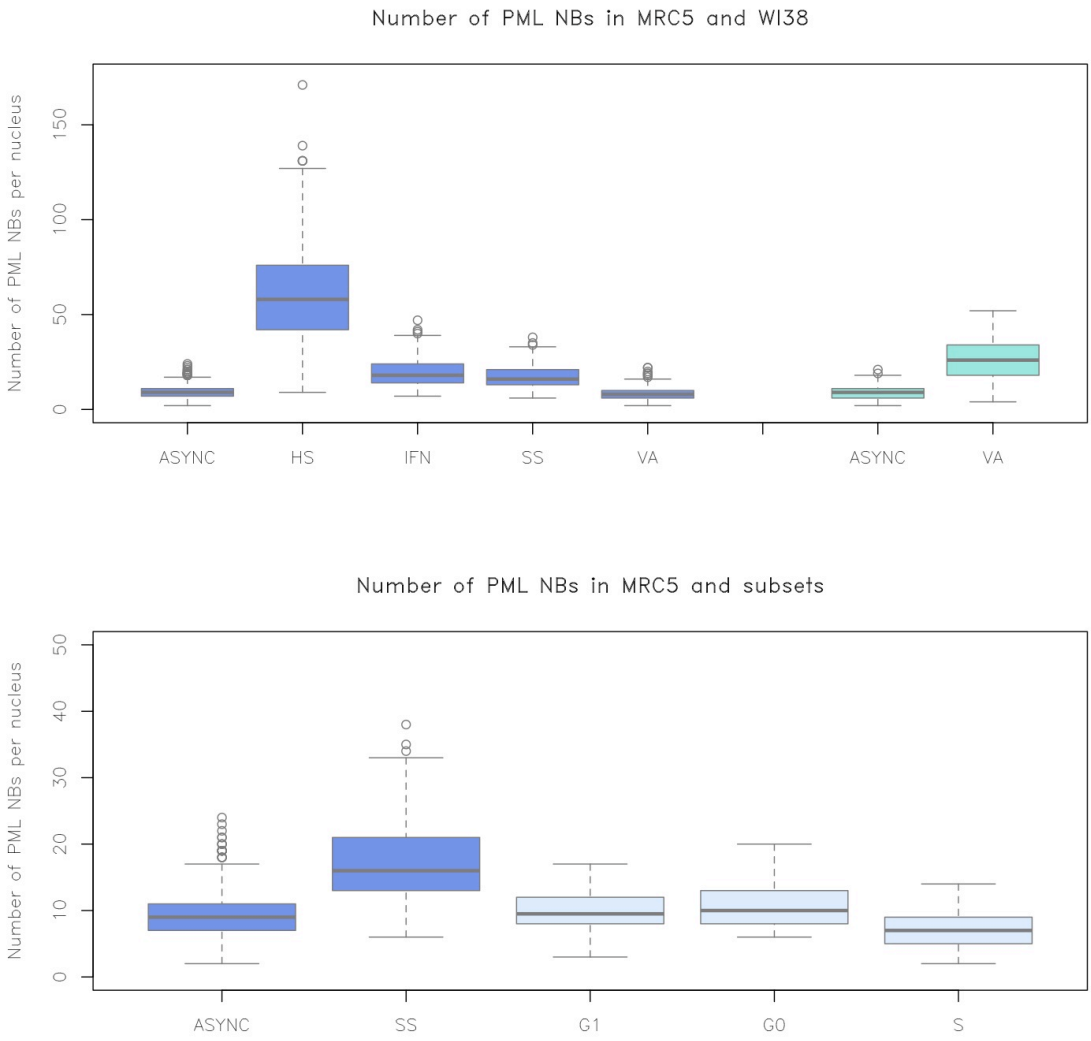


Figure 17 PML NB number in MRC5 and WI38 fibroblasts

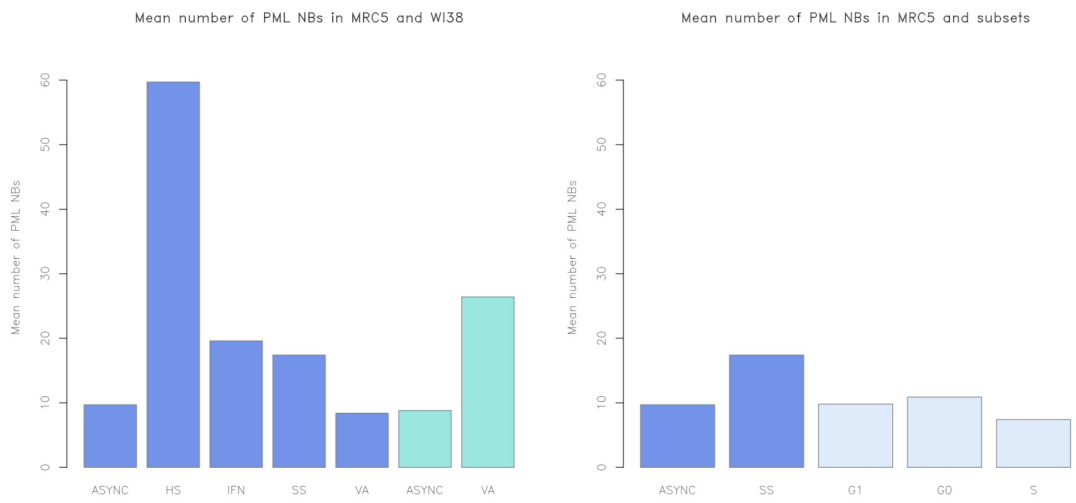


Figure 18 Mean PML NB number in MRC5 and WI38 fibroblasts

3.3.5 PML NB size (volume)

Since the SCT algorithm was able to segment all PML NBs within a nucleus, this information could be used to plot the voxel count (as an estimate of volume) of each PML NB in the data set. As we make the assumption that PML NBs are spherical, their volume is therefore closely related to their diameter. It must be noted that PML NB volume is a different (but related) measure to the (total) mean PML volume per cell (which is presented in Section 3.3.7).

3.3.5.1 PML NB size in MRC5 ASYNC, HS, IFN, SS, VA nuclei

If the MRC5 data sets in Figure 19 (upper) are ordered by median PML NB size (in voxels) HS had the smallest bodies, followed by VA, SS, ASYNC, and lastly IFN with the largest median body size. All of the datasets had many outliers, showing that there is quite a lot of variation in PML NB size even in ASYNC populations. In HS especially there was an exceptional number of outliers, with voxel counts ranging from about 170 to over 2500 voxels. In contrast the largest outlier body was at around 1500 voxels in the ASYNC data set. This indicates that in the HS dataset there is potentially more than one population of PML NBs, (that of the tiny bodies, and also of the large bodies). However, it seems that the larger bodies which one might expect to be the standard PML NBs seen in ASYNC are still very large in comparison to those in ASYNC.

From visual inspection it did not appear that the HS larger bodies were particularly large in size in comparison to those in MRC5 ASYNC. Therefore is possible that the presence of these outliers is instead due to a thresholding artefact. In order to segment the small PML NBs produced as a result of the heat shock treatment, the threshold had to be set manually. This meant that although the threshold was appropriate to segment the small bodies, the bigger ones could be overestimated, a problem that may also have appeared again in the total PML volume estimate (see Section 3.3.7). However it is possible that heat shock results in an increase in size of the larger PML NBs as well as the creation of smaller bodies. However, where this "extra" PML protein originates from is unclear.

Treatment with IFNβ resulted in an increase in the median body size, and which were the largest bodies of the five datasets. This dataset also included the biggest range of body sizes (excluding outliers), athough their distribution was skewed towards a smaller body size. This agrees with the literature in that IFNβ treatment upregulates PML protein and increases body size (Lavau et al., 1995). In VA nuclei the PML NBs were second smallest, and this concurs with what was seen in the IF, and that transformation results in a reduction in PML NB size when compared to ASYNC. In SS cell nuclei PML NBs are (very) slightly smaller than in ASYNC, which makes sense under the conditions of no new PML synthesis due to the cell being in a state of quiescence, but continual degradation of existing PML protein.

3.3.5.2 PML NB size in MRC5 subsets (G1, G0, S)

In the MRC5 G0 subset the median PML NB size was much greater than that of both the MRC5 ASYNC and SS datasets, and even the IFNβ treated one (Figure 19, lower). This does not match the SS result at all, where the median body size was decreased in comparison to ASYNC. Therefore it seems very likely that SS is stimulating a stress response that makes the PML NBs in serum starved cells differs from those in the G0 subset.

In the MRC5 G1 subset the median PML NB size was greater than MRC5 ASYNC, and there was a wider range of PML NB sizes too. However, as mentioned before due to the difficulties in classification this subset may have included some non-G1 nuclei, which

could affect the results, and therefore we should not place too much emphasis on the results from this dataset.

The S subset nuclei contained PML NB sizes with a median almost as small as the HS cells, which should indicate that these are cells from late S phase (as PML NBs would have split at this point (Dellaire et al., 2006b). However, they were fewer in number than in MRC5 ASYNC, and if they had indeed split we might have expected a higher number of bodies than average. It could instead be that the segmentation of PML NB in the MRC5 S subset was not completed correctly as smaller bodies are sometimes missed from the analysis (especially if they are not very intensely stained, as was the case of heat shocked PML NBs). Otherwise it is difficult to account for this result.

3.3.5.3 PML NB size in WI38 ASYNC and VA nuclei

The median PML NB size for WI38 ASYNC was similar to that of MRC5 ASYNC, and the same can be said for WI38 VA and MRC5 VA, which also shared a similar median body size (Figure 19, upper). Therefore transformation with SV40 has likely resulted in a decreased median PML NB size, but that whilst in MRC5 VA it has no effect on PML NB number, in WI38 VA cell nuclei it dramatically increases the number of NBs per cell nucleus.

3.3.5.4 PML NB size (volume) and number in MRC5

In MRC5 HS we saw that whilst the number of PML NBs was greatly increased per nucleus, the median size of those bodies actually decreased in comparison to ASYNC. However there was still the persistence of a population of large PML NBs, which are likely to be those that existed prior to heat shock treatment, and were possibly the source of the small PML NB fragments produced. In MRC5 IFN we saw that both PML NB number and size increased when in comparison to that of MRC5 ASYNC. In MRC5 SS although PML NB size remained similar to that in ASYNC, the number of PML NBs per nucleus increased. However, this may have been a result of stress induced by serum starvation treatment as the converse was seen in the G0 data set (where there are larger PML NBs than in ASYNC, but they are similar in number per nucleus). In MRC5 VA

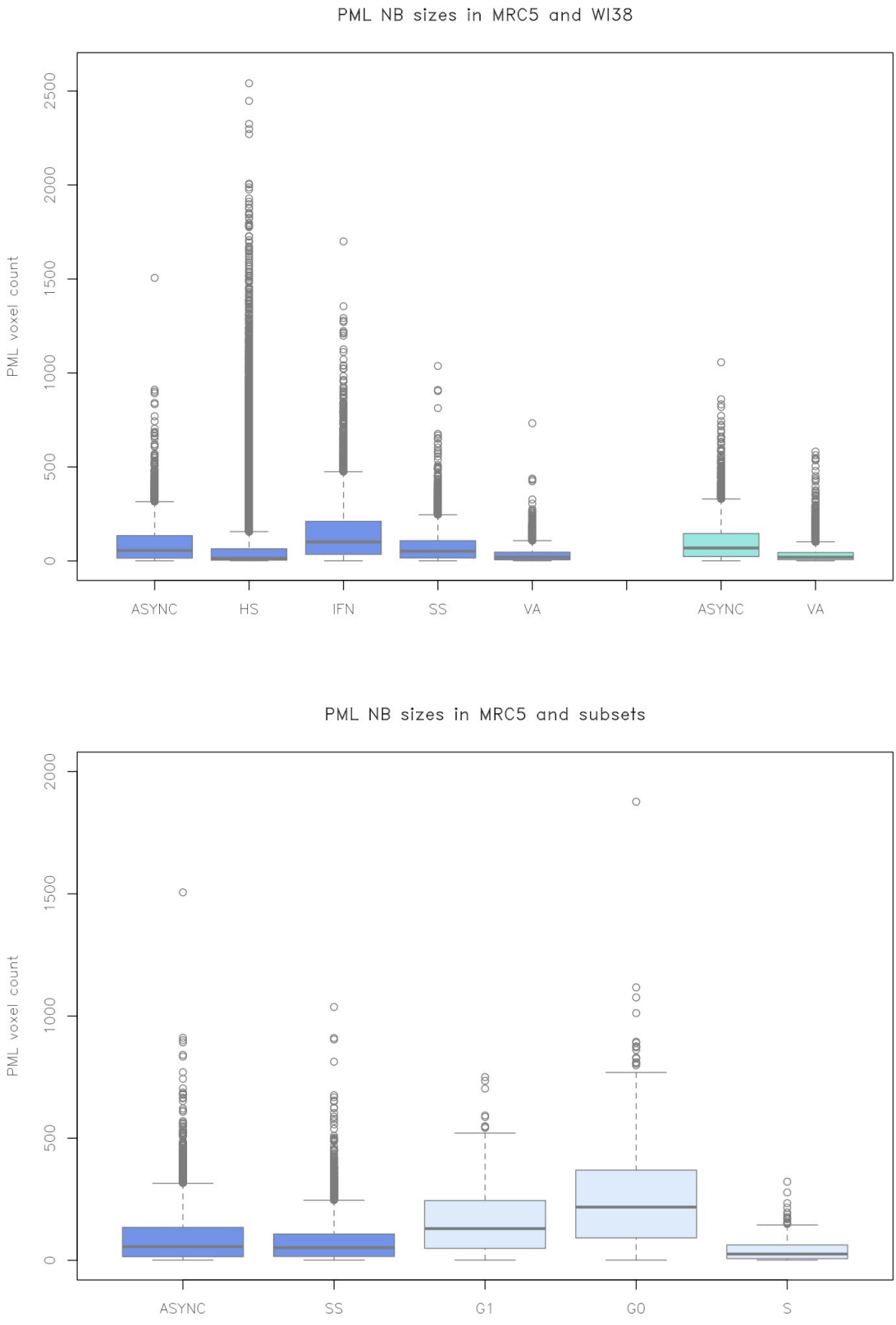


Figure 19 PML NB size in MRC5 and WI38 fibroblasts

whilst PML NB number was similar to that of ASYNC, the size of the bodies was much smaller, and this is therefore likely a consequence of the transformation of the cell.

3.3.5.5 Summary of mean PML NB size and number for MRC5 and WI38 datasets

Figure 20 and Figure 21 summarise the mean PML NB size versus mean PML NB number for MRC5 and WI38 cell lines and treatments, and MRC5 subsets respectively. These plots help to reveal the trends shown in Figure 17, Figure 18, and Figure 19 with regard to how SV40 transformation, heat shock, IFN treatment, serum starvation and cell cycle phase appear to exert influence over both PML NB size and number in the nucleus.

In Figure 20 the mean PML NB size was plotted versus the mean PML NB number for the MRC5 ASYNC, VA, HS, IFN, and SS datasets, and the WI38 ASYNC and VA datasets. MRC5 ASYNC had a mean PML NB size of about 95 voxels, and WI38 ASYNC had a slightly larger mean PML NB size of about 105 voxels. However, both MRC5 ASYNC and WI38 ASYNC had a very similar mean PML NB number (at around 10 bodies). MRC5 VA and WI38 VA had the smallest mean PML NB size at just over 35 voxels, indicating that SV40 transformation results in a decrease in the average PML NB size in comparison to their ASYNC cell line counterparts. Interestingly, WI38 VA had a greater mean PML NB number than MRC5 VA (25 versus 10 bodies), indicating there is variation in the consequences of transformation even if the originator cell lines shared a similar mean PML NB number. Overall MRC5 ASYNC and MRC5 VA shared a similar mean PML NB count (10 bodies), but the mean PML NB size in MRC5 VA was much smaller (35 voxels in MRC5 ASYNC compared to 95 voxels in MRC5 ASYNC).

With SV40 transformation the mean PML NB size dramatically decreased to 35 voxels in WI38 VA, in comparison to the mean PML NB size in WI38 ASYNC (105 voxels), but the mean PML NB number was greater in WI38 VA (25 bodies, in comparison to 10 bodies in WI38 ASYNC).

The mean PML NB size in MRC5 HS was similar to that of MRC5 ASYNC (about 95

voxels), however the mean PML NB number was much greater at about 60 bodies (in comparison to 10 bodies in MRC5 ASYNC). This gives a good indication that extra PML NBs do form in the nucleus when it is subjected to the stress of heat shock treatment.

In the IFN treated MRC5 mean PML NB size was much greater than that of MRC5 ASYNC (150 voxels versus 95 voxels), and there was also a greater mean PML NB number (around 18 bodies in MRC5 IFN, compared to 10 bodies in MRC5 ASYNC). It is likely that the PML protein production induced by IFN treatment leads to this increase in mean PML NB size, and also that the stress response induced by such treatment results in the increase in the mean number of PML NBs.

The effects of serum starvation upon PML NBs could also be seen as the MRC5 SS dataset had a smaller mean PML NB size than MRC5 ASYNC (around 80 voxels compared to 95 voxels in MRC5 ASYNC). However MRC5 SS had slightly more bodies on average (with a mean PML NB count of about 18, in comparison to 10 in MRC5 ASYNC). It is likely that the decrease in mean PML NB size is due to a halt in the manufacture of PML protein in the serum starved cell in combination with a degradation of existing PML protein. The increase in PML NB number is likely to be a response to the stress of serum starvation. This concurs with the increase in PML NB number seen in both heat shocked and IFN-treated MRC5 cells discussed above.

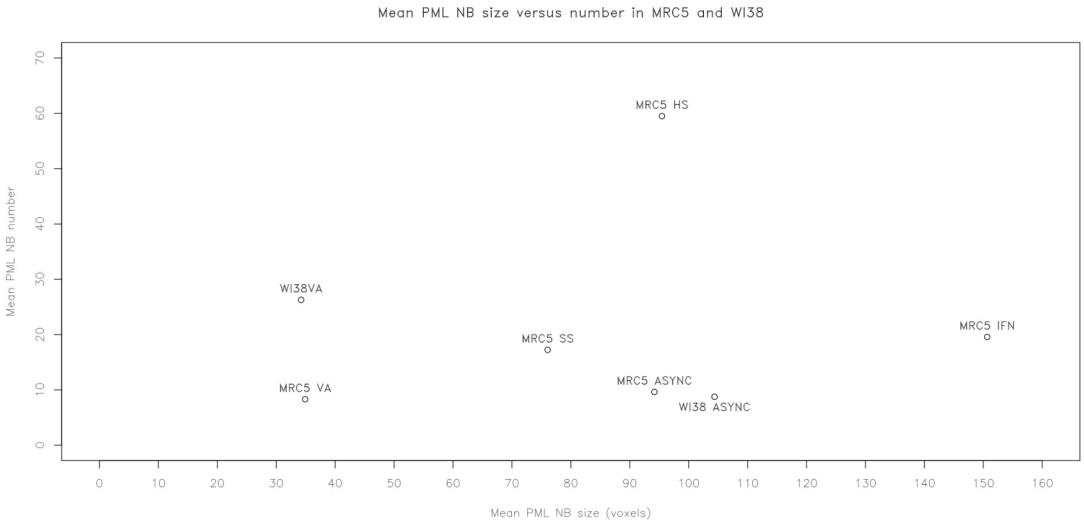


Figure 20 Mean PML NB size and number in MRC5 and WI38

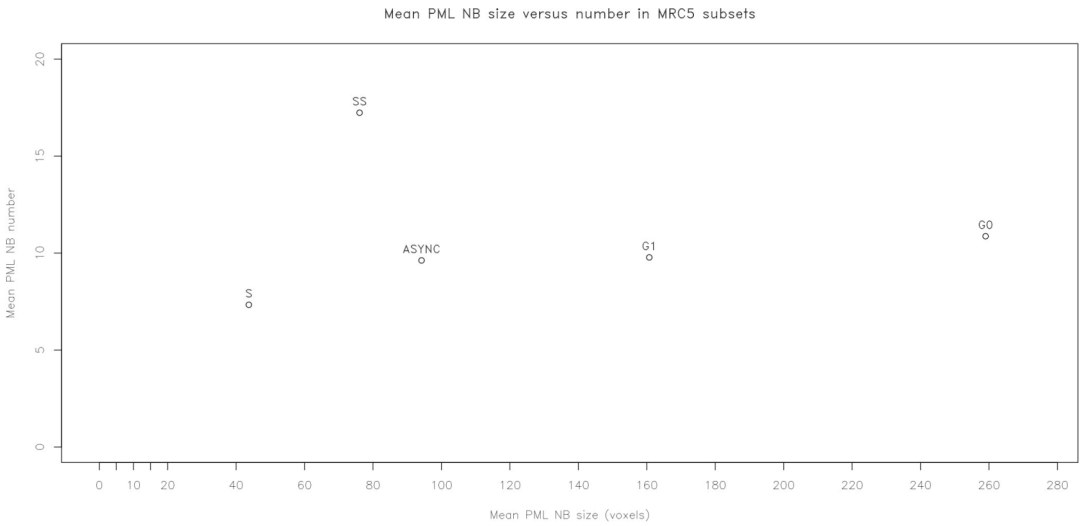


Figure 21 Mean PML NB size and number in MRC5 subsets

In Figure 21 the mean PML NB size was plotted versus the mean PML NB number for the MRC5 ASYNC, SS, and subset (G0, G1, and S) datasets. The mean PML NB size for MRC5 ASYNC was 95 voxels, and the mean PML NB number was about 10 bodies. Interestingly the MRC5 G1 dataset showed a similar mean PML NB number (about 10 bodies), but a much greater mean PML NB size (around 160 voxels). Since PML NBs have been shown to reform in early G1 and increase in volume as the cell cycle progresses it is difficult to account for the high mean PML NB size in the G1 dataset in comparison to the mean PML NB size for ASYNC. For the MRC5 S subset the mean PML NB number was about 7, which was slightly smaller than that for ASYNC, and the mean PML NB NB size was smaller too, at 45 voxels. Since PML NBs are thought to double in number in S phase by a fission mechanism it is not obvious why there should be a lower mean PML NB number for the S dataset, in comparison to ASYNC. However, as the mean PML NB size was also smaller, it may be that in S phase PML NBs have split but that some of these bodies are too small to be correctly thresholded, therefore lowering the mean PML NB size but not resulting in an increase in mean PML NB number.

The MRC5 SS dataset mean PML NB size was slightly smaller than the ASYNC, at about 80 voxels, and the mean PML NB number was about 17 bodies. As mentioned above this is likely due to PML protein degradation without *de novo* synthesis (PML NB size decrease) and a stress response to serum starvation (PML NB number increase). However in the MRC5 G0 subset the mean PML NB size was about 260 voxels, and the

mean PML NB number was very similar to that of MRC5 ASYNC. This is in disagreement with the MRC5 SS results. The discrepancy in mean PML NB number may be accounted for as G0 nuclei have not undergone the stress of serum starvation to become quiescent (as they were selected as Ki67 negative using indirect IF staining), and therefore would not show an increase in PML NB number. However, it is less clear as to why the mean PML NB size would increase in such quiescent nuclei.

3.3.6 ECDF of PML NB volume in MRC5 and WI38 nuclei

To further investigate the processes that underlie PML NB size, we plotted the Empirical Cumulative Distribution Function (ECDF) of PML NB volume in MRC5 and WI38 cell nuclei (Figure 22 and Figure 23).

It was apparent that in the MRC5 SS (blue line) and VA (purple line) datasets the PML NB size (in voxels) was smaller than that of ASYNC (red line). In SS this was probably due to a degradation of PML protein over the eight-day serum starvation period. The IFN (green line) PML NB size was greater than that of ASYNC. For MRC5 ASYNC, IFN, SS and VA nuclei the ECDF curves exactly followed an exponential distribution. This was unexpected, and meant that the mean PML NB size is likely to be controlled by only one parameter. However for the HS (yellow line) nuclei, PML NB size does not follow such a distribution. Interestingly, the mean size of PML NBs in both ASYNC and HS datasets, were the same. This should therefore result in the curves falling at the same location on the ECDF plot (as the mean size determines where the curve lies). Therefore despite the HS dataset containing many small and large PML NBs (which results in the ECDF curve not following the exponential for HS), a mechanism exists to ensure that mean PML NB size is maintained between datasets where PML protein has not been upregulated or degraded, (such as in the ASYNC and HS datasets).

For WI38 we also plotted the ECDF of PML NB size, and found that the VA dataset mean PML NB size was smaller than that in ASYNC. Both curves also followed the exponential distribution meaning that this is probably intrinsic to PML NB mean size. Overall, what parameter controls mean size in unclear as we were unable to produce a non-exponential curve for PML NB size where mean body size was also perturbed.

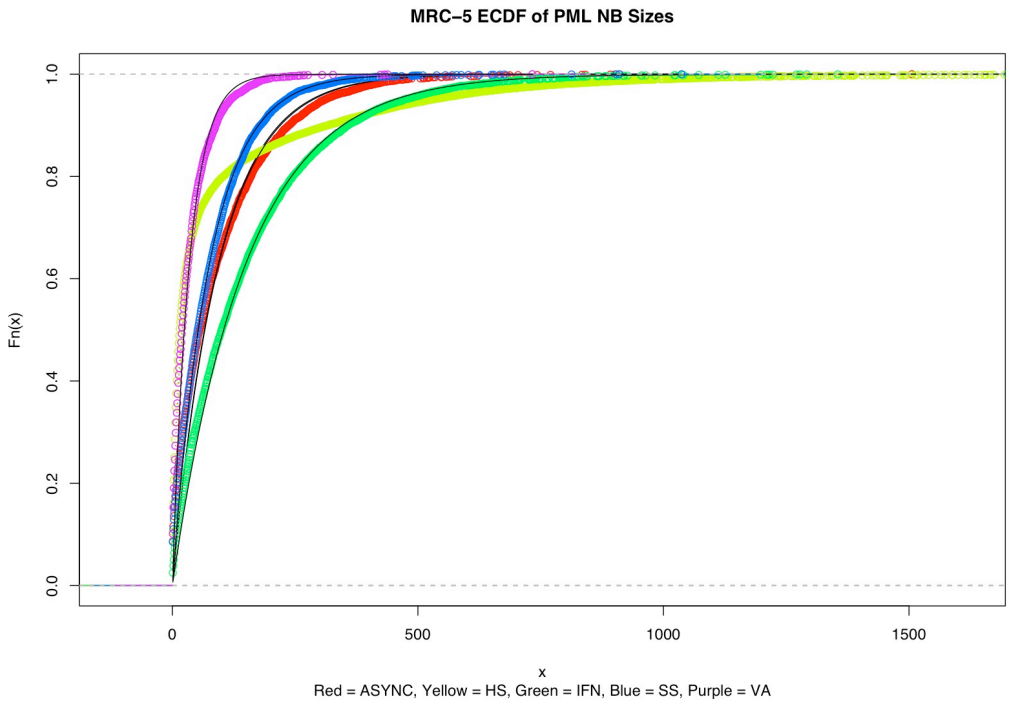


Figure 22 MRC5 EDCF of PML NB sizes

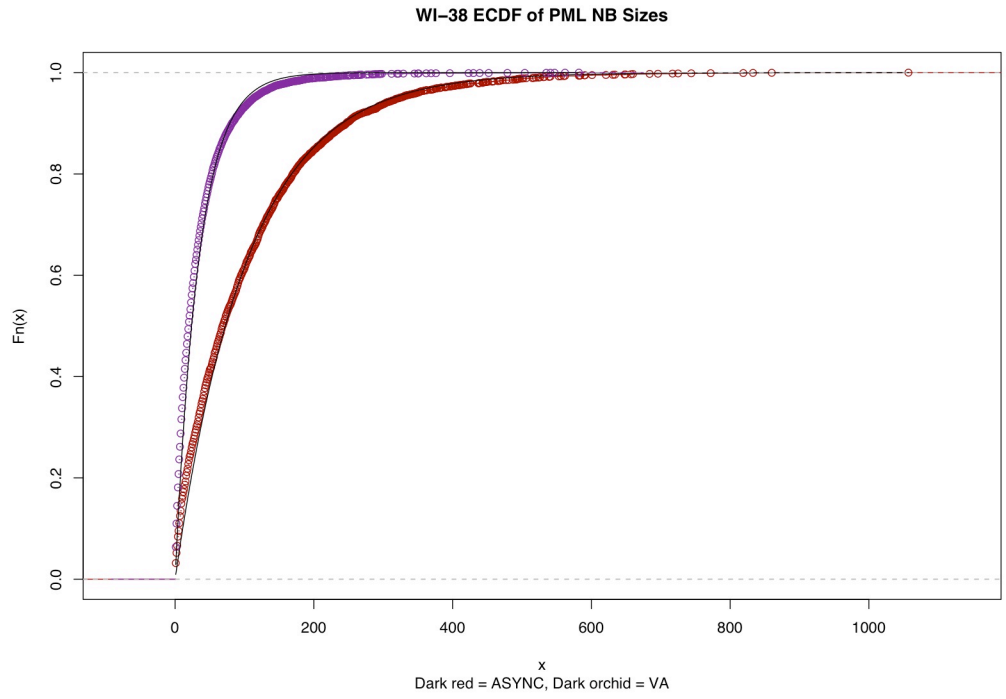


Figure 23 WI38 ECDF of PML NB sizes

3.3.7 PML volume

The average voxels of PML per nucleus (estimated using the green voxel segmentation from the collated results for each cell line and treatment) were presented as a barplot in Figure 24. This can be used as an approximation of the volume of PML protein in the nucleus.

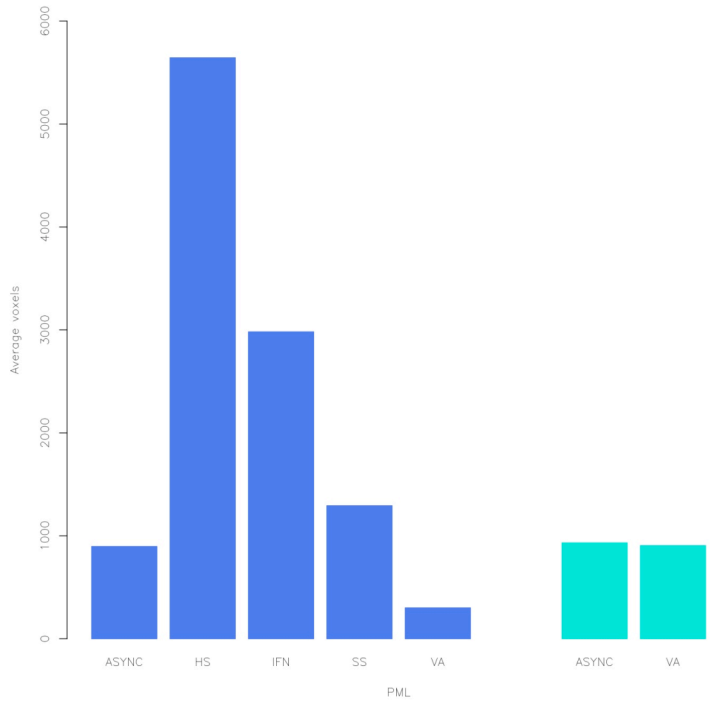


Figure 24 Average PML voxels per nucleus for MRC5 and WI38 fibroblasts

Effects of heat shock, IFNβ, and serum starvation treatment, and SV40-transformation on PML protein levels. Barplot of average PML voxels per cell in MRC5 ASYNC, HS, IFN, SS, VA and WI38 ASYNC and VA nuclei. Based upon segmentation using the SCT algorithm of nuclei immunofluorescently stained for PML protein.

3.3.7.1 PML volume in MRC5 ASYNC, HS, IFN, SS and VA nuclei

The smallest average voxel count was found in MRC5 VA nuclei at around 400 voxels per nucleus. In ASYNC nuclei the average voxel count was just under 1000, in SS this was about 1400, and in IFN it was about 3000 voxels per nucleus. Therefore in VA cells the average amount of PML per nucleus decreased by about 50%, in SS cells it increased by about 50%, and in IFN cells it trebled in comparison to MRC5 ASYNC.

For SS this is logical as although the median body size is similar (Figure 19, upper) (although apparently slightly less according to the EDCF curves in Figure 22), there were more of them, and therefore more PML protein was required to make them. However, if this PML was newly synthesised or brought out of solution by SUMOylation is unclear. In IFN there are a greater number of bigger bodies which accounts for the increase in average PML voxel count per nucleus. In VA nuclei there were smaller PML NBs, but of about the same number which accounts for the fewer PML voxels per nucleus on average.

In HS cells there was a very large average PML voxel count per nucleus, at 5500 voxels, over five times the volume for ASYNC. We saw that the median PML NB size was smaller in HS than in ASYNC, but that the number of PML NBs per cell was greatly increased by the treatment. This could possibly account for the large increase in PML volume. However the volume of PML should have been similar to that in ASYNC since the heat shock treatment was only administered for 30 mins, during which there was not enough time to synthesize excessive amounts of PML protein.

However, there are a number of explanations that may account for this situation. Firstly, PML protein could itself be being taken out of solution to form bodies by the treatment – there is a known diffuse PML protein component in the nucleoplasm which if it became insoluble could account for this *de novo* extra PML. However it would need to be SUMOylated to come out of solution, and Eskiw et al (Eskiw et al., 2003) suggests that PML heat shock bodies are not.

Secondly, the act of the bodies being disrupted by fission of smaller fragments from pre-existing PML NBs may expose a greater area of PML protein to the antibody used to detect it. Since we know that the heat shock fragment bodies are of lower intensity than normal PML NBs it could be that the existing amount of PML has been "stretched" to create more signal, since true PML NBs are probably saturated in terms of the amount of PML protein required for a signal to be present. Therefore since intensity is only really taken into account at low levels to aid in the separation of bodies from background signal, (if the signal exceeds a particular threshold and is greater than one voxel in size it is classed as a body), it is possible to "make" more PML than is found in the ASYNC from the ASYNC PML component.

Lastly, it could be that (as mentioned previously) because the thresholding of the HS dataset was done manually due to the smaller bodies being missed by the thresholding algorithm, whilst correctly segmenting the smaller fragment PML NBs, the larger PML NBs were over-segmented and their size was estimated as larger than they truly were. This is a caveat of the way the SCT algorithm works at the moment and should be addressed in the future, since it affects compartments with populations of different sized bodies (as can happen with PML NBs), and may lead to inaccuracies in the way that volumes are estimated.

In Appendix 7.2 a western blot was completed to compare PML protein levels in all the cell lines and conditions tested. It was apparent that IFNβ treatment resulted in an upregulation of PML protein whereas heat shock did not (in comparison to MRC5 ASYNC). Therefore it is likely to be an imaging or segmentation issue, rather than extra PML being produced during heat shock treatment.

3.3.8 Summary

IF – PML protein and PML NBs

PML NBs were stained using indirect immunofluorescence and one of three equivalent anti-PML antibodies (raised in rabbit, mouse or goat). From the IF they were seen to vary in size and/or number in a cell line and treatment dependent manner. They appeared to show a random spatial organisation except in MRC5 SS where PML NBs appeared to be clustered centrally in the nucleus. Other PML structures (rings, cytoplasmic bodies and MAPPs) could also be detected using the same anti-PML antibodies.

PML NB number

Using the SCT algorithm, PML NBs that fell within the nuclear volume were segmented. Cells containing non-PML NB structures within the nucleus were discarded prior to analysis. A boxplot of PML NB number per nucleus for each nucleus of a dataset was plotted for all the cell lines and treatments. Upon arrangement by median PML NB number per nucleus, the MRC5 subset S contained the least number of PML NBs per nucleus. MRC5 HS contained the most. SV40 transformation resulted in a decrease in the median PML NB number per nucleus (compared to MRC5 ASYNC), whereas serum

starvation, IFNβ treatment and heat shock increased the median PML NB number per nucleus. However, SV40 transformation in WI38 actually resulted in an increase in the median number of PML NBs per nucleus. The median PML NB number per nucleus in MRC5 SS was slightly higher than in the MRC5 subset G0.

PML NB size (volume)

PML NB size (volume) data for every PML NB within a cell line or treated cell line were plotted as a boxplot. When arranged by median PML NB size (Figure 25), the MRC5 HS and WI38VA data sets contained the smallest PML NBs. The MRC5 subset G0 contained the largest PML NBs. SV40 transformation resulted in the reduction in median PML NB size in both MRC5 and WI38 cells. Heat shock, SV40 transformation and serum starvation resulted in a decrease in median PML NB size in MRC5 nuclei (compared to MRC5 ASYNC), whereas IFNβ treatment resulted in an increase. Once again the MRC5 subset G0 differed from MRC5 SS, where G0 nuclei contained larger PML NBs than MRC5 SS data set.



Figure 25 PML NB size arranged by median

ECDF of PML NB volume

The empirical cumulative distribution function for MRC5 ASYNC, HS, IFN, SS and VA nuclei, and for WI38 ASYNC and VA was plotted. For all datasets bar MRC5 HS, the curve followed an exponential distribution. The gradient of the curve was controlled by the mean PML NB size; therefore mean body size in the MRC5 SS and VA datasets was smaller than in the ASYNC. However, mean PML NB size in MRC5 IFN was greater. Mean body size in WI38 VA was smaller than in WI38 ASYNC. Since the curves were exponential, it is likely that a single parameter controls mean PML NB size. Interestingly the MRC5 HS dataset shared a mean PML NB size with MRC5 ASYNC despite the former not following an exponential distribution.

PML volume (voxel count)

Since PML protein was always labelled green when performing indirect IF the voxel count in the green channel after image segmentation could be used as an estimate of total PML protein volume in the nucleus (excluding the diffuse nucleoplasmic component). The average PML voxel count per nucleus was measured, and was 50% lower in MRC5 VA nuclei than in MRC5 ASYNC. It was 50% and 300% higher in serum starved and IFNβ-treated cells respectively. Unexpectedly, PML volume in MRC5 HS was 550% that of PML in MRC5 ASYNC.

3.4 PML NB distance relationships – NND analysis

3.4.1 Introduction

The proximity of PML NBs to other PML NBs, the nuclear boundary and centroid can be described using data gathered from image segmentation. Here we used the total minimum NNDs to characterise PML NB distance relationships for MRC5 and WI38 nuclei. Distances are measured in voxels.

3.4.2 Inter – PML NB-PML NB total minimum NNDs

3.4.2.1 Inter – PML NB total minimum NNDs MRC5 ASYNC, HS, IFN, SS and MRC5VA nuclei

From the total inter – PML NNDs in Figure 26 (upper) (the minimum NND between every PML NB in every nucleus of a dataset to its closest neighbouring PML NB), we could see the following trends. PML NBs that were closest together according to median distance were HS bodies, followed by SS and IFN, then ASYNC. VA PML NBs were furthest apart, and were further apart than ASYNC PML NBs. They also had the biggest inter-quartile range (IQR). HS PML NBs were about three times closer to each other than ASYNC, and this was a function of the increased number of PML NBs in the HS dataset compared to ASYNC.

PML NBs in IFN and SS nuclei had a fairly similar distribution of total minimum NNDs, with an almost identical median at about 30 voxels.

3.4.2.2 Inter – PML NB total minimum NNDs MRC5 G1, G0 and S subsets

Figure 26 (lower) shows that in general the G0, G1 and S subsets had fewer outliers (compared to the other MRC5 datasets), presumably because they came from a more homogeneous cell population (in terms of cell cycle phase).

The median of the G0 dataset indicated that PML NBs were further apart in this subset than in MRC5 SS nuclei. Interestingly the G0 nuclei have fewer PML NBs per nucleus than SS nuclei do, which would account for this distance difference. However, the distribution of PML NBs NNDs in the G0 cells is instead similar to that of the ASYNC population. The distribution of the G1 cells is also very similar, but with a slightly further median distance. The S phase subset shared its median with the G1 cells, but had the largest IQR of the three. It also had the fewest PML NBs per nucleus

3.4.2.3 Inter PML NB total minimum NNDs in WI38 ASYNC and VA nuclei

From the distance measurements collected, we were able to plot the total minimum inter – PML NB NNDs for ASYNC and VA in WI38 cell nuclei (Figure 26, upper).

In all of the data sets the total minimum inter – PML NB NNDs start at a distance of just over 0 voxels. The closest PML NBs were found in WI38VA, at a distance of about 25 voxels, followed by WI38 ASYNC. The distributions for MRC5 ASYNC and WI38 ASYNC were very similar overall, but the median for WI38 VA, compared to MRC5 VA, was much lower, meaning that the bodies were much closer together than in MRC5 VA. This is interesting because in the MRC5 cell line transformation resulted in PML NBs being further apart than in the ASYNC data set, but in the WI38 the transformation it resulted in the bodies moving closer together. This is probably due to the number of bodies decreasing in MRC5 VA compared to ASYNC, but increasing in WI38 VA compared to the ASYNC. All four data sets contained a large number of outliers.

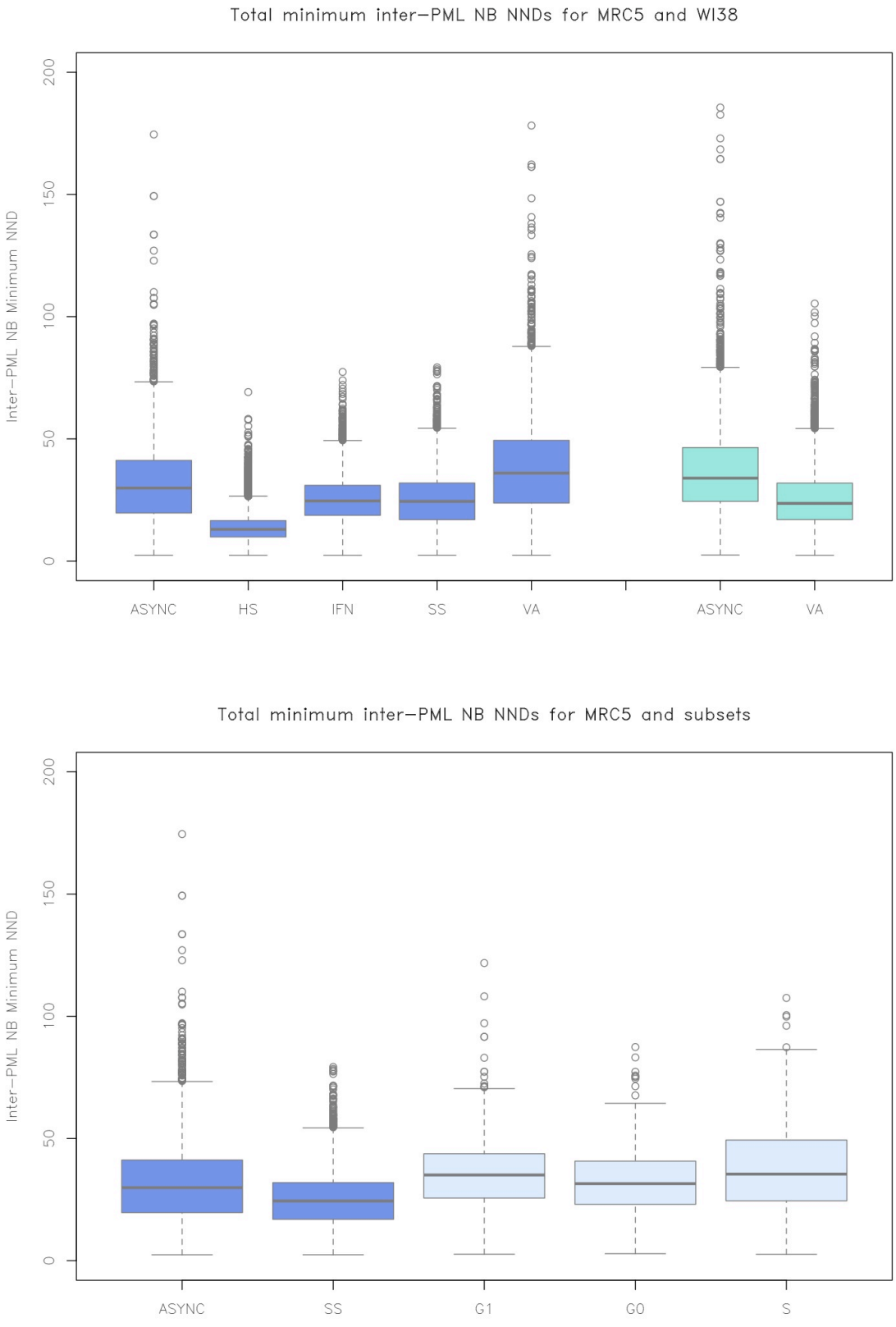


Figure 26 Inter - PML NB NNDs for MRC5 and WI38

Overall, it can be seen that an increase in the number of PML NBs translates as a visible decrease in the NNDs between PML NBs.

3.4.3 PML NB-nuclear boundary total minimum NNDs

3.4.3.1 PML NB – boundary total minimum NNDs in MRC5 ASYNC, HS, IFN, SS and VA nuclei

In Figure 27 (upper) an obvious feature is that in all the datasets there is an "edge-effect" whereby PML NBs tended to locate away from the nuclear boundary, (as most of the data (the box) is found at a distance of between 10 and 20 voxels). The ASYNC median PML NB-boundary NND was 13, the lower and upper quartiles spanned 10-20, and the smallest and largest non-outlier NNDs at 1 and 34 respectively. There were a large number of outliers showing that some PML NBs were located very deeply within the nucleus. The median PML NB-boundary NNDs for HS, IFN and SS datasets (and indeed the distribution of their total NNDs) were very similar, with almost identical medians at about 11.5, which was less than for ASYNC. Therefore these stresses result in PML NBs being located slightly closer to the nuclear boundary than in ASYNC cells (and supports the observation that PML NBs in quiescent cells appear to cluster towards the nuclear centre). Again, this could be a function of the increased number of PML NBs per nucleus found in each of these datasets. For VA, the median and distribution is again similar to that of ASYNC, showing that in transformed cells the edge-effect is not disrupted.

3.4.3.2 PML NB – boundary total minimum NNDs in MRC5 subsets

Figure 27 (lower) shows that in G0 cells the median PML NB-boundary NND was greater than in ASYNC or SS, meaning that the PML NBs are more central in terms of their location within the nucleus. The same is true for the G1 and S datasets.

3.4.3.3 PML NB – boundary total minimum NNDs in WI38 ASYNC and VA

In the WI38 ASYNC dataset the median PML NB-boundary minimum NND was less than in MRC5 ASYNC (Figure 27, upper), meaning that PML NBs were slightly closer to

the boundary, despite the two datasets having a very similar median (and mean) number of PML NBs per nucleus. The largest non-outlier value for PML NB-boundary NND was also smaller than for MRC5 ASYNC, as was the IQR. For WI38 VA the median PML NB – boundary minimum NND was slightly greater than in WI38 ASYNC, which is very interesting because the number of PML NBs was greater than in WI38 ASYNC, meaning that they should probably be closer to the nuclear boundary if they were arranged according to random. WI38 VA had a bigger IQR than MRC5 VA, and so there was more variation in the minimum PML NB-boundary NNDs in these nuclei.

3.4.4 PML NB- nuclear centroid total minimum NNDs

Overall the medians and distributions of PML NB-nuclear centre NNDs were similar for all datasets (Figure 28, upper), with all medians being between 60 and 80 voxels. Only in WI38 VA was the median noticeably higher than in the other datasets. Therefore it is questionable how useful this measurement is in terms of quantifying nuclear organisation. For example we can see that there is almost no difference between the medians and distributions of the MRC5 SS and G0 datasets (Figure 28, lower), which in every test until now had been exhibiting differing behaviour, suggesting that the two populations were not the same. Since this is equivalent to the total radial distance measurements for every PML NB from the centre of the nucleus it does not apparently tell us anything very interesting about PML NB organisation under the different cell lines and conditions. Furthermore, there was no evidence to support the IF observation that PML NBs in MRC5 SS nuclei cluster towards the centre of the nucleus.

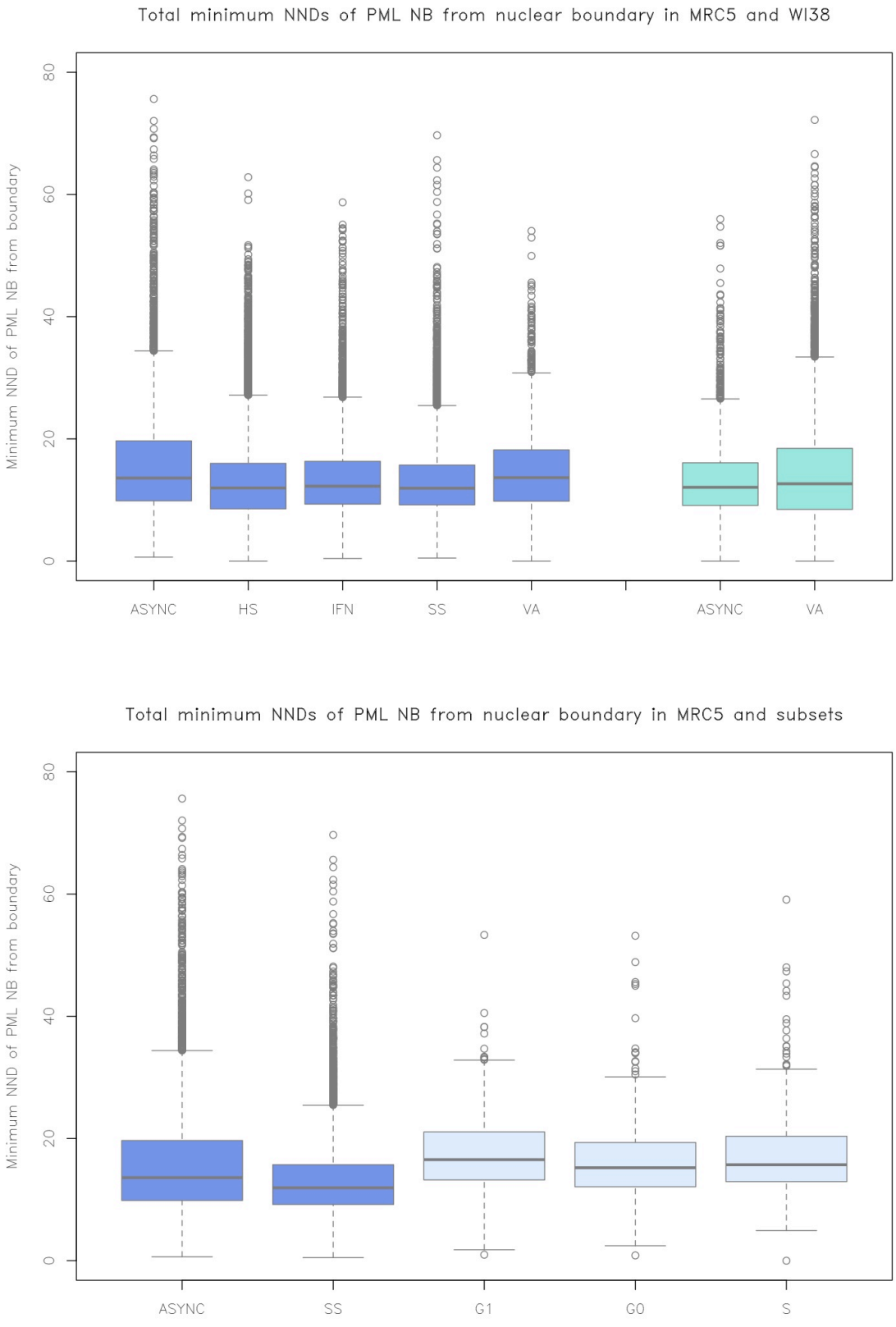


Figure 27 PML NB - nuclear boundary NNDs in MRC5 and WI38

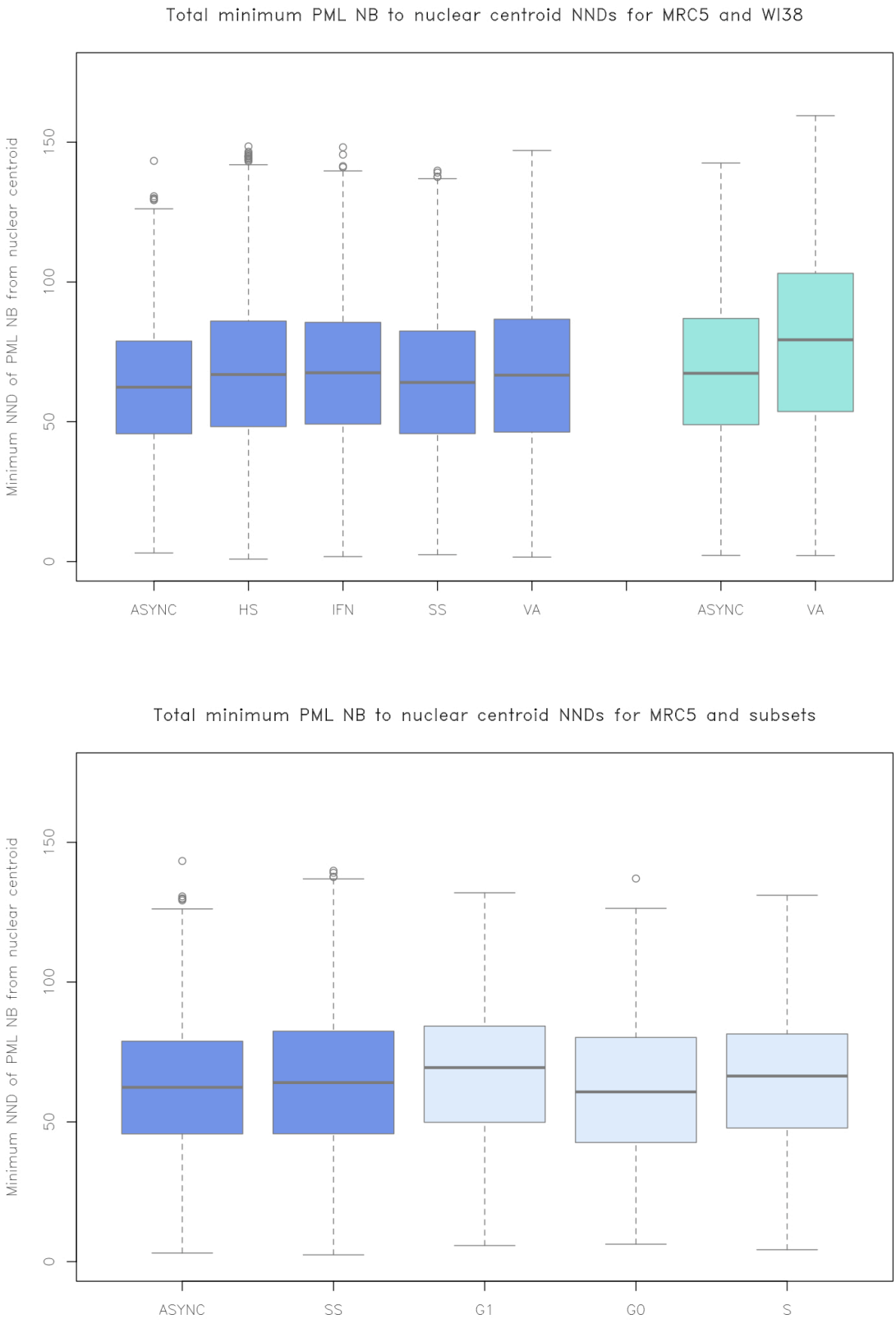


Figure 28 PML NB - nuclear centroid NNDs for MRC5 and WI38

3.4.5 Summary

PML NB – PML NB NNDs

After segmentation the centroid of each PML NB in every nucleus was defined as an *xyz* coordinate. This allowed the distance between the centroid of each PML NB in a nucleus to be measured. Then the minimum NND for each PML NB (that is the distance between every PML NB and its closest neighbouring PML NB) in every nucleus of a dataset was plotted on a boxplot. Once arranged according to the median value of minimum NND (Figure 29), the dataset with the closest together PML NBs was MRC5 HS, and those that were furthest apart were in MRC5 VA. Conversely, SV40 transformation in WI38 resulted in a shorter median value for the minimum NND between PML NBs. Heat shock, IFNβ treatment and serum starvation result in PML NBs being positioned closer together than in MRC5 ASYNC, according to the median value. The median minimum inter – PML NB NND distance in MRC5 subset G0 was greater than that in the MRC5 SS dataset.



Figure 29 Inter PML NB NND hierarchy

Summary of the median PML NB distance hierarchy from the nearest PML NB in MRC5 ASYNC, HS, IFN, SS, VA and WI38 ASYNC and VA nuclei. Data sets are ordered by median minimum nearest neighbour distance (NND) between PML NB and the nearest PML NB. Closest to furthest from the bodies (left to right).

PML NB – nuclear boundary NNDs

The distance between the centroid of each PML NB in a nucleus and the nuclear boundary, as delineated by lamin B or DAPI staining, was measured. The minimum NND between each PML NB in every nucleus of a dataset and the nuclear boundary of their corresponding nucleus was then plotted on a boxplot. Once arranged according to median minimum NND (Figure 30), the datasets with the shortest PML NB to nuclear boundary distances were jointly MRC5 HS, MRC5 SS and WI38 ASYNC. The dataset with PML NBs the furthest from the nuclear boundary was the MRC5 subset G1. SV40 transformation resulted in PML NBs being located a greater distance from the nuclear boundary compared to those in their ASYNC counterparts in both MRC5 and WI38

ASYNC nuclei. Heat shock, serum starvation and IFNβ treatment of MRC5 cells resulted in shorter median minimum PML NB – boundary NND. The median minimum NND PML NB – boundary distance in MRC5 subset G0 was greater than that in the MRC5 SS dataset. In all cell lines and treatments PML NBs exhibited an "edge-efect" whereby they were repulsed by the nuclear boundary. This was a consistent observation regarding PML NB organisation in the nucleus of different cell lines.



Figure 30 PML NB - nuclear boundary NND hierarchy

Summary of the median PML NB distance hierarchy from the nearest nuclear boundary in MRC5 ASYNC, HS, IFN, SS, VA and WI38 ASYNC and VA nuclei. Data sets are ordered by median minimum nearest neighbour distance (NND) between PML NB and the nearest nuclear boundary. Closest to furthest from the bodies (left to right).

PML NB – nuclear centroid NNDs

The distance between the centroid of each PML NB in a nucleus and the nuclear centroid was measured. The minimum NND between each PML NB in every nucleus of a dataset and their corresponding nuclear centroid was plotted on a boxplot. After arranging according to the median value (Figure 31), the dataset with the closest PML NBs to the nuclear centroid was the MRC5 subset G_0, and that with the furthest PML NB to nuclear centroid minimum NND was WI38 VA. Serum starvation, heat shock, SV40 transformation and IFNβ treatment resulted in PML NBs locating further away from the nuclear centroid than in MRC5 ASYNC nuclei. The same was true for SV40 transformed WI38, in which the minimum PML NB to nuclear centroid NND was greater than in WI38 ASYNC cells. However, overall there was very little difference between the PML NB – nuclear centroid total minimum NNDs in all the cell lines and conditions studied.



Figure 31 PML NB - nuclear centroid NND hierarchy

Summary of the median PML NB distance hierarchy from the nuclear centroid in MRC5 ASYNC, HS, IFN, SS, VA and WI38 ASYNC and VA nuclei. Data sets are ordered by median minimum nearest neighbour distance (NND) between PML NB and the nuclear centroid. Closest to furthest from the bodies (left to right).

3.5 PML NB spatial organisation – CSR analysis

3.5.1 Introduction

We also wished to investigate PML NBs in relation to each other, the nuclear boundary, and the geometric centre of the nucleus in terms of their spatial (rather than distance-based) organization. This incorporated SPP theory using complete spatial randomness as a null hypothesis for PML NB spatial organization in the nucleus.

3.5.2 Inter – PML NB spatial organisation

We were interested in the inter – PML NB spatial organisation in of each of the cell lines and treatments that we studied. After IF staining and segmentation of PML NBs, the interbody distances could be calculated, and then the minimum observed PML NB inter-distance for each cell was compared to that obtained from simulation of the PML NBs for that cell under the null hypothesis of complete spatial randomness (CSR). CSR was rejected if PML NBs were either closer or further from the object the distances were measured between than expected under CSR.

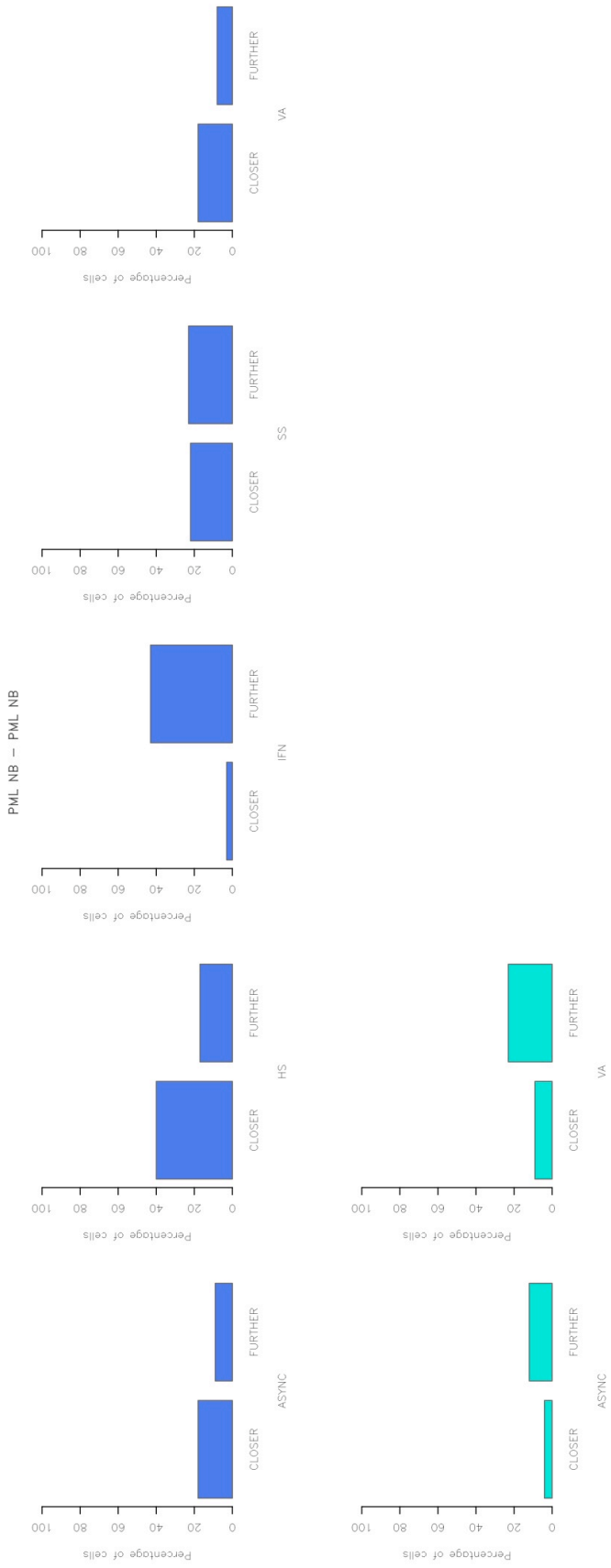


Figure 32 Inter PML NB spatial organisation under CSR

Percentage of nuclei rejecting CSR according to observed minimum inter-PML NB NND. Observed minimum inter-PML NB NNDs for each nucleus in a dataset were compared with simulations for the same PML NBs under CSR. PML NBs were either closer to or further from the nearest PML NB than expected under CSR. Row 1 MRC5: ASYNC, HS, IFN, SS and VA. Row 2 WI38: ASYNC and VA.

3.5.2.1 Inter – PML NB CSR analysis for MRC5 ASYNC, HS, IFN, SS and VA nuclei

Figure 32 shows thatin the asynchronous MRC5 cell population 18% (n = 435) of the cells tested contained PML NBs that were significantly closer to each other than we would expect under CSR. In HS nuclei this figure was higher, with 40% (n = 438) of cells containing PML NBs that were closer to each other than expected. In IFN, SS, and VA nuclei the percentages of cells containing PML NBs that were closer to each other than expected were as follows: 3% (n = 378), 22% (n = 409), and 18% (n = 409) respectively.

Therefore a similar proportion of the cells in the ASYNC, SS and VA cells contained PML NBs that were closer to each other than expected under CSR (between 18 and 22% of cells). However, in the HS dataset almost double the amount of cells contained PML NBs that were closer to each other than expected. In IFN nuclei the proportion was much lower than in all of the other cell populations, dropping to 3%. This means that the vast majority of cells contained PML NBs that were CSR with respect to each other.

In the ASYNC MRC5 cell population 9% (n = 435) of the cells tested contained PML NBs that were significantly further from each other than we would expect under CSR. In HS this figure was higher, with 17% (n = 438) of cells containing PML NBs that were further from each other than expected. In IFN, SS, and VA nuclei the percentages of cells containing PML NBs that were further from each other than expected were as follows: 43% (n = 378), 23% (n = 409), and 8% (n = 409) respectively.

Again, a similar proportion of ASYNC and VA cells in the populations tested (9% and 8% respectively) contained PML NBs that were further from each other than we would have expected. This is slightly higher for HS and SS cells, and with IFN treatment over 40% of cells contained PML NBs that were further apart than expected under CSR. Therefore stresses on the cell seem to induce a re-organisation of PML NBs away from the asynchronous arrangement.

3.5.2.2 Inter – PML NB CSR analysis for WI38 ASYNC and VA nuclei

In WI38 ASYNC nuclei 4% (n = 421) were classified as containing PML NBs that were closer to another PML NB than expected under the condition of CSR, and this was slightly higher at 9% (n = 376) for WI38VA cells (Figure 32). This is dissimilar to that seen in MRC5 nuclei where 18% of both ASYNC and VA nuclei contained PML NBs that were closer to another PML NB than expected.

In WI38 ASYNC nuclei 12% (n = 421) were classified as containing PML NBs that were further from another PML NB than expected under the condition of CSR, and this was almost doubled at 23% (n = 376) for VA cells. This was dissimilar to that seen in MRC5 nuclei; where 9% and 8% of ASYNC and VA nuclei, respectively, contained PML NBs that were further from another PML NB than expected.

3.5.3 PML NB-nuclear boundary spatial organisation

This measurement concerns the distance of the nearest PML NB in each nucleus to the nuclear boundary, which has been delineated using either immunofluorescent staining of lamin B, or DAPI (which intercalates with DNA). If the observed distances for the PML NBs are compared to that of PML NBs simulated under the null hypothesis of CSR, it can be determined if they are closer, further (or both), or CSR with respect to the nuclear boundary.

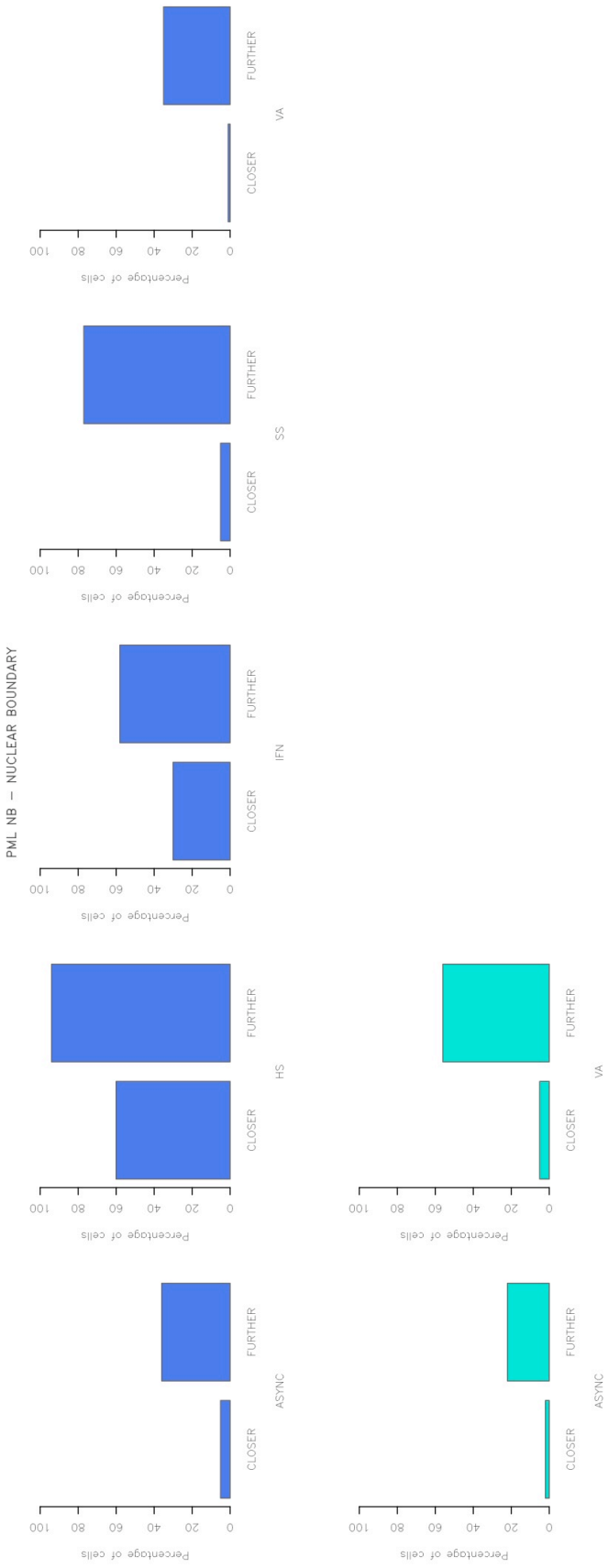


Figure 33 PML NB - nuclear boundary spatial organisation under CSR

Percentage of nuclei rejecting CSR according to observed minimum PML NB - nuclear boundary NND. Observed minimum PML NB - nuclear boundary NNDs for each nucleus in a dataset were compared with simulations for the same PML NBs under CSR. PML NBs were either closer to or further from the nuclear boundary than expected under CSR. Row 1 MRC5: ASYNC, HS, IFN, SS and VA. Row 2 WI38: ASYNC and VA.

3.5.3.1 PML NB – boundary CSR analysis for MRC5 ASYNC, HS, IFN, SS and VA nuclei

In MRC5 ASYNC 5% (n = 435) of the cells tested contained PML NBs that were significantly closer to the nuclear boundary than we would expect under CSR (Figure 33). In HS cells this figure was dramatically higher, with 60% (n = 438) of cells containing PML NBs that were closer to the boundary than expected. In IFN, SS, and VA nuclei the percentages of cells containing PML NBs that were closer to the boundary than expected were as follows: 30% (n = 378), 5% (n = 409), and 1% (n = 409) respectively.

Cells which were not being stressed (ASYNC and VA), or are have been serum-starved do not appear to be closer to the nuclear boundary in more than 5% of the population, and therefore can be considered to be CSR with respect to the boundary. However, in IFN and HS cells these stresses appear to change the organisation of PML NBs with respect to the nuclear boundary, as there were much greater proportions of cells in these populations in which PML NBs are closer to the boundary than we would expect under CSR. This is particularly apparent in the HS population.

It is likely that these "closer" to the boundary PML NBs are the smaller bodies induced by heat shock, and those extra bodies produced in response to IFNβ-treatment. In the case of heat shocked cells the small bodies are likely to be more mobile fragments of PML (as opposed to true bodies), and are therefore able to move within smaller channels, into the chromatin, and closer to the edge of the nucleus.

In MRC5 ASYNC cell population 36% (n = 435) of the cells tested contained PML NBs that were significantly further from the nuclear boundary than we would expect under CSR. In HS this figure was far higher, with 94% (n = 438) of cells containing PML NBs that were further from the boundary than expected. In IFN, SS, and VA the percentages of cells containing PML NBs that were further from the boundary than expected were as follows: 58% (n = 378), 77% (n = 409), and 35% (n = 409) respectively.

Once again, unstressed cells (ASYNC and VA) appeared to show a similar trend, and in this case have a similar proportion of cells in which the PML NBs were classified as being further from the nuclear boundary than expected under CSR. This indicates that in all cells there is a condition that requires PML NBs to be organised so as to be placed away from the boundary, which we have termed the "edge-effect" (seen in at least a third of all cells in the MRC5 population). However, upon the application of stress to the cells, the proportion that contain PML NBs that are further away from the boundary than we would expect under CSR increases (thus increasing the prevalence of the "edge-effect"). In HS cells this meant that up to 94% of cells tested contained PML NBs that were further from the boundary than expected, with the next highest proportion being in SS cells (77%). Therefore in these stressed cells PML NBs undergo reorganization, which causes them to be positioned away from the nuclear boundary.

It should be noted that tt is possible for the PML NBs from a particular cell to be classified as both significantly closer *and* further from either other PML NBs or the boundary at the same time. This indicates that there is potentially more than one population of PML NBs within the nucleus. In IFN, and in HS cells particularly, there was a population of cells that contained PML NBs that were significantly closer and further from the nuclear boundary. It is interesting that it is the IFN and HS populations that are affected since these treatments have the most obvious effect upon PML NB morphometrics and organisation. Such changes in PML NBs can therefore be quantified successfully using the methods employed here.

3.5.3.2 PML NB – boundary CSR analysis for WI38 ASYNC and VA nuclei

In WI38 ASYNC fibroblast nuclei 2% (n = 421) could be classified as containing PML NBs that were closer to the nuclear boundary than expected under the condition of CSR, and this was slightly higher at 5% (n = 376) for WI38VA cells (Figure 33). This result was similar to that seen in MRC5 nuclei; 5% and 1% for ASYNC and VA nuclei respectively.

In WI38 ASYNC nuclei 22% (n = 421) were classified as containing PML NBs that were further from the nuclear boundary than expected under the condition of CSR, and this was over two and a half times higher at 56% (n = 376) for WI38VA cells. This is

dissimilar to that seen in MRC5 nuclei, where 36% and 35% of ASYNC and VA nuclei, respectively, contained PML NBs that were further from the nuclear boundary than expected.

3.5.4 PML NB-nuclear centroid spatial organisation

Many association studies use the radial distance to look for association between objects. From the NND sections we saw that this was not a particularly useful measurement. However, we wished to see if this measure became more informative when used to characterise PML NBs by comparing the observed value with respect to their distance from the centre of the nucleus when simulated under the null hypothesis CSR, (Figure 34).

3.5.4.1 PML NB – nuclear centroid CSR analysis for MRC5 ASYNC, HS, IFN, SS and VA nuclei

In Figure 34 MRC5 ASYNC, SS and VA nuclei, PML NBs appeared to be significantly closer to the nuclear centroid in 5-10% of cells tested (8% ASYNC, n = 435; 10% SS, n = 409; 5% of MRC5 VA cells, n = 409). However, upon HS treatment this rose to 57% of cells containing PML NBs that could be classified as being significantly closer to the nuclear centroid than expected under CSR, and in IFNβ-treated cells this proportion was also higher, at 32% of the cells tested. This is a similar trend to the proportion of cells that were significantly closer to the nuclear boundary for each of the data sets tested. Therefore the heat shock and IFNβ treatments result in a measurable change in minimum radial distance from the nuclear centroid.

In particular, the case if having PML NBs significantly closer to the nuclear centroid was often seen in conjunction with them also being classified as being both significantly closer and significantly further from the nuclear boundary. This situation most often occured in the HS cell population, followed by the IFN nuclei.

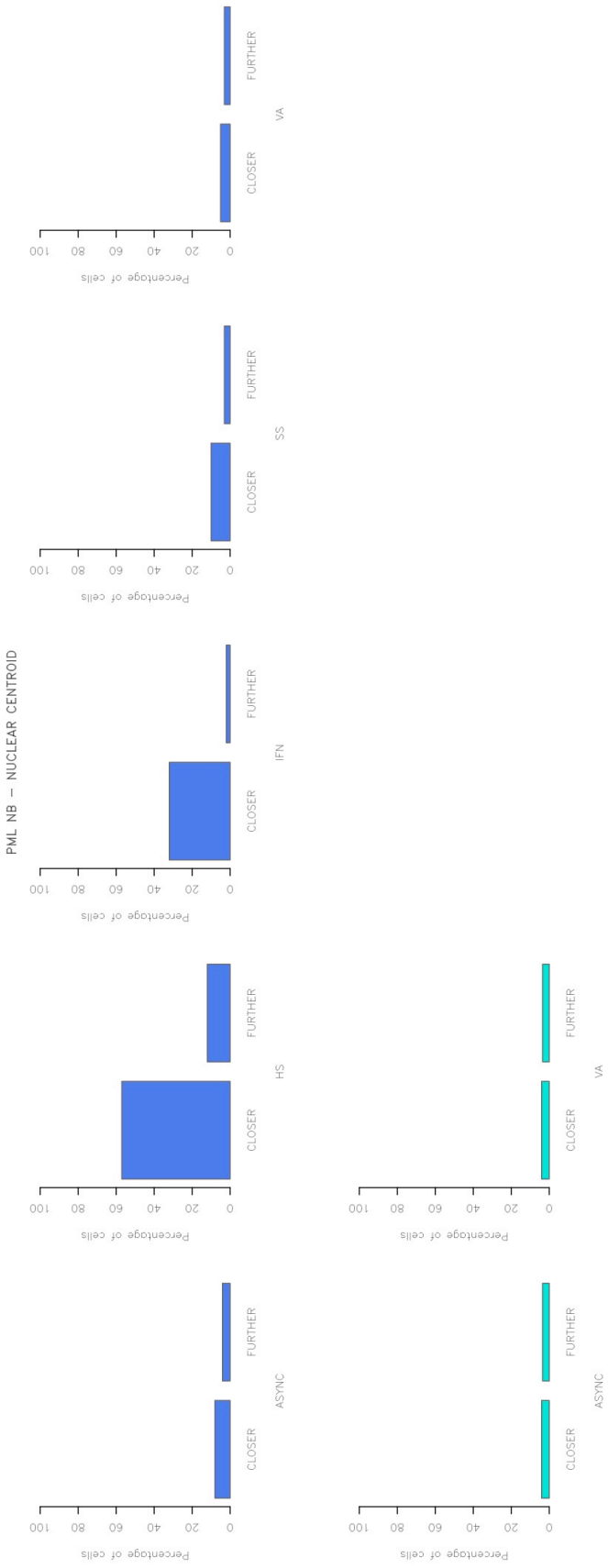


Figure 34 PML NB - nuclear centroid spatial organisation under CSR

Percentage of nuclei rejecting CSR according to observed minimum PML NB - nuclear centroid NND. Observed minimum PML NB - nuclear centroid NNDs for each nucleus in a dataset were compared with simulations for the same PML NBs under CSR. PML NBs were either closer to or further from the nuclear centroid than expected under CSR. Row 1 MRC5: ASYNC, HS, IFN, SS and VA. Row 2 WI38: ASYNC and VA.

The ASYNC, IFN, SS and VA cells all seem to show a similar trend where between 2-4% of the nuclei tested were classified as containing PML NBs that were further from the nuclear centroid than expected under CSR, (4% ASYNC, n = 435; 2% IFN, n = 378; 3% SS, n = 409; 3% of VA cells, n = 409). Therefore it is most common for the PML NBs in a cell to be CSR with respect to the nuclear centroid. HS seemed to increase the proportion of cells where PML NBs were significantly further from the nuclear centroid in comparison to ASYNC, as was seen in 12% of cells tested (n = 438), and therefore this was the most interesting observation.

3.5.4.2 PML NB – boundary CSR analysis for WI38 ASYNC and VA nuclei

In Figure 34 both 4% ASYNC and VA WI38 nuclei (n = 421, n = 376, respectively) could be classified as containing PML NBs that were closer to the nuclear centre than expected under the condition of CSR. This is dissimilar to that seen in MRC5 nuclei; where 8% and 5% of asynchronous cells and MRC5VA respectively, contained PML NBs that were closer to the nuclear centre than expected.

In both WI38 ASYNC and VA nuclei 3.5% could be classified as containing PML NBs that were further from the nuclear centre than expected under the condition of CSR. This is similar to that seen in MRC5 nuclei; where 4% and 3% of ASYNC and VA nuclei, respectively, contained PML NBs that were closer to the nuclear centre than expected. Overall, there is no strong association between PML NBs and the nuclear centroid in WI38 ASYNC or VA nuclei.

3.5.5 Summary

PML NB – PML NB CSR

As well as by simply using distance measurements which pool results across nuclei within datasets, the spatial organisation of PML NBs was tested in every individual nucleus of each cell line and treatment by comparing a cumulative distribution function plot of the

observed minimum inter – PML NB NND distances for every PML NB in the nucleus with the equivalent distances for the same PML NBs simulated 999 times under the null hypothesis of CSR. This was repeated for all nuclei in the dataset. If the observed curve fell out of the simulation envelope it was either closer to or further from (as appropriate) other PML NBs than expected under CSR. If it stayed within the simulation envelope, the PML NBs in that particular nucleus were arranged according to complete spatial randomness. PML NBs were closer to other PML NBs than expected under CSR in 18%, 40%, 3%, 22% and 18% of MRC5 ASYNC, HS, IFN, SS and VA nuclei respectively. They were further than expected in 9%, 17%, 43%, 23% and 8% of MRC5 ASYNC, HS, IFN, SS and VA nuclei respectively. Therefore heat shock treatment increased the percentage of MRC5 nuclei that contain PML NBs that are closer than expected under CSR, and IFNβ-treatment increases the percentage of nuclei that contain PML NBs that are further from PML NBs than expected under CSR, as do heat shock and serum starvation to some extent. Interestingly this means that heat shock treatment is responsible for increasing both the percentages of nuclei containing PML NBs that are both closer and further from each other than expected under CSR. In WI38 ASYNC and VA cells 4% and 9% of nuclei contained PML NBs that were closer than, and 12% and 23% that were further than expected from nearest neighbouring PML NBs under CSR.

PML NB – nuclear boundary CSR

The cumulative distribution function plot of the observed minimum PML NB – nuclear boundary NND distances for every PML NB in the nucleus was compared with the equivalent distances for the same PML NBs simulated 999 times under the null hypothesis of CSR. This was repeated for all nuclei within the dataset. PML NBs were closer to the boundary than expected under CSR in 5%, 60%, 30%, 5% and 1% of MRC5 ASYNC, HS, IFN, SS and VA nuclei respectively. Heat shock and IFNβ-treatment greatly increased the percentage of nuclei with PML NBs that were closer to the boundary than expected under CSR in comparison to MRC5 ASYNC nuclei. They were further from the boundary in 36%, 94%, 58%, 77% and 35% of MRC5 ASYNC, HS, IFN, SS and VA nuclei respectively. Heat shock, IFNβ-treatment and serum starvation increased the percentage of nuclei with PML NBs that were further from the boundary than expected under CSR. Therefore heat shock and IFNβ-treatment cause an increase in the percentage of nuclei containing PML NBs that locate both closer to and

further from the nuclear boundary than expected under CSR. In WI38 ASYNC and VA cells 2% and 5% of nuclei contained PML NBs that were closer than, and 22% and 56% that were further than expected under CSR. In all of MRC5 and WI38 ASYNC and VA nuclei, PML NBs were more commonly found to be further from the nuclear boundary than expected under CSR, than closer to it indicating a natural repulsion from the boundary, termed the "edge-effect".

PML NB – nuclear centroid CSR

The cumulative distribution function plot of the observed minimum PML NB – nuclear centroid NND distances for every PML NB in the nucleus was compared with the equivalent distances for the same PML NBs simulated 999 times under the null hypothesis of CSR. This was repeated for all nuclei within the dataset. PML NBs were closer to the centroid than expected under CSR in 8%, 57%, 32%, 10% and 5% of MRC5 ASYNC, HS, IFN, SS and VA nuclei respectively. Heat shock and IFNβ-treatment greatly increased the percentage of nuclei with PML NBs that were closer to the nuclear centroid than expected under CSR in comparison to MRC5 ASYNC nuclei. They were further from the boundary in 4%, 12%, 2%, 3% and 3% of MRC5 ASYNC, HS, IFN, SS and VA nuclei respectively. Heat shock slightly increased the percentage of nuclei with PML NBs that were further from the nuclear centroid than expected under CSR. Therefore heat shock causes an increase in the percentage of nuclei containing PML NBs that locate both closer to and further from the nuclear centroid than expected under CSR. In both WI38 ASYNC and VA cells 4% of nuclei contained PML NBs that were closer than, and 3.5% that were further than expected under CSR, an unremarkable result.

3.6 Chapter summary

The morphology, number and size of PML NBs in MRC5 normal human fibroblasts cell populations (untreated asynchronous, heat shocked, IFNβ-treated and serum starved), the SV40-transformed MRC5 VA cell line, three subsets of MRC5 (G0, G1 and S), WI38 untreated asynchronous normal human fibroblasts and the SV40-transformed WI38 VA cell line were investigated using indirect immunofluorescence of nuclear PML protein and collection of 3D confocal image stacks. The SCT algorithm was used to segment

PML NBs and describe their location within the volume of the nucleus. Number, size (volume), distance relationships and spatial organisation of PML NBs were described, in addition to total PML protein levels (via voxel counts and western blotting). In line with published data they were found to vary according to cell line and treatment, presenting the SCT algorithm as an excellent tool for the quantification of PML NB organisation.

4

PML NBs and Nuclear Compartments

4.1 Introduction

The inter – PML NB, PML NB – boundary, and PML NB – nuclear centroid distance and spatial relationships were presented in Chapter 3, for the normal, treated and virally-transformed fibroblast cell lines MRC5 and WI38. In Chapter 4 we extend this analysis to look at the PML NB – functional compartment distance and spatial relationships in the same cell lines. This allowed us to explore PML NB function and organisation in relation to functional compartments within the nucleus.

Table 12 shows a summary of the datasets for which PML NB relationships to the functional compartments shown were collected.

Table 12 Summary of data sets and compartments for which the PML NB - compartment relationship is described

Cell line and treatment		Nuclear Compartment										
		ACA	TELO	ACHIS	MEHIS	RNA	RNAPII	B23	SC35	CB	19S	11S
MRC5	ASYNC	✓	✓	✓	✓	✓	✓	✓	✓	✗	✓	✓
	HS	✓	✓	✓	✓	✓	✓	✓	✓	✗	✓	✓
	IFN	✓	✓	✓	✓	✗	✓	✓	✓	✗	✓	✓
	SS	✓	✓	✓	✓	✓	✗	✓	✓	✗	✓	✓
	VA	✓	✓	✓	✓	✓	✓	✓	✓	✓	✓	✓
WI38	ASYNC	✓	✓	✓	✓	✓	✓	✓	✓	✗	✓	✓
	VA	✓	✓	✓	✓	✗	✓	✓	✓	✓	✓	✓

Functional groups are as follows: chromosome topology (yellow), transcriptional compartments (blue), post-transcriptional compartments (orange) and proteolysis (pink).

4.2 Immunofluorescence of nuclear compartments in different cell lines and conditions

4.2.1 Introduction

Firstly we visually characterised the immunofluorescence pattern for each of the antibodies we used as functional compartment markers (Figure 35, Figure 36, and Figure 37). Pattern, organisation in the nucleus, association with PML NBs and change in appearance (if any) upon treatment was described. Immunofluorescence was carried out as described in Chapter 2.

4.2.2 Chromosomal topology compartments

4.2.2.1 Chromosomes (ACA)

Centromeres were detected using the anti centromere antibody (ACA) antibody which is produced as an autoantibody against human centromeric proteins. They were visualised as large, discrete foci in the MRC5 and WI38 ASYNC and VA cell lines, as well as the treated MRC5 nuclei. They appeared to be arranged randomly within the nucleus, with no colocalisation occuring between PML NBs and centromeres other than that expected by chance. Treatment of MRC5 ASYNC cells with heat shock (HS), IFNβ (IFN), or serum-starvation (SS) did not appear to alter the appearance or arrangement of centromeres. MRC5 and WI38 ASYNC cells are of normal ploidy (see Table 8), and the majority of cells should contain 46 centromeres. Cells from the MRC5 and WI38 VA cell lines should contain upwards of this number (see Table 8). However, from visual study of the projection images it was apparent that many nuclei did not contain as many as 46 foci. Therefore it was likely that centromeres were clustering to form kinetochores (Solovei et al., 2004) which are structures formed at certain times during the cell cycle.

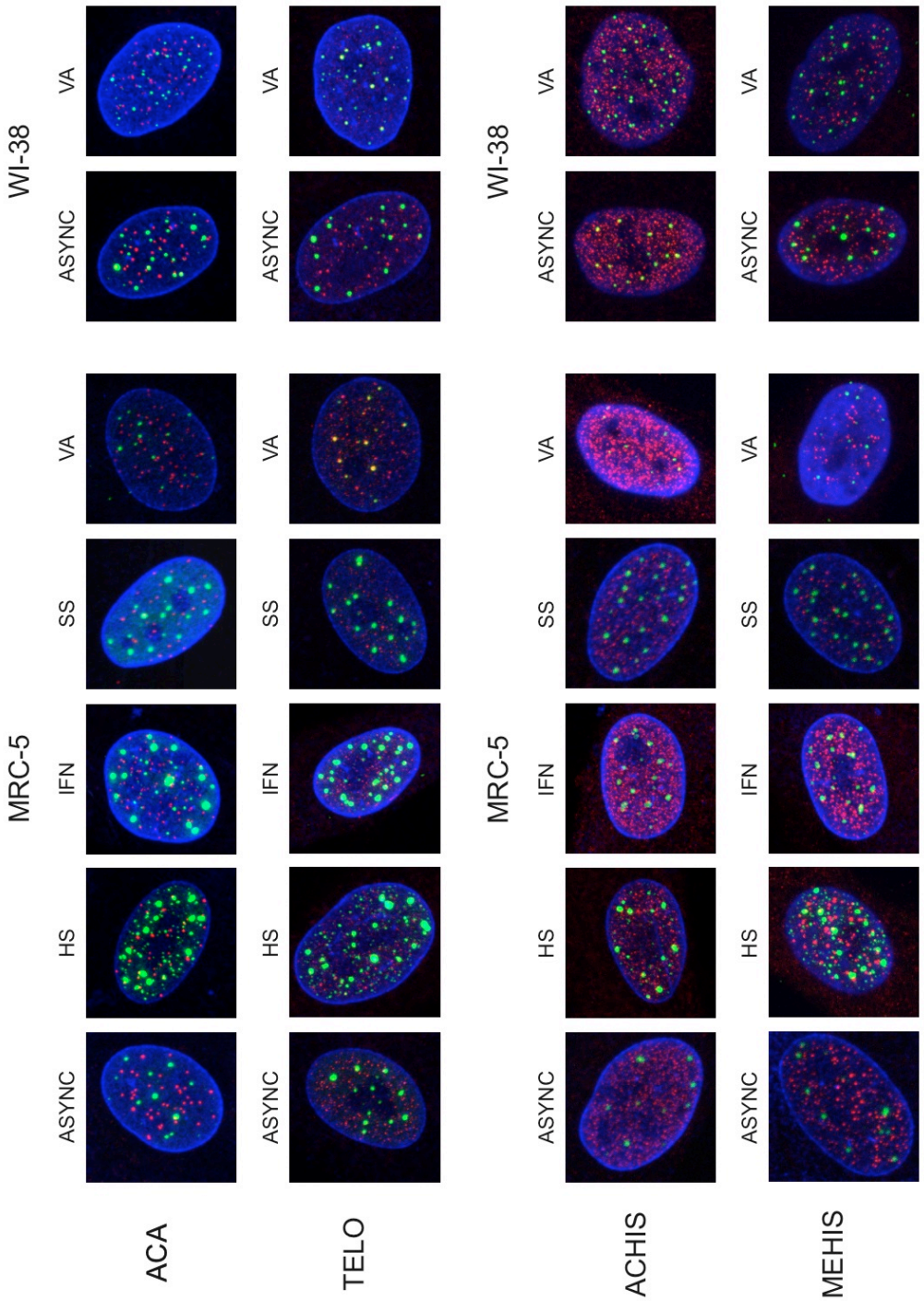


Figure 35 Centromeres, telomeres, acetylated histone, and methylated histone in MRC5 normal and treated fibroblasts, WI38 normal fibroblasts, and the SV40-transformed cell lines MRC5 VA and WI38 VA

Projection images of various functional compartments as labelled (red), PML NBs (green) lamin B (blue). Scale bar 5µm.
Row 1 - Centromeres (ACA). Row 2 - Telomeres (TELO). Row 3 - Acetylated histone H4 K12 acetylation (ACHIS). Row 4 - Methylated histone H3 K9, K27 methylation (MEHIS).

4.2.2.2 Telomeres (TELO)

Telomeres were detected using an anti-human telomeric-repeat binding factor-1 (TRF-1) antibody. This binds to the TRF-1 protein which itself binds to the telomeric DNA repeats at the ends of the chromosomes. Therefore the size of the foci detected is related to the length of the telomeric repeats. From the IF it can be seen that there were a greater number of telomeric foci than centromeres in all of the cell lines studied (as telomeres are present at the ends of chromosomes there will naturally be twice the number of them as centromeres), and all appear to be randomly arranged (with respect to their location in the nucleus, and to PML NBs) except for in the MRC5 VA and WI38 VA nuclei. In these two cell lines there was a clear colocalisation between some of the larger telomeres and PML NBs. This is because they are both Alternative lengthening of telomeres (ALT) positive cell lines, and such PML NBs are named ALT-associated PML NBs (APBs). It must be noted that "telomeres" in ALT positive cell lines may actually be lengths of free telomeric DNA repeats (which play a role in the ALT mechanism), and potentially PML NBs may colocalise with these repeats rather than telomeres themselves. None of the HS, IFN or SS treatments appeared to alter the number or size of telomeres present in MRC5 cells.

4.2.3 Transcriptional compartments

4.2.3.1 Acetylated histones (ACHIS)

Acetylated histones were detected using an antibody directed against histone H4 acetylated on K12, which is associated with an environment favourable to gene expression (Jiang et al., 2004). In all of the cell lines and conditions the IF pattern revealed a large number of similarly-sized foci distributed uniformly throughout the nucleus, except for in nucleoli where they were absent. In MRC5 SS nuclei there appeared to be fewer foci of ACHIS than in the other MRC5 nuclei. There were too many foci to suggest if there were any associations between ACHIS foci and PML NBs visually.

4.2.3.2 Methylated histones (MEHIS)

Methylated histones were detected using an antibody raised against histone H3 dimethlated at K9 and K27, which corresponds to areas of repression of gene expression (Jiang et al., 2004; Lachner et al., 2003). The foci were more variable in size than those of ACHIS, but were seemingly organised randomly throughout the nuclei of all the cell lines and conditions studies. In MRC5 HS there appeared to be a greater amount of the larger foci compared to the other MRC5 nuclei. In MRC5 SS there appeared to be fewer (and smaller) foci than in MRC5 ASYNC. Due to the large number of foci it was not possible to assess if there was any association between MEHIS foci and PML NBs by qualitative methods.

4.2.3.3 Nascent RNA (RNA)

Nascent RNA, visualised by incorporation of BU for 10 mins (or 15 mins for MRC5 SS) and then detected using an anti-BrdU antibody revealed RNA as a pattern of hundreds of small foci distributed evenly throughout the nucleus, but excluded from nucleoli (as BU is not efficiently incorporated by RNA polymerase I into rRNA transcripts). In MRC5 and WI38 VA nuclei the staining appeared to be more diffuse - however this was due to an increased number of smaller foci than in their ASYNC counterparts. This meant that in WI38 VA RNA could not be segmented correctly by the SCT algorithm and so could not be used in the analysis. Also, the staining in MRC5 IFN was too poor to use in the majority of nuclei. Due to the number of foci it was not possible to suggest if there was an association between nascent RNA and PML NBs in any of the cell lines or conditions studied.

When staining nascent RNA in SV40 transformed cells, although able to incorporate BU, it was not possible to get punctate foci that could be segmented by the SCT algorithm. Instead the RNA formed a fuzzy signal, from which points could not be segmented, and thus it was not possible to formally compare the nascent RNA relationship with PML NBs in WI38 and WI38 VA nuclei. However, it is interesting that the $RNAPII_O$ foci could be segmented for WI38 VA cells. In contrast, for MRC5 serum starved (SS) cells it was not possible to detect $RNAPII_O$ foci, but nascent RNA foci could be segmented after 15min BU incorporation.

4.2.3.4 RNA polymerase II_O (RNAPII)

The active (elongation) form of RNA polymerase II (RNAPII) (which is hyperphosphorylated on its CTD tail) was detected using the H5 antibody, and an RNase inhibitor VRC was used to ensure RNA did not degrade during the staining process. Such foci indicate sites of active mRNA transcription in the nucleoplasm, and are excluded from the nucleolus where other forms of RNAPII dominate. Foci numbered in the hundreds (exceeding the count of RNA) and were punctate. The number of foci appeared to be lower in MRC5 HS, and higher in MRC5 IFN, than in MRC5 ASYNC. It was not possible to collect nuclei with a strong enough signal to be accurately segmented in MRC5 SS cells. MRC5 and WI38 VA contained a more diffuse pattern of RNAPII but this was likely due to the same reasons as occurred in the RNA staining of these nuclei - a greater number of smaller foci than in their ASYNC counterparts. It was not possible to tell if there was association between RNAPII foci and PML NBs from visual inspection alone.

4.2.3.5 Nucleoli (B23)

Nucleoli were visualised with an antibody directed at B23, also known as nucleophosmin. Nucleoli themselves are sites of ribosomal RNA (rRNA) synthesis and ribosome biogenesis. In all of the cell lines studied nucleoli typically numbered between one and five (usually one or two in the ASYNC cells, but upwards of four in VA cells), and in MRC5 ASYNC, HS and IFN, as well as WI38 ASYNC displayed either irregular or rounded edges. However in MRC5 and WI38 VA nuclei they were typically rounded or circular on the projection images. In MRC5 and WI38 ASYNC, and in MRC5 IFN B23 could be stained solidly throughout the nucleolus, but in MRC5 HS, SS and VA, and WI38 VA only the edges of the nucleoli were strongly stained for B23 protein. In MRC5 HS, VA and WI38 VA there was a diffuse B23 staining in the nucleoplasm (including some small foci in HS nuclei). Typically nucleoli were found at the centre of the nucleus, with occasional nucleoli touching the nuclear lamina. There did not appear to be an association between nucleoli and PML NBs in ASYNC cells, but in those cells treated with HS or IFN, or that were VA cell lines there were occasionally small PML NBs that associated with the edge of the nucleolus, or were found within. B23 also occasionally colocalised with PML ring structures that can be found in stressed cells (data not shown).

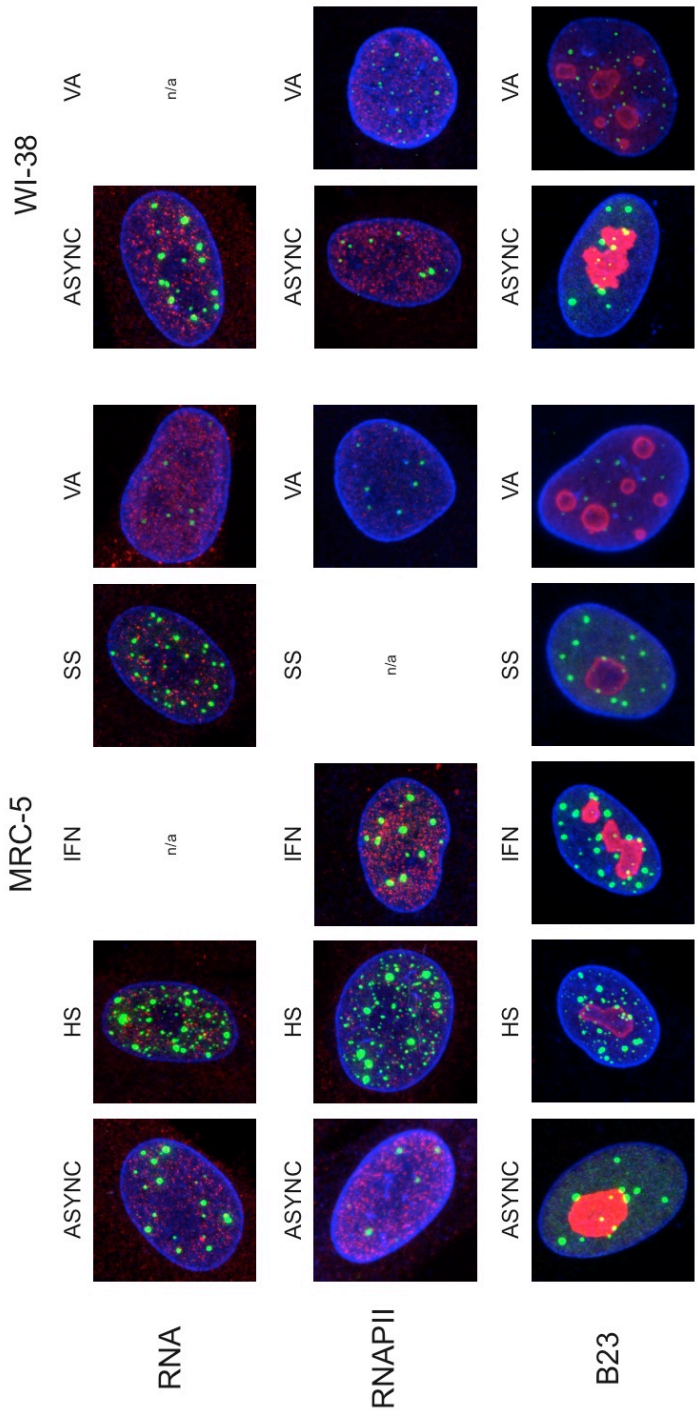


Figure 36 Nascent RNA, RNA polymerase II (elongation) and nucleoli in MRC5 normal and treated fibroblasts, WI38 normal fibroblasts, and the SV40-transformed cell lines MRC5 VA and WI38 VA

Projection images of various functional compartments as labelled (red), PML NBs (green) lamin B (blue). Scale bar 5μm. Row 1 - Nascent RNA (RNA). Row 2 - RNA polymerase II elongation form (RNAPII). Row 3 - Nucleoli (B23).

4.2.4 Post-transcription compartments

4.2.4.1 Splicing speckles (SC35)

Splicing speckles were detected using an anti-SC35 antibody. SC35 is an integral splicing factor component of the splicing speckles, found in a mesh-like network throughout the nucleus. SC35 was strongly stained in all of the cell lines studied, and the speckles themselves were typically irregularly shaped, except in MRC5 HS and SS where they were rounded. They were irregular in size, with the MRC5 and WI38 VA cell lines containing the smallest speckles in general. In MRC5 IFN there was a strong diffuse nucleoplasmic component visible, although this was present to some extent in all of the cell types and treatments. They were arranged randomly throughout the nucleolus except that they were clearly excluded from nucleoli. Quite often there appeared to be a PML NB directly adjacent to a speckle, but there was little or no colocalisation between the two compartments.

4.2.4.2 Cajal bodies (CB)

Cajal bodies were detected using an anti-Coilin antibody, which detects the protein Coilin. Of the cell lines tested, Cajal bodies were not found in MRC5 or WI38 ASYNC nuclei, and were only seen in MRC5 and WI38 VA nuclei. In MRC5 VA there were typically one to three foci, of similar size to PML NBs. In WI38 VA there were between one and five foci of PML NB size amongst a background of many smaller foci. They seemed show random arrangement within the nucleus, yet typically it appeared that at least one of the Cajal bodies within a nucleus was adjacent to a PML NB.

4.2.5 Proteolysis compartments

4.2.5.1 19S core proteasome regulator (19S)

The 19S proteasome regulator was detected using an anti-19S antibody which was raised against the yta2 ATPase subunit (a yeast homologue of human TBP-7, found in the human 26S proteasome). It was present in all the cell lines and conditions tested as

multiple foci, slightly larger than that of nascent RNA (with some variation between the sizes of individual foci), and appeared to be uniformly distributed throughout the nucleus. The number of foci seemed similar in all of the MRC5 and WI38 ASYNC nuclei (including MRC5 HS, IFN and SS), but in MRC5 and WI38 VA nuclei appeared to be lower. There was also positive staining for 19S in the cytoplasm. There appeared to be occasional association between 19S foci and PML NBs in the cell lines and conditions tested.

4.2.5.2 11S immunoproteasome regulator (11S)

The 11S immunoproteasome regulator was detected using an anti-11S antibody which was raised against the PA28α subunit, and plays a role in recruiting the core proteasome into the immunoproteasome, such as in response to IFN production upon viral infection (Fabunmi et al., 2001). The immunofluorescence pattern was similar to that of 19S in all the cell lines and conditions tested, consisting of multiple small foci uniformly distributed throughout the nucleus. There was also positive staining in the cytoplasm. Interestingly, the number of foci was greatly increased in MRC5 IFN nuclei, compared to the MRC5 ASYNC nuclei. It seemed that quite often there was a focus of 11S adjacent to a PML NB, however since the total number of foci was very high it was not possible to tell if this association was due to chance or a functional relationship from visual inspection alone.

4.2.6 Summary

There were a number of different types of patterns of nuclear compartments that can be visualised by immunofluorescence detection. These are point pattern, diffuse and solid. Examples of these are centromeres, some parts of the splicing speckle pattern (and PML diffuse nucleoplasm staining), and nucleoli, respectively. Typically the point patterns were easiest to segment using the SCT algorithm. By simply studying projection images of such compartments it was not possible to accurately describe or understand the relationships between these functional compartments and PML NBs, and therefore quantitative methods should be used.

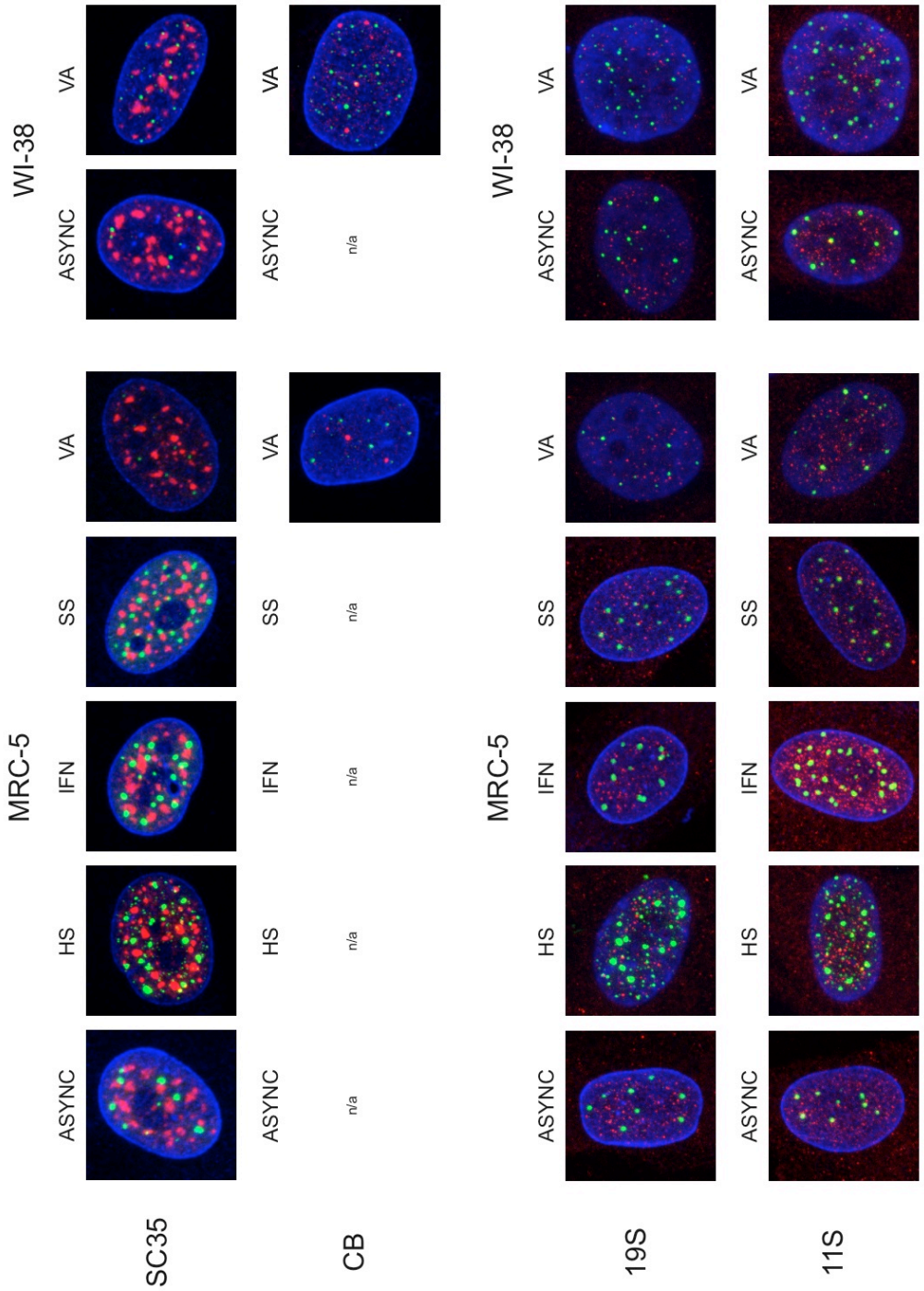


Figure 37 SC35 domains (splicing speckles), Cajal bodies, 19S core proteasome regulator, and 11S immunoproteasome regulator in MRC5 normal and treated fibroblasts, WI38 normal fibroblasts, and the SV40-transformed cell lines MRC5 VA and WI38 VA

Projection images of various functional compartments as labelled (red), PML NBs (green) lamin B (blue). Scale bar 5μm.
Row 1 - SC35 domains (SC35). Row 2 - Cajal bodies (CB). Row 3 - 19S core proteasome regulator (19S). Row 4 - 11S immunoproteasome regulator (11S).

4.3 Average voxels of functional compartments per nucleus

4.3.1 Introduction

To describe the volumes occupied by each functional compartment within the nucleus the volumes of different nuclear subcompartments were estimated by calculating the average red voxel counts per nucleus for each compartment, under each condition, and within each cell line. They were based on measurements from between 30 and 50 cell nuclei each. Average PML voxels per nucleus are included for comparison.

4.3.2 Average voxels of functional compartments in MRC5 and WI38 nuclei

4.3.2.1 Chromosome topology

In MRC5 the mean volumes per cell were as follows (Figure 38). For centromeres (ACA) the volumes were quite similar across the conditions, between 390 and up to a maximum of 821 voxels of red. The highest count per cell was seen in the HS population (821), and the lowest in SS nuclei (390). The voxel count in VA was slightly higher than in ASYNC (612 versus 560), which was as expected since MRC5VA cells have a more than diploid karyotype. None of the perturbations except for VA should affect volume of ACA found within the cell (since they do not cause new centromeres to form, or extra material to be deposited at them, whereas the transformed cells do have an altered karyotype compared with normal MRC5 fibroblasts). The HS data set result, which showed the highest average voxel count, might be accounted for by a redistribution of centromere proteins due to heat shock treatment, which may have increased the total volume of protein that could be detected by the antibody. Since all the data sets except for SS contain asynchronous cell populations, it would be expected that the volumes might be variable since centromeres can exist as separate structures that divide during mitosis, or may form fusions with other centromeres to form chromocentres. As these populations contain cells at various stages of the cell cycle, this

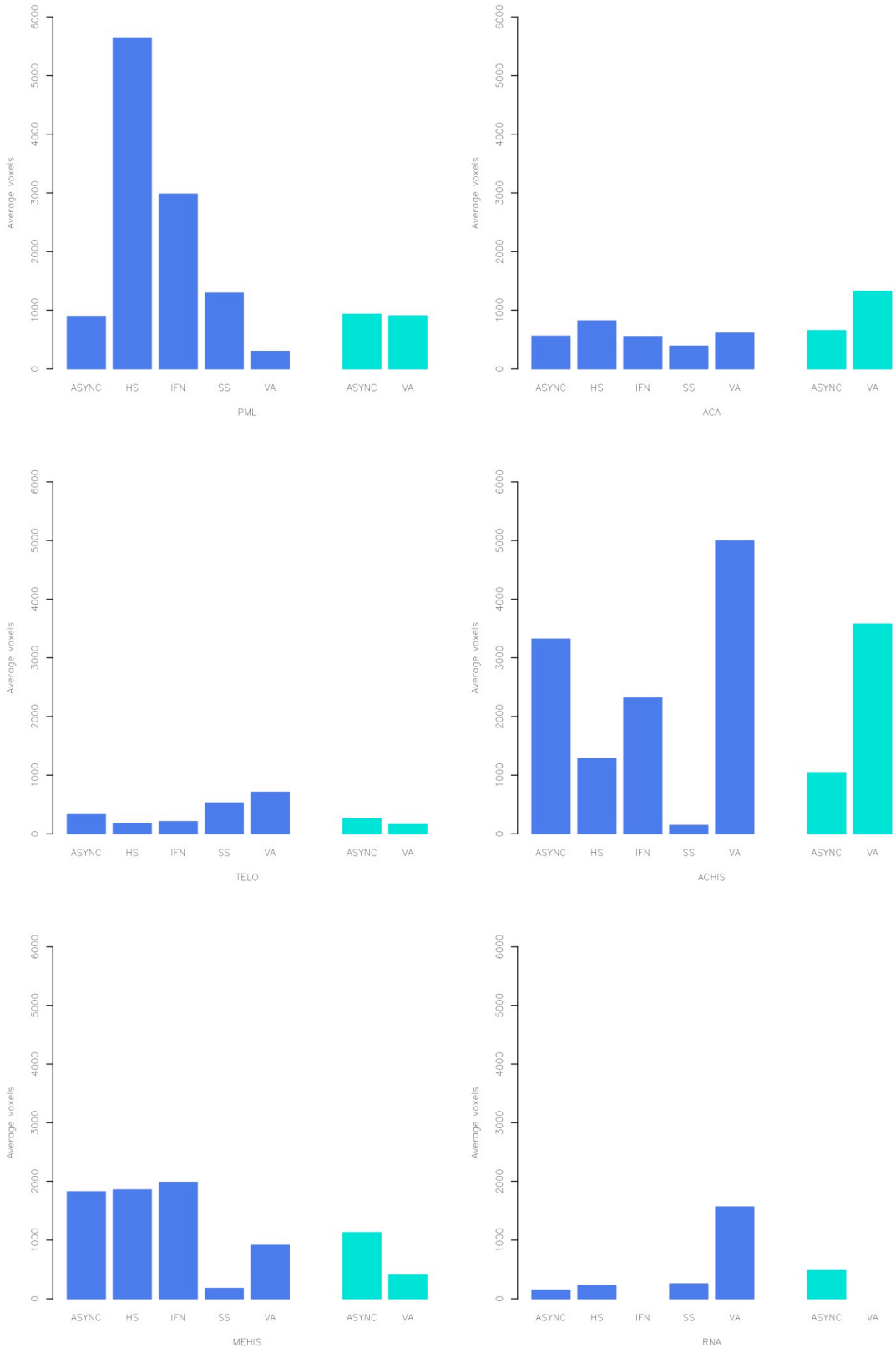


Figure 38 Average voxels of ACA, TELO, ACHIS, MEHIS and RNA per nucleus

Effects of heat shock, IFNβ, and serum starvation treatment, and SV40-transformation on functional compartment levels. Based upon segmentation using the SCT algorithm [ref] of nuclei immunofluorescently stained for each of the functional compartments.

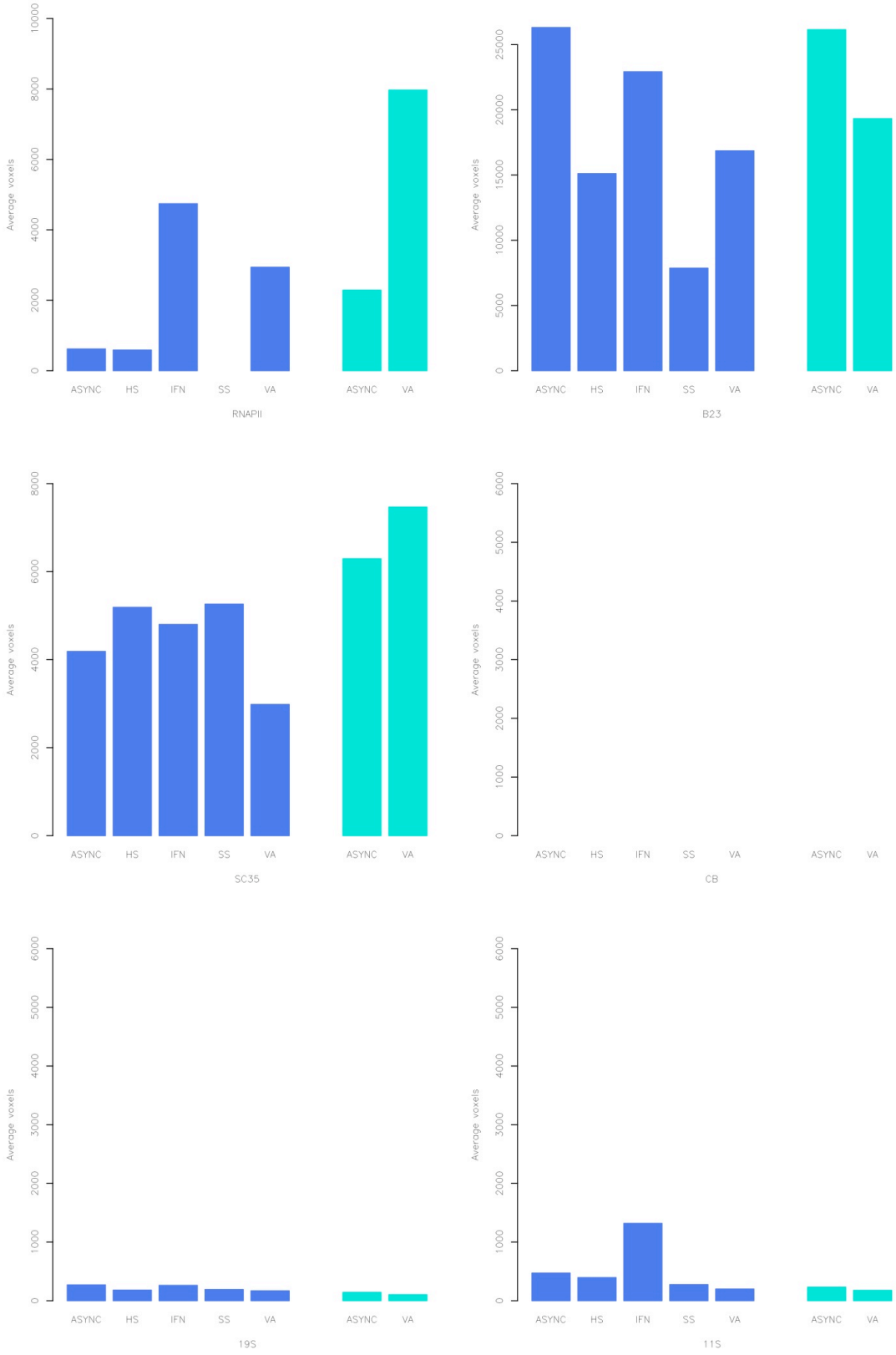


Figure 39 Average voxels of RNAPII, B23, SC35, CB, 19S and 11S per nucleus

Effects of heat shock, IFNβ, and serum starvation treatment, and SV40-transformation on functional compartment levels. Based upon segmentation using the SCT algorithm [ref] of nuclei immunofluorescently stained for each of the functional compartments.

might lead to the differences in volumes of ACA seen. This also applies to centromere number (which is not investigated here). It is interesting that in the SS cells the volume is lowest – these cells should mostly be in G_0 where there has been no duplication of centromeres yet.

In WI38 ASYNC and VA the mean volumes were 655 and 1326 voxels respectively. Transformation appears to have resulted in a greater than diploid cell line in WI38 VA which could account for the higher average ACA voxels in these nuclei. The ASYNC mean volume was in the same range as for MRC5 ASYNC indicating no difference between the two.

For MRC5 telomeres (TELO) the marker used was the TRF1 protein, which efficiently binds to telomeric DNA. Average voxels across the data sets were in a similar range to that of ACA, at the scale of between 210 and 711 per cell, with the lowest being in HS cell nuclei, and the highest being in VA cells (Figure 38). HS, IFN and SS treatments were not expected to result in an increase in the average TELO voxel count per cell, and accordingly there was little difference between the average voxel counts for these datasets and ASYNC. In VA cells however, the increase in chromosome number obviously results in an increase in telomere number too. Therefore the higher average voxel count in the VA cells (at 711) is logical. Interestingly MRC5VA are ALT positive cells, which means that in order to preserve their immortality their telomeres are lengthened via a mechanism that involves a particular class of PML NB, and may also result in the presence of extra-chromosomal telomeric DNA. The marker protein used in the study also binds to this extra DNA, and therefore the overall amount of TELO signal was higher in this dataset than in any of the other data sets.

In WI38 ASYNC and VA the mean volumes were 259 and 158 voxels respectively. These were in the same range as for MRC5, but the VA mean voxel count was lower than expected considering that WI38 VA are also ALT positive cells. In general telomere staining with IF was weak (which affected segmentation), and this could account for the lower than expected result.

4.3.2.2 Transcriptional compartments

For MRC5 acetylated histones (ACHIS) (Figure 38) the average voxel counts per cell were much more highly variable between cell conditions, ranging from around 145 in SS cells, to 4997 in VA cells. In ASYNC cells an average of 3320 voxels per cell was seen, whereas in HS cells this was much lower at 1281 voxels, and in IFN cells this was 2317 voxels per cell. This concurs with VA cells being much more transcriptionally active than ASYNC, and SS cells are much less transcriptionally active than ASYNC cells (as we might expect in serum-starved cells). Interestingly both HS and IFN cells show lower average voxel counts than ASYNC cells. However, in both these conditions specialised transcriptional pathways are turned on which may not greatly increase global transcription levels, and indeed could still occur despite the overall transcription level being decreased relative to ASYNC cells.

In WI38 ASYNC and VA cells the average ACHIS voxels were 1045 and 3577, respectively. The voxel count was tripled in VA in comparison to ASYNC. The increase between ASYNC and VA cells also occurred in MRC5, but the average voxel count in MRC5 ASYNC was higher to start with (at 3320).

For MRC5 methylated histones (MEHIS) (Figure 38) the average voxel counts per cell were between 178 and 1986 voxels across the data sets. These were fairly similar in ASYNC, HS and IFN cells (at 1856 and 1986 voxels per cell), greatly decreased in SS cells (at 178 voxels per cell), and were about half the ASYNC level in VA cells (912 voxels per cell). It is interesting that the average voxel count was decreased in both SS and VA cells – this might be expected in VA cells since a higher global transcription level might require that areas of histone methylation be reduced to allow an open chromatin structure. However, in SS cells one might expect that such areas of closed chromatin were more widespread, and hence the amount of MEHIS should increase when in comparison to ASYNC cells. However, global condensation of chromatin may be controlled by another repression marker in quiescent cells (and not the one chosen by us), and therefore we would not be able to see an increase in of MEHIS in SS cells – it could just be a marker of local repression sites in cycling cells for instance.

In WI38 ASYNC and VA cells the average MEHIS voxels were 1129 and 405, respectively. The voxel count halved in VA in comparison to ASYNC. This increase was similar in trend to that seen between MRC5 ASYNC and VA.

Overall, voxel counts for ACHIS were more variable and typically higher than for MEHIS in MRC5 and WI38, except in MRC5 SS cells, which were non-cycling. In the other data sets all cells were cycling and thus transcriptionally active.

For nascent RNA foci (RNA) in MRC5 nuclei (Figure 38) the average voxel count was lowest in ASYNC at 150, and highest in VA at 1566 voxels. There was little difference between the voxel counts for ASYNC, HS and SS nuclei. There was no value for IFN as it was not possible to segment the IFN MRC5 RNA pattern. The increase in average voxel count between ASYNC and VA was ten fold, indicating that the level of transcription was much higher in VA nuclei than in ASYNC.

In WI38 ASYNC nuclei the average voxel counts for RNA was 481, which was higher than that of MRC5 ASYNC. There was no average voxel count available for VA as the nascent RNA pattern of WI38 VA nuclei could not be segmented.

For RNA polymerase II_O (RNAPII) foci in MRC5 nuclei (Figure 39) the average voxel counts per nucleus ranged from 618 (in ASYNC) to 4744 (in IFN). In HS nuclei the average voxel count was similar to ASYNC at 587, and in VA nuclei it was much higher than ASYNC (at 2939 voxels). There was no count available for SS nuclei.

In WI38 ASYNC and VA nuclei the voxel counts for RNAPII foci were 2290 and 7972, respectively. As in MRC5 nuclei there was also an increase in the amount of RNAPII between ASYNC and VA cells, indicating a much higher level of transcriptional activity in the virally-transformed cells.

The trend of an increase in the transcriptional activity of the transformed VA nuclei in comparison to their ASYNC counterparts was seen for both the RNA and RNAPII markers in MRC5 and WI38 cells. However the increase in average RNAPII voxels in IFN nuclei in comparison to ASYNC could not be reinforced with a similar finding for RNA in MRC5, due to the missing IFN RNA dataset.

Nucleoli (B23) are clearly the most common compartment in the nucleus in terms of mean voxel count per cell. Voxel counts in MRC5 (Figure 39) ranged from between 7865 (in SS cells) to 26318 in ASYNC cells. In SS cells the voxel count may underestimate nucleoli voxels as the localisation of the B23 marker is altered in such cells. Instead of the nucleolus being labelled throughout, only the outer shell contained nucleophosmin. Due to the way that the SCT algorithm works, the volume inside these nucleoli is not included in the analysis, and thus they appear hollow (as only red voxels are counted as compartment). However, this did not affect the SS PML NB – nucleoli distance and spatial measurements in Section 4.4.2.2 as the NNDs were measured from PML NB centroid to the edge of the nucleolus. Therefore the voxel count only truly applies to nucleophosmin as a nucleolar component, and not the nucleolus in SS cells. In HS cells the average voxel count per cell was 15117 voxels, which was lower than in ASYNC cells. This could be due to a delocalisation of B23 into the nucleoplasm under conditions of heat shock. Any marker in the nucleoplasm would probably be discounted as signal by the SCT algorithm. In VA cells the average voxel count per cell is lower than that in ASYNC cells at 16861 voxels. This may be due to differences in nucleolar morphology. In ASYNC cells are larger, irregularly shaped nucleoli that are labelled solidly, whereas in VA cells they are rounded and only labelled at the edges.

In WI38 ASYNC and VA nucleoli the voxel counts were in a similar range to that of MRC5, and also decreased between ASYNC and VA (at 26153 and 19332, respectively).

4.3.2.3 Post-transcription compartments

For splicing speckles (SC35) the average voxel counts in MRC5 (Figure 39) were fairly similar across the cell conditions, at between 2983 voxels (VA) and 5263 voxels (SS) per cell. In ASYNC the voxel count per cell was 4188 voxels, and in HS and IFN it was at 4801 voxels per cell. Interestingly here the highest average voxel count was seen in the condition where most of the splicing speckle components are being stored within the speckle (SS) as the cell is completing less transcription. The high voxel count for HS cells could be accounted for by disruption of splicing speckles by the heat shock treatment, which could result in SC35's diffusion away from the speckles. In VA cells, where transcription levels should be fairly high, the voxel count for SC35 was lower than

in ASYNC cells, indicating a greater presence of SC35 as a diffuse component of the nucleoplasm (and thus not segmented by the SCT algorithm as SC35).

In WI38 ASYNC and VA nuclei the voxel counts for SC35 were 6295 and 7468, respectively. Unlike between MRC5 ASYNC and VA, the voxel count was increased upon transformation, which is difficult to account for. Overall, the voxel counts were elevated in comparison to those for MRC5 nuclei.

4.3.2.4 Proteolysis

For the 19S core proteasome regulator (19S) in MRC5 (Figure 39) the average voxel count per cell was very similar across the conditions for MRC5, at between 163 and 271 voxels per cell. This indicates that the core proteasome regulator is required under all cell conditions, and is not overexpressed under conditions of IFN-β treatment. If required in greater amounts to deal with complications such as protein denaturation due to heat shock treatment, the treatment time was too short to indicate an increase in the average 19S voxel counts in the cell nucleus. It is possible that this might be seen at a later timepoint.

In WI38 ASYNC and VA the 19S average voxel counts were similar to each other, and to those in MRC5 at 144 and 105 voxels, respectively.

For the 11S immunoproteasome regulator (11S) the average voxel count per cell was similar across the ASYNC, HS, SS and VA data sets at around 400 voxels per cell, and this was similar to the voxel count seen for the 19S data sets. However, in the IFN data set the average voxel count increased to 1500 voxels per cell, and this is likely to be a consequence of 11S overexpression in response to treatment with IFN-β. It is interesting as the 11S regulator is required to help form the immunoproteasome, which forms part of the immune response induced by IFN-β. The 11S regulator displaces the 19S regulator from the core proteasome, which may explain why 19S levels are unaffected by IFN-β treatment (Fabunmi et al., 2001; Rechsteiner et al., 2000). The increase in the average 11S voxel count also coincides with an increase in the average PML voxel count per cell in IFN-β treated cells, and the two are closely linked.

In WI38 ASYNC and VA nuclei the 11S average voxel counts were 233 and 178, respectively. These were similar in range to those in MRC5, although slightly lower in the case of ASYNC.

4.3.3 Summary

The average voxel counts per nucleus for each functional compartment investigated in conjunction with PML NBs could be estimated from the red channel segmentation. This provided a simple way to determine if cell lines and treatments had an effect upon particular functional compartment presence within the nucleus. Of interest was the increase in average voxels of ACA between ASYNC and VA cells, since transformed nuclei are hyperdiploid and therefore contain more centromeres than ASYNC. VA nuclei also contained much higher average TELO voxel counts due to the ALT positive status of MRC5 VA and WI38 VA cells. B23 (nucleoli) had the highest average voxel counts of any of the functional compartments per nucleus by far. The average voxel counts for the proteolysis compartments 19S and 11S proteasome regulators were the lowest counts of all the functional compartments. Interestingly, IFN treatment induced an increase in the 11S voxel count (as it did the PML average voxel count), indicating a possible functional homology.

4.4 PML NB – functional compartment NNDs

4.4.1 Introduction

Here we plot the PML NB – functional compartment total minimum NNDs (the minimum PML – functional compartment NND for every PML in each cell of a dataset) as boxplots.

We also use the PML NB – functional compartment minimum NND to represent each nucleus when pooled for each data set (across 50 cells) (minimum NNDs) to construct a boxplot for all of the PML NB – functional compartment NNDs within a cell line or

treatment. They are summarised in a diagram of distance hierarchies at the end of Section 4.4.4.

4.4.2 PML NB – functional compartment total minimum NNDs in MRC5 and WI38

To discover how the NND relationships between specific functional compartments and PML NBs changed across the different cell lines and conditions investigated, the total minimum PML – compartment NND (that is the minimum NND for each PML in every nucleus of a dataset) was plotted as a boxplot. The total minimum NND was chosen so as to allow us to look at the entire range of minimum NNDs, instead of using just one (the shortest minimum NND) as the representative for a particular nucleus within the data set.

4.4.2.1 Chromosomal topology

When ordered by median, ACA was closest to PML NBs in SS nuclei in MRC5, followed by ASYNC (which shared a very similar median), then VA and IFN, and was furthest from PML NBs in HS nuclei (Figure 40). ACA in VA, IFN and HS nuclei all shared the largest IQR, and also had almost identical values for the median PML-ACA NND. The range of total minimum NNDs (including outliers) for ASYNC (0 to 40) was almost half that of IFN (0 to 80). In WI38 ASYNC and VA nuclei ACA had very similar median minimum NNDs to PML NBs, and the bigger IQR was in VA nuclei at around 10 voxels.

TELO were closest to PML NBs in MRC5 VA nuclei when ordered by median, followed by SS, ASYNC, and IFN, and finally they were furthest from PML NBs in HS nuclei. The biggest IQR was in HS nuclei, and the smallest IQR was found in SS nuclei. Surprisingly TELO were closest to PML NBs in WI38 ASYNC nuclei, rather than VA according to median minimum NNDs. This was unexpected due to the associations between PML NBs and telomeres found in ALT positive cells such as WI38 VA. However, the IQR was greatest in the VA nuclei meaning that many more of the NNDs contained within the box (which contains 50% of the data points) were very close to or

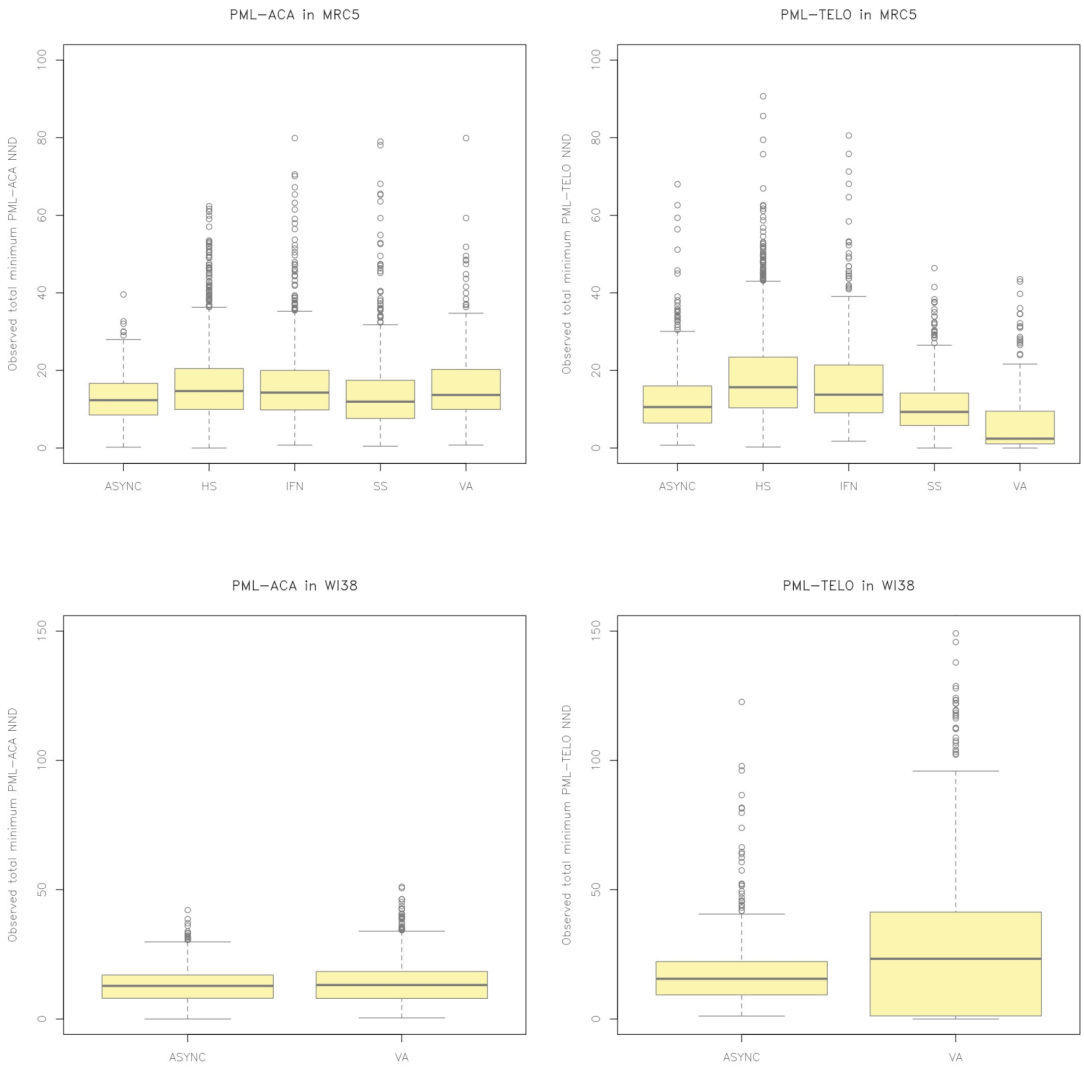


Figure 40 Boxplot of PML NB - chromosome topology compartments total minimum NNDs in MRC5 and WI38

Total minimum NNDs between PML NB and chromosome topological compartments, for MRC5 ASYNC, HS, IFN, SS and VA, and WI38 ASYNC and VA. The box represents 50% of the data points, and the median bar crosses the box. Row 1 MRC5: ACA (left) and TELO (right). Row 2 WI38: ACA (left) and TELO (right).

were touching PML NBs, especially as the lower quartile was found at almost 0 voxels away from PML NBs (indicating colocalisation).

4.4.2.2 Transcription compartments

ACHIS were closest to PML NBs in MRC5 ASYNC and VA nuclei, which shared similar median minimum NNDs, followed by those found in IFN and SS cells, and were furthest from PML NBs in SS cells (Figure 41). In ASYNC cells the IQR for ACHIS

was smallest, and it was largest in SS cells. The median minimum NND for WI38 ACHIS was very similar in both ASYNC and VA nuclei, but slightly closer in ASYNC nuclei, which also had the biggest IQR (Figure 42).

IN MRC5 MEHIS were closest to PML NBs according to median minimum NND in ASYNC and IFN nuclei, followed by HS and VA nuclei. They were furthest from PML NBs in SS nuclei, which also had the largest IQR. The smallest IQR was found in IFN nuclei for MEHIS. The median minimum NND for WI38 MEHIS was closest to PML NBs in ASYNC nuclei than in VA nuclei. The bigger IQR was found in VA nuclei.

In MRC5 VA nuclei RNA was closest to PML NBs according to median minimum NND, followed by SS nuclei. RNA was (equally) furthest from PML NBs in ASYNC and HS nuclei. The biggest IQR was for the PML NB – RNA minimum NND in ASYNC nuclei, and the smallest IQR was found in VA nuclei. There was no result for IFN nuclei as it was not possible to collect the PML-RNA data set under this treatment due to the signal being poor. In WI38 nuclei it was only possible to capture data for nascent RNA in ASYNC nuclei due to the more diffuse nature of the RNA staining which made the segmentation of foci extremely difficult. However, the median minimum NND for RNA in ASYNC nuclei was at 10 voxels and the IQR was roughly 10 voxels at between 8 and 16 voxels.

The closest median minimum NNDs for PML NB – RNAPII in MRC5 were in both IFN and VA nuclei, followed by ASYNC. The furthest RNAPII from PML NBs were in HS nuclei, which also had the biggest IQR. The smallest IQR was found in IFN nuclei. There was no result for SS nuclei, as in serum starved cells there were very few foci of $RNAPII_O$ and a very poor signal, meaning that it could not be segmented accurately during image processing. $RNAPII_O$ were closer to PML NBs in WI38 VA nuclei than in ASYNC, according to median minimum NNDs. The bigger IQR was found in ASYNC nuclei.

When arranged by the median minimum NND for MRC5, nucleoli were closest to PML NBs in VA cells, and then shared almost identical median minimum NNDs in ASYNC, HS, IFN and SS nuclei. The biggest IQR was in SS nuclei, and the IQR for the other four nuclei types were smaller, and very similar to each other. The median minimum

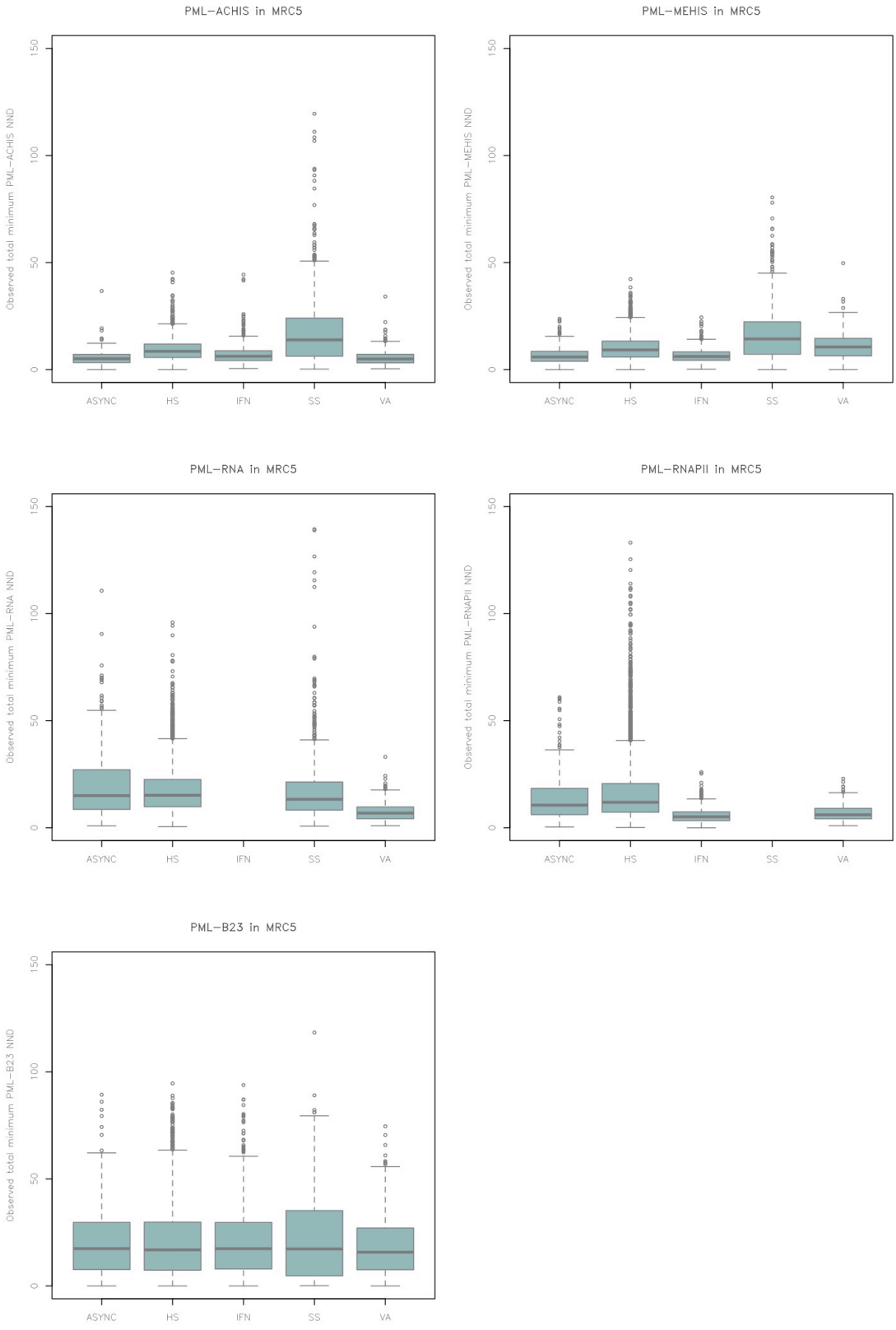


Figure 41 Boxplot of PML NB - transcriptional compartments total minimum NNDs in MRC5

Total minimum NNDs between PML NB and transcriptional compartments for MRC5 ASYNC, HS, IFN, SS and VA. The box represents 50% of the data points, and the median bar crosses the box. Row 1 MRC5: ACHIS (left) and MEHIS (right). Row 2 MRC5: RNA (left) and RNAPII (right). Row 3 MRC5: B23.

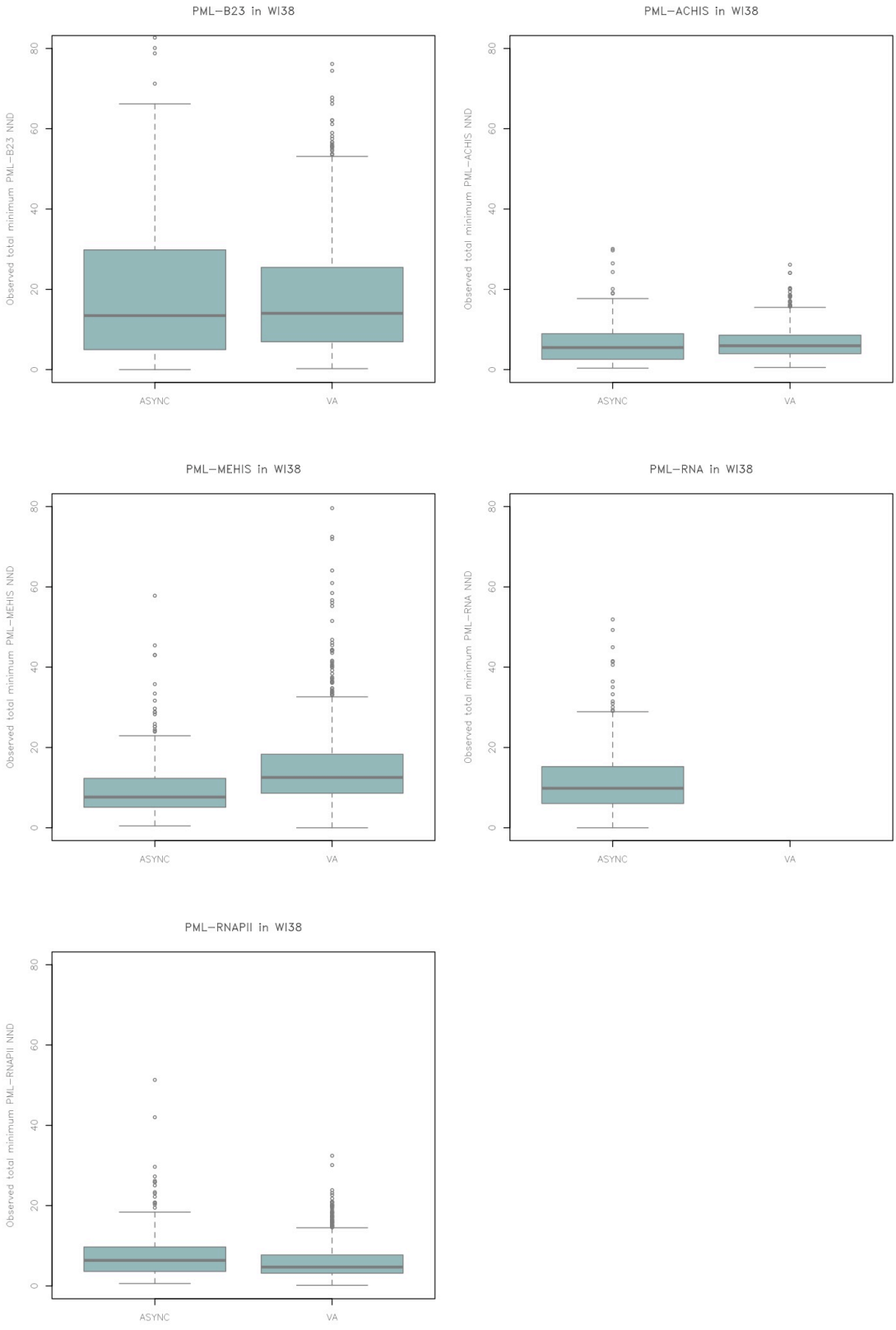


Figure 42 Boxplot of PML NB - transcriptional compartments total minimum NNDs in WI38

Total minimum NNDs between PML NB and transcriptional compartments for WI38 ASYNC and VA. The box represents 50% of the data points, and the median bar crosses the box. Row 1 WI38: B23 (left) and ACHIS (right). Row 2 WI38: MEHIS (left) and RNA (right). Row 3 WI38: RNAPII.

NNDs for nucleoli (B23) to PML NBs were the same in both ASYNC and VA nuclei of WI38 cells. However, ASYNC nuclei NNDs spanned a greater IQR.

4.4.2.3 Post-transcriptional compartments

The closest median minimum NND in MRC5 for splicing speckles (SC35) was in ASYNC nuclei, which also had the smallest IQR (Figure 43). Second closest to PML NBs were both IFN and SS nuclei, followed by HS, and VA nuclei in which splicing speckles were furthest from PML NBs as arranged by median minimum NNDs. VA nuclei also had the biggest IQR for PML-SC35 minimum NNDs. Splicing speckles were closer to PML NBs in WI38 ASYNC nuclei than in VA according to the median minimum NNDs. The VA SC35-PML NB NNDs had a greater IQR than those in ASYNC nuclei.

Since Cajal bodies are not present in normal MRC5 cell nuclei, there was only one result, which was for VA nuclei (Figure 46). The median minimum NND between CB and PML NBs fell at about 15 voxels with the IQR being between 10 and 20. As for MRC5 cells, Cajal bodies were not found to be present in normal WI38 cell nuclei. However, in WI38 VA the median minimum NND fell at about 40 voxels, which is quite a large distance in terms of inter-object distances in the nucleus.

4.4.2.4 Proteolysis compartments

For the 19S core proteasome regulator (19S) in MRC5, arranging by median minimum PML NNDs showed that 19S was closest to PML NBs in ASYNC nuclei, followed by IFN, SS and HS nuclei, and was furthest from PML NBs in VA nuclei (which also had the largest IQR) (Figure 44). The smallest IQR for 19S was found in IFN nuclei. 19S were closer to PML NBs in WI38 ASYNC nuclei than in VA, and the largest IQR was seen in VA nuclei.

The 11S immunoproteasome regulator (11S) was closest to PML NBs (by looking at median minimum NND) in both MRC5 ASYNC and IFN nuclei, followed by SS and HS nuclei, and was furthest from PML NBs in VA nuclei (Figure 47). The biggest IQR was

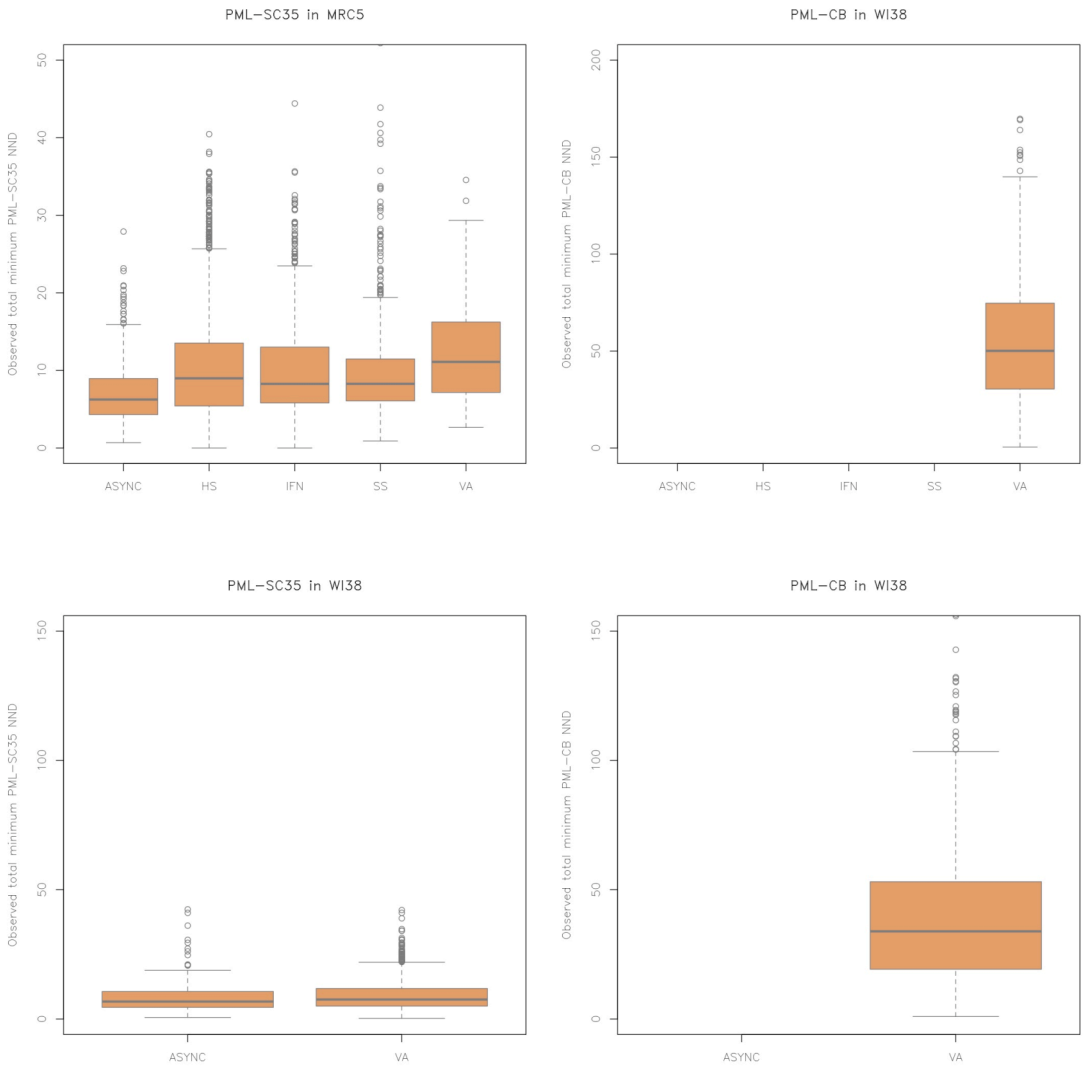


Figure 43 Boxplot of PML NB - post-transcriptional compartments total minimum NNDs in MRC5 and WI38

Total minimum NNDs between PML NB and chromosome topological compartments, for MRC5 ASYNC, HS, IFN, SS and VA, and WI38 ASYNC and VA. The box represents 50% of the data points, and the median bar crosses the box. Row 1 MRC5: SC35 (left) and CB (right). Row 2 WI38: SC35 (left) and CB (right).

found in SS nuclei, and the smallest was in IFN nuclei. According to median minimum NND, 11S were closer to PML NBs in WI38 ASYNC nuclei than in VA, and the larger IQR was seen in the VA nuclei.

4.4.3 Distance hierarchies for all compartments from PML NBs

To understand the NND relationships between all the functional compartments studied and PML NBs for each cell line or perturbation, boxplots of the minimum PML NB –

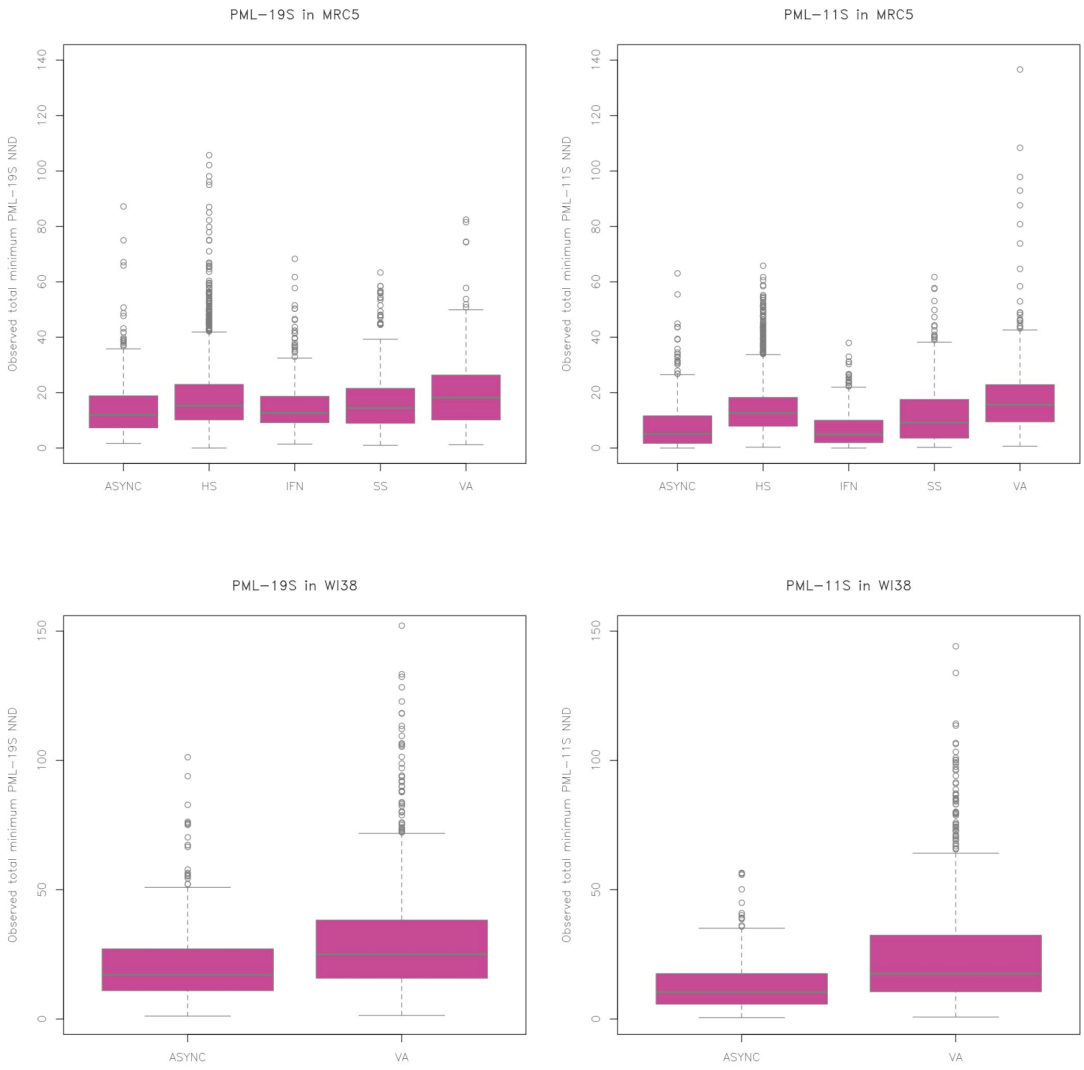


Figure 44 Boxplot of PML NB - proteolysis compartments total minimum NNDs in MRC5 and WI38

Total minimum NNDs between PML NB and proteolysis compartments, for MRC5 ASYNC, HS, IFN, SS and VA, and WI38 ASYNC and VA. The box represents 50% of the data points, and the median bar crosses the box. Row 1 MRC5: 19S (left) and 11S (right). Row 2 WI38: 19S (left) and 11S (right).

functional compartment distances for all the compartments within each cell line and condition were plotted. This allowed a hierarchy of compartments in relation to their median minimum NND from PML NB for each dataset to be constructed. The minimum NNDs from PML NBs are shown for the range of compartments in the study for each cell line and perturbation in Figure 45, Figure 46, and Figure 47. A graphical summary (Figure 48) can be found in Section 4.4.4.

4.4.3.1 MRC-5

In MRC-5 ASYNC the closest compartment to PML NBs was 11S, a compartment involved in proteolysis, followed by ACHIS, B23, and MEHIS, which are all involved in transcription. The next furthest compartment from PML NBs was SC35, then TELO, RNAPII, 19S, ACA, and finally RNA was the furthest from PML NBs according to the median value for the minimum NNDs.

For MRC-5 HS, the trend was different, and B23 was actually the closest functional compartment to PML NBs. It was followed by another transcriptional compartment MEHIS, then by SC35, 11S, and then the two chromosomal topological compartments ACA and TELO. Further away still from the bodies was ACHIS and RNA (which shared their median values), then RNAPII, and finally 19S which was furthest from PML NBs in HS MRC5 nuclei.

In MRC-5 nuclei treated with IFNβ (IFN), once again 11S was closest to PML NBs. Interestingly the median value for the minimum NND for 11S to PML NBs in MRC-5 ASYNC and IFN was the same. The next closest compartment to PML NBs was RNAPII, followed by the other transcriptional compartments B23, MEHIS, and ACHIS. Further away from PML NBs was SC35, followed by the chromosomal topology compartments TELO and ACA. 19S was once again furthest from PML NBs in distance according to the median minimum NND value.

For MRC-5 SS, 11S compartment was closest to PML NBs (however it was further from them than 11S in both ASYNC and IFN MRC-5 nuclei). The next closest functional compartment was B23, followed by MEHIS, TELO, ACHIS, ACA, SC35 and 19S. The transcriptional compartment RNA was furthest from PML NBs in SS nuclei.

In MRC-5 VA nuclei the closest functional compartment to PML NBs according to median minimum NND was TELO. The transcriptional compartments were the next closest to PML NBs, in the order of ACHIS, B23 and RNA (which shared a median minimum NND), RNAPII, and lastly MEHIS. The next furthest compartments were 19S, followed by 11S, which are both involved in proteolysis. Second furthest from

PML NBs was SC35, and lastly ACA were the furthest compartment from PML NBs in VA nuclei.

There were some interesting trends overall. In three of the data sets (ASYNC, IFN and SS) 11S was the closest compartment to PML NBs. Conversly, the other compartment involved in proteolysis, 19S was always one of the furthest compartments from PML NBs. Interestingly, only in VA nuclei were 19S and 11S found at a similar distance away from PML NBs (and in this case 11S seemed to be particularly far away from PML NBs). It may be that in these cells the proteolytic pathway requiring 11S is downregulated for some reason.

Other trends are that the compartments with known transcriptional functions were mostly near to PML NBs (shown by the prevalence of blue compartments on the left hand side of Figure 45). The exception is RNA, which is often found quite far away from PML NBs in terms of the compartment hierarchy, except in MRC-5 VA nuclei. Suprisingly MEHIS was closer to PML NBs than ACHIS in HS, IFN and SS nuclei, but not in ASYNC or VA. However, overall this supports a transcriptional function for PML NBs. The chromosome topology compartments ACA and TELO were amongst those furthest away from PML NBs, and were commonly found close to (ASYNC, SS) or directly next to each other (HS, IFN). This indicates that PML NBs are unlikely to play a major role in functions that may occur at centromeres or telomeres. The exception to this was in the MRC-5 VA nuclei where TELO and ACA are found at opposite ends of the spectrum in terms of median minimum NND from PML NBs. TELO are closest to PML NBs, whereas ACA are furthest. This highly supports the evidence for the association that PML NBs have with telomeric DNA in ALT positive cell lines, of which MRC-5 VA is one. It also still provides evidence for a lack of shared functions with centromeres.

4.4.3.2 WI-38

As shown in Figure 47, in WI38 ASYNC nuclei the closest nuclear compartment to PML NBs according to the median minimum NND was ACHIS, followed by B23, 11S, MEHIS, RNA and RNAPII. Next furthest from PML NBs was SC35, followed by the

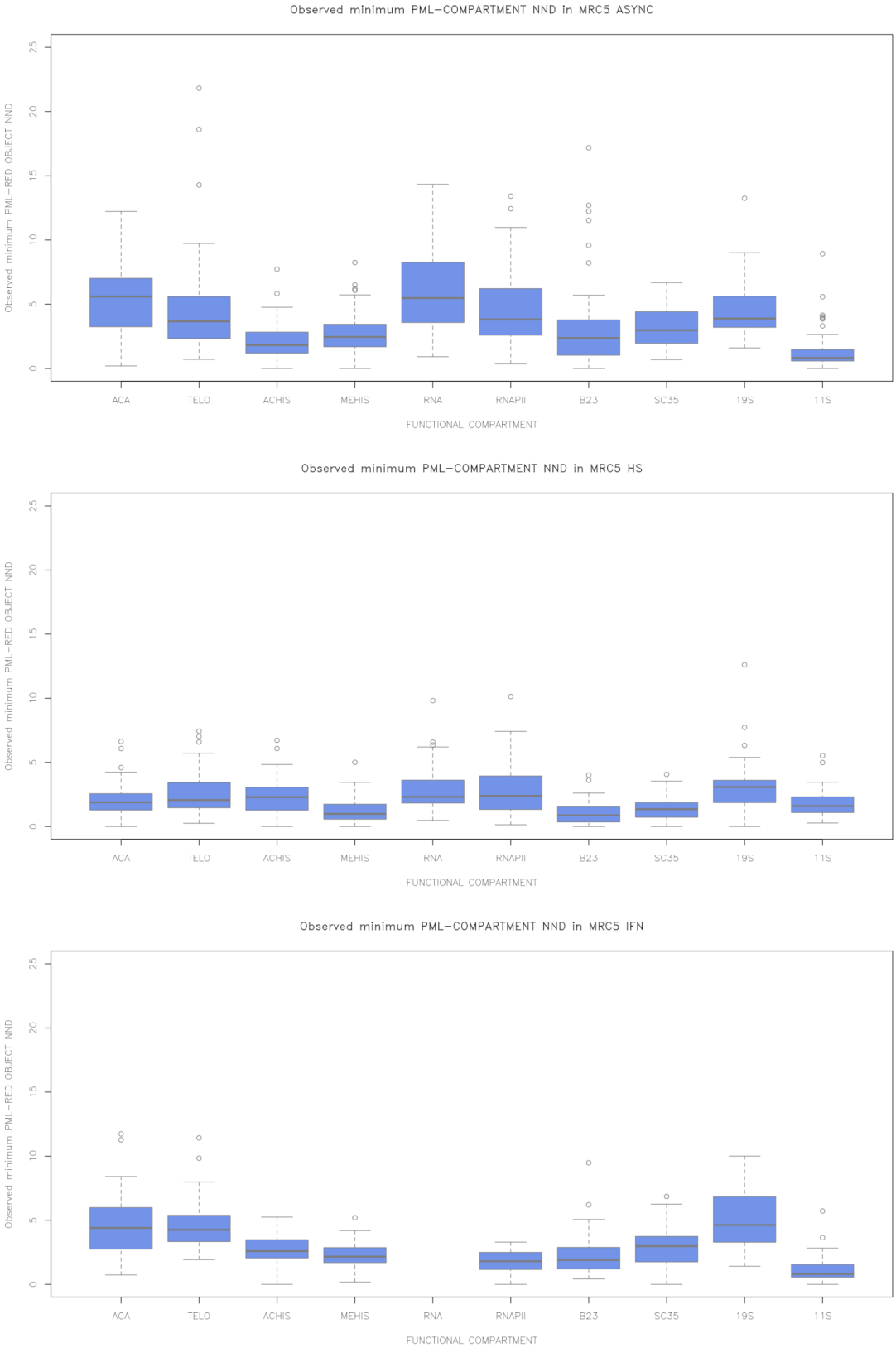


Figure 45 Boxplot of PML NB - functional compartment total minimum NNDs in MRC5 ASYNC, HS and IFN

Minimum NNDs between PML NB and functional compartments, for MRC5. The box represents 50% of the data points, and the median bar crosses the box. Row 1 MRC5 ASYNC: ACA, TELO, ACHIS, MEHIS, RNA, RNAPII, B23, SC35, 19S and 11S (left to right). Row 2 MRC5 HS: ACA, TELO, ACHIS, MEHIS, RNA, RNAPII, B23, SC35, 19S and 11S (left to right). Row 3 MRC5 IFN: ACA, TELO, ACHIS, MEHIS, RNAPII, B23, SC35, 19S and 11S (left to right).

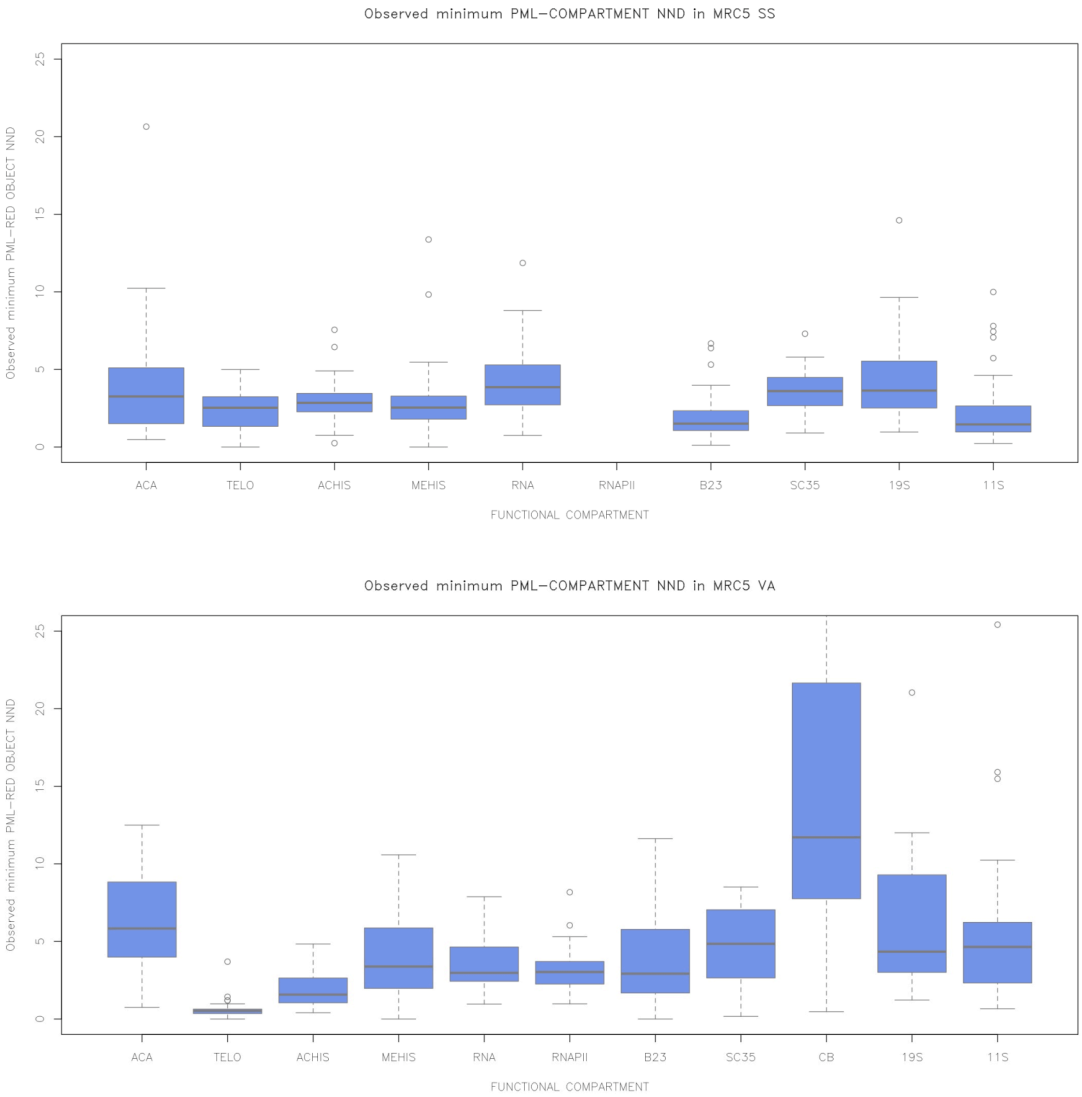


Figure 46 Boxplot of PML NB - functional compartment total minimum NNDs in MRC5 SS and VA

Minimum NNDs between PML NB and functional compartments, for MRC5. The box represents 50% of the data points, and the median bar crosses the box. Row 1 MRC5 SS. Functional compartments ACA, TELO, ACHIS, MEHIS, RNA, B23, SC35, 19S and 11S (left to right). Row 2 MRC5 VA. Functional compartments ACA, TELO, ACHIS, MEHIS, RNA, RNAPII, B23, SC35, CB, 19S and 11S (left to right).

chromosome topology markers ACA and TELO (which was joint furthest from PML NBs with 19S).

In WI38 VA nuclei (Figure 47) the closest compartment to PML NBs was TELO. It was followed by three transcriptional compartments: RNAPII, ACHIS and B23. The next furthest compartment from PML NBs was ACA, and then SC35 and MEHIS. The two proteolytic compartments 11S and 19S followed, and surprisingly CB was the furthest compartment from PML NBs in WI38 VA.

Overall trends included 11S being close to PML NBs in WI38 ASYNC, whilst 19S was far away from PML NBs in both ASYNC and VA nuclei. Interestingly in WI38 VA nuclei 11S was directly adjacent to 19S (with both far away from PML NBs), as was seen in MRC5 VA nuclei also. This shows that the close proximity between PML NBs and 11S also becomes less of a requirement in WI38 VA, as is the case in MRC5 VA nuclei

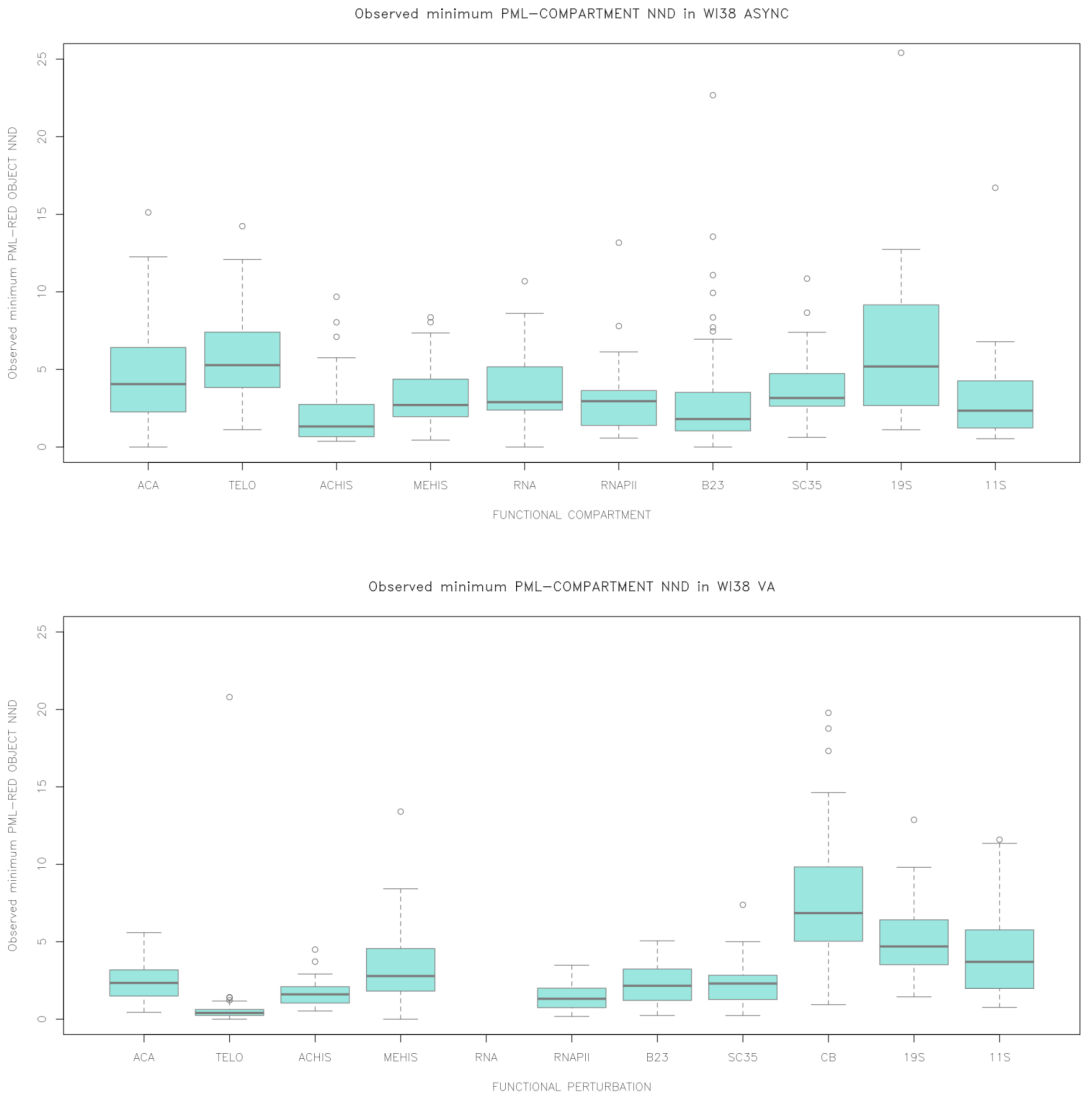


Figure 47 Boxplot of PML NB - functional compartment total minimum NNDs in WI38 ASYNC and VA

Minimum NNDs between PML NB and functional compartments, for WI38. The box represents 50% of the data points, and the median bar crosses the box. Row 1 WI38 ASYNC. Functional compartments ACA, TELO, ACHIS, MEHIS, RNA, RNAPII, B23, SC35, 19S and 11S (left to right). Row 2 WI38 VA. Functional compartments ACA, TELO, ACHIS, MEHIS, RNAPII, B23, SC35, CB, 19S and 11S (left to right).

too. In WI38 ASYNC ACA and TELO were adjacent to each other, as seen in some of the MRC5 nuclei data sets. The transcriptional compartments were once again on the

left hand side of the figure, and grouped together, indicating their relative closeness to PML, in both WI38 ASYNC and VA nuclei. In WI38 VA TELO was the closest compartment to PML NBs (unlike in WI38 ASYNC where it was joint furthest), and this situtation mirrored that which occurred in MRC5 VA nuclei. WI38 VA (like MRC5 VA) are also an ALT positive cell line (Draskovic et al., 2009). Lastly, CB was the furthest from PML NBs according to median minimum NND, which was surprising given the level of association often quoted between the two compartments.

4.4.4 Summary

In Figure 48 functional compartments are arranged according to their median minimum NND from PML NBs, where the nuclear compartment on the left is the closest to PML NBs according to median minimum NND, and those to the right are sequentially found further away in distance from PML NBs. The compartments are also coloured, where yellow compartments indicate chromosome topology markers, blue compartments are involved in transcription, orange compartments have post-transcriptional functions in the nucleus, and pink compartments are involved in proteolysis.

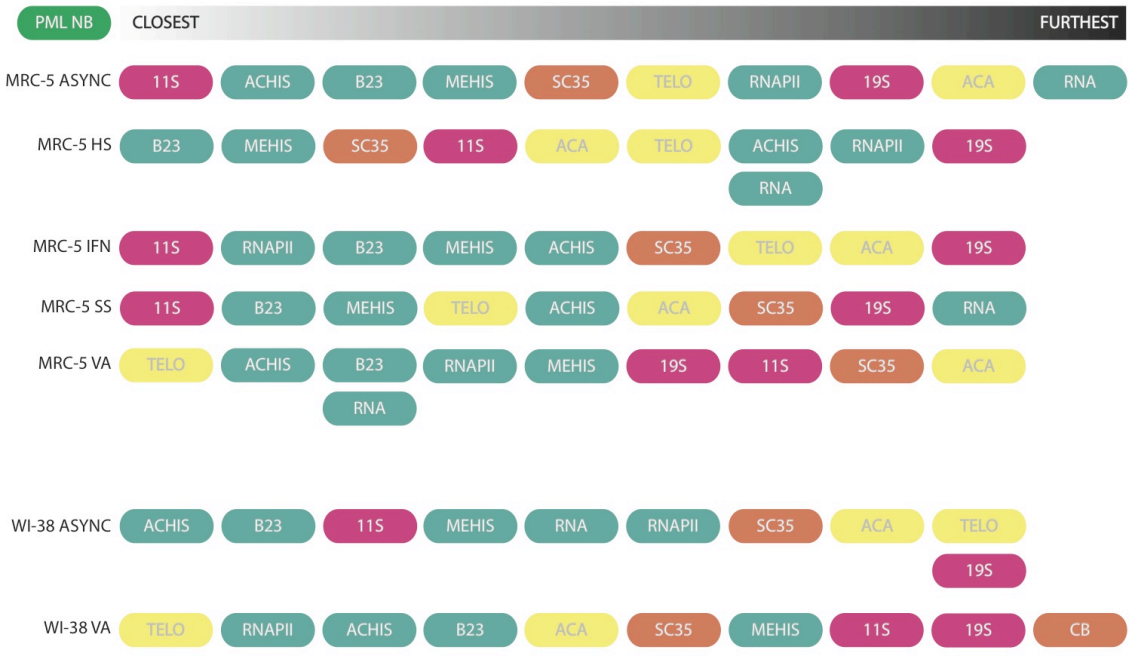


Figure 48 Summary of the median PML NB distance hierarchy from the PML NB to nearest functional compartment in MRC5 ASYNC, HS, IFN, SS, VA and WI38 ASYNC and VA nuclei

Data sets are ordered by median minimum nearest neighbour distance (NND) between PML NB and the functional compartment. Closest to furthest from the bodies (left to right).

4.5 PML NB – functional compartment CSR analysis for MRC5 and WI38

4.5.1 Introduction

The spatial organization of PML NBs with respect to functional nuclear compartments was tested using CSR analysis. The NND between each PML NB in a nucleus and the nearest compartment voxel was plotted and the curve compared to a simulation envelope created by simulating the location of the same PML NBs 999 times within the nucleus according to the CSR SPP. Strong functional relationships between PML NBs and other compartments may be indicated by a high percentage of nuclei containing PML NBs that are closer to the functional compartment than expected under the hypothesis of CSR. Weak relationships (indicating no shared function) may be revealed when a low number or no nuclei in a dataset contain PML NBs that are closer to the compartment than expected. Repulsion between compartments may even be indicated by nuclei containing PML NBs that are further from the compartment than expected under CSR. Effects of a treatment or transformation upon the PML NB – compartment relationship may be shown as an increase or decrease in the percentage of PML NBs that are classified as being closer to a compartment than in the corresponding ASYNC dataset.

4.5.2 PML NB – functional compartment CSR analysis

4.5.2.1 Centromeres (ACA)

There are cells in which centromeres (ACA), as shown by the foci immunofluorescently stained by a human autoantibody raised against centromeric proteins, are significantly closer to PML NBs than we would expect under CSR in all of the asynchronous, heat shocked, IFNβ-treated, and serum starved MRC5 cell populations tested, but not in SV40 T-Ag transformed MRC5 cell populations (Figure 49). Only in the SV40 T-Ag transformed MRC5 data set were there cells in which ACA foci were significantly further from PML NBs than we would expect under CSR, but which are a very small proportion of the total cells tested.

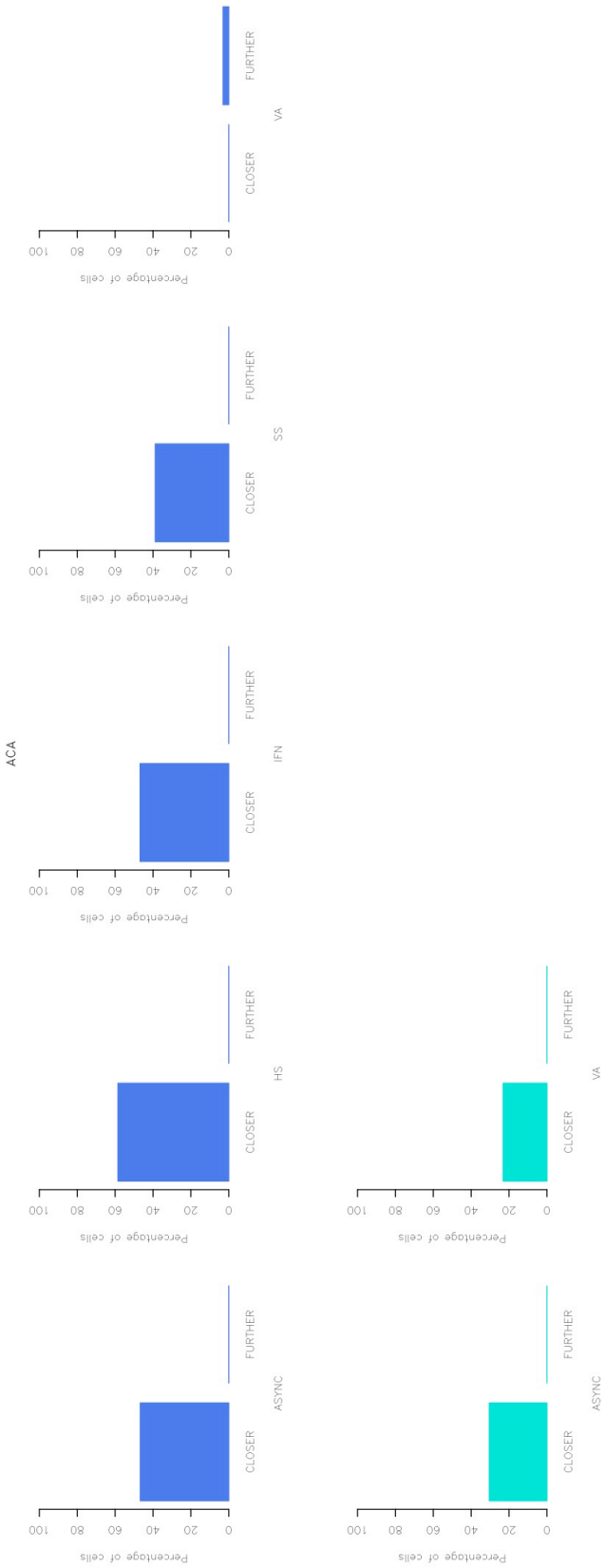


Figure 49 PML NB - centromeres spatial organisation under CSR

Percentage of nuclei rejecting CSR according to observed minimum PML NB - compartment NNDs. Observed minimum PML NB - compartment NNDs for each nucleus in a dataset were compared with simulations for the same PML NBs under CSR. PML NBs were either closer to or further from chromosome topology compartments than expected under CSR. Row 1 MRC5: ASYNC, HS, IFN, SS, VA. Row 2 WI38: ASYNC, VA.

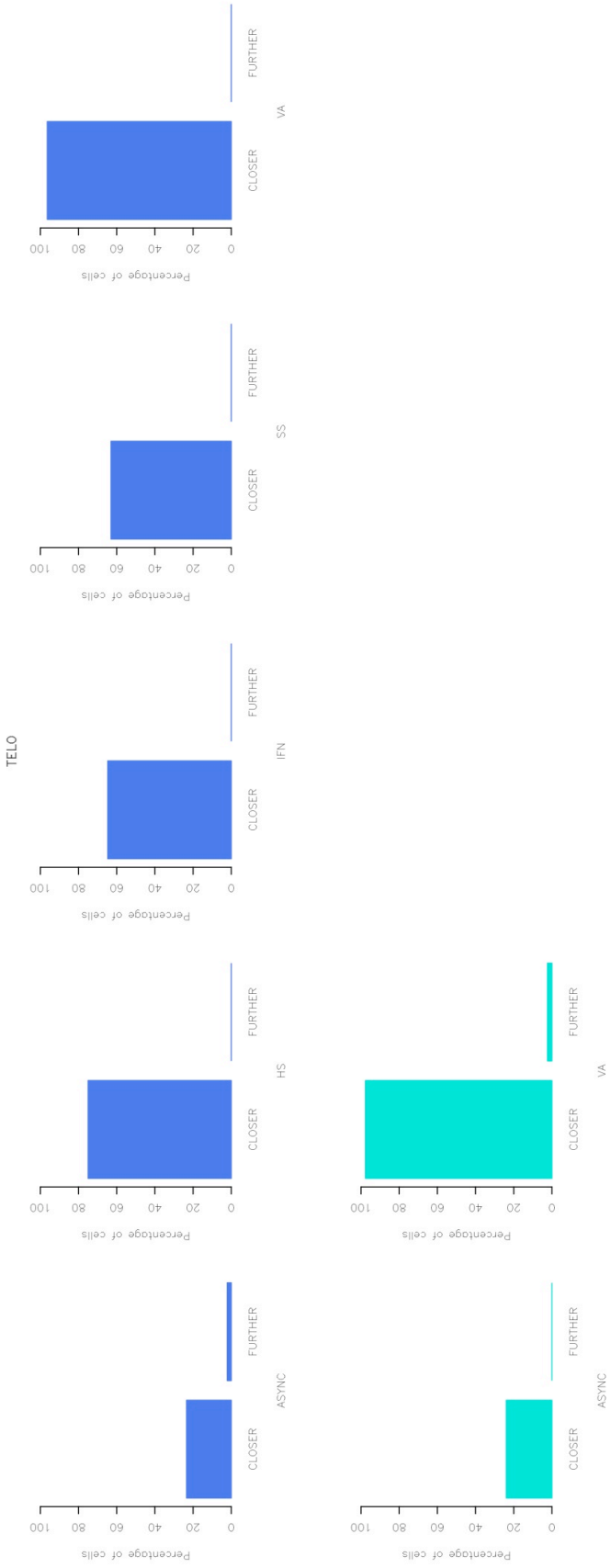


Figure 50 PML NB - telomeres spatial organisation under CSR

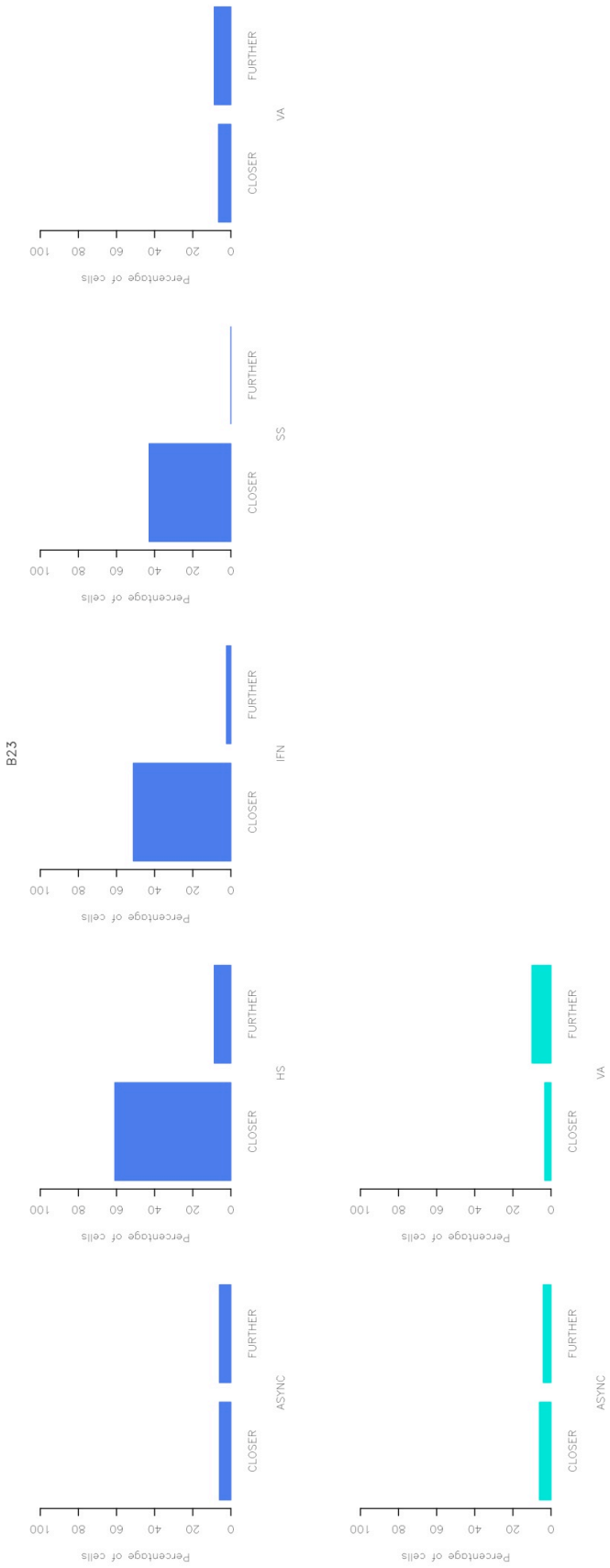


Figure 51 PML NB - nucleoli spatial organisation under CSR

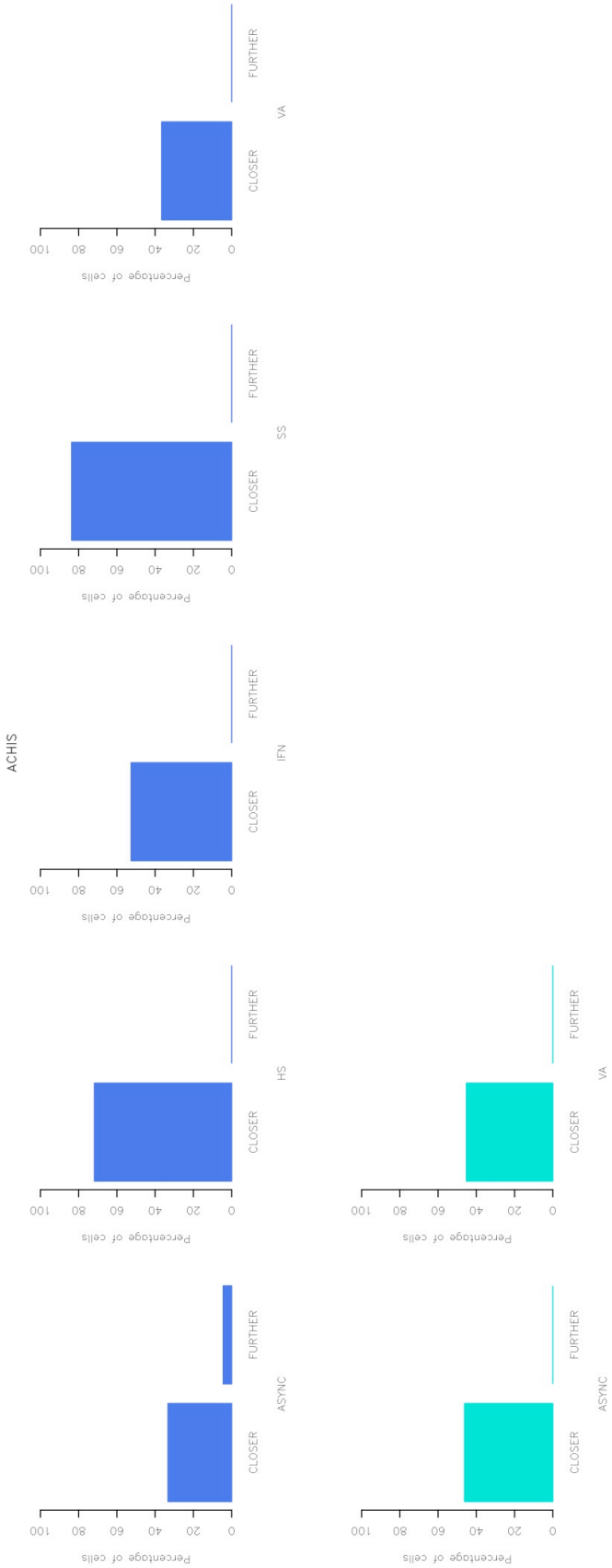


Figure 52 PML NB - acetylated histone spatial organisation under CSR

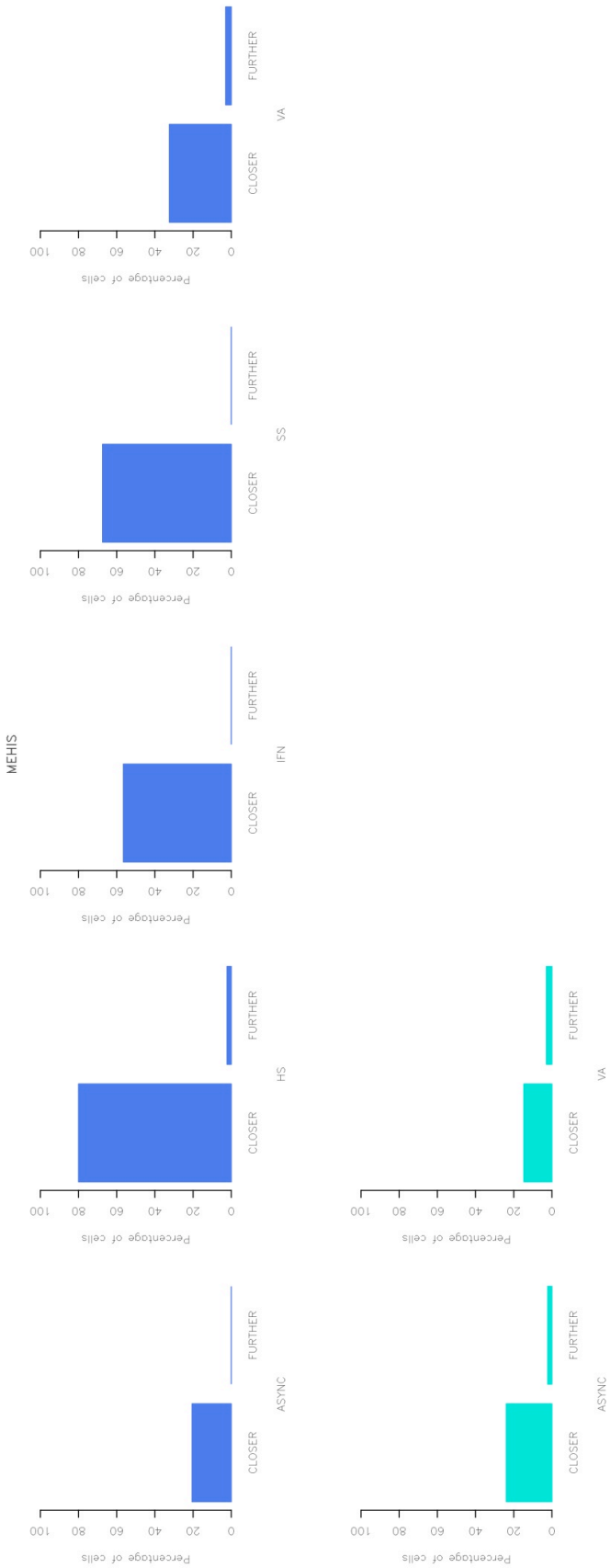


Figure 53 PML NB - methylated histone spatial organisation under CSR

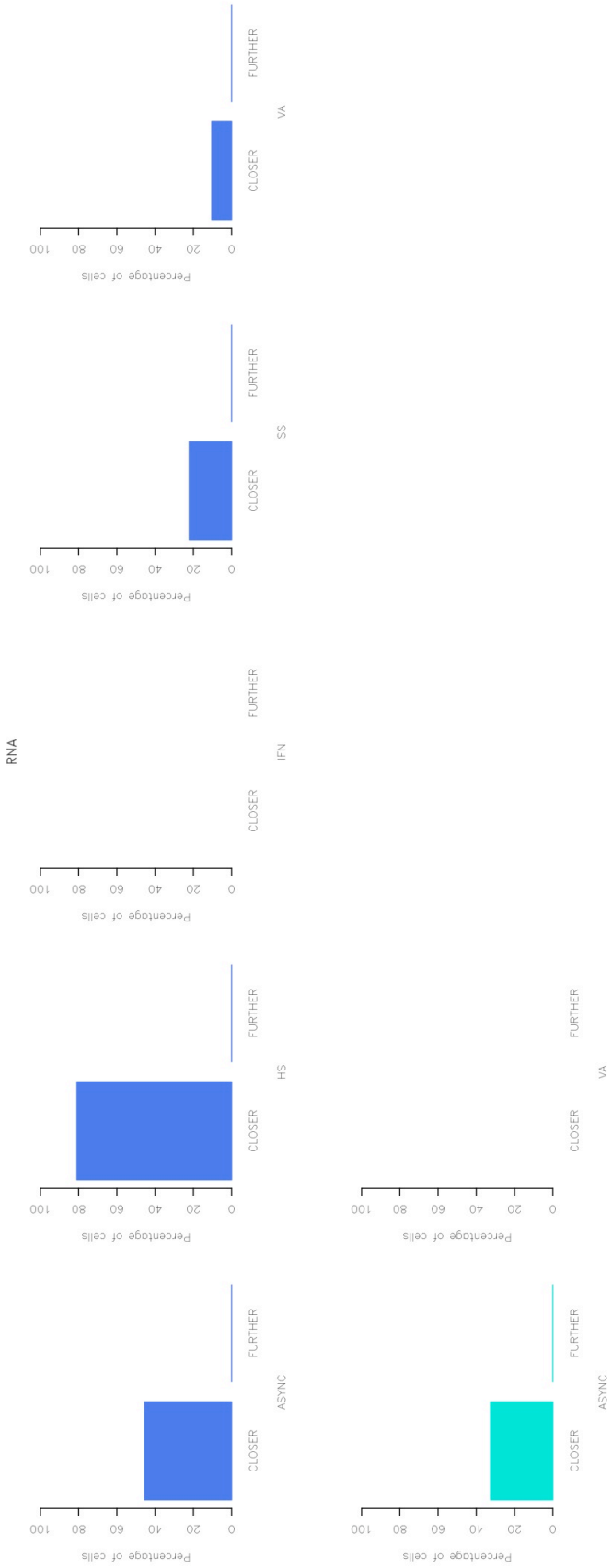


Figure 54 PML NB - nascent RNA spatial organisation under CSR

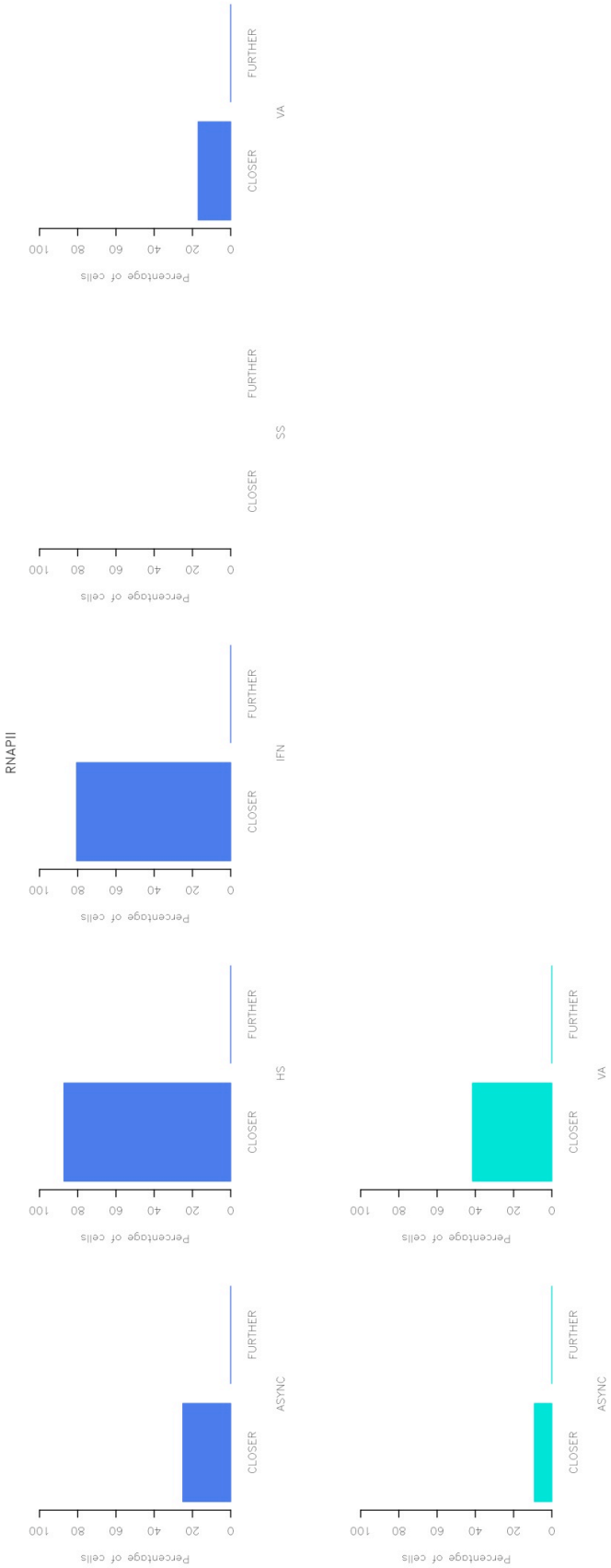


Figure 55 PML NB - RNA polymerase II spatial organisation under CSR

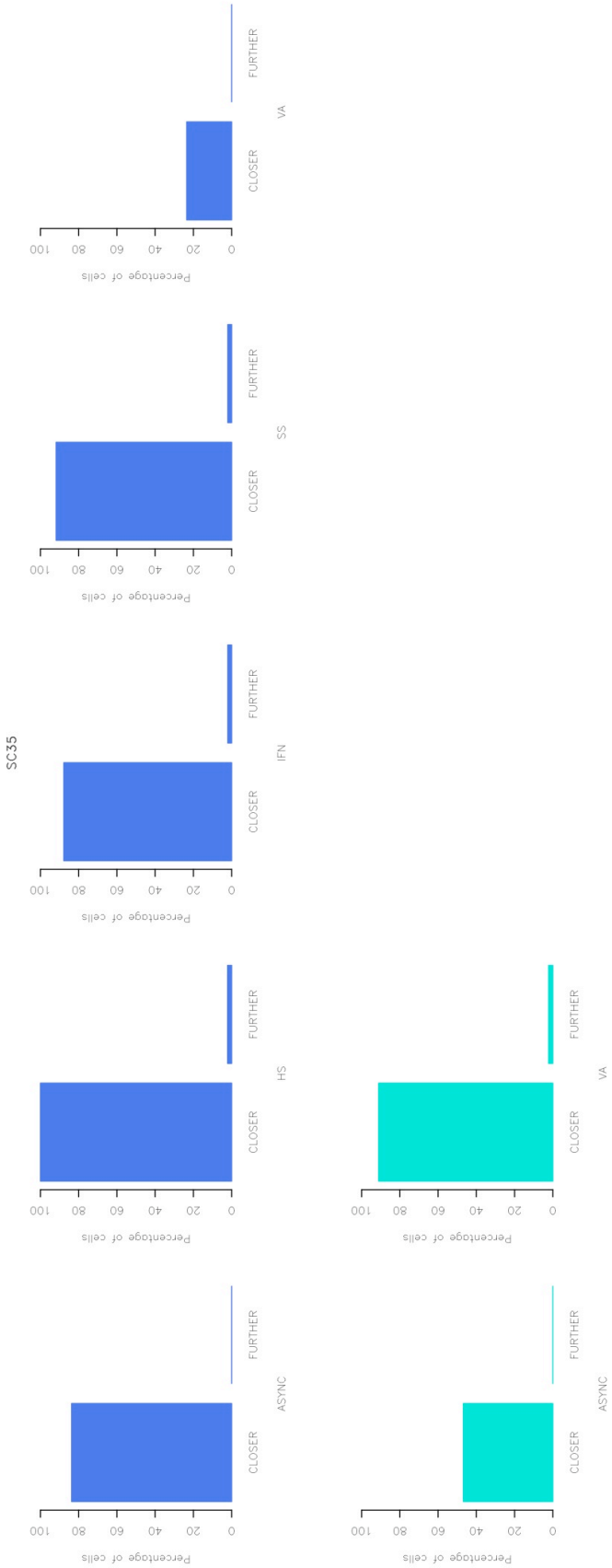


Figure 56 PML NB - SC35 domains spatial organisation under CSR

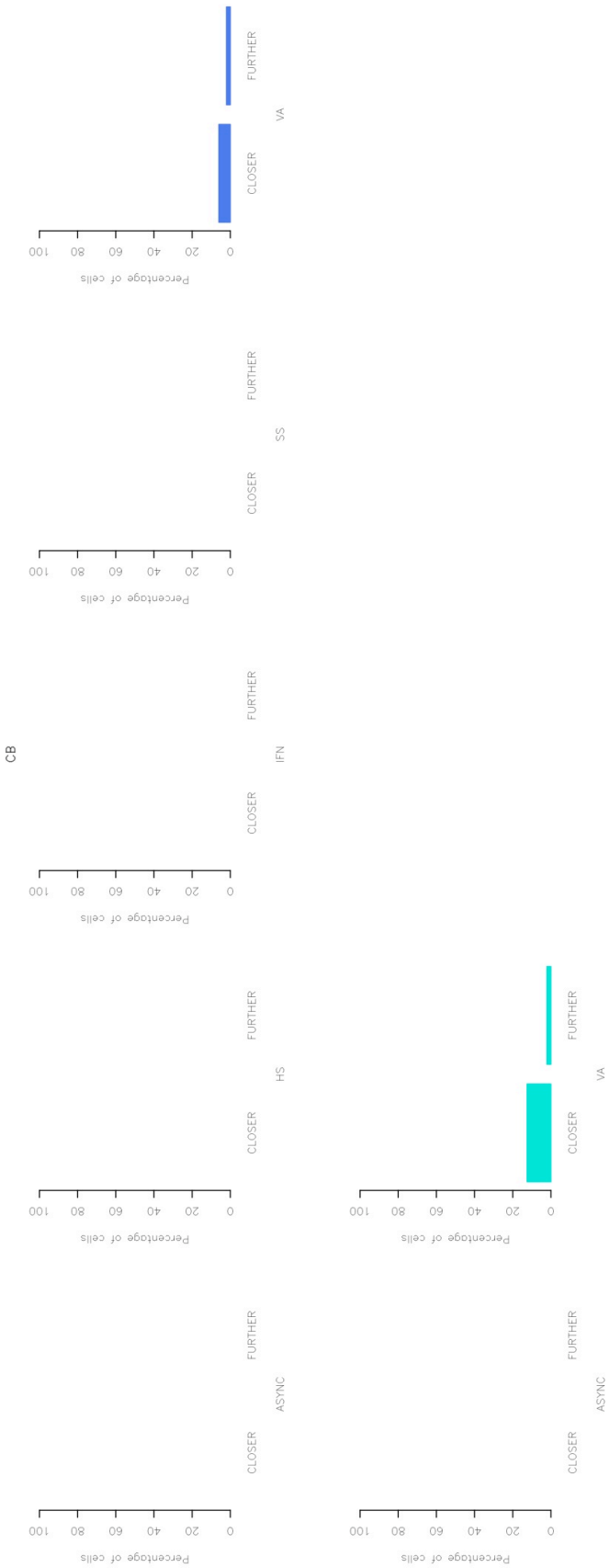


Figure 57 PML NB - Cajal bodies spatial organisation under CSR

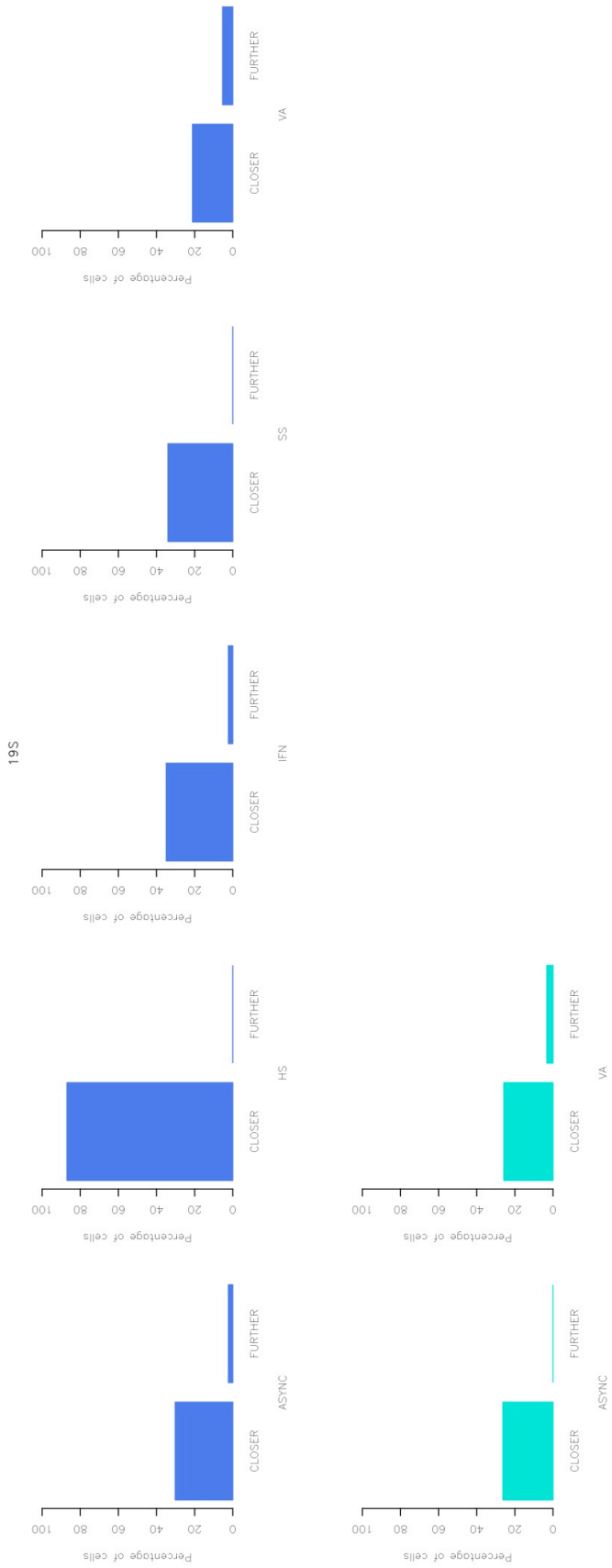


Figure 58 PML NB - 19S spatial organisation under CSR

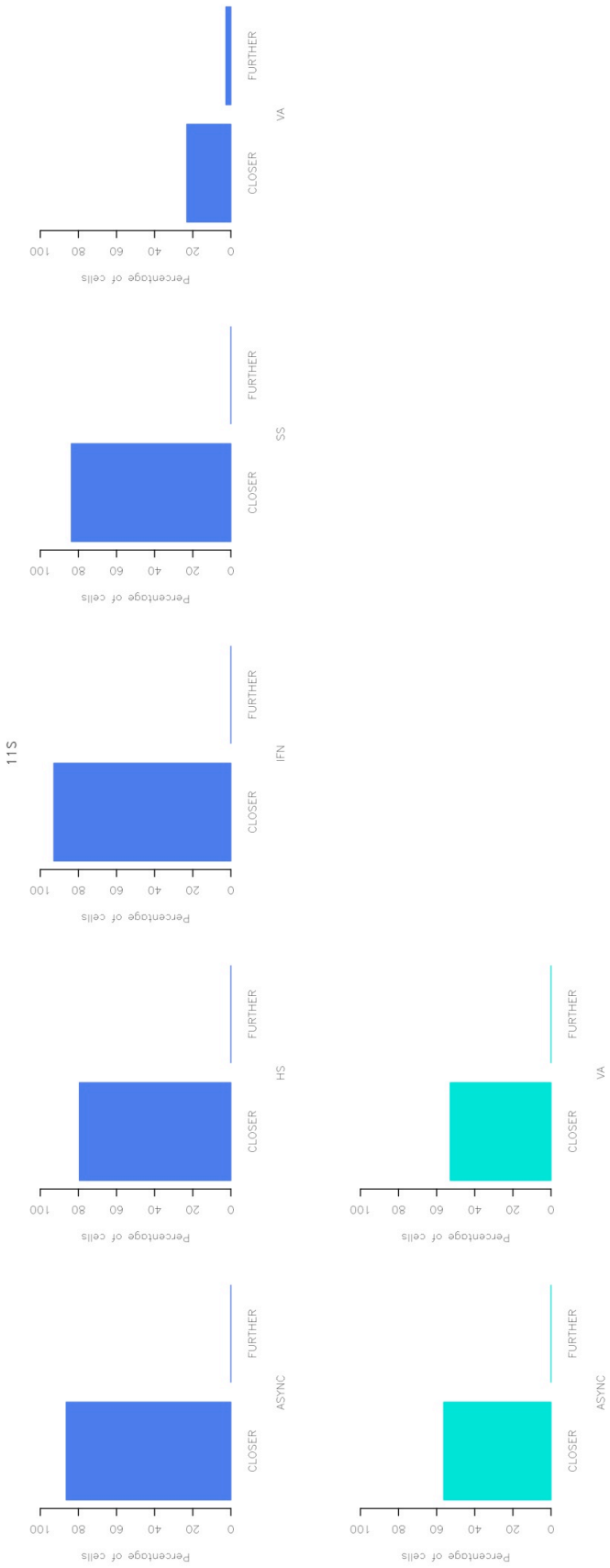


Figure 59 PML NB - 11S spatial organisation under CSR

In asynchronous MRC5 cells there is a significantly closer association between ACA foci and PML NBs in 46.7% of the cells tested (n = 45). Under conditions of heat shock this association rose to 58.5% of cell nuclei (n = 41) containing ACA foci that are closer to PML NBs than expected under CSR. In IFNβ-treated cells a similar percentage of cells to the asynchonrous data set (46.8% (n = 47)) showed ACA foci significantly closer to PML NBs than we might expect under CSR. In serum starved cells, 38.8% percent of the cells tested had ACA foci showing a significantly closer association with PML NBs, (n = 49), and in SV40 T-Ag transformed no cells at all showed ACA foci that were significantly closer to PML NBs than expected under CSR (0% (n = 33).

There appears to be an association between centromeres and PML NBs in quite a large proportion of the cells in all the data sets bar MRC5VA cell nuclei. Therefore we see some kind of association between centromeres and PML NBs in about half of all asynchronous cells tested in a population. Treatment with IFNβ overnight does not apparently affect this association at all. An increase in the proportion of cells containing centromeres that were significantly closer to PML NBs in heat-shocked cells (compared to the asynchronous population) indicates that this stress may be inducing this association further. A decrease in the proportion of cells in which centromeres show a significantly closer association with PML NBs than expected under CSR in serum-starved cells indicates that there may be some reorganisation in these cells, which lessens the association. The MRC5VA cell populations also contained some cells that showed ACA foci that were classified as being significantly further from PML NBs than expected under CSR, in a very small proportion of cells (about 3%, n = 33). This is unlikely to be meaningful.

In WI38 ASYNC nuclei 30.4% (n = 46) contained PML NBs that were closer to ACA than expected under CSR, and in WI38 VA nuclei this was true in 23.1% (n = 39). However no nuclei contained PML NBs that were further from ACA than expected in either ASYNC or VA cells. This was different to that seen for MRC5 ASYNC and VA.

4.5.2.2 Telomeres (TELO)

There are cells in which telomeres, as represented by immunofluorescent staining of TRF-1, a protein which binds telomeric DNA, are significantly closer to PML NBs than

we would expect under CSR in all of the asynchronous, heat shocked, IFNβ-treated, serum starved and SV40 T-Ag transformed MRC5 cell populations (Figure 50). Only in the asynchronous data set were there cells in which telomeres were significantly further from PML NBs than we would expect under CSR, but which are a very small proportion of the total cells tested.

In asynchronous MRC5 cells there is a significantly closer association between telomeres and PML NBs in 23.4% of the cells tested (n = 47). Under conditions of heat shock this association increased, rising to 75% of cell nuclei (n = 40) containing telomeres that are closer to PML NBs than expected under CSR. In IFNβ-treated cells a slightly smaller proportion of cells tested (64.7% (n = 34)) showed telomeres significantly closer to PML NBs than we might expect under CSR. In serum starved cells, a simlar percentage of the cells tested had telomeres showing a significantly closer association with PML NBs, (63% (n = 46)), and in SV40 T-Ag transformed cells showed the highest percentage of cells containing telomeres that are significantly closer to PML NBs than expected under CSR (96.4% (n = 28). This is a particularly strong association between telomeres and PML NBs which can be seen in almost all MRC5VA cell nuclei, compared to only about a quarter of the asynchronous MRC5 cells. This indicates that the transformation of MRC5 fibroblasts with the SV40 T-Ag has resulted in this increased association, and is likely due to MRC5VA being an ALT positive cell line. The high percentage of cells containing telomeres that show significantly closer associations with PML NBs than we would expect in the heat shock, IFNβ-treated, and serum-starved populations highlights that cellular stresses may also lead to an increase in closer telomere – PML NB associations.

Telomere morphology is varied between asynchronous MRC5 cells and their transformed counterparts, MRC5VA, and this is a direct result of the latter's ALT positive status.

Only in the asynchronous MRC5 cell population were there some cells that showed telomeres that were classified as being significantly further from PML NBs than expected under CSR, and this was only in a very small proportion of cells (2.1%, n = 47). This is unlikely to be meaningful.

In asynchronous WI38 cell nuclei 23.9% (n = 46) of cells tested contained PML NBs that were closer to telomeres than expected under CSR, but in WI38VA cells this rose dramatically to 97.7% (n = 43) of cells containing such PML NBs. This is very similar to that seen in MRC5 nuclei; where 23.4% and 96.4% of asynchronous cells and MRC5VA respectively, contained PML NBs that were closer to telomeres than expected under CSR. Therefore it is likely that there is a normal association between telomeres (or telomeric DNA) and PML NBs, but that this is attenuated in SV40 T-Ag cells, due to the cells becoming ALT positive as a consequence of their transformation.

These similar trends for telomeres in MRC5 and WI38 cell nuclei also serve to show that it is a suitable comparison (and a positive control) between the MRC5 and WI38 cell lines, as trends like this can be seen, but any differences seen may therefore be cell line specific.

2.3% of nuclei in WI38 ASYNC contain PML NBs that were further from telomeres than expected. This is very similar to that seen in MRC5 nuclei; where 2.1% and 0% of asynchronous cells and MRC5VA respectively, contained PML NBs that were further from telomeres than expected under CSR.

4.5.2.3 Acetylated histones (ACHIS)

There are cells in which acetylated histone (ACHIS) are significantly closer to PML NBs than we would expect under CSR in all of the asynchronous, heat shocked, IFNβ-treated, serum starved and SV40 T-Ag transformed MRC5 cell populations (Figure 52). Only in the asynchronous data set were there cells in which ACHIS foci were significantly further from PML NBs than we would expect under CSR, but which are a very small proportion of the total cells tested.

In asynchronous MRC5 cells there is a significantly closer association between ACHIS foci and PML NBs in 33.3% of the cells tested (n = 45). Under conditions of heat shock this association doubled, rising to 71.8% of cell nuclei (n = 39) containing ACHIS foci that are closer to PML NBs than expected under CSR. In IFNβ-treated fewer cells that were tested (52.6% (n = 38)) showed ACHIS foci significantly closer to PML NBs than we might expect under CSR. In serum starved cells, over 80% of the cells tested had

ACHIS foci showing a significantly closer association with PML NBs, (83.7% (n = 43)), and in SV40 T-Ag transformed cells showed a similar percentage of cells to the asynchronous population containing ACHIS foci that were significantly closer to PML NBs than expected under CSR (36.6% (n = 41). This is interesting as it shows a similar trend to the $RNAPII_O$ and MEHIS foci in that asynchronous MRC5 and MRC5VA show a similar percentage of cells whose foci show a significantly closer association to PML NBs that would be expected under CSR. Maybe this means that this relationship is not affected by transformation of the cell. Once again the infliction of a stress upon the cell population seems to induce an association between the compartment (here ACHIS foci) and PML NBs in much higher proportion of cells tested in these data sets. The effect was most pronounced in serum-starved cells. This was unexpected because one might expect ACHIS foci to be less active in serum-starved cells due to a lower global activity and growth rate of the cell. However, it should be considered that ACHIS foci are ACHIS foci whatever the transcriptional status of the cell, and therefore if the association between PML NBs needs to be maintained then it would still exist. However, it is not obvious why the association should increase. It could be that due to compaction of DNA in serum starved cells the areas of ACHIS are more accessible to PML NBs as the channels are wider?

The asynchronous cell populations also contained some cells that showed ACHIS foci, which were classified as being significantly further from PML NBs than expected under CSR, in a very small proportion of cells (4.4%, n = 45). This is unlikely to be meaningful.

In WI38 ASYNC and VA nuclei 46.2% (n = 39) and 45.2% (n = 31), respectively, contained PML NBs that were closer to ACHIS than expected under CSR. No nuclei in either contained PML NBs that were further from ACHIS than expected.

4.5.2.4 Methylated histones (MEHIS)

There are cells in which methylated histone (MEHIS), as shown by foci immunofluorescently stained by an antibody raised against the histone H3 K9 K27 dimethylation marker, are significantly closer to PML NBs than we would expect under CSR in all of the asynchronous, heat shocked, IFNβ-treated, serum starved and SV40 T-

Ag transformed MRC5 cell populations (Figure 53). Only in the heat shock and SV40 T-Ag transformed MRC5VA data set were there cells in which MEHIS foci were significantly further from PML NBs than expected under CSR, but which are a very small proportion of the total cells tested.

In asynchronous MRC5 cells there is a significantly closer association between MEHIS foci and PML NBs in 20.5% of the cells tested (n = 39). Under conditions of heat shock this association greatly increased, rising to 80% of cell nuclei (n = 45) containing MEHIS foci that are closer to PML NBs than expected under CSR. In IFNβ-treated fewer cells that were tested (56.5% (n = 46)) showed MEHIS foci significantly closer to PML NBs than we might expect under CSR. In serum starved cells, almost 70% percent of the cells tested had MEHIS foci showing a significantly closer association with PML NBs, (67.4% (n = 46)), and in SV40 T-Ag transformed cells showed a greater percentage of cells to the asynchronous population containing MEHIS foci that were significantly closer to PML NBs than expected under CSR (32.4% (n = 34). Once again the infliction of a stress upon the cell population seems to induce an association between the compartment (here MEHIS foci) and PML NBs in much higher proportion of cells tested in these data sets. The effect was most pronounced in heat-shocked cells.

The heat shock and MRC5VA cell populations also contained some cells that showed MEHIS foci which were classified as being significantly further from PML NBs than expected under CSR, in a very small proportion of cells (2.2%, n = 45, and 2.9%, n = 34 for heat shock and MRC5VA respectively). This is unlikely to be meaningful.

In WI38 ASYNC and VA nuclei 23.9% (n = 46) and 14.7% (n = 34), respectively, contained PML NBs that were closer to MEHIS foci than expected under CSR. 2.2% (n = 46) and 2.9% (n = 34), of ASYNC and VA nuclei respectively, contained PML NBs that were further from MEHIS than expected under CSR. This was unlikely to be significant.

4.5.2.5 Nascent RNA (RNA)

Sites of nascent RNA transcription are significantly closer to PML NBs than expected under CSR in asynchronous MRC5 cells, and also in SV-40 T-Ag transformed MRC5

cells, and asynchronous MRC5 cells which have been subjected to the stress of either being heat shocked or serum-starved (Figure 54). There were no cells in which sites of nascent RNA were significantly further from PML NBs than we would expect under CSR.

In asynchronous MRC5 cells there is a significant association between sites of nascent RNA transcription and PML NBs in just under half of the cell population tested (45.5%, n = 33). Under conditions of heat shock this association is significantly increased, rising to 80.9% of cell nuclei (n = 47) with nascent RNA sites being closer to PML NBs than expected under CSR. However in both serum starved and SV40 T-Ag transformed cells, a much smaller proportion of cells had nascent RNA foci showing a significant association with PML NBs, (22.2% (n = 45) and 10.4% (n = 48) respectively). This is interesting because globally one might expect serum starved and transformed MRC5 cells to be at opposite ends of the spectrum transcriptionally, yet nascent RNA foci from both show little significant association with PML NBs.

There is no result for IFNβ-treated MRC5 cells because it was not possible to collect a data set where the nascent RNA formed sufficiently punctate foci to allow accurate and representative segmentation using the SCT algorithm.

32.6% (n = 46) of WI38 ASYNC nuclei contained PML NBs that were closer RNA foci than expected under CSR. No ASYNC nuclei contained PML NBs that were further from RNA than expected under CSR.

4.5.2.6 RNA polymerase II_O (RNAPII)

In the asynchronous, heat shock, IFNβ-treated, and SV40 T-Ag transformed cell populations tested there are cells in which the elongation form of RNA polymerase II ($RNAPII_O$) is significantly closer to PML NBs than we would expect under CSR (Figure 55).

In asynchronous MRC5 cells there is a significantly closer association between $RNAPII_O$ foci and PML NBs than expected under CSR in 25% of the cells tested (n = 40). Under conditions of heat shock the percentage of cells classified as having association greatly

increased, rising to 87.2% of cell nuclei (n = 47) containing $RNAPII_O$ foci that are closer to PML NBs than expected under CSR. In IFNβ-treated cells a slightly smaller proportion of cells tested (80.6% (n = 36)) showed $RNAPII_O$ foci significantly closer to PML NBs than we might expect under CSR. Unexpectedly, SV40 T-Ag transformed cells showed an association level similar to that of asynchronous cells, with only 17% of cells (n = 47) containing $RNAPII_O$ foci that are significantly closer to PML NBs than expected under CSR.

It seems stressing the cells with either heat shock, or the addition of IFNβ overnight leads to an increase in cells which have $RNAPII_O$ foci significantly closer to PML NBs.

There are no cells in any of the populations (asynchronous, heat shock, IFNβ-treated, or SV40 T-Ag transformed) that contained RNAPII that was shown to be significantly further from PML NBs than expected under CSR.

There is no result for serum-starved MRC5 cells because staining of $RNAPII_O$ was extremely weak and unusable by the SCT algorithm. This indicates that there is little active transcription going on in these cells.

Compared to 9.1% (n = 33) of WI38 ASYNC nuclei that contained PML NBs that were closer to $RNAPII_O$ foci than expected under CSR, four times as many (41.5%, n = 41) cells were classified as having PML NBs that were closer in WI38VA cells. This is dissimilar to that seen in MRC5 nuclei; where 25% and 17% of asynchronous cells and MRC5VA respectively, contained PML NBs that were closer to $RNAPII_O$ foci than expected under CSR.

No WI38 nuclei contained PML NBs that were closer to RNAPII foci than expected. This is very similar to that seen for MRC5 nuclei; where 0% of both asynchronous cells and MRC5VA, contained PML NBs that were closer to $RNAPII_O$ foci than expected under CSR.

Overall it can be seen that there are some differences between the VA nuclei for both cell lines regarding their closeness to $RNAPII_O$ foci.

4.5.2.7 Nucleoli (B23)

There are cells in which nucleoli, as represented by immunofluorescent staining of nucleophosmin (B23), are significantly closer to PML NBs than we would expect under CSR in all of the asynchronous, heat shocked, IFNβ-treated, serum starved and SV40 T-Ag transformed MRC5 cell populations (Figure 51). However, there are also some cells in all of those data sets (except serum-starved) where nucleoli are significantly further from PML NBs than we would expect under CSR, but in much lower proportions.

In asynchonous MRC5 cells there is a significantly closer association between nucleoli and PML NBs in only about 6% of the cells tested (n = 50). Under conditions of heat shock this association was much higher, rising to about 60.9% of cell nuclei (n = 46) containing nucleoli that are closer to PML NBs than expected under CSR. In IFNβ-treated cells about half of cells (51.2% (n = 43)) showed nucleoli significantly closer to PML NBs than we might expect under CSR. In serum starved cells, a slightly smaller proportion of cells had nucleoli showing a significant association with PML NBs, (42.9% (n = 35)), and in SV40 T-Ag transformed only about 6.5% of cells (n = 46) contain nucleoli that are significantly closer to PML NBs than expected under CSR. This clearly indicates that stresses on the cell, be they of different types, seem to induce a significantly closer association between nucleoli and PML NBs. It has been shown that certain stresses on the cell can result in PML being dragged to nucleoli (Bernardi et al., 2004; Condemine et al., 2007). One might therefore also expect that nucleoli in MRC5VA cells to be closer in a large proportion of cells tested, but this was not the case.

It is important to consider the different morphologies of nucleoli across the data sets, with the most significant difference being seen between asynchronous, serum starved and SV40 transformed MRC5 cells. However, this cannot account for the much higher proportion of nucleoli significantly closer to PML NB cells in the heat shock and IFNβ-treated data sets where appearance of nucleoli is similar to that in asynchronous cells.

Percentages of cells with nucleoli that are significantly further from PML NBs than expected under CSR are under 10% for all data sets (asynchronous (6%), heat shock (8.7%), IFNβ-treated (2.3%), and VA cells (8.7%). In serum starved cells there are no cells in which nucleoli are significantly further from PML NBs than we would expect

under CSR. This shows that stresses do not appear to induce movement of PML NBs away from nucleoli, and also that in an asynchronous cell population PML NBs are not typically arranged to be particularly far or close to nucleoli. This confirms the view that PML NBs do not typically associate with nucleoli for a shared function (and may indeed be excluded from them) until stress induces a movement of PML towards the nucleolus. This is not just a movement of PML protein as might be expected from Bernardi et al, but there is an actual rearrangement of PML NBs towards nucleoli.

In WI38 ASYNC and VA nuclei 6.1% (n = 49) and 3.3% (n = 30), respectively, contained PML NBs that were closer to B23 than expected under CSR. 4.1% and 10%, of ASYNC and VA nuclei respectively, contained PML NBs that were further from B23 than expected under CSR. None are these results show any particular association between PML NBs and nucleoli in WI38 ASYNC and VA nuclei.

4.5.2.8 Splicing speckles (SC35)

In 83.7% of MRC5 ASYNC nuclei (n = 49) PML NBs are closer to SC35 splicing speckles than expected under the hypothesis of CSR (Figure 56). This rose to 100% of HS nuclei (n = 48) containing PML NBs that were closer to SC35 than we would have expected. In IFN treated cells 87.8% (n = 49) of nuclei contained PML NBs that were closer than expected, and in SS cells this was slightly higher at 91.8% (n = 49). 23.5% of VA cells contained such PML NBs, where n = 34. Interestingly in HS, IFN and SS cells 2.1, 2.0 and 2.0 % of nuclei respectively also contained PML NBs, which were further from splicing speckles than we would expect under CSR.

In 46.8% of WI38 ASYNC nuclei (n = 47) PML NBs were closer to SC35 than expected under CSR. In VA nuclei 91.1% of nuclei (n = 45) contained PML NBs who were closer to SC35 than expected. There were no nuclei with PML NBs further from SC35 than expected in ASYNC, but there were in 2.2% of VA nuclei. This is not significant.

4.5.2.9 Cajal bodies (CB)

In only 6% of MRC5 VA nuclei (n = 50) were there PML NBs that were closer to Cajal bodies than expected (Figure 54). Cajal bodies are not present in ASYNC cell populations and so could not be quantified in these. 2.0% of VA nuclei also contained PML NBs that were further from CB than expected under the hypothesis of CSR.

In 12.5% of WI38 VA nuclei (n = 48) PML NBs were closer to Cajal bodies (CB) than expected under the hypothesis of CSR. In 2.1% of VA nuclei PML NBs were further from PML NBs than expected. There were no Cajal bodies present in ASYNC nuclei, and therefore this could not be looked at in that cell line. The association between PML NBs and Cajal bodies in both MRC5 VA and WI38 VA is lower than expected, especially according to other findings (Grande et al., 1996; Sun et al., 2005). This is likely to be due to differences in object number between PML NBs and Cajal bodies, and is discussed further in Section 6.3.4.2.1.

4.5.2.10 19S core proteasome regulator (19S)

There are cells in which 19S proteasome regulator (19S) are significantly closer to PML NBs than we would expect under CSR in all of the asynchronous, heat shocked, IFNβ-treated, serum starved MRC5 cell populations, and in SV40 T-Ag transformed MRC5 cell populations (Figure 58). In the asynchronous, IFNβ-treated, and SV40 T-Ag transformed MRC5 data set there were also cells in which 19S foci were significantly further from PML NBs than we would expect under CSR, but which are a small proportion of the total cells tested.

In asynchronous MRC5 cells there is a significantly closer association between 19S foci and PML NBs in 30.2% of the cells tested (n = 43). Under conditions of heat shock this association rose greatly to about 87% of cell nuclei (n = 46) that contained 19S foci that are closer to PML NBs than expected under CSR. In IFNβ-treated cells 34.9% (n = 43)) showed 19S foci significantly closer to PML NBs than we might expect under CSR. In serum starved cells, 34% percent of the cells tested had 19S foci showing a significantly closer association with PML NBs, (n = 47), but in SV40 T-Ag transformed only 21.1% of cells showed 19S foci that were significantly closer to PML NBs than expected under

CSR (n = 38).

In all the data sets bar HS cell nuclei there appears to be an association between 19S foci and PML NBs in about 20-35% of cells tested, and thus this appears to be a standard relationship that is not affected by stressing the cell with IFNβ-treatment or serum-starvation. However in the heat shocked cell population of MRC5 fibroblasts 19S foci are significantly closer to PML NBs than expected under CSR in the vast majority of cells (87% of those tested). This particular treatment seems to greatly increase this association. It could be that heat shock induces protein denaturation on a global scale, and thus there is a need for the core proteasome to suddenly move into action. (This may not be seen so much in the 11S proteasome data sets because HS would not just induce immunoproteasome-related proteolysis, but would link it to increasing the core proteasome association with PML NBs instead. The 11S proteasome regulator probably has a high association with PML NBs in general anyway, which is increased slightly when the cells are treated with IFNβ, which mimics viral infection and thus immuno-linked proteolysis). In SV40 T-Ag transformed MRC5 cells there is an even lower percentage association than in the asynchronous data set (21.1% of cells) between 19S foci and PML NBs, and that this may be a consequence of transformation, similar to the loss seen for the 19S proteasome regulator.

The asynchronous, IFNβ-treated and MRC5VA cell populations were the only ones to also contain some cells that showed 19S foci which were classified as being significantly further from PML NBs than expected under CSR, in a very small proportion of cells (about 2.3%, n = 43, 2.3%, n = 43, and 5.3%, n = 38, for asynchronous, IFN and MRC5VA respectively). This is unlikely to be meaningful.

In WI38 ASYNC and VA nuclei 26.3% (n = 38) and 25.8% (n = 31), respectively, contained PML NBs that were closer to 19S than expected under CSR. 0% and 3.2%, of ASYNC and VA nuclei respectively, contained PML NBs that were further from 11S than expected under CSR. The association between PML NBs in a quarter of nuclei tested stands for both ASYNC and VA cells, and therefore is not a relationship that is affected by the viral transformation.

4.5.2.11 11S immunoproteasome regulator (11S)

There are cells in which 11S proteasome regulator (11S) is significantly closer to PML NBs than we would expect under CSR in all of the asynchronous, heat shocked, IFNβ-treated, serum starved MRC5 cell populations, and in SV40 T-Ag transformed MRC5 cell populations (Figure 59). Only in the SV40 T-Ag transformed MRC5 data set were there cells in which 11S foci were significantly further from PML NBs than we would expect under CSR, but which are a very small proportion of the total cells tested.

In asynchronous MRC5 cells there is a significantly closer association between 11S foci and PML NBs in 86.4% of the cells tested (n = 44). Under conditions of heat shock this association was seen in 79.5% of cell nuclei (n = 39) that contained 11S foci that are closer to PML NBs than expected under CSR. In IFNβ-treated cells 92.9% (n = 42)) showed 11S foci significantly closer to PML NBs than we might expect under CSR. In serum starved cells, 83.7% percent of the cells tested had 11S foci showing a significantly closer association with PML NBs, (n = 49), but in SV40 T-Ag transformed only 23.1% of cells showed 11S foci that were significantly closer to PML NBs than expected under CSR (n = 39).

In all the data sets bar MRC5VA cell nuclei there appears to be an extremely high association between 11S foci and PML NBs. Even in an asynchronous cell population of MRC5 fibroblasts 11S foci are significantly closer to PML NBs than expected under CSR in the vast majority of cells. Treatment with cellular stresses does not seem to attenuate this already high association except in the case of overnight IFNβ-treatment, where it rises to almost 93% of cells containing 11S foci that are closer to PML NBs than we would expect. It is apparent that SV40 T-Ag transformation of MRC5 cells seems to result in a much lower percentage association (almost four times as low at 23.1% of cells) between 11S foci and PML NBs, and that this may be a consequence of transformation.

In fact the MRC5VA cell population was the only one to also contain some cells that showed 11S foci which were classified as being significantly further from PML NBs than expected under CSR, in a very small proportion of cells (2.6%, n = 39). This is unlikely to be meaningful. Therefore this could mean that 11S loses its association with PML NBs in these cells, and may even move away. Within the nucleus11S is not necessarily in

active proteasome units (but may just be aggregated for storage and kept in close proximity for when needed, such as upon viral infection).

In WI38 ASYNC and VA nuclei 56.3% (n = 32) and 52.9% (n = 34), respectively, contained PML NBs that were closer to 19S than expected under CSR. None of ASYNC and VA nuclei contained PML NBs that were further from 11S than expected under CSR. There is a high association between PML NBs and 11S in both normal and transformed WI38, and therefore seems to be strong relationship that exists normally in all cells.

4.5.2.12 General trends for PML NB – functional compartment CSR analysis

In general functional compartments tended to be closer to PML NBs, rather than further from them than we would expect under the hypothesis of CSR. High percentages of nuclei within a dataset showing PML NBs that are closer to the functional compartment than expected indicate that a functional relationship exists between the two.

The treatments used in MRC5 nuclei (heat shock, interferon and serum starvation), seemed to increase the percentage of nuclei containing PML NBs that were closer to a functional compartment than we would expect. This could possibly reflect compartment-specific reorganizations towards PML NBs upon certain treatments, but might instead indicate the dysregulation of nuclear organisation. Since PML NBs seem to move closer to many different compartments upon different treatments (and therefore not really in a compartment specific manner) it could be more likely that this instead reflects a general spatial dysregulation in the nucleus.

Interestingly, as in some of the PML CSR analysis from Chapter 3, there also exists a case where PML NBs from the same nucleus are classified as being both closer to, and further from, a specific compartment. As mentioned previously, this could indicate that there is more than one population of PML NBs in that nucleus that show different associations with the same functional compartment.

4.5.3 Summary

PML NB – Chromosome topological compartments CSR

As well as by simply using distance measurements which pool results across nuclei within datasets, the spatial organisation of PML NBs in relation to a range of functional compartments in the nucleus was tested in every individual nucleus of each cell line and treatment by comparing a cumulative distribution function plot of the observed minimum PML NB to compartment edge NND distances for every PML NB in the nucleus with the equivalent distances for the same PML NBs simulated 999 times under the hypothesis of CSR. If the observed curve falls out of the simulation envelope it is either closer to or further from (as appropriate) the functional compartment than expected under CSR. If it stays within the simulation envelope, the PML NBs in that particular nucleus are arranged according to complete spatial randomness with respect to the functional compartment.

The cumulative distribution function plot of the observed minimum PML NB to the edge of the ACA or TELO compartment NND distances was constructed as above.

PML NBs were closer to ACA than expected under CSR in 47%, 59%, 47%, 39% and 0% of MRC5 ASYNC, HS, IFN, SS and VA nuclei respectively. The HS treatment slightly increased the percentage of nuclei containing PML NBs that locate closer to ACA than expected under CSR, whereas IFN, SS and VA all decreased the percentage of such nuclei (dramatically in the case of VA). PML NBs were further from ACA than expected under CSR in 3% of MRC5 VA nuclei only. In WI38 ASYNC and VA PML NBs were closer to ACA than expected under CSR in 30% and 23% of nuclei respectively. They were further than expected in none of the nuclei.

PML NBs were closer to TELO than expected under CSR in 23%, 75%, 65%, 63% and 96% of MRC5 ASYNC, HS, IFN, SS and VA nuclei respectively. The HS, IFN, SS and VA treatments increased the percentage of nuclei containing PML NBs that locate closer to TELO than expected under CSR, (dramatically so in the case of VA). PML NBs were further from TELO than expected under CSR in 2% of MRC5 ASYNC nuclei only. In WI38 ASYNC and VA PML NBs were closer to TELO than expected under CSR in

24% and 96% of nuclei respectively. They were further than expected in 2% of WI38 ASYNC nuclei only.

PML NB – Transcriptional compartments CSR

The cumulative distribution function plot of the observed minimum PML NB to the edge of the ACHIS, MEHIS, RNA, RNAPII or B23 compartment NND distances was constructed as previously described.

PML NBs were closer to ACHIS than expected under CSR in 33%, 72%, 53%, 84% and 37% of MRC5 ASYNC, HS, IFN, SS and VA nuclei respectively. The HS, IFN and SS treatments all dramatically increase the percentage of nuclei containing PML NBs that locate closer to ACHIS than expected under CSR. PML NBs were further from ACHIS than expected under CSR in 4% of MRC5 ASYNC nuclei respectively only. In WI38 ASYNC and VA PML NBs were closer to ACHIS than expected under CSR in 46% and 45% of nuclei respectively. They were further than expected in neither of WI38 ASYNC or VA nuclei.

PML NBs were closer to MEHIS than expected under CSR in 21%, 80%, 57%, 67% and 32% of MRC5 ASYNC, HS, IFN, SS and VA nuclei respectively. The HS, IFN and SS treatments all dramatically increased the percentage of nuclei containing PML NBs that locate closer to MEHIS than expected under CSR. PML NBs were further from MEHIS than expected under CSR in 2% of MRC5 HS and 3% of VA nuclei only. In WI38 ASYNC and VA PML NBs were closer to MEHIS than expected under CSR in 24% and 14% of nuclei respectively. They were further than expected in 2% and 3% of WI38 ASYNC and VA nuclei respectively.

PML NBs were closer to RNA than expected under CSR in 45%, 81%, 22%, and 10% of MRC5 ASYNC, HS, SS and VA nuclei respectively. The HS treatment dramatically increased the percentage of nuclei containing PML NBs that locate closer to RNA than expected under CSR, however the SS and VA reduced the percentages of such nuclei. PML NBs were further from RNA than expected under CSR in none of the MRC5 cell lines and treatments. In WI38 ASYNC PML NBs were closer to RNA than expected under CSR in 33% of nuclei. They were further than expected in 0% of WI38 ASYNC nuclei.

PML NBs were closer to RNAPII than expected under CSR in 25%, 87%, 81% and 17% of MRC5 ASYNC, HS, IFN and VA nuclei respectively. The HS and IFN treatments both dramatically increased the percentage of nuclei containing PML NBs that locate closer to RNAPII than expected under CSR. PML NBs were further from RNAPII than expected under CSR in none of the MRC5 cell lines and treatments. In WI38 ASYNC and VA PML NBs were closer to MEHIS than expected under CSR in 9% and 42% of nuclei respectively. They were further than expected in none of WI38 ASYNC and VA nuclei respectively.

PML NBs were closer to B23 than expected under CSR in 6%, 61%, 51%, 43% and 7% of MRC5 ASYNC, HS, IFN, SS and VA nuclei respectively. The HS, IFN and SS treatments all increase the percentage of nuclei containing PML NBs that locate closer to B23 than expected under CSR. PML NBs were further from B23 than expected under CSR in 6%, 9%, 2%, 0% and 9% of MRC5 ASYNC, HS, IFN, SS and VA nuclei respectively. In WI38 ASYNC and VA PML NBs were closer to B23 than expected under CSR in 6% and 3% of nuclei respectively. They were further than expected in 4% and 10% of WI38 ASYNC and VA nuclei respectively.

PML NB – Post-transcriptional compartments CSR

The cumulative distribution function plot of the observed minimum PML NB to the edge of the SC35 or CB compartment NND distances was constructed as previously described.

PML NBs were closer to SC35 than expected under CSR in 84%, 100%, 89%, 92% and 24% of MRC5 ASYNC, HS, IFN, SS and VA nuclei respectively. All of the MRC5 ASYNC, HS, IFN and SS datasets contained a very high percentage of nuclei containing PML NBs that locate closer to SC35 than expected under CSR, however in VA this percentage was dramatically decreased. PML NBs were further from SC35 than expected under CSR in 2% of all of MRC5 HS, IFN and SS nuclei. In WI38 ASYNC and VA PML NBs were closer to SC35 than expected under CSR in 47% and 91% of nuclei respectively. They were further than expected in 0% and 2% of WI38 ASYNC and VA nuclei respectively.

PML NBs were closer to CB than expected under CSR in only 6% of MRC5 VA nuclei only, and were not further from CB than expected under CSR in any of MRC5 VA nuclei. In WI38 VA PML NBs were closer to CB than expected under CSR in 13% of nuclei.

PML NB – Proteolytic compartments CSR

The cumulative distribution function plot of the observed minimum PML NB to the edge of the 19S or 11S compartment NND distances was constructed as previously.

PML NBs were closer to 19S than expected under CSR in 30%, 87%, 35%, 34% and 21% of MRC5 ASYNC, HS, IFN, SS and VA nuclei respectively. The MRC5 HS dataset contained a very high percentage of nuclei containing PML NBs that locate closer to 19S than expected under CSR, however in VA this percentage was slightly decreased in comparison to MRC5 ASYNC. PML NBs were further from 19S than expected under CSR in 2%, 2% and 5% of MRC5 ASYNC, IFN and VA nuclei respectively. In WI38 ASYNC and VA PML NBs were closer to 19S than expected under CSR in 26% of both datasets. They were further than expected in 0% and 3% of WI38 ASYNC and VA nuclei respectively.

PML NBs were closer to 11S than expected under CSR in 86%, 80%, 93%, 84% and 23% of MRC5 ASYNC, HS, IFN, SS and VA nuclei respectively. All of the MRC5 ASYNC, HS, IFN and SS datasets contained a very high percentage of nuclei containing PML NBs that locate closer to 11S than expected under CSR, with highest percentage being in the MRC5 IFN dataset, but in VA the percentage was greatly decreased in comparison to MRC5 ASYNC. PML NBs were further from 11S than expected under CSR in 3% of MRC5 VA nuclei only.

In WI38 ASYNC and VA PML NBs were closer to 11S than expected under CSR in 56% and 53% of nuclei respectively. They were further than expected in none of the WI38 ASYNC and VA nuclei.

4.6 Chapter Summary

The average voxel counts per nucleus of eleven of different functional compartments in the nucleus (centromeres, telomeres, acetylated histones, methylated histones, nascent RNA, RNA polymerase II_O, nucleoli, SC35 domains, Cajal bodies, 19S proteasome regulator, and 11S immunoproteasome regulator) were characterised in normal, treated, and SV40 transformed MRC5 fibroblasts, and normal and transformed WI38 fibroblasts. The distance relationships and spatial organisation of PML NBs were investigated in relation to all of the compartments above. PML NBs were found to show close relationships with a number of functional compartments, which may indicate their functional role(s) in the nucleus.

5

Aggregate Maps of Nuclear Compartments

5.1 Introduction – Making the Aggregate Maps

The aggregate map (AM) is a visually appealing and interesting way to represent the data obtained from the image segmentation of the raw image files, by showing the spatial preference of nuclear compartments over an "average" nucleus. It is progress towards creating a map of an average nucleus, where similarities and differences in the spatial preference of functional compartments in normal cells, and under different treatments and viral transformation can be viewed.

An AM is created by first modelling the average cell nucleus morphology (in terms of size, shape and volume) for each of the appropriate categories: ASYNC, HS, IFN, SS and VA, in MRC5 and WI38 cell lines. Then, the raw segmentation data for each of the functional compartments can be plotted by transformation of the data onto the "average cell nucleus" using landmarks. Initially this results in a field with no discernable structure as voxels are marked as either having a functional compartment present, or not (0 or 1), which basically covers the entire field of the nucleus with signal. However, by applying an intensity threshold, regions where the compartment is found more often appear. From these, certain patterns of nuclear localisation can be determined.

The maps represent a 3D view of the nucleus, but here we only show the *xy* projection. This is because the *xz* and *yz* plots do not reveal much extra useful information about the spatial organisation of the compartments, and the resolution in the *z* axis is not as high as in the *x* or *y*, due to the nature of the confocal image stacks.

5.2 Mean Nucleus shape

When thinking about the organisation of the nucleus, and how this might differ across cell lines, we decided to look at the mean shape of the nucleus for each of the cell lines and treatments studied.

It must be noted that whilst being relevant to the population of cells used in this study, the mean nucleus shape may not be representative of the total population of cells in culture, ince extremes (nuclei which were larger than a ROI, the size of which was selected to include most of the cells in the population for the analysis) were not included.

The first step in AM construction required plots of the average cell nucleus shape for each of the cell lines and conditions looked at. Since the most variation is seen in the *xy*, we show here the projection images of the *xy* plot only.

5.2.1 Mean nucleus shape for MRC5 nuclei

The cell line with the smallest nuclear footprint was MRC5 ASYNC (Figure 60). The next largest were MRC5 HS and SS, which overlapped somewhat and were longer than MRC5 ASYNC nuclei. It was not expected that MRC5 HS should have a dramatically different mean nucleus shape than MRC5 ASYNC, as there was not enough time during the treatment to alter nuclear shape. However, for the SS cells this elongation can be accounted for by a general lengthening and a "squaring" of the nucleus often seen in populations of fibroblasts that have been serum starved. MRC5 SS cells were also flatter (in addition to being longer) than MRC5 ASYNC, therefore differing from HS cells in that respect. The next largest the WI38 ASYNC mean nucleus, meaning that the area of WI38 ASYNC fibroblasts was on average bigger than that of MRC5 ASYNC. Interestingly, although the area was bigger, the volume of the WI38 ASYNC was smaller than that of the MRC5 ASYNC, meaning that WI38 ASYNC cells are flatter. The next largest average nucleus was that of MRC5 IFN, followed by WI38 VA and finally MRC5 VA, which had the largest nuclear footprint of all.

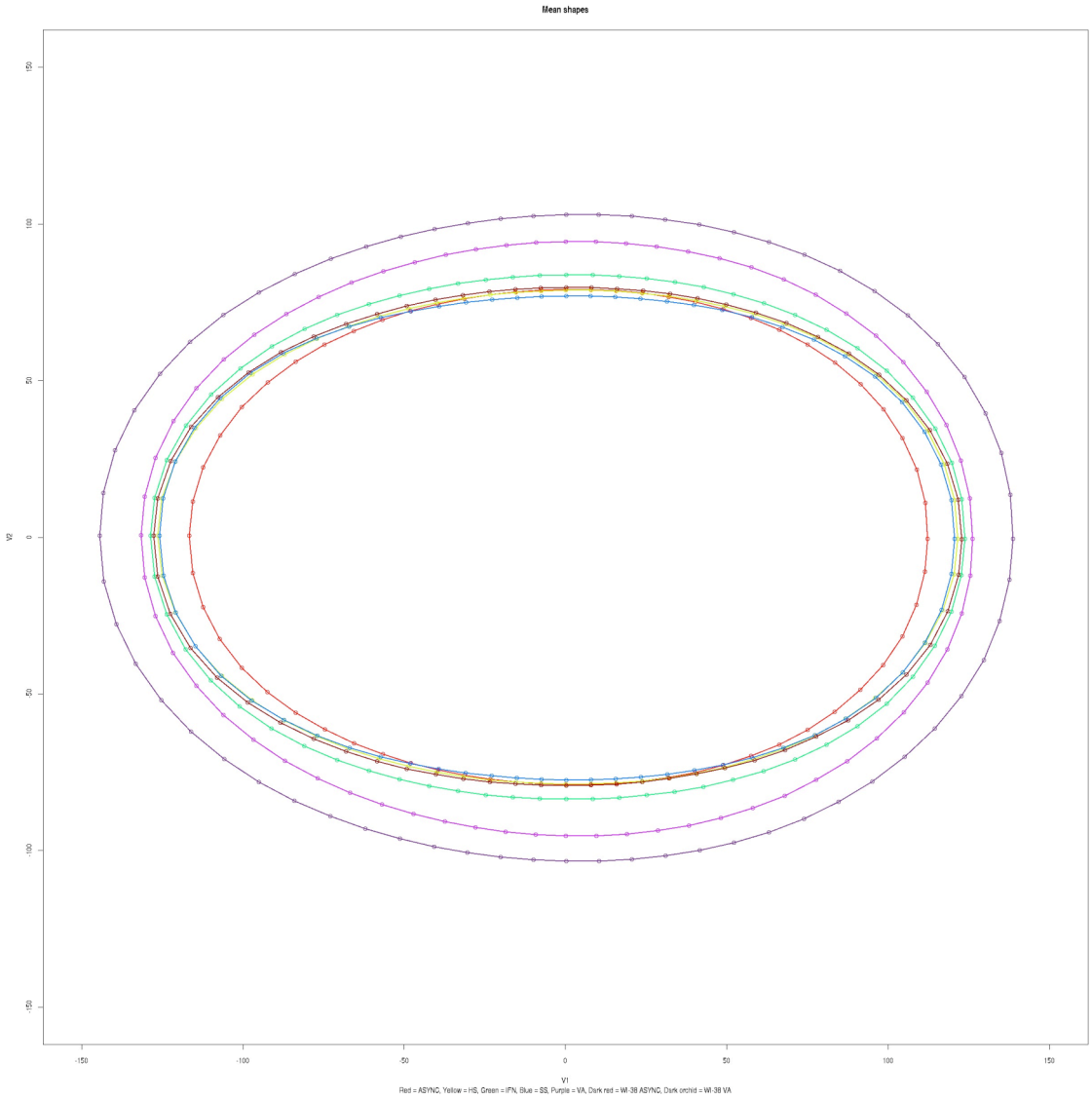


Figure 60 Mean nucleus shape for MRC5 and WI38 fibroblasts

The mean nucleus shape in 3D was calculated for MRC5 ASYNC (red), HS (yellow), IFN (green), SS (blue) and VA (purple), and WI38 ASYNC (dark red) and VA (dark orchid) according to a series of landmarks, and is shown as a projection of the mean nucleus footprint for each of the cell lines and treatments.

5.2.2 Summary

One of our aims was to visualise where functional nuclear compartments reside within an "average" nucleus, and to investigate if compartments showed particular spatial preferences. Before this could be achieved it was necessary to model average nucleus morphology (size (volume), and shape) for each of the cell lines and treatments. MRC5 ASYNC had the smallest nuclear footprint, followed by the slightly larger MRC5 HS and SS nuclei. Interestingly according to the nuclear volume data presented in Chapter 3 (Section 3.2.3) the median nuclear volume of MRC5 SS nuclei was smaller than that of

MRC5 ASYNC. The next largest nuclear footprint was WI38 ASYNC nuclei, but which has a smaller volume than MRC5 ASYNC and hence is flatter. They were followed by MRC5 IFN, WI38 VA, and finally MRC5 VA, which had the largest nuclear footprint.

5.3 Aggregate maps

Using the cell nuclei previously collected our colleagues in the Department of Mathematics were able to construct aggregate maps for the following compartments, under the conditions of ASYNC, HS, IFN, SS and VA for MRC5 cells, and in ASYNC and VA WI38 cells.

5.3.1 Aggregate map pattern description

There were four types of pattern for spatial preference in the nucleus seen in the AMs that follow. The type of pattern seen can be summarised as below.

5.3.1.1 Diffuse

To be classified as completely spatially random (CSR) the compartment is found throughout the field of the nucleus, with no preference for particular locations. The field does not have to be covered uniformly (for instance there could be high intensity of voxels in one area but none in another).

It should be noted that if a pattern is classified as being CSR, this could be because it is indeed CSR, or potentially because there is not enough data to prove otherwise (as it is again the null hypothesis).

5.3.1.2 Core

There is a spatial preference for the centre of the nucleus by the compartment.

5.3.1.3 Annular

The compartment is found in a ring around the area that would be the core (but lacks voxels in this case).

5.3.1.4 Polar

The compartment shows spatial preference for the poles of the nucleus, and not for the core, or the regions to the side of the core.

5.3.2 AMs for PML NBs and functional compartments in MRC5 and WI38 nuclei

The aggregate maps are found in Figure 61 to Figure 76, which show the 3D projections for the aggregate maps of nuclear compartments in the *xy* for the average MRC5 nuclei of in normal, transformed, and treated cells, and of WI38 ASYNC and VA nuclei.

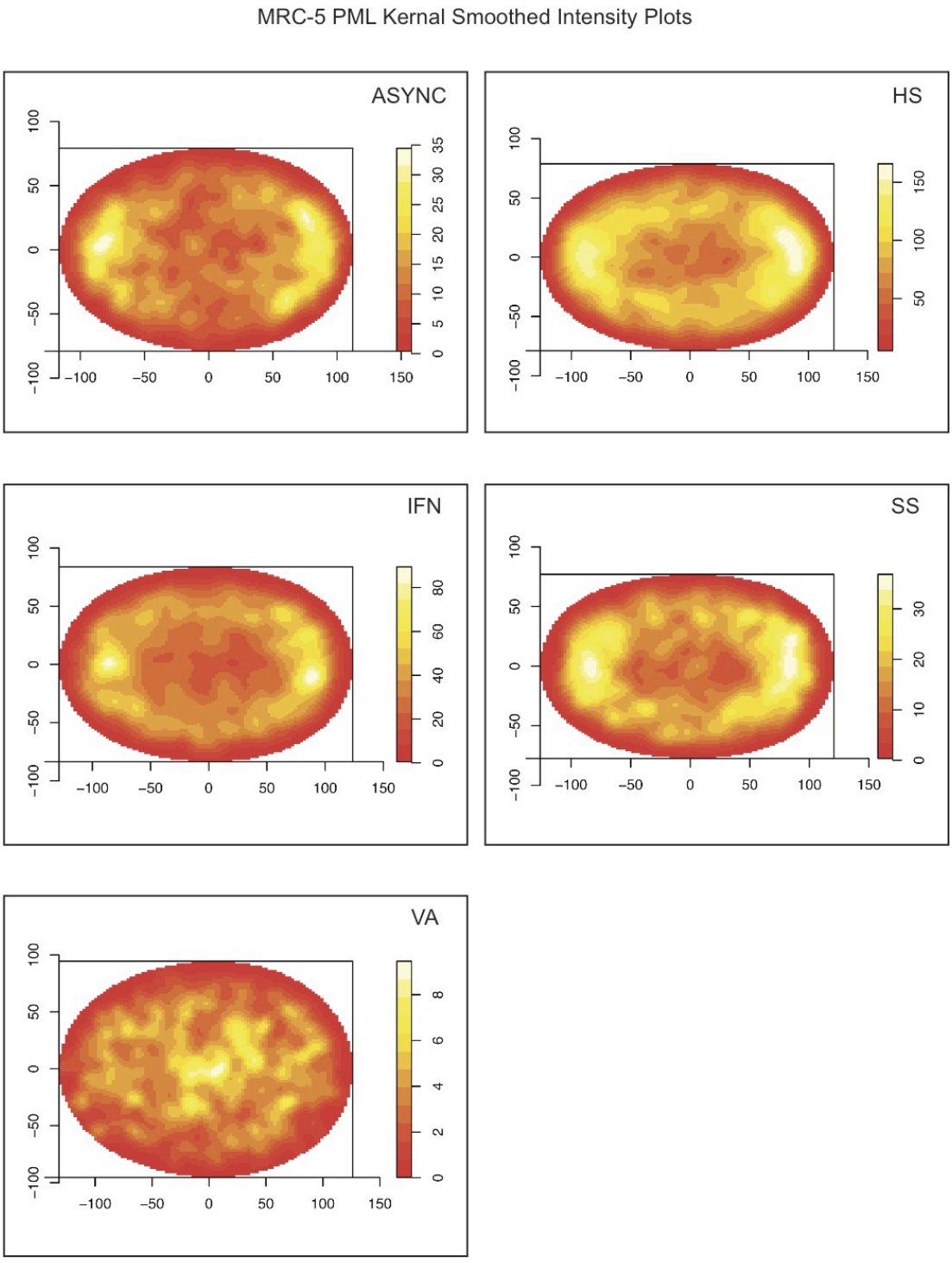


Figure 61 Aggregate map of PML NB spatial preference in MRC5

Aggregate maps of spatial preference of PML NBs in MRC5 ASYNC, HS, IFN, SS and VA nuclei were plotted by transforming the segmented PML voxels onto the mean nucleus shapes for the appropriate cell line and condition. A threshold of sigma = 5 was applied to reveal the spatial preference of the compartment. The colour range indicating intensity is found to the right of the map.

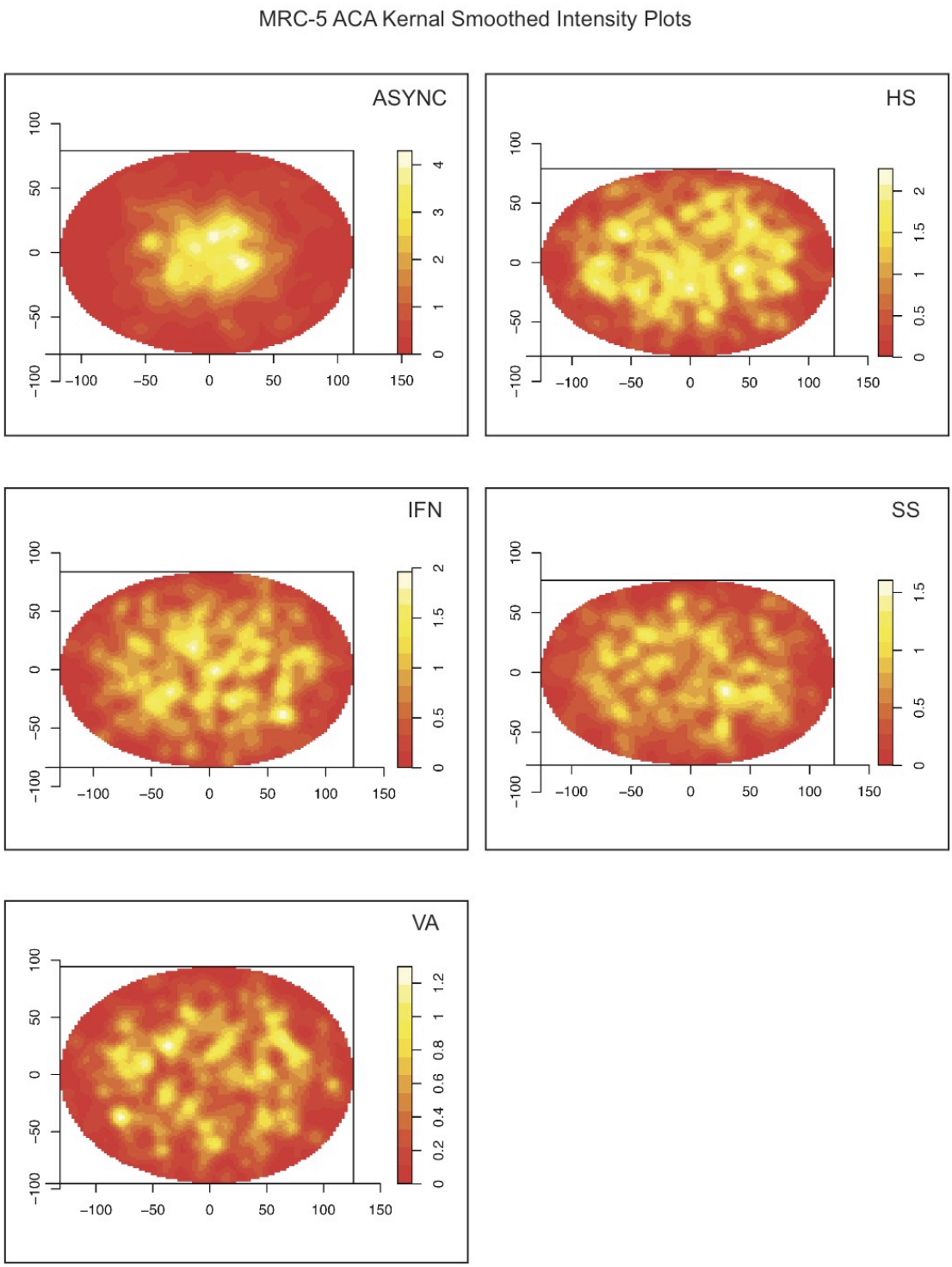


Figure 62 Aggregate map of centromere spatial preference in MRC5

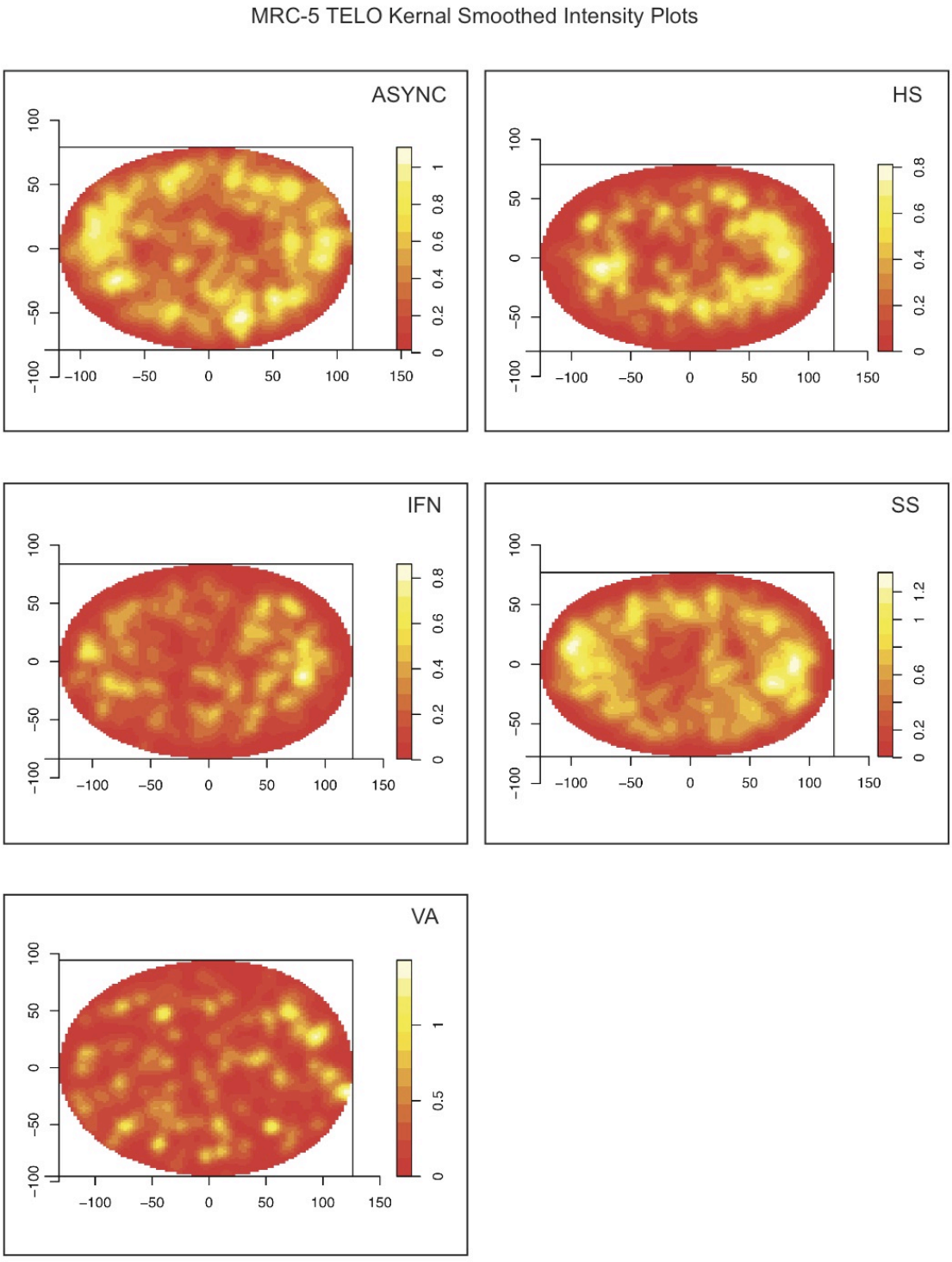


Figure 63 Aggregate map of telomere spatial preference in MRC5

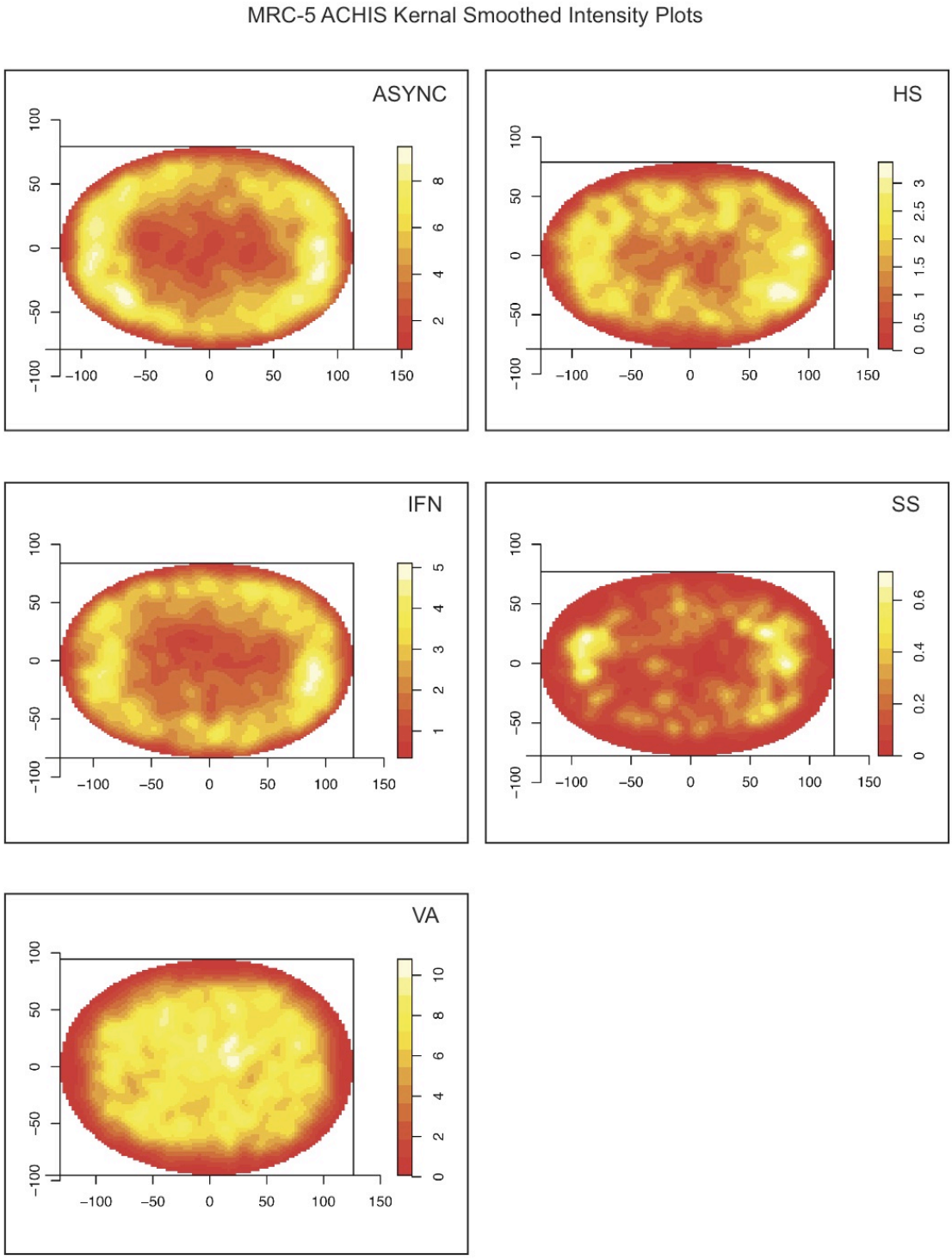


Figure 64 Aggregate map of acetylated histone spatial preference in MRC5

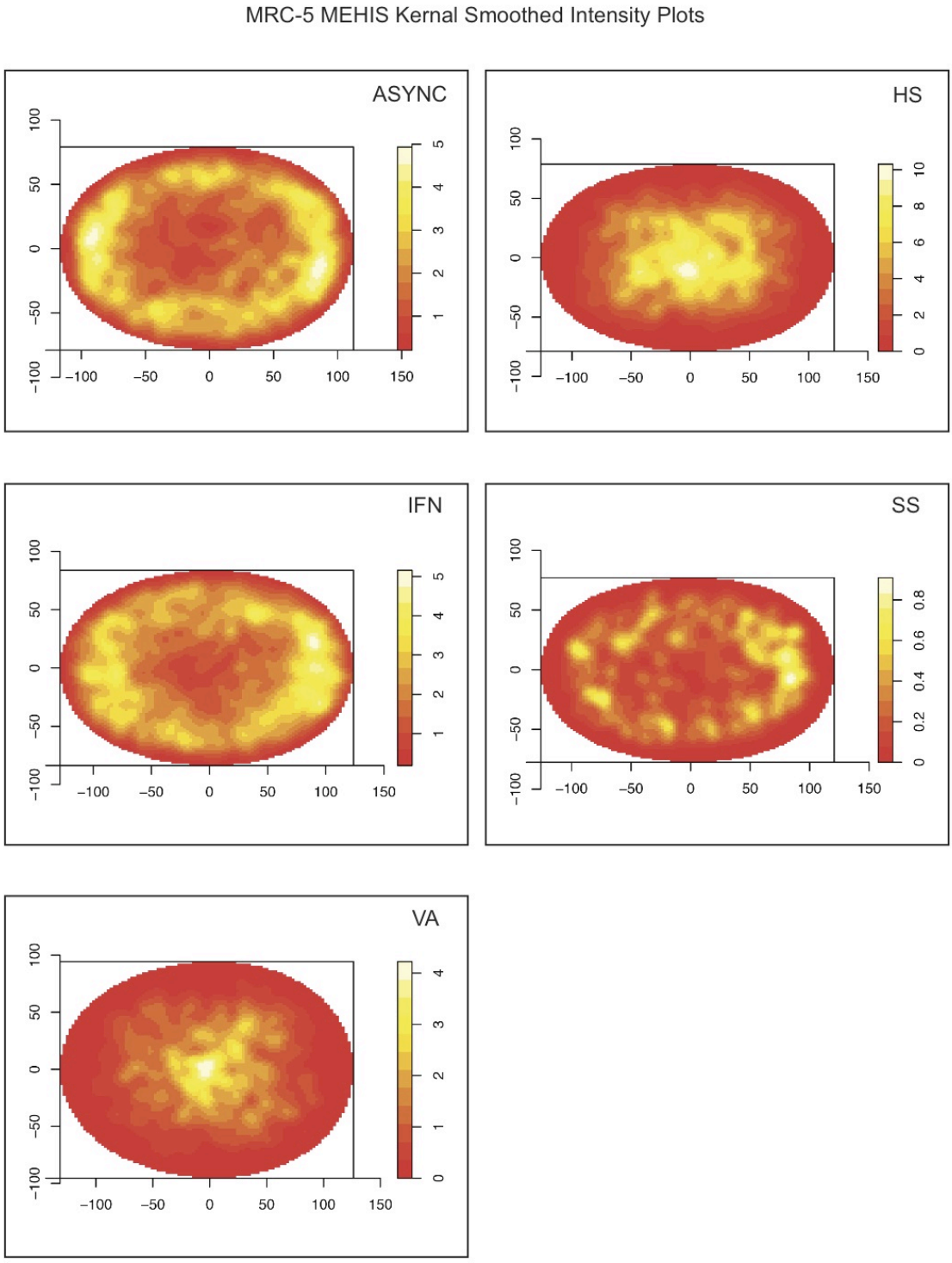


Figure 65 Aggregate map of methylated histone spatial preference in MRC5

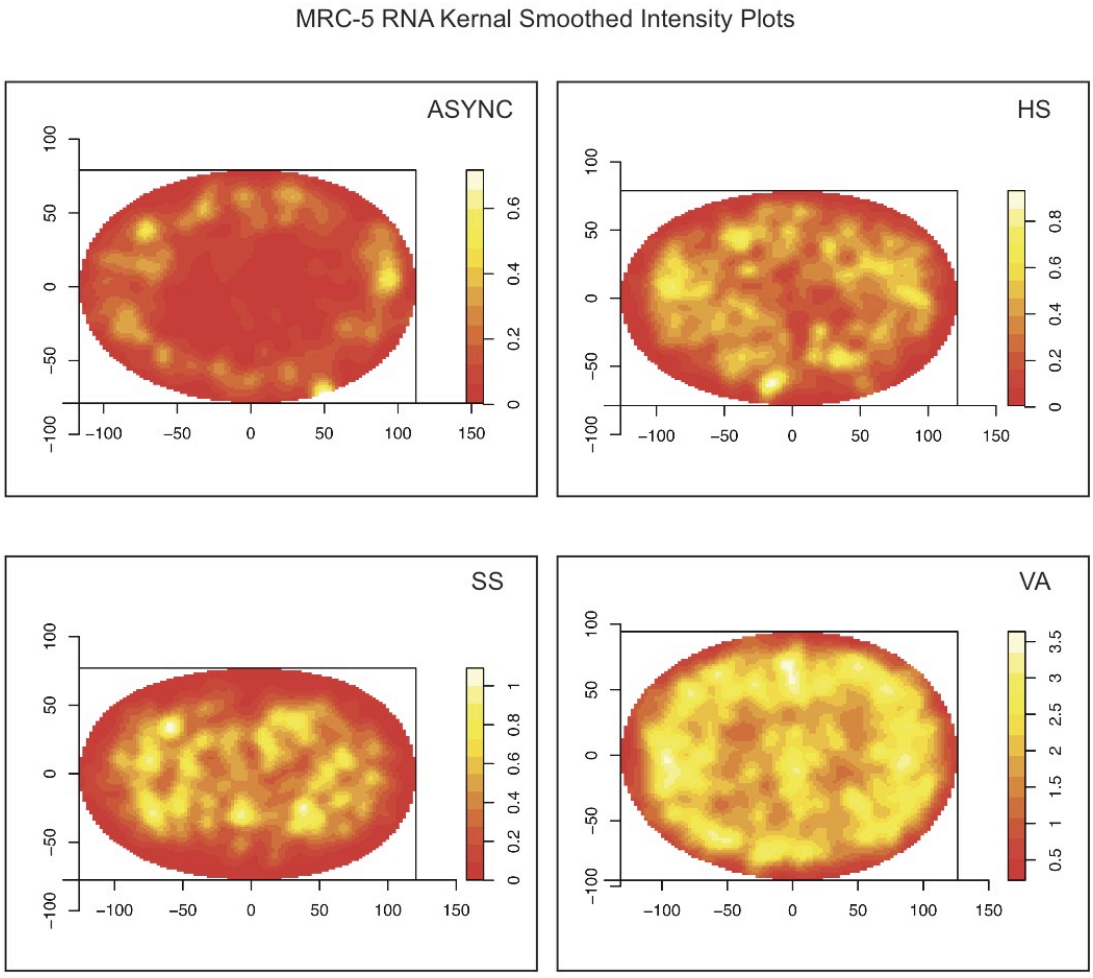


Figure 66 Aggregate map of nascent RNA spatial preference in MRC5

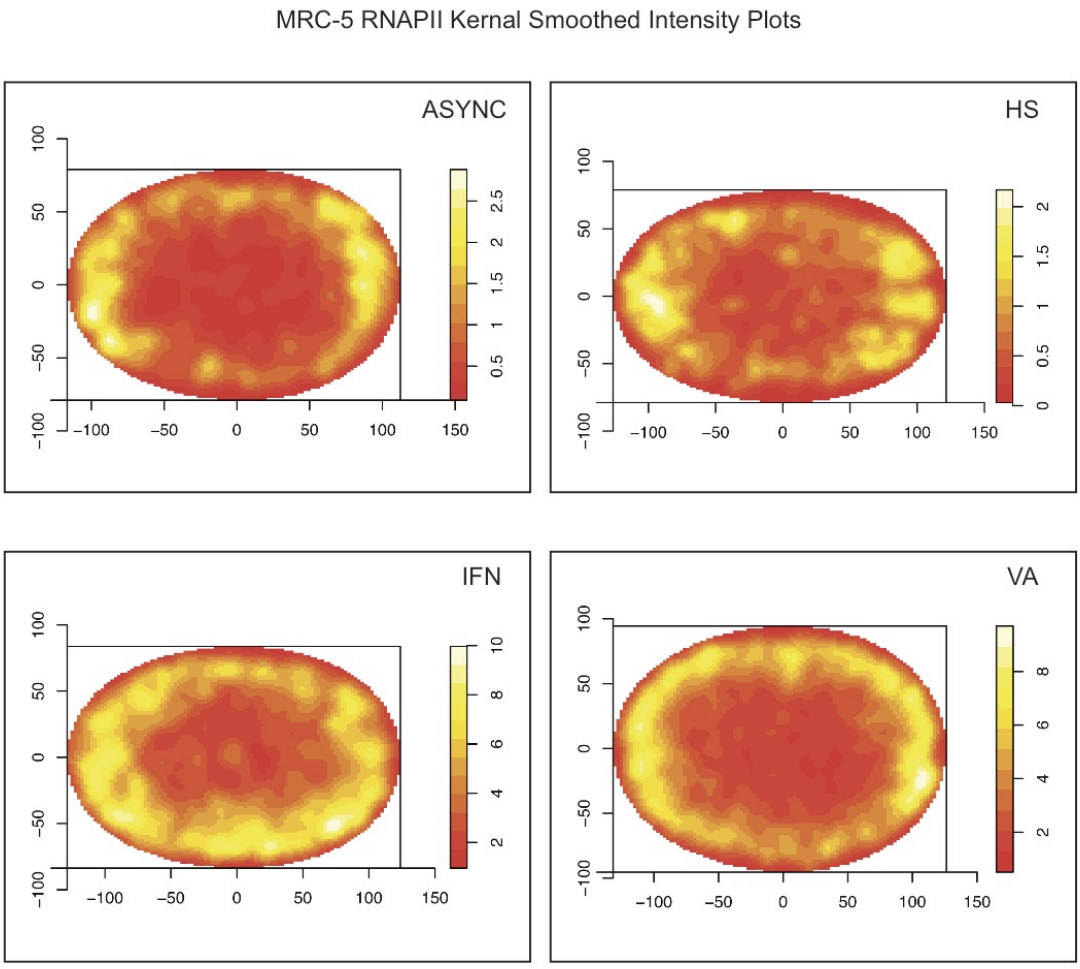


Figure 67 Aggregate map of RNA polymerase II spatial preference in MRC5

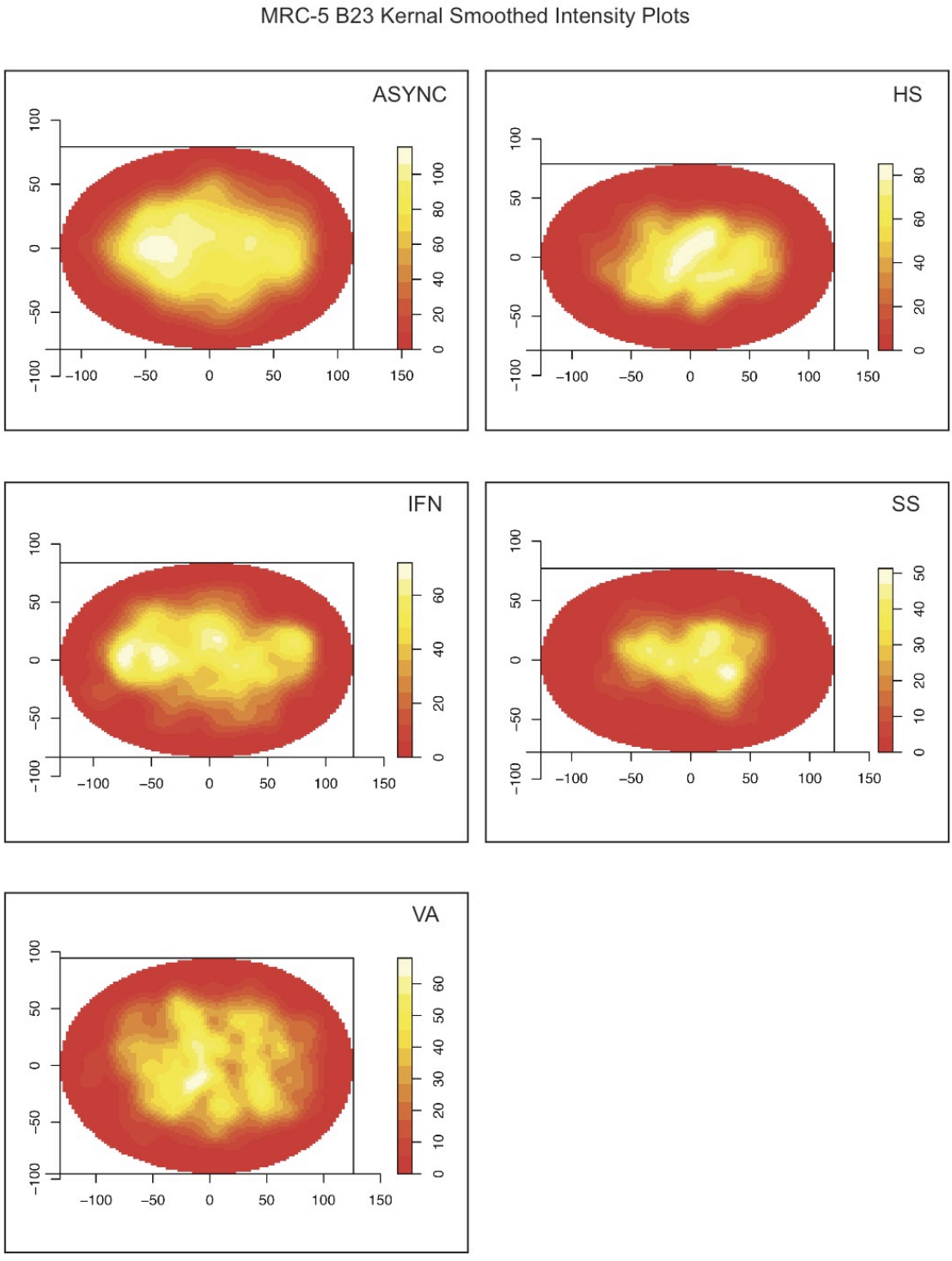


Figure 68 Aggregate map of nucleolus spatial preference in MRC5

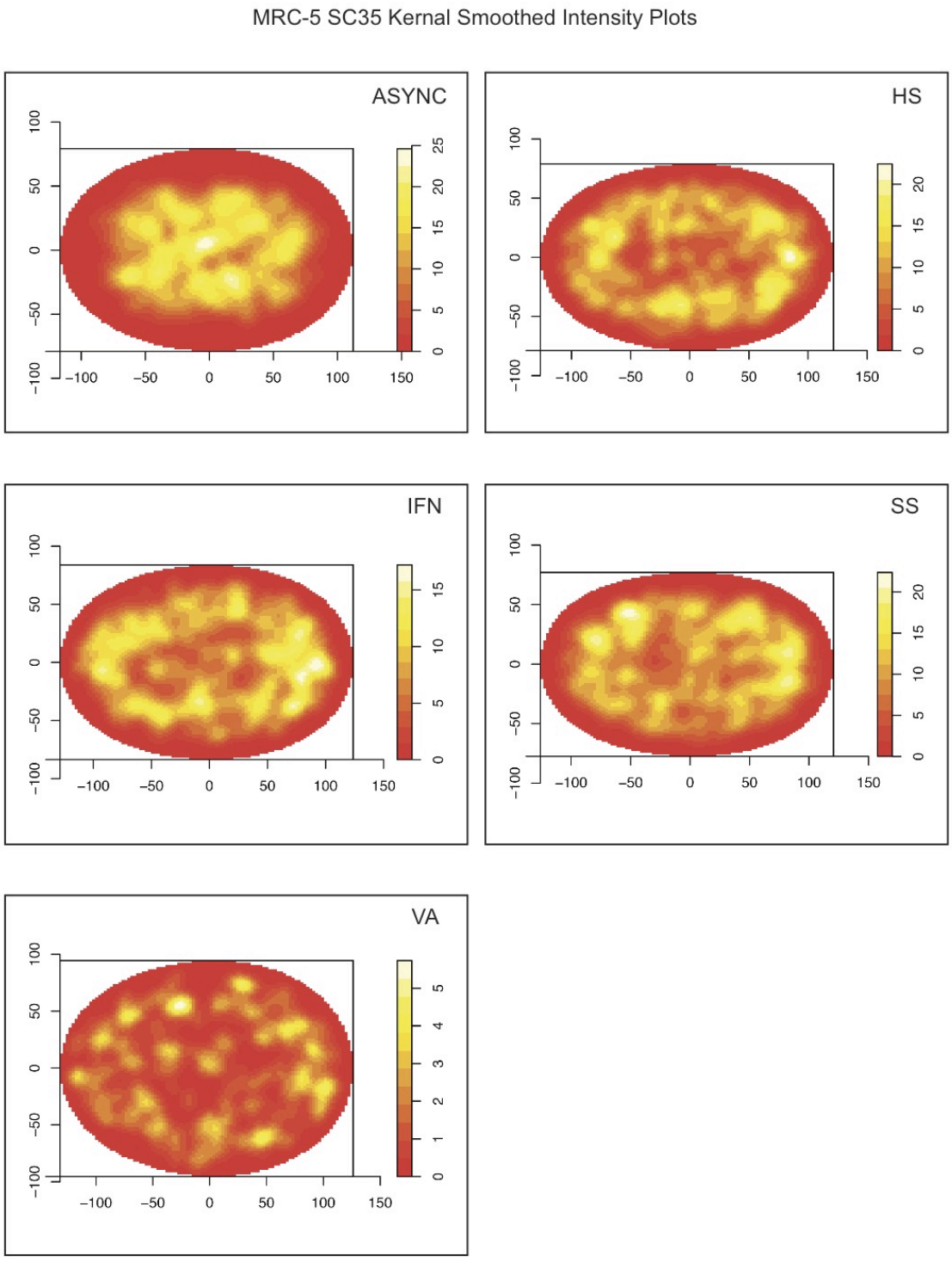


Figure 69 Aggregate map of SC35 domain spatial preference in MRC5

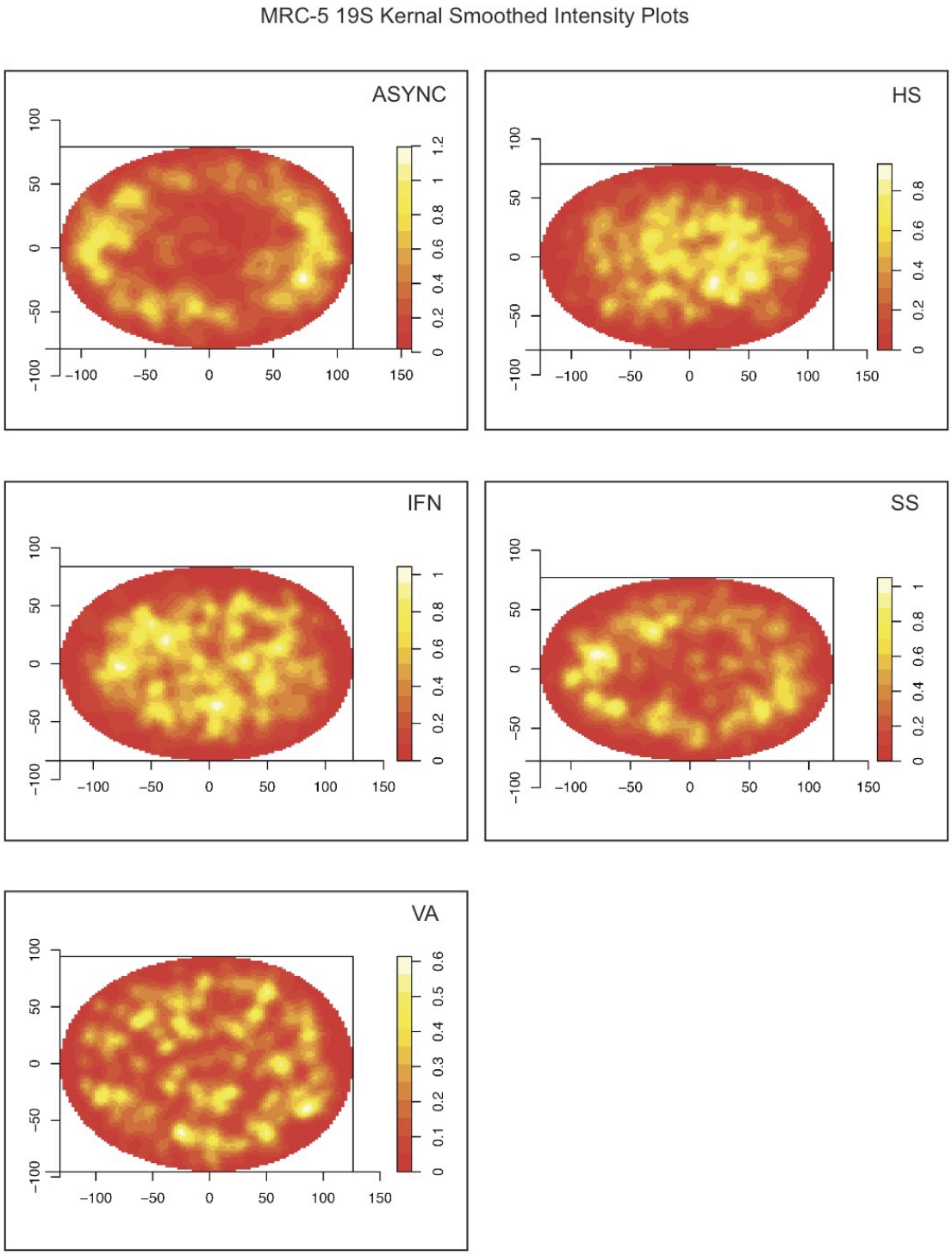


Figure 70 Aggregate map of 19S proteasome regulator spatial preference in MRC5

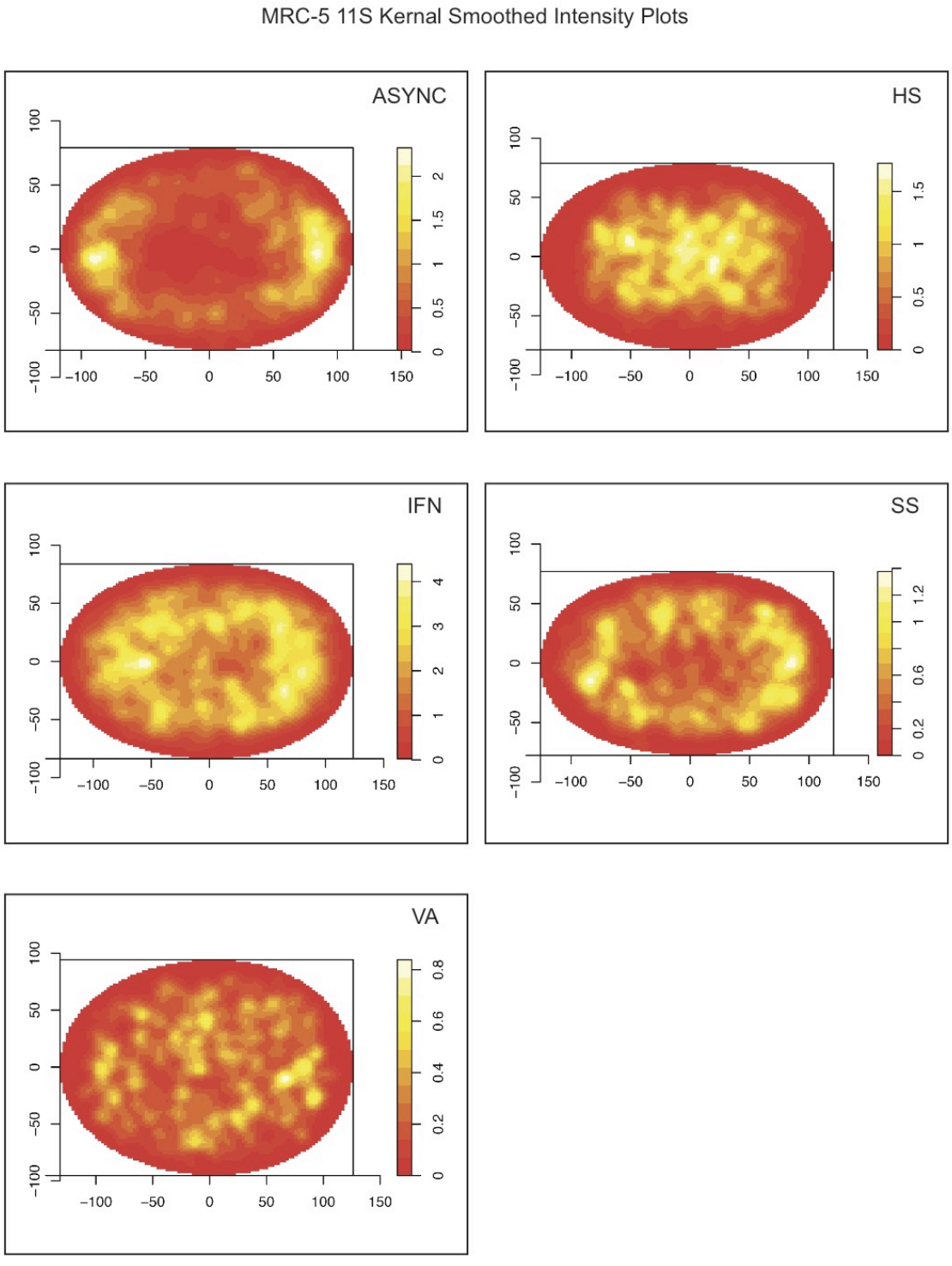


Figure 71 Aggregate map of 11S immunoproteasome regulator spatial preference in MRC5

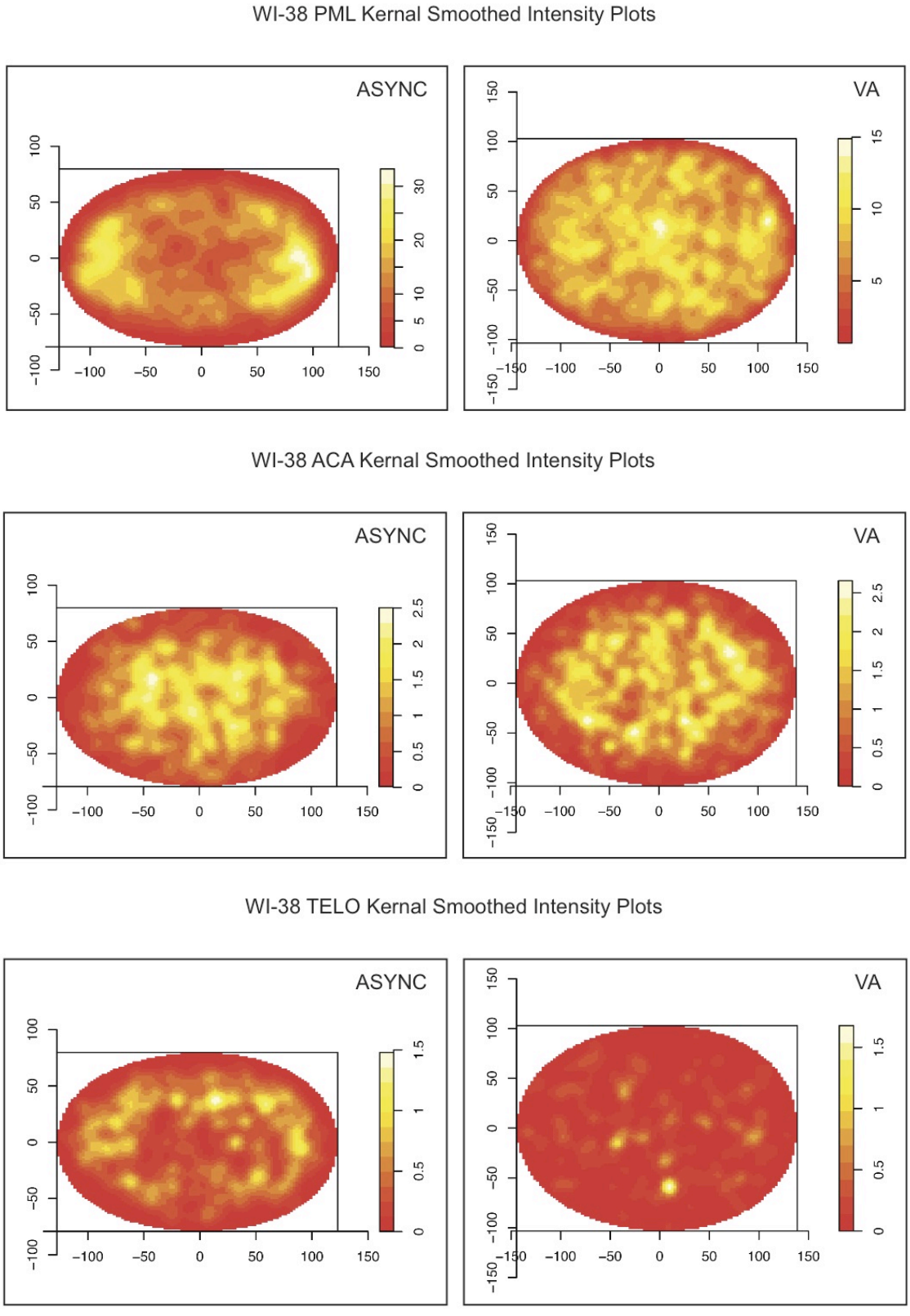


Figure 72 Aggregate map of PML NB, centromere, and telomere spatial preference in WI38

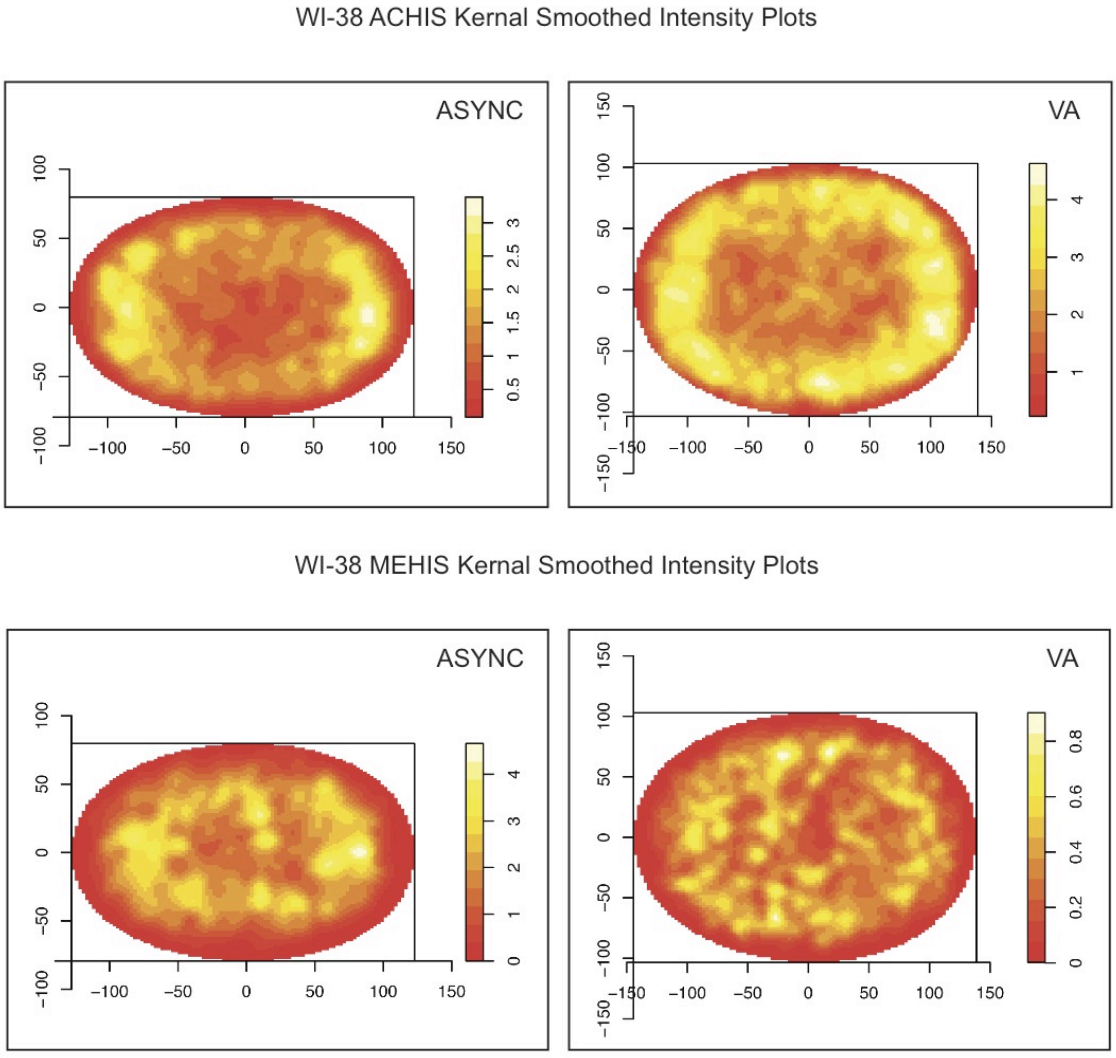


Figure 73 Aggregate map of acetylated and methylated histone spatial preference in WI38

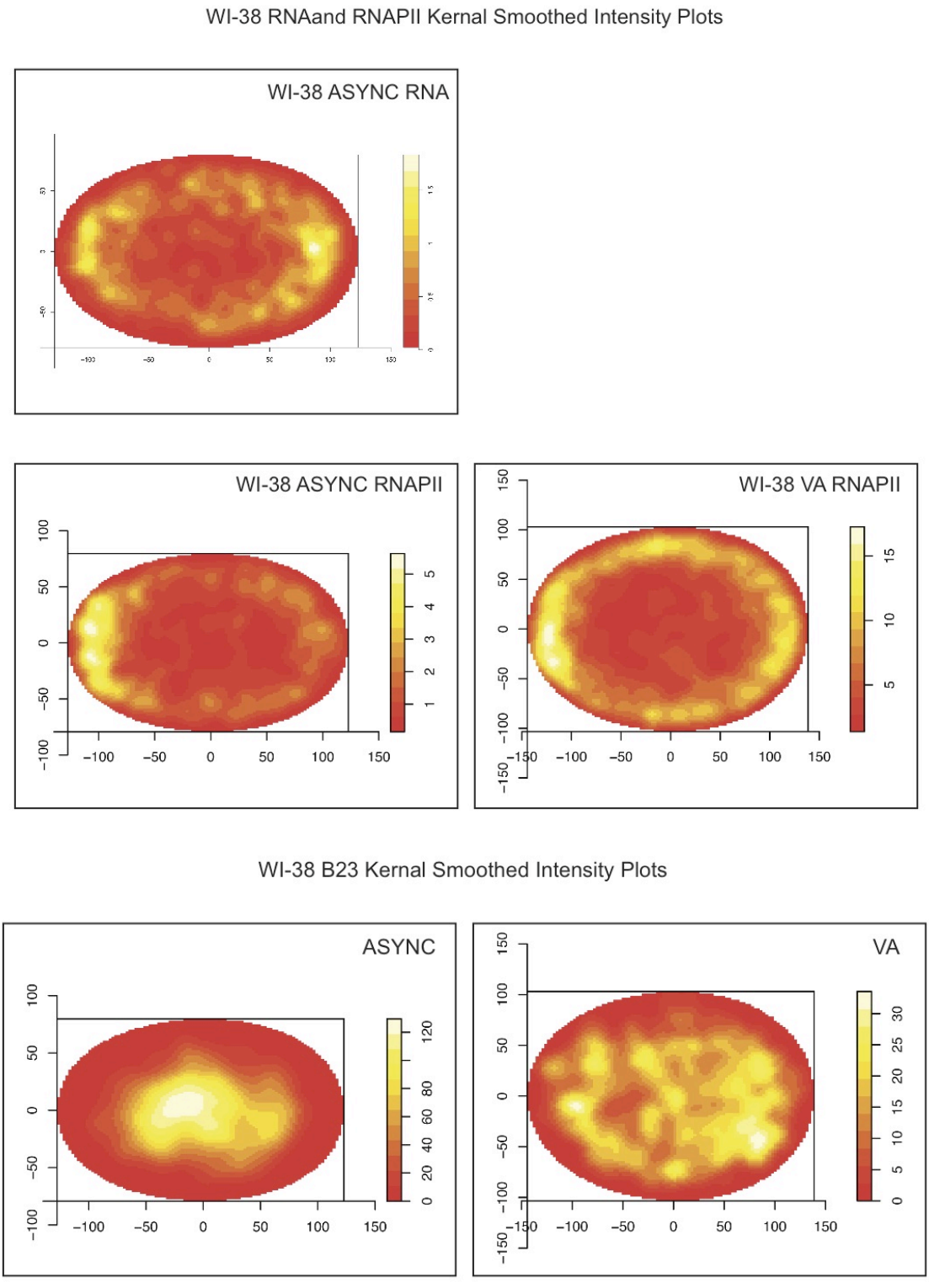


Figure 74 Aggregate map of nascent RNA, RNA polymerase II, and nucleolus spatial preference in WI38

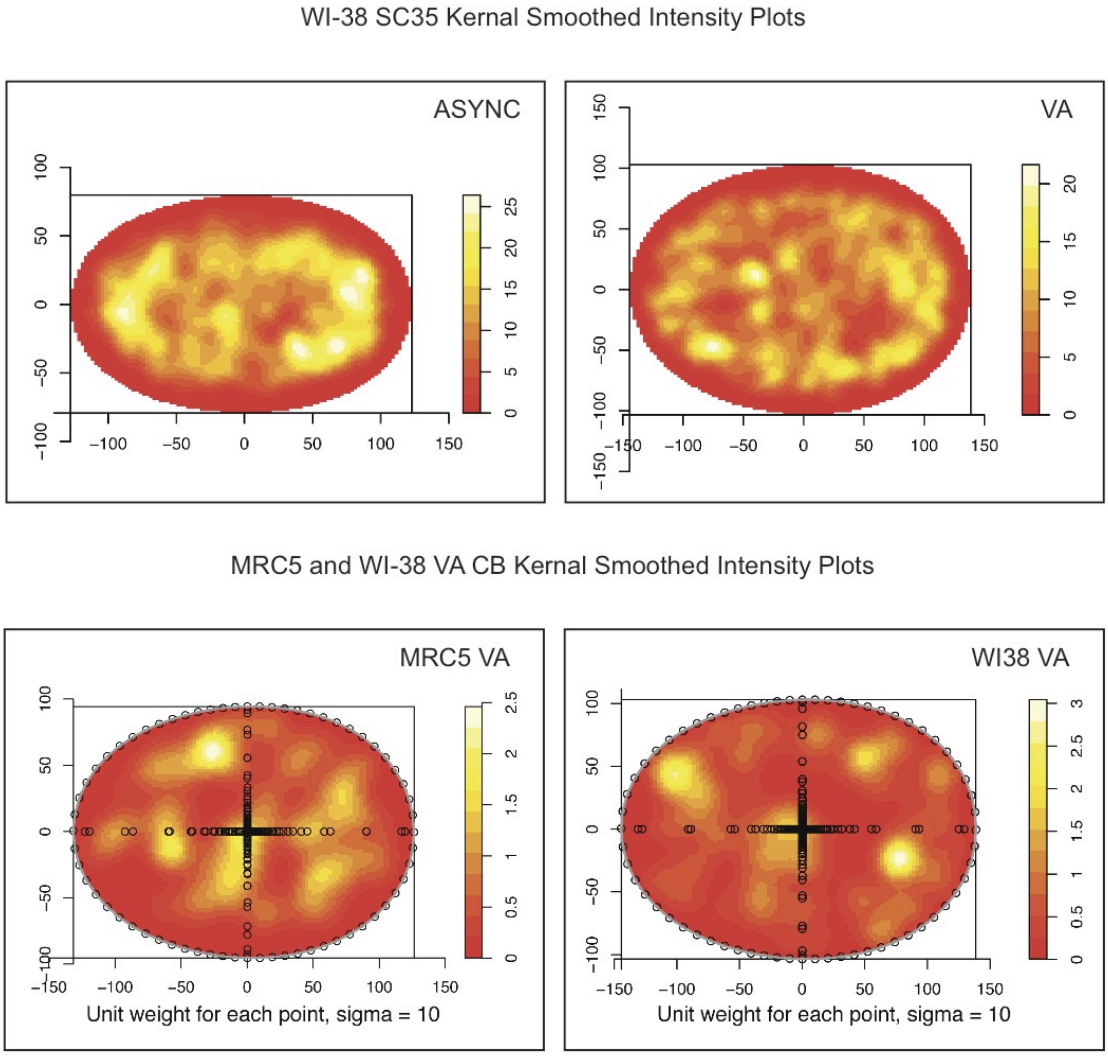


Figure 75 Aggregate map of SC35 domain spatial preference in WI38, and Cajal body spatial preference in MRC5 VA and WI38 VA

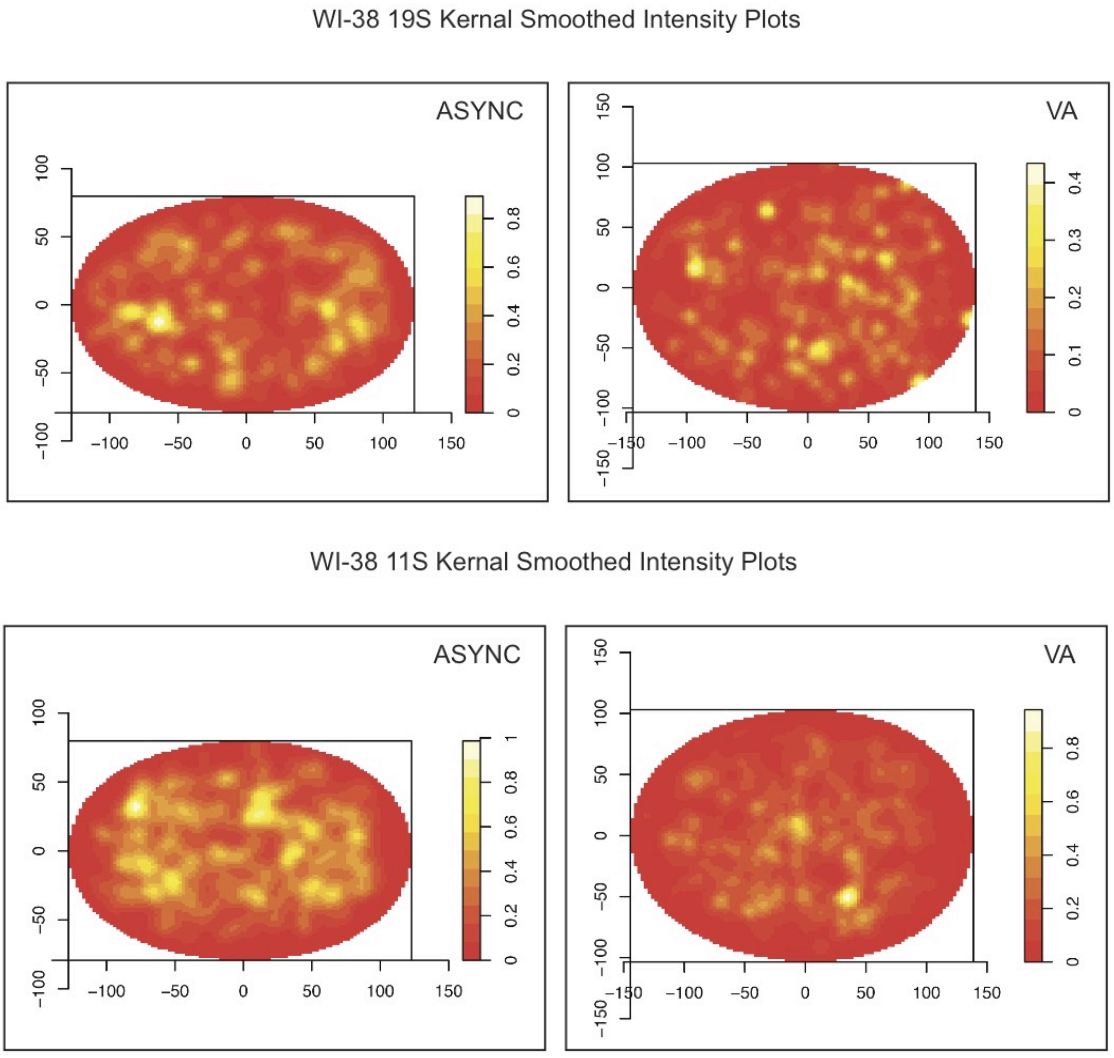


Figure 76 Aggregate map of 19S and 11S proteasome regulator spatial preference in WI38

5.3.2.1 Summary of AM classification for the data set

Table 13 Maximum intensities for each aggregate map

Function	Compartment	MRC-5					WI-38	
		ASYNC	HS	IFN	SS	VA	ASYNC	VA
?	PML	35	150	90	35	9	30	15
Chromosome topology	ACA	4	2	2	1.5	1.2	2.5	2.5
	TELO	1	0.8	0.8	1.2	1.5	1.5	1.5
Transcription	ACHIS	10	3.5	5	0.7	10	3.5	5
	MEHIS	5	10	5	0.8	4	4.5	0.9
	RNA	0.7	0.9	n/a	1	3.5	2	n/a
	RNAPII	2.5	2	10	n/a	10	5	15
	B23	120	80	70	50	70	120	30
Post-transcription	SC35	25	20	17	20	6	25	20
	CB	n/a	n/a	n/a	n/a	5	n/a-	7
Proteolysis	19S	1.2	0.9	1	1	0.6	0.8	0.4
	11S	2.5	1.5	4	1.4	0.8	1	0.9

Table 14 summarises the AM classification for the data set. Key: A = annular, P = polar, D = diffuse, and C = core. n/a means aggregate map not available.

Table 14 Summary of aggregate map classifications for functional compartments in the nucleus

Function	Compartment	MRC-5					WI-38	
		ASYNC	HS	IFN	SS	VA	ASYNC	VA
?	PML	P	A	P	A	D	P	D
Chromosome topology	ACA	C	D	D	D	C	C	C
	TELO	A	A	D	P	D	A	D
Transcription	ACHIS	A	A	A	P	D	A	D
	MEHIS	A	C	A	A	D	A	C
	RNA	A	D	n/a	D	D	A	n/a
	RNAPII	A	A	A	n/a	A	A	A
	B23	C	C	C	C	C	C	C
Post-transcription	SC35	C	A	A	A	D	C	D
	CB	n/a	n/a	n/a	n/a	D	n/a-	D
Proteolysis	19S	D	D	D	A	D	A	D
	11S	P	C	A	A	D	P	D

5.3.2.2 Overall AM trends

There is an obvious "edge-effect" whereby the functional compartments do not show a strong spatial preference for the nuclear boundary. Of course this does not mean that functional compartments are never found there, but it is less common.

Table 13 shows the maximum intensity for each dataset (which is also found in the vertical bar plotted next to each AM. The intensity ranges are different for each map

because they have been constructed from different amounts of segmented voxels. Therefore those AMs constructed for functional compartments with low voxel counts (such as telomeres, 19S, and 11S) are less reliable for the determination of spatial preference. In some cases this may lead to a spatial preference classification of diffuse, when in fact there was just not enough signal to determine the true pattern.

5.3.2.3 Spatial preference trends for functional compartments in MRC5 and WI38

5.3.2.3.1 Spatial preference trends of PML NB in MRC5 and WI38

Across the conditions of MRC5 ASYNC, HS, IFN, SS and VA, PML NBs can be classified as all of the categories of aggregate map pattern. In asynchronous nuclei PML voxels were found in a polar distribution (Figure 61 and Figure 72 (top)), found at both poles of the nucleus, but not within the core. However, with heat shock treatment the distribution was altered to be annular, whereby there is a ring of voxels that surrounds a core devoid of voxels. In cells treated with IFNβ the spatial preference of PML is still polar, and this indicates that there was no change in the organisation of PML upon this treatment. Upon serum starvation the localisation of PML was annular, and therefore there was a change that occurs in PML NB organisation under this treatment. However, in VA cells the localisation of PML was diffuse, which is completely different to that in the other data sets.

Interestingly in WI38 ASYNC PML was also polar as it was in MRC5 ASYNC, and in WI38 VA it was also diffuse (as in MRC5 VA).

5.3.2.3.2 Chromosome topology markers

In MRC5 ASYNC and VA cell nuclei centromeres appear to have a spatial preference for the core of the nucleus. However, in all the other data sets (heat shock, IFNβ-treated and serum starved nuclei) the localisation was diffuse. It seems unlikely that a reorganisation could occur during the 30 min treatment for heat shock. (However overnight, or over eight days (for interferon and heat shock, respectively) is probably

more likely). In WI38 ASYNC and VA, ACA were also found in the core pattern, and therefore the same distribution as in MRC5 ASYNC and VA nuclei.

In MRC5 asynchronous nuclei, telomeres were found within an annular region, and this was similar in heat-shocked cells. However in IFNβ-treated, SS and VA nuclei their spatial preference was diffuse. In WI38 ASYNC and VA TELO was found with the same spatial preference as in MRC5 ASYNC and VA nuclei – annular and diffuse respectively.

5.3.2.3.3 Spatial preference trends for transcriptional compartments

ACHIS in MRC5 ASYNC, HS and IFN was found in an annular region. In SS nuclei and in VA nuclei it was diffuse. For WI38 ASYNC and VA it was (as in MRC5 ASYNC and VA) found in an annular and diffuse region respectively.

MEHIS was found in an annular location in MRC5 ASYNC, IFN and SS nuclei. However, it had a spatial preference for the core in HS nuclei, and was found in a diffuse pattern in MRC5 VA. In WI38 ASYNC it was found to be annular as in MRC5 ASYNC, but in WI38 VA it was found in a core pattern unlike in MRC5 VA. Therefore MEHIS is the only compartment in which the spatial preference in MRC5 VA and WI38 VA differs.

In MRC5 ASYNC RNA was found in an annular region. In MRC5 HS and SS RNA was found to be diffuse. Unfortunately it was not possible to create the AM for RNA in MRC5 IFN or VA, or WI38 VA due to poor signal segmentation. In WI38 ASYNC it was also found in an annular region.

RNAPII was found to have an annular spatial preference in all of MRC5 and WI38 ASYNC and VA nuclei, and also in MRC5 HS. Unfortunately it was not possible to collect RNAPII in MRC5 SS.

Of interest was that B23 (nucleoli) showed a spatial preference for the core of the nucleus in every cell line and condition tested (MRC5 ASYNC, HS, IFN, SS and VA, and WI38 ASYNC and VA). This shows it has a strong preference for being at the centre of

the nucleus that does not change even under conditions of heat shock, IFNβ treatment or serum starvation.

5.3.2.3.4 Spatial preference trends for post-transcriptional compartments

In ASYNC nuclei (both MRC5 and WI38) SC35 showed a preference for the core of the nucleus, and in VA nuclei (both MRC5 and WI38) it was found to be diffuse. In MRC5 HS, IFN and SS SC35 was instead located in an annular region.

Cajal bodies (CB) were only found within the VA cell lines, and in both MRC5 and WI38 VA nuclei their spatial preference was diffuse. Therefore they fall within the same region as PML NBs, but since this region is wide (the whole nucleus) there is little evidence for a specific association that is hinted at in some publications.

5.3.2.3.5 Spatial preference trends for proteolysis compartments

19S in MRC5 ASYNC, HS, IFN and VA nuclei was found in a diffuse pattern. In SS however, it was found in an annulated region, as it was in WI38 ASYNC. In WI38 VA, as in MRC5 VA, 19S was found in a diffuse pattern. Therefore 19S is the only compartment where the spatial preference in MRC5 and WI38 ASYNC nuclei differs. Overall 19S is only found in a diffuse or annular region.

In MRC5 ASYNC 11S was found to have the same spatial preference as PML – polar, as it was also in WI38 ASYNC. In MRC5 HS 11S showed a core pattern, and in IFN and SS it showed an annular pattern. In MRC5 VA it was diffuse, as it was also in WI38 VA.

5.3.3 Summary

Across the ASYNC nuclei for each functional compartment there is an obvious correlation between spatial preference, which is also seen for VA nuclei. This shows that spatial preference for a particular compartment in likely to be similar in similar cell types (for example in both MRC5 and WI38 ASYNC PML shows a polar preference, ACA shows a core preference, and TELO shows an annular preference). Therefore they

appear to share similar organisations. However, the HS, IFN and SS treatments in MRC5 often do have an effect upon spatial preference (and are therefore affecting nuclear organisation) when compared to MRC5 ASYNC data set. Unfortunately the resultant change in spatial preference does not appear to be predictable, for example a core compartment in ASYNC becomes either diffuse (in the case of ACA) or annular (for SC35) in the MRC5 HS, IFN and SS data sets.

5.3.4 Functional compartment trends for cell lines and condition in MRC5 & WI38

5.3.4.1 Spatial preference trends for compartments in ASYNC nuclei

In MRC5 ASYNC nuclei all four of the AM patterns were found – PML and 11S were polar; TELO, ACHIS, MEHIS, RNA and RNAPII were annular; ACA, B23 and SC35 were core; and 19S was diffuse. In WI38 ASYNC there were no compartments showing a diffuse pattern, but PML and 11S were (as in MRC5 ASYNC) polar; ACA, B23 and SC35 were core (also as in MRC5 ASYNC); TELO, ACHIS, MEHIS, RNA, and RNAPII were annular (as in MRC5 ASYNC) but so was 19S in addition.

It is interesting that all the compartments involved in transcription show an annular distribution in ASYNC nuclei except for B23, which is found in a core location. Also of note is that only PML and 11S share the same location (both being polar in MRC5 and WI38 ASYNC).

5.3.4.2 Spatial preference trends for compartments in HS nuclei

In MRC5 HS, PML showed an annular pattern; ACA, RNA and 19S showed a diffuse pattern; TELO, ACHIS, RNAPII and SC35 were annular; and MEHIS, B23 and 11S were found in the core of the nucleus. In comparison to MRC5 ASYNC, certain compartments showed a reorganisation – PML changed from being polar to annular; ACA was no longer core, but was diffuse instead; MEHIS was not annular but changed to a core distribution; SC35 changed from core to annular; RNA switched from annular to core, and 11S switched from a polar organisation to a core one. Therefore heat shock

treatment appears to cause a redistribution of functional compartments in nuclei, which can be visualised using the AM.

5.3.4.3 Spatial preference trends for compartments in IFN nuclei

In MRC5 IFN once again all four AM patterns were found. PML was polar; ACA, TELO and 19S were diffuse; ACHIS, MEHIS, RNAPII, SC35 and 11S were found in an annular distribution; and B23 was found at the core. In IFN nuclei there was a slight reorganisation of some functional compartments (ACA, TELO, SC35, 11S) within the nucleus compared to MRC5 ASYNC nuclei. It is notable however that PML does not change its location with IFNβ treatment, and remains in a polar distribution.

5.3.4.4 Spatial preference trends for compartments in SS nuclei

In MRC5 SS PML showed an annular pattern, as did MEHIS, SC35, 19S and 11S. ACA, TELO, ACHIS, and RNA were diffuse; and B23 was core. This is very different from the organisation of functional compartments within MRC5 ASYNC nuclei, with many compartments sharing their distribution with PML (annular) or becoming diffuse.

5.3.4.5 Spatial preference trends for compartments in VA nuclei

In MRC5 VA nuclei there was a distinct trend with PML, TELO, ACHIS, MEHIS, SC35, CB, 19S and 11S all found in a diffuse pattern. ACA and B23 were found in the core region, and RNAPII was annular. In WI38 VA the result was extremely similar, with PML, TELO, ACHI, RNA, SC35, CB, 19S and 11S all found as diffuse patterns. ACA and B23 were once again found in the core, but with MEHIS in addition showing this distribution. RNAPII was once again annular.

Therefore transformation has resulted in a reorganisation of the nucleus in VA cells (of both MRC5 and WI38), which is probably more accurately described as a disorganisation. There is a trend for functional compartments, including PML to be found over a much less specific region of the nucleus, and hence them being found in a diffuse pattern.

Figure 77 shows a cartoon of the different AM patterns, with examples below of corresponding results.

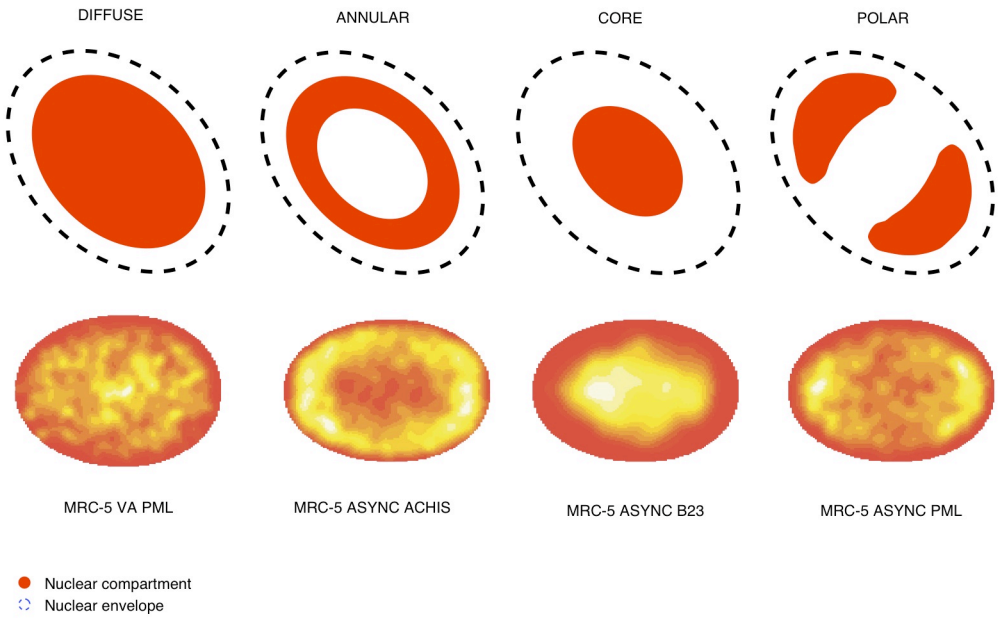


Figure 77 Summary of aggregate map patterns of spatial preference

Row 1: Four patterns of spatial preference were found; diffuse, annular, core and polar (left to right. Row 2: depicts examples of real AMs that fit the pattern descriptions; compartment, compartment, compartment, compartment (left to right).

5.4 Chapter summary

In order to create the aggregate maps the segmented nuclear compartments were transformed onto the templates of the appropriate cell line or treatment average nucleus. Interestingly four patterns of spatial preference in the nucleus were found. These were: diffuse, annular, core and polar. In all cases there was repulsion from the edge of the nucleus. Table 14 is a summary of the classification for AMs were generated for PML NBs, chromosome topological, transcriptional, post-transcriptional and proteolysis compartments in all cell lines and treatments except for the following; MRC5 VA IFN and RNA, MRC5 SS RNAPII. AMs for Cajal bodies were only made for MRC5 and WI38 nuclei, as they were not found in normal fibroblasts. Only PML NBs and 11S show a polar spatial preference. Nucleoli were found in the core regardless of the cell line or treatment, and RNA polymerase II_O was always annular in spatial preference. In

fact the functional compartments grouped under transcription were most commonly found in an annular pattern except for nucleoli. Centromeres showed a core spatial preference except in the heat shocked, IFNβ-treated and serum starved MRC5 nuclei. The 19S core proteasome regulator was most commonly found to show a diffuse spatial preference. Interestingly there is an obvious disruption of the spatial preference of nearly all the functional compartments in the SV40 transformed MRC5 and WI38 VA (in comparison to their ASYNC counterparts) whereby almost all present in a diffuse pattern.

It is possible to classify the average localisation for compartments within the nucleus in normal, transformed, and treated cells using the aggregate mapping method. There are four main patterns that can be classified; CSR, core, annular and polar. For some nuclear subcompartments the pattern varies depending on the cell and what it has been treated with. For others, such as B23, the localisation always remains as core, and this is indicative of the need for that compartment to stay where it is no matter what the cellular environmental conditions are.

Obviously, bigger sample sizes lead to more accurate mapping of where compartments are found within an average nucleus in a particular cell type.

6

Discussion and conclusions

6.1 Introduction

In Chapter 6 the findings and implications of the results are considered with respect to PML NBs and their spatial relationships in normal, treated and virally transformed fibroblast cell lines. The technical issues that arose during the project are also discussed. Overall conclusions are drawn about PML NBs and their spatial organisation in relation to other PML NBs, nuclear landmarks, and functional compartments within the nucleus, and the value of the image segmentation and statistical tools used to quantify their relationships are assessed.

6.2 PML NBs – organisation and function in the nucleus

6.2.1 Discussion of nuclear volume and PML NB findings in asynchronous normal and virally transformed fibroblasts

- **Nuclear volume increases as a consequence of viral transformation**

Nuclear volumes were higher in both the virally transformed cell lines of MRC5 and WI38 than their ASYNC counterparts. Therefore an increase in nuclear volume is a likely function of transformation.

The mean nuclear shape according to footprint can be summarised as MRC5 ASYNC < WI38 ASYNC < WI38 VA < MRC5 VA. Since WI38 ASYNC nuclei share a similar

mean volume to MRC5 ASYNC this means that WI38 ASYNC have slightly flatter nuclei. From the nuclear volume increase attributed to transformation it was expected that the nuclear footprints of the VA cells would also be greater than their ASYNC counterparts.

- **Transformation results in an increase in median PML NB number in WI38 but not MRC5 VA nuclei**

The median number of PML NBs in MRC5 ASYNC nuclei was about 10, and this was the same for MRC5 VA. Therefore transformation has no effect upon PML NB number in MRC5 cells. WI38 ASYNC nuclei had a similar median number of PML NBs per nucleus to MRC5 ASYNC, however viral transformation in WI38 cells resulted in a two and a half-fold increase in PML NB number. Therefore viral transformation does not always result in the same effect upon infected cell lines.

The mean PML NB was also plotted, and was found to be very similar to that of the median PML NB number. Therefore either the median or mean were suitable values chosen to represent data sets.

- **PML NB median size decreases with SV40 viral transformation**

In MRC5 ASYNC the median PML NB size was about 50 voxels. In MRC5 VA this was smaller. WI38 ASYNC and VA nuclei showed the same trends with median PML NB sizes (and overall range of sizes) the same as their MRC5 counterparts. Therefore viral transformation with SV40 results in a decrease in median PML NB size. Also, PML NB size is maintained between different fibroblast and virally transformed cell lines. Interestingly though, as mentioned previously, there were a greater number of PML NBs in WI38 VA than in MRC5 VA, although their size was similar. This means that we would expect there to be more PML protein in WI38 VA nuclei than in MRC5 VA nuclei.

- **The average PML protein voxel count per nucleus is a reflection of the median PML NB size and number in normal and transformed nuclei**

In MRC5 ASYNC the average PML voxel count per nucleus was about 1000 voxels, and this decreased in MRC5 VA. Since there were the same number of PML NBs in VA as ASYNC, but those bodies were smaller, this result can be explained.

In WI38 ASYNC the PML voxel count was the same as for MRC5 ASYNC, which was expected, as PML NB size and number were the same for both cell lines. The WI38 VA PML voxel count was also similar, and this was because although the PML NBs were smaller in size than in WI38 ASYNC, there were greater in number.

- **Mean PML NB size is only controlled by one parameter in normal and transformed nuclei**

From the ECDF plot VA < ASYNC in terms of mean PML NB size for both MRC5 and WI38 nuclei. All curves followed an exponential distribution, meaning that mean PML NB size is likely to be controlled by only one parameter.

- **Transformation may result in an increase, decrease, or no change in the average voxel counts of functional compartments in the nucleus**

For ACA the average voxel count per cell was slightly higher in WI38 VA than the other ASYNC and VA datasets, which could be due to an increased ploidy due to transformation. For TELO the voxel count doubled in MRC5 VA in comparison to ASYNC, which was due to the ALT positive status of the MRC5 VA cells. However, this increase was not seen in WI38 VA, but could have been due to a relatively poor TELO signal overall from the antibody used. If repeated a PNA FISH probe against telomeric DNA, in combination with DAPI staining could be used to achieve a better signal. This was not done previously because of imaging limitations (there was no UV laser available at the time), and lamin B was delocalised during the FISH procedure.

For ACHIS the voxel count increased in VA nuclei, but was lower in WI38 ASYNC than in MRC5 ASYNC. In MEHIS the voxel count slightly decreased in VA cells. This may

have been due to there being less repression foci due to the increase in acetylation (and hence increased transcription). RNA voxels also increase in VA nuclei in comparison to ASYNC, as did the RNAPII voxel count. Therefore overall the voxel counts for transcriptional compartments are increased in VA nuclei, indicating a greater level of global transcription levels. The B23 voxel count was similarly high in ASYNC and VA nuclei.

In SC35 the voxel count decreased in MRC5 VA cells in comparison to ASYNC. Since above we deduce that such nuclei are highly transcriptionally active, this can only be accounted for when we consider that active SC35 is found as a diffuse component, and not in splicing speckles where it is stored. Since diffuse staining is not well segmented by the SCT algorithm active splicing speckles may well be underestimated in size (Russell et al., 2009). This should be improved in future versions of the SCT algorithm. For 19S and 11S the average voxel counts were low in both ASYNC and VA nuclei, showing that levels are low in ASYNC nuclei, and that transformation has no effect upon the levels.

- **Inter – PML NB distance is probably a reflection of the median nuclear volume and the number of PML NBs per nucleus in normal and transformed nuclei**

In MRC5 ASYNC the median minimum inter – PML NB NND was at around 30 voxels, but in MRC5 VA this increase to about 40 voxels. This means that the PML NBs were further apart from each other, a change which could be attributed to the increase in nuclear volume, which accompanies transformation. Since the PML NB number did not alter, PML NBs in such cells have a greater space through which to spread, and if locating according to CSR (as the majority do (see below)) we would naturally expect to see an increase in inter – PML NB NND.

For WI38 ASYNC the median minimum inter – PML NB NND was at around 40 voxels (further than for MRC5), and in WI38 VA the median minimum inter – PML NB NND decreased to around 30 voxels. Since the inter – PML NB NND was longer in WI38 ASYNC than in MRC5 ASYNC this may be a difference that exists between the cell lines. The decrease in inter – PML NB NND between WI38 ASYNC and VA can be accounted for by the large increase in PML NB number in the VA nuclei (which is also

large enough to counteract the effect of the WI38 VA nucleus being of greater volume than ASYNC).

- **PML NBs are organised according to CSR with respect to each other in the majority of normal and transformed nuclei**

From the CSR results it can be interpreted that objects that are closer together than expected under CSR are clustered, and objects that are further apart from one another than expected are more regularly spaced than when arranged according to complete spatial randomness.

The percentages of cells containing PML NBs that were closer to each other, or further from each other than expected under CSR were similar for MRC5 ASYNC and VA (about 20% and 10%, respectively). Overall this shows that the majority of PML NBs are organised according to CSR with respect to their nearest neighbouring PML NB. Also, it shows that transformation has not really had an affect upon the spatial organisation of PML NBs in comparison to the asynchronous population. This may be because PML NB number is maintained between MRC5 ASYNC and VA nuclei.

In WI38 cells there was a decrease in the percentage of cells where PML NBs were classified as closer than expected in comparison to MRC5. However in there was also an increase in the percentage of cells where PML NBs were further from each other than expected in comparison to MRC5. Therefore, there are subtle differences in the spatial organisation of PML NBs in MRC5 and WI38 cell lines (PML NBs are slightly more randomly or regularly spaced in WI38), but overall these differences are minor.

In WI38 VA cells there were more cells where PML NBs were closer than expected to each other in comparison to WI38 ASYNC, which can be accounted for by the increase in PML NB number seen in WI38 VA cells in comparison to ASYNC. However in WI38 VA cells there were also more cells that contained PML NBs that were further from each other than in WI38 ASYNC. Therefore this is a complicated trend that is difficult to account for.

- **PML NBs in normal and transformed nuclei show repulsion from the nuclear boundary**

The PML NB – nuclear boundary median minimum NND was very similar for all of the MRC5 and WI38 ASYNC and VA datasets, at a distance of about 13 voxels. Therefore the "edge-effect" could be seen between PML NBs and the nuclear boundary in all the cell lines studied, and must therefore be intrinsic to the organisation of PML NBs within the nucleus.

In MRC5 and WI38 ASYNC and VA cell populations there was a similarly small percentage of cells that contained PML NBs that were closer to the boundary than expected. This indicates that PML NBs do sometimes locate near to the boundary, but in most cases they are placed according to CSR with respect to the boundary. In these same cell populations there was also a moderate percentage of cells in which PML NBs were further from the boundary than expected under CSR. This is evidence to support the "edge-effect" which is present in all cell lines and treatments tested, and suggests that PML NBs are repelled from the nuclear boundary and locate more centrally than we would expect.

- **PML NBs do not show preference for a central nuclear location in normal and transformed cells**

In MRC5 ASYNC and VA nuclei the PML NB – nuclear centroid median minimum NNDs were similar at around 60 voxels. In WI38 ASYNC and VA these were slightly longer. These measurements show that PML NBs are typically found quite far away from the centre of the nucleus, and this is likely to be due to the presence here of the nucleolus, from which we show there is repulsion of PML NBs.

The percentage of cells that contained PML NBs that were closer to or further from the nuclear centroid in the MRC5 and WI38 ASYNC and VA populations was very low, and therefore PML NBs were mostly arranged according to CSR with respect to the nuclear centroid.

- **In normal cells PML NBs share strong spatial associations with SC35 domains and the 11S immunoproteaseome regulator, and a very weak association with nucleoli**

The association levels between PML NBs and functional compartments were very similar between MRC5 ASYNC and VA cells for the majority of compartments. For ACA, TELO, ACHIS, MEHIS, RNAPII, and 19S there was a moderate percentage of ASYNC cells that contained PML NBs that were closer than expected under CSR to the compartments. In B23 there was a very low percentage of ASYNC cells that contained PML NBs that were closer than expected to nucleoli, and a similar low percentage that were actually further than expected. For SC35 and 11S there was a moderate (WI38) to high (MRC5) percentage of ASYNC cells that contained PML NBs that were closer than expected under CSR to the compartments.

- **In transformed cells PML NB spatial associations with centromeres, nascent RNA, and 11S immunoproteasome regulator are lost, and a very strong association with telomeres is gained**

There did not appear to be a big difference in the CSR relationships described for PML NBs in ASYNC cells in the virally transformed VA cells. However, for ACA, RNA, and 11S, their association between PML NBs was lost in VA cells. This may be a sign of disorganisation in transformed nuclei. For RNAPII the association with PML NBs increased in WI38 VA, but not in MRC5 VA. For SC35, whilst an association with PML NBs was lost in MRC5 VA cells, it actually strongly increased in WI38 VA cells. Interestingly, for TELO a very strong association between PML NBs was gained in both MRC5 VA and WI38 VA cells, and which was not seen as strongly in the ASYNC cells. This was due to the ALT positive status of both VA cell lines, which induces a relationship between TELO and PML NBs. This was also true for CB, although the association was only seen in a low percentage of cells, and was non-existent in ASYNC since Cajal bodies do not form in normal cell lines.

- **The spatial preference of different functional compartments is conserved between MRC5 and WI38 normal fibroblast cell lines, and also between MRC5 VA and WI38 VA transformed cell lines**

There were four patterns of spatial preference found for the functional compartments looked at in the study. These were diffuse, core, annular, and polar. Similar spatial preferences for individual functional compartments were seen within the MRC5 and WI38 ASYNC AMs, and between the MRC5 and WI38 VA AMs. This shows that the spatial preference results for each functional compartment are comparable between the two fibroblast lines, and that transformation has had a similar effect upon the spatial preference of functional compartments in both VA cell lines.

- **The spatial preference of functional compartments, including that of PML NBs, is disrupted upon transformation**

However, there was a discrepancy between the spatial preferences of the majority of functional compartments in the ASYNC AMs in comparison to the VA AMs. There was a disorganisation from polar, core, or annular patterns to diffuse, and this was even seen for PML NBs. This was likely to be a function of the transformation, which can be shown to have a huge impact upon the organisation of functional compartments within the nucleus. However, this was not obvious from simply comparing projection images of nuclei from both normal and transformed cells. It was also not apparent from the NND and CSR analysis between PML NBs and functional compartments in ASYNC and VA nuclei. This was because there was also a major disruption of the PML NB spatial preference, meaning that overall many PML NB – functional compartment associations remained intact. This suggests that that the function(s) of PML NBs remain the same in both normal and transformed cell lines.

- **The spatial preference of transcriptional compartments tends to be annular in both normal and transformed nuclei, except for nucleoli which show a preference for the centre of the nucleus**

Spatial preference of transcriptional compartments was often found to be in the annular region for both MRC5 and WI38 ASYNC and VA, indicating a region in the nucleus

where transcription tends to occur. This also overlaps with where PML NBs are found, reinforcing the NND and CSR evidence that PML NBs may play a transcriptional role in the nucleus.

Interestingly RNAPII and B23 maintained their spatial preference (annular and core, respectively, even under HS, IFN, and SS treatment) between ASYNC and VA nuclei, which indicates that this requirement probably integral to their correct functioning within the nucleus, and essential to maintain its viability. AS for B23, ACA was core in ASYNC and VA. This is interesting as IF reveals centromeres to often be found within nucleoli, due to the fact that many nucleolar organising regions are near centromeric regions.

- **Functional compartments with strong associations with PML NBs share overlapping, but not necessarily the same spatial preferences**

TELO and CB (shown to have strong associations with PML NBs in VA cells in the NND and CSR analysis by us, and in the literature, respectively,) were found to be diffuse in VA nuclei, which coincided with the PML NB spatial preference. However, there may not have been enough signal to determine their correct pattern due to low voxel counts overall.

6.2.2 Discussion of nuclear volume and PML NB findings in normal fibroblasts treated with heat shock, interferon β, and serum starvation

- **Nuclear volume is conserved in heat shocked and interferon treated normal fibroblasts, but decreases in serum starved cells**

Nuclear volumes were similar for MRC5 ASYNC, HS, and IFN cells, which was as expected because there would not be much time for a change in nuclear volume to occur during the treatment periods (30 mins and 16 hours respectively). In SS cells there was a slight decrease in nuclear volume. Since the cells were left in 0.1% FCS medium for eight days it is possible that with no active growth there was no increase in nuclear volume. Also, since the cells were induced into quiescence, chromatin compaction is likely to have occurred which may also have contributed to the slight decrease in nuclear volumes of this dataset.

The mean nuclear shape according to footprint can be summarised as MRC5 ASYNC < HS, SS < IFN. For SS a bigger nuclear footprint than ASYNC can be explained as despite there was being slight decrease in median nuclear volume in SS nuclei compared to ASYNC, in serum starved cells appear to be longer and thinner which accounts for both a smaller volume and a bigger footprint. The different shape of MRC5 HS and IFN to ASYNC was unexpected since they were all of similar median nuclear volume. Since the treatments times are short for both HS and IFN, it seems unlikely that a big change in nuclear footprint could occur during this timescale. However, it could simply be an artefact due to the shapes of the particular nuclei found within the sample.

- **Heat shock, interferon treatment, and serum starvation increase PML NB number**

There was a six-fold increase in PML NB number in the MRC5 HS dataset, in comparison to ASYNC (where the median PML NB number was 10). In the IFN and SS datasets there was a two-fold increase in the median number of PML NBs. Since all treatments affected PML NB number, this may be a stress response, exhibited by the cell upon heat shock damage (HS), viral infection response (IFN), or growth inhibition (SS).

- **PML NBs increase in size with IFN treatment, but decrease in size with HS and SS treatment**

Median PML NB size decreased in MRC5 HS nuclei in comparison to MRC5 ASYNC. This was due to fission of small PML fragment bodies from the pre-existing normal PML NBs found in MRC5 ASYNC. These pre-existing PML NBs persist in the HS dataset. The high number of large sized outliers may indicate a potential segmentation problem, since the pre-existing bodies actually appear to increase in size due to heat shock treatment. It is possible that PML protein may become diffuse around the pre-existing bodies, which could lead to their over-segmentation by the SCT algorithm. PML NB size increased in the IFN dataset (due to increased levels of PML protein expression), and decreased slightly in the SS dataset (perhaps due to degradation of PML protein over the eight day serum starvation period).

- **The average PML voxel count increases in interferon treated nuclei and (unexpectedly) in heat shock nuclei**

The average PML voxels per nucleus in MRC5 HS was increased in comparison to ASYNC, which was unexpected because the extra PML NB found in HS nuclei are thought to form via fission from pre-existing bodies. Therefore there could be a potential segmentation problem attached to this dataset, which is discussed further in Section 6.3.3.2.1.2. The PML voxel count in MRC5 IFN was increased, as expected, due to an increase in PML protein expression upon IFN treatment (demonstrated in Appendix II). However, the slight decrease in SS PML voxels was not expected, as PML NBs were slightly smaller in size, but slightly greater in number than in MRC5 ASYNC, and therefore the average PML voxel counts should have been similar. However it was only a slight difference from what was expected, and was therefore likely not to be significant.

- **Mean PML NB size is only controlled by one parameter in heat shocked, and interferon treated nuclei**

From the ECDF plot SS < ASYNC < IFN in terms of mean PML NB size. MRC5 SS and IFN followed an exponential curve (as did MRC5 ASYNC and VA) meaning that mean body size was likely to be controlled by only one parameter. However MRC5 HS did not follow the exponential, and this is likely to do with the two differently sized PML NB populations in these nuclei. Interestingly the mean body size for HS was the same as for ASYNC, indicating that there is some mechanism to maintain mean size where PML protein levels remain the same.

- **Chromosome topology voxel counts are unaffected by heat shock, interferon treatment, and serum starvation**

For ACA, the average voxel count per nucleus was similar for all of MRC5 ASYNC, HS, IFN, and SS nuclei, and as expected none of these treatments affected the number of centromeres. For TELO the same trend was seen.

- **The effects of heat shock, interferon treatment, and serum starvation upon transcriptional compartment voxel counts are variable**

For ACHIS, the voxel count decreased in HS, IFN, and SS nuclei in comparison to MRC5 ASYNC, and for MEHIS it remained the same in HS and IFN nuclei, but decreased in SS nuclei. For SS both trends can be accounted for since ACHIS (as a marker of active transcription) would decrease where overall transcriptional levels are lower (for example serum starved cells), and MEHIS might be replace by a marker of global repression in such cells. RNA voxel counts did not alter in HS or SS cells, and nor did RNAPII in HS cells. However in IFN nuclei the RNAPII voxel count increased. For B23 there was a decrease in both HS and SS nuclei. In HS B23 became diffuse and consequently was not well segmented, and in SS B23 was only found at the edges of nucleoli. Nucleoli in both were therefore underestimated in terms of voxel count.

- **Interferon treatment results in an increase in the average 11S immunoproteasome regulator voxel count**

SC35 voxel counts were high in all of the ASYNC, HS, IFN and SS datasets. 19S had low voxel counts in all, as did 11S except in IFN where it was upregulated due to its requirement in the immunoproteasome. (IFN treatment mimics the cell's initial response to viral infection).

- **Heat shock results in a decrease in the inter – PML distance, but interferon treatment and serum starvation do not**

In MRC5 HS there was an decrease in the median minimum inter – PML NB NND in comparison to MRC5 ASYNC, and this was due to the increase in number of bodies within the same nuclear volume. In IFN and SS the inter – PML NB NND remained the same as for ASYNC despite the increase in median PML NB number for these datasets.

- **Interferon treatment and serum starvation lead to a more regular spacing between PML NBs, as does heat shock, which in addition also results in a clustering of PML NBs**

In MRC5 HS nuclei there was an increase in the percentage of cells where PML NBs were closer to each other than expected under CSR compared to MRC5 ASYNC. This means that there was a clustering of PML NBs in HS cells, which is probably due to the increase in PML NB number. In HS, IFN, and SS nuclei there was an increase (slight for HS) in the percentage of cells where PML NBs were further from each other than expected under CSR, therefore indicating a more regular spacing of PML NBs in such nuclei. This means that in HS nuclei there are two populations of PML NBs, (probably consisting of the heat shock fragments and the larger, normal bodies from which they split).

- **The repulsion of PML NBs from the nuclear boundary is maintained in heat shocked, interferon treated, and serum starved nuclei**

The PML NB – nuclear boundary median minimum NND was very similar for all of the MRC5 ASYNC, HS, IFN and SS datasets (at about 13 voxels) showing that the "edge-effect" is maintained even in treated MRC5 cells.

- **Heat shock and interferon treatment both increase the association with, and repulsion from, the nuclear boundary simultaneously, but under serum starvation there is only an increased "edge-effect"**

In both HS, and IFN nuclei there was an increase in both the percentages of cells containing PML NBs that were closer to and further from the nuclear boundary than we would expect under CSR in comparison to the MRC5 ASYNC population. However, the increase in both for IFN was less than for the HS population. This is evidence of an increased "edge-effect" for both populations, and further clustering towards a central nuclear location. There is also evidence to suggest that at least some of the PML NBs move towards the nuclear boundary in the nuclei of such treated cells. It could be that there are two populations of PML NBs (which certainly could explain the result for the HS dataset. In this case the smaller (and more mobile) PML NBs might be able to move

closer to the nuclear boundary than the pre-existing bodies from which they split). Therefore both HS and IFN treatments alter the spatial organisation of PML NBs. In SS cells there was only an increase in the percentage of cells where PML NBs were further from the boundary than expected under CSR. Although PML NBs are still repulsed from the boundary in SS nuclei, there is no increased effect, as for HS or IFN. However, this still supports the IF observation that PML NBs in serum-starved cells appeared to cluster towards the centre of the nucleus.

- **Heat shock, interferon treatment, and serum starvation do not affect PML NBs' distance from the nuclear centroid according to NND analysis**

The PML NB – nuclear centroid median minimum NNDs for MRC5 HS, IFN, and SS were similar to that of MRC5 ASYNC, at around 60 voxels. This distance is set by the typical presence of the nucleolus towards the centre of the nucleus. Therefore such treatments do not appear to influence the minimum NNDs of PML NBs to the nuclear centre. Of course there will always be some PML NBs that are found extremely close to the centre of the nucleus, but these are not often seen, as PML NBs are typically repulsed by the nucleolus.

- **PML NBs cluster towards the nucleus in a low percentage of cells as a result of heat shock, interferon treatment, and serum starvation according to CSR analysis**

In HS, IFN, and SS cells there was an increase in the percentage of cells in which PML NBs were closer to the nuclear centroid than expected under CSR, the biggest of which was seen in HS nuclei. Therefore there was some limited evidence to support a clustering towards the centre of the nucleus in such treated cells, although the percentages were generally low.

- **Heat shock increases the association between PML NBs and transcriptional compartments**

Heat shock treatment induced the most increases in association between PML NBs and functional compartments (for the seven compartments TELO, ACHIS, MEHIS, RNA,

RNAPII, B23, and 19S). This was interesting as PML NBs were closer to all the transcriptional compartments than expected under CSR in HS treated cells.

- **Interferon treament increases the association between PML NBs and many functional compartments, including the 11S immunoproteasome regulator**

IFN treatment induced an increase in association between PML NBs and six compartments – TELO, ACHIS, MEHIS, RNAPII, B23, and 11S. For 11S the association was already very high in ASYNC cells, and so the increase was only slight overall.

- **Heat shock, interferon treatment, and serum starvation all increase PML NB association with telomeres, acetylated and methylated histones, and nucleoli**

Serum starvation induced an increase in association between four compartments and PML NBs – TELO, ACHIS, MEHIS, and B23. PML NBs were actually induced to become closer than expected under CSR to all of TELO, ACHIS, MEHIS, and B23 when cells were treated with HS, IFN or SS. Since PML protein has been shown to associate with nucleoli under conditions of stress cells (Bernardi et al., 2004; Condemine et al., 2007; Janderova-Rossmeislova et al., 2007) it is likely that the relationship between PML NBs and B23 is induced by the HS, IFN and SS treatments acting as a stress upon the cells. For ACHIS and MEHIS the increase in association upon HS, IFN or SS treatment could be due to changes in transcriptional activity in such cells, and indicate a transcriptional role for PML NBs. However, it was not obvious why the association between TELO and PML NBs should increase upon such treatments.

- **Heat shock, interferon treatment, and serum starvation result in changes to spatial preferences for many different functional compartments**

As mentioned previously, four patterns of spatial preference (diffuse, core, annular, or polar) were found for the functional compartments studied in the nucleus. HS, IFN, and SS treatments resulted in changes in spatial preferences for many compartments from

those in ASYNC nuclei, although the differences were not as striking as the change between ASYNC and VA nuclei. For example, in all three treatments ACA changed from a core to a diffuse spatial preference, and SC35 changed from core to annular. RNAPII and B23 remained annular and core, respectively, even upon treatment. PML NBs showed different spatial preferences in HS and SS nuclei from ASYNC, but not in IFN cells.

6.2.3 PML NBs in MRC5 cell-cycle subsets

- **Nuclear volume measurements of MRC5 cell-cycle subsets do not concur with those of MRC5 ASYNC or SS**

The nuclear volumes of G1, G0, and S MRC5 subsets were greater than that of MRC5 ASYNC. This was converse to what was expected since MRC5 ASYNC also contains large G_2 cells, which should contribute to an increased median volume. However, these are probably only a small proportion of the entire ASYNC population, and may not make much of a difference overall. Also, the MRC5 subsets had small sample sizes in comparison to ASYNC (50 cells versus 500), and so any particularly large cells in these samples would bias the median values to a greater extent. It is interesting though that the G0 median nuclear volume was greater than that of MRC5 SS, which indicated potential differences between the two populations, even though they are supposed to represent equivalent cells.

- **PML NB number in MRC5 cell-cycle subsets is not as expected**

In the MRC5 subsets, G1 and G0 cells shared a median PML NB number with that of MRC5 ASYNC. There was a slight decrease in PML NB number in the S subset. However, it was expected to have stayed the same or increased (since PML NB number doubles during the course of S phase (Dellaire et al., 2006b). Therefore we cannot support this previous finding. The median PML NB number in the G0 subset was less than that of MRC5 SS, again showing these datasets may not represent the same population of cells. Since PML NB number seems to increase upon cellular stresses it may be that serum starvation is stressing cells, which results in them moving into quiescence.

- **PML NB size in MRC5 cell-cycle subsets is not as expected**

In the MRC5 subsets the median PML NB size was the same for S as it was for MRC5 ASYNC. It was increased in both G1 and G0 subsets. The median PML NB size in G0 was greater than in MRC5 SS, reinforcing that these two datasets did not represent the same populations.

- **Inter - PML NB distances for MRC5 cell-cycle subsets are similar to those in MRC5 ASYNC**

The minimum inter – PML NB NNDs for the G1, G0, and S subsets were very similar to that of MRC5 ASYNC. For G0 the inter – PML NB NND was increased in comparison to MRC5 SS, due to there being fewer bodies in a larger volume.

- **PML NB repulsion from the nuclear boundary is also seen in MRC5 cell-cycle subsets**

The "edge-effect" could also be seen between PML NBs and the nuclear boundary in the G1, G0 and S MRC5 subsets too, and must therefore be intrinsic to the organisation of PML NBs within the nucleus.

- **PML NBs in MRC5 cell-cycle subsets are also positioned away from the nuclear centroid**

The MRC5 subsets G1, G0, and S all shared similar PML NB – nuclear centroid median minimum NNDs, and therefore the PML NBs in these datasets were also found quite a distance away from the centre of the nucleus.

6.2.4 PML NB functional insights

A number of functional roles in the nucleus were indicated for PML NBs by our analysis. These also support existing knowledge about PML NB function in the literature.

The PML NB - 11S immunoproteasome regulator relationship was found to be strong in

normal asynchronous MRC5 nuclei, and even stronger in cells treated with interferon, which supports previous findings (Fabunmi et al., 2001; Lafarga et al., 2002; Lallemand-Breitenbach et al., 2001). In comparison, the PML NB relationship with the 19S core proteasome regulator was almost non-existant, despite evidence to suggest otherwise (Dino Rockel and von Mikecz, 2002; Wojcik and DeMartino, 2003). Since the 11S immunoproteasome regulator is always found close to PML NBs even in untreated asynchronous MRC5 cells, this is likely to be related to an important function for which PML NBs and 11S need to be closely located. Interestingly, the association between 11S and PML NBs was abrogated in SV40-transformed nuclei, and in such nuclei we also showed that PML NB size was decreased. In interferon treated cells we saw that the expression of PML protein was upregulated as part of the anti-viral response (Section 3.3.7 and Appendix), and that this coincided with an increase in 11S voxel counts (Section 4.3.2.4). Since PML protein has anti-viral properties (Everett and Chelbi-Alix, 2007) it obviously presents invading viruses with an obstacle, and therefore levels must be lowered in order to allow viral replication and protein production, which may lead to transformation of the cell depending upon the virus. In addition, the association between PML NBs and 11S must also be removed for virally-infected cells (such as MRC5 VA) to persist. PML NBs probably play a more passive role in the proteolysis of viral proteins, such as those of herpesviruses, which are known to target and disrupt PML NBs (Everett et al., 2006; Salsman et al., 2008). Since the relationship between PML NBs and 11S became stronger upon interferon treatment, it is likely that the 11S regulator becomes active upon viral infection so that viral proteins found at PML NBs can be quickly degraded for presentation as MHC class I antigenic peptides at the cell surface (Rechsteiner et al., 2000). Such cells are then targeted for destruction by T cells as part of the immune response. Paradoxically, viral genomes are found to replicate at PML NBs (Everett, 2006; Ishov and Maul, 1996; Maul et al., 1996), which would suggest that they provide an environment suitable for viral transcription. Yet viruses still attempt to disrupt PML NBs and downregulate PML protein expression. Therefore in the long run the anti-viral properties of PML protein, and its association with 11S that encourages MHC class I presentation of viral proteins must be more of a disadvantage to viruses than the advantage of exploiting the transcriptional environment of the bodies, which they are able to use to their advantage upon initial infection.

The PML NB - telomere relationship was shown to be extremely strong in the SV40-transformed MRC5 and WI38 VA cell lines. This strongly supports existing evidence for the functional role of PML NBs in ALT positive cells, which includes the clustering of true telomeres at APBs (Draskovic et al., 2009). However, we also saw a slight association between PML NBs and telomeres (which was not expected under CSR) in normal asynchronous cells, which do not employ the ALT mechanism to maintain telomere length. This is difficult to account for. Previously, telomeres have been shown to be randomly distributed in both normal and transformed cells (Luderus et al., 1996), attached to the nuclear matrix (de Lange, 1992), found as a disk in G_2 (Chuang et al., 2004), and to cluster at the perinucleolar region (Ramirez and Surralles, 2008). Therefore the evidence for PML NB association with telomeres in normal and transformed cells has often been contradictory. Brouwer et al saw the *de novo* formation of PML NBs at telomeres in several cell lines where PML NBs had previously been dissembled using the DNA demethylating agent MMS, (including in non ALT cells) (Brouwer et al., 2009). They suggest that PML NBs nucleate at telomeres, and in non-ALT cells they dissociate after formation. This could account for why we saw a low proportion of cells where PML NBs were closer to telomeres than expected under CSR in normal asynchronous fibroblasts. However, since the study was completed in cells treated with MMS, it is difficult to make a fair comparison between our findings and those made by Brouwer et al.

Our analysis was unable to confirm that Cajal bodies shared a strong relationship with PML NBs, as published previously (although never quantified) (Grande et al., 1996; Sun et al., 2005). Despite evidence gained by examining image stacks immunofluorescently stained for PML protein and coilin, where Cajal bodies were often found in close proximity to PML NBs, this was not reflected in the NND or CSR analyses. This was probably due to the much lower object number of Cajal bodies in comparison to PML NBs in MRC5 VA and WI38 VA nuclei, meaning that only one of the total PML NB - CB minimum NND was very short. Any association between PML NBs and Cajal bodies is unlikely to relate to a shared post-transcriptional function, since there is much greater evidence to suggest that PML NBs are an environment that encourages transcription, as opposed to post-transcriptional processing. Therefore it may be that, (as for the PML NB - SC35 domain relationship described below), PML NBs and Cajal bodies form a post-transcriptional processing hub.

Interestingly, a strong PML NB - SC35 domain relationship was revealed by our analysis in normal MRC5 cells and those treated with heat shock, interferon, and serum starvation. We previously showed that PML NBs and SC35 domains are closer to each other than expected in normal asynchronous and serum starved nuclei, which indicated that their juxtaposition may create a transcriptional processing hub set up to respond to the transcriptional requirements of the cell as appropriate (Russell et al., 2009). However, we now see that this association is almost completely lost in SV40 transformed MRC5 VA nuclei. Since PML NBs and SC35 domains have been shown to function in transcription and post-transcriptional roles, respectively, they may form a processing hub for transcriptional products (Russell et al., 2009). If PML NBs and SC35 domains do function as such a hub, it is not obvious why this would be lost in VA cells, which are more transcriptionally active than either ASYNC or SS cells. One explanation is that active SC35 actually leaves splicing speckles to become a diffuse component in the nucleoplasm (Fay et al., 1997; Lamond and Spector, 2003). As diffuse staining is less well segmented by the SCT algorithm it may be that SC35 domains are incorrectly segmented in VA cells (due to high levels of activity) and therefore the association between PML NBs is seemingly lost. Alternatively, as there is little evidence for a shared post-transcriptional function between PML NBs and SC35 domains, since both are found within the ICD this could instead account for their close spatial proximity.

PML NBs were often found in close proximity to, and to have strong spatial relationships with, transcriptional compartments such as nascent RNA, RNA polymerase II, and acetylated and methylated histones as previously suggested (Boisvert et al., 2000; Grande et al., 1996; Kiesslich et al., 2002; LaMorte et al., 1998; von Mikecz et al., 2000). This suggests that PML NBs do function as an environment conducive to transcription. Interestingly, the number and pattern of transcription factories was conserved in heat-shocked cells (Mitchell and Fraser, 2008) indicating that although heat shock should result in a shutdown of transcription (except for the production of particular proteins produced in response to heat stress), the spatial associations they share with PML NBs may not necessarily be abrogated. However we can see from our results that there was not a strong spatial relationship between PML NBs and nucleoli under normal conditions, but this does not mean that PML NBs are never found to be associated with nucleoli in normal cells. However the association did slightly increase upon treatments that were likely to trigger stress response pathways in the cell, such as heat shock,

interferon, and serum starvation, and there is evidence in the literature to suggest that PML protein colocalises with nucleolar proteins under conditions of stress or DNA damage (Bernardi et al., 2004; Condemine et al., 2007; Janderova-Rossmeislova et al., 2007). Areas of heterochromatin, which is transcriptionally repressive, are often found in perinucleolar regions (see (Zhao et al., 2009)), which given PML NBs' role transcriptional role may also account for why they appear to be repelled from the nucleolus (in a similar manner to the "edge-effect"). Therefore it seems likely that PML NBs do not to share a functional role with nucleoli in normal asynchronous fibroblasts.

6.2.5 PML NB organisational insights

Interestingly, the minimum inter - PML NB distances are far greater than any of the other PML NB - functional compartment minimum distances, at around 30 or 40 voxels. Spacing appears to be related to the number of bodies present within a nucleus, as when the body number increases, the spacing between bodies decreases. We also saw that PML NBs in the nuclei of normal and transformed cells appear to be organised according to CSR with respect to each other. This could indicate that PML NBs locate within the nucleus so that collectively they cover as much of the nuclear volume as possible, and that different PML NBs within the same nucleus have separate functional roles. It may also mean that PML NBs are positioned non-randomly according to other functional compartments within the nucleus, which at least for telomeres, the 11S proteasome regulator, transcriptional comparments, and SC35 domains, this seems to be the case. There also appears to be an "edge-effect" whereby PML NBs are repelled from the nuclear boundary, and this may relate to PML NBs' transcriptional role, since the environment at the edge of the nucleus is typically repressive towards gene transcription (Deniaud and Bickmore, 2009; Towbin et al., 2009; Zhao et al., 2009).

Heat shock, interferon, and serum starvation were all shown to affect PML NB number and or size, which could be clearly seen when the data describing PML NB size and number in MRC5 and WI38 normal, treated and transformed cell lines (Figure 17, Figure 18, and Figure 19) was combined and presented as Figure 20 and Figure 21. This provided a useful way of presenting both PML NB size and number data in a way that allowed the effects of transformation, heat shock, IFN treatment, and serum starvation upon the PML NB populations of MRC5 and WI38 cells to be visualised. However, it

did not provide any insight as to why PML NB size and number differs between different cell lines, other than illustrating that they do differ, even between primary cell lines of similar origin, and that transformation with SV40 results in an decrease in mean PML NB size. It might be interesting to correlate the PML NB size and number data for many different cell lines with other information available about the cells (such as originator tissue, age, enzyme expression) to see if any trends could be found that may predict the PML NB morphometrics of a particular cell line.

The effect of serum starvation upon PML NBs was shown to be an increase in size, and a slight decrease in number in normal MRC5 fibroblasts, which has not been observed before. However, other evidence (from the comparison of the MRC5 SS dataset and the MRC5 cell-cycle G0 subset) suggests that the two populations may not be the same. This means that although the SS dataset was shown to be synchronised in G0 (see appendix controls), and therefore could be classified as quiescent (like the cells selected in G0 phase by their negative Ki67 staining), it is likely that the SS cells were also stressed by being forced into G0 through serum starvation. Therefore inducing quiescence via serum starvation may not create a good model for G0 cells, as there are also stress responses going on in which may mask or affect what we expect to happen.

When we quantify PML NB spatial organisation it is possible that we are also investigating where the bodies can exist within the nucleus. Evidence presented above suggests that PML NBs are not typically found within the centre of the nucleus, probably due to the presence of the nucleolus. PML NBs are thought to lie within the channels and lacunae of the ICD (Gorisch et al., 2004), migrating within a chromatin corral. Therefore we could inform the SPPs used to simulate PML NB spatial organisation within the nucleus using information regarding levels of chromatin condensation, as determined by the intensity of DAPI staining, since PML NBs should be found within less intensely stained regions. However, from our own aggregate maps we saw that PML NBs have a definite spatial preference (polar or annular), which often coincides with the region that other compartments found within the ICD (SC35 domains for example) and chromatin (nascent RNA, RNA polymerase II, acetylated and methylated histones) show spatial preference for (typically annular). In VA cells PML NB preference becomes diffuse, showing that PML NBs can be found almost anywhere within the nucleus, including the nucleoli. It may therefore be better to use this PML NB spatial preference

to inform the CSR analysis as to where PML NBs are often found within the nucleus, and to use this to determine if PML NBs are closer to functional compartments than expected under the informed SPP, as opposed to a CSR-based simulation.

The polar spatial preference of PML NBs in normal asynchronous cells was unexpected and is difficult to account for. Interestingly, the poles are found at the edges of the nucleus that are adjacent to the growing edges of the cell, and which extend to contact other cells that have also attached to the culture flask. Since IF staining was completed after 48 hours, most cells in the flask would by then have grown so that they were touching other cells, and be affected by contact inhibition. PML protein has been shown to be a negative growth regulator and tumour supressor (Wang et al., 1998) and therefore it is possible that it could play a role in this by stopping further growth in ASYNC cells from these polar regions. Interestingly in VA cells, which no longer undergo contact inhibition, PML NB spatial preference is diffuse, and PML NBs are smaller in size. PML protein expression has been knocked down in order to limit its tumour suppressive and negative growth regulator activities. In cells treated with interferon, PML NBs share the same polar spatial preference as ASYNC nuclei. Interferon β has been shown to lengthen S phase in squamous carcinoma cell lines (Vannucchi et al., 2000), and as seen in this report also increases PML protein expression levels (see Appendix 7.2). PML over-expression was also shown to reproduce S phase lengthening, meaning that PML may be part of interferon induced growth suppression (Vannucchi et al., 2000). In virally infected cells (but not transformed) it would be logical to inhibit growth in an attempt to prevent virion production, and spread of the virus to other cells.

6.3 Technical limitations: Problems and resolution

6.3.1 Biological issues - can these influence PML spatial relationships?

6.3.1.1 Choice of experimental time points

From the examples discussed it is clear that there are different subpopulations of PML NBs, and that when imaging PML NBs it is likely that all populations will be included in the analysis, especially in unsynchronised cells. Isoform-specific antibodies for PML will help to reveal any relationships that are related to particular isoforms in normal primary cells. Currently the vast majority of cell imaging is done in fixed cells, and not live ones. For PML microstructures that show movement, and are derived from larger PML NBs, their relationship with other nuclear compartments will be fairly dynamic, and imaging methods using fixed cells will only capture a snap shot of this PML NB population in time.

6.3.1.2 Effects of stress and handling of cells upon PML NBs

It is clear that PML NBs react to cellular stresses with changes in number, size and morphology (Dellaire and Bazett-Jones, 2004; Eskiw et al., 2003). When subjected to stress (including UV-C radiation, IR-γ, and transcription or proteasome inhibition) endogenous PML (likely to be PML I) forms nucleolar caps (Condemine et al., 2007). In response to type I interferon (IFN) PML expression is induced, resulting in a greater number of PML NBs, which are also larger in size than normal (Chelbi-Alix et al., 1995; Lavau et al., 1995). Although the stresses above will not occur in cells outside of experimental protocols, it may be that stresses on the cell resulting from culturing procedures and handling could also potentially have an effect on PML NB spatial relationships.

6.3.2 Methods related factors – can these influence PML spatial relationships?

6.3.2.1 Fixation, permeabilization and immunofluorescence

Fixation and permeabilization are essential for the immunofluorescent staining and visualisation of mammalian cells at particular time points. Different methods may be used, usually those historical to the lab but this has an effect upon the distribution of proteins in the fixed cell, especially that of nuclear proteins. As an example, different cell fixation and permeabilization methods can be correlated with the relocation of active RNA polymerase II complexes to splicing speckles where conditions did not preserve cellular ultrastructure (Guillot et al., 2004). Ominously the same methods also caused some redistribution of PML staining from PML NBs, but did not affect labelling of SC35 (splicing speckles) or coilin (Cajal bodies).

Some antibodies used in immunofluorescence recognise antigens better than others, and hence use of different antibodies to stain the same nuclear compartments in different publications may, in the extreme, result in noticeable differences in associations detected.

In this study PML protein was initially immunofluorescently stained using one of two anti-PML antibodies, based upon the species requirements for the particular IF detection combination. PML stained with the mouse anti-PML monoclonal antibody (from Santa Cruz) was typically weaker than that stained with the rabbit anti-PML polyclonal antibody. This did not pose a major problem for the SCT algorithm because if the overall intensity of the staining of the PML NBs is low, then the automatic threshold employed is low too. However, in a few cases it seemed that some of the smaller bodies were not correctly segmented where the mouse anti-PML antibody was used.

This issue was avoided later on in the project as a confocal microscope that had a UV laser became available. We could therefore image DAPI to delineate the nucleus (as an alternative to using the goat anti lamin B antibody). In turn, this allowed the much better goat anti PML polyclonal antibody to be used to detect PML, thus avoiding the problem of the weak signal.

6.3.2.2 Blocking

In addition to the well-defined pattern of PML NBs in the nucleus, there is a diffuse nuclear component consisting of PML protein that has not been SUMO-modified (Zhong et al., 2000a). Therefore blocking to avoid background staining of PML protein in the nucleus is futile. It is common not to include blocking steps, with clean images being achieved through thorough testing of highly specific antibodies, and well-executed wash steps. Since we are only interested in signal that falls within the nucleus, non-specific cytoplasmic background has little implications for data collection.

6.3.2.3 Reliability of using cell cycle markers to determine PML NB spatial organisation in subset of MRC5 nuclei

We attempted to use markers for G_0, G_1 and S phase to categorise nuclei to allow us to determine the PML NB spatial organisation for these phases in MRC5 ASYNC nuclei. It was hoped that they would present clear information regarding PML NB organisation from which we could return to the asynchronous MRC5 cells and use to extract cell cycle phase specific information. This approach was not successful. Unfortunately the information gained regarding PML NBs in S phase did not correlate to that already published (Dellaire et al., 2006b), however it was done in different cell lines. Also there was no specific information published regarding PML NB organisation in specific cell cycle phases for human fibroblasts. The sample sizes of 50 cells were probably not big enough to tell us about PML NB either. It was not possible to determine precisely if nuclei in the G1 subset indeed were in G1 as it was difficult to pick out G1 specific patterns for Ki67 staining. Lastly, the results obtained for the MRC5 G0 subset (chosen by their lack of positive staining for Ki67) and MRC5 SS differed. MRC5 SS population were shown to be mostly negative for Ki67 staining too (see Appendix), and so we would have expected them to show similar PML NB size, number and organisation. However this was not the case meaning that the "quiescent" cells obtained through serum starvation are not exactly equivalent those those picked out from an untreated asynchronous MRC5 population. It is likely that serum starvation subjects cells to stress and pushes them into quiescence, which is reflected in its PML NBs (which show signs of response to stress, and are know stress-responders in the nucleus as mentioned in Section 6.3.1.2)

6.3.2.4 Labelling

In general there is an amplification of the signal using IF to detect proteins in the nucleus. There is a risk that compartment size maybe over estimated. However we showed that the average PML NB size as determined through segmented by the SCT algorithm was in the correct range for that expected from both IF and electron microscopy measurements of PML NBs (Russell et al., 2009). Therefore this provides us with confidence that the distance measurements obtained from methods used herein are reliable and comparable to other existing methods available.

6.3.3 Imaging methods

Widefield and confocal microscopy are commonly used in the imaging of co-localization studies in the cell nucleus. The resolution limit of light microscopy poses a constant problem for the confirmation of true co-localization between two nuclear compartments. In 3D confocal imaging a further potential difficulty is the difference in resolution between the z-axis and those of the x and y. To some extent deconvolution can help resolve both drawbacks, but advances in imaging will be needed to improve the accuracy of quantification in association studies.

6.3.3.1 Data collection

To ensure accurate thresholding it was important to avoid background noise and unspecific staining as much as possible, and this was especially important in the red and blue channels. This was achieved by using highly specific antibodies, and by following IF procedures precisely to avoid leaving antibodies on the samples for too long. Using IF protocols already established in our lab it was found to be unnecessary to use blocking steps, and as demonstrated in the Appendix, there was no apparent difference between the level of background in blocked and non-blocked cells. However, the SCT algorithm was in general very able to cope with such noise and unspecific signals, and as such other issues found in correctly stained cells were the main source of thresholding problems, and are listed below.

6.3.3.2 Automatic Thresholding

In the majority of cases the SCT algorithm was successfully able to segment the red, green and blue channel images from the confocal data stacks. However, in some cells there were problems with some or all colour segmentation. For truly automated thresholding, as required for high throughput data analysis, this needs to be improved.

6.3.3.2.1 Main sources of thresholding problems

Because the data collected in each of the coloured channels was different, and reserved for particular nuclear compartments, different problems affected the image segmentation for each. The SCT algorithm was written bearing in mind that the red channel was reserved for the nuclear compartment, the green for PML protein, and the blue for the stain or protein that was used to delineate the nucleus.

6.3.3.2.1.1 Red channel

Sometimes the SCT algorithm did not choose the most appropriate threshold. This occurred in three cases. The first was where the signal was weak, and thus not detected even at low thresholds. The second was when the signal was diffuse, which is difficult for the algorithm to reduce to a focus or region. The third was when the signal consisted of foci of variable in size and or intensity. This led to an inappropriately high threshold being chosen, which eliminated small true, but weak, foci from the analysis. In such cases the threshold chosen was typically too high, resulting in the loss of signal where it should be present as seen in the image stack.

6.3.3.2.1.2 Green channel

In nuclei where there are PML NBs of a variety of intensities. The problem is similar to that of the red channel, where there are variably sized foci of different intensities. Two particular cases where this became important were in the HS MRC5 cells (where small PMLs undergo fission from pre-existing larger bodies), and in WI38VA cells, which appear to have a large number of particularly small PML NBs. A short-term resolution was to segment using manually chosen thresholds, but in the long term this is

unsustainable due to the large number of cells that would need to be checked. Also, the idea of automatic thresholding is that subjective user-oriented thresholding can be removed, thus allowing high throughput microscopy techniques, and removed variability introduced by different thresholders (despite user-thresholding being the described as the "gold standard") (Russell et al., 2009).

6.3.3.2.1.3 Blue channel

The blue signal from lamin B, used to delineate the nucleus, was occasionally weak at various points in the mesh, and the algorithm ignored this section of the cell, leaving it truncated, and the volume inadequately represented. Also, red and green signal that fell within the truncated area are not included in the segmentation. When the nuclear volume was stained with DAPI, as was possible in the latter part of the research timeline, a similar problem as that for the lamin B above also occurred. The code was then modified to cope with the DAPI, and this could also be used to avoid the previous problem in the lamin B data sets. However, the fix introduced a different problem to the DAPI data sets, whereby it was no longer possible to exclude blue signal that originated from another nucleus partially captured in the image stack, or from blebs nearby the nucleus. This led to an extension of the blue segmentation beyond the true edge of the nucleus, and therefore an over-representation of the nuclear volume. A temporary solution was to manually mask or remove the blue signal in regions of the slide that did not correspond to the nucleus, and reprocess the individual nuclei again.

6.3.3.3 Inter – PML NB and PML NB – functional compartment distance measurements

Upon segmentation of the images PML NB centroids were defined as an *xyz* coordinate within the 3D volume of the nucleus. Red objects were represented by segmented red voxels and did not have a centroid (even when possessing a body-like morphology such as Cajal bodies or centromeres). The distance between two PML NBs was defined as the distance between their two centroids. The distance between a PML NB and the nearest compartment was defined as the distance between the centroid of the PML NB and the edge of the red voxels of the compartment. This is an appropriate proximation in most cases but in certain cases can result in error. This is illustrated in Figure 78.

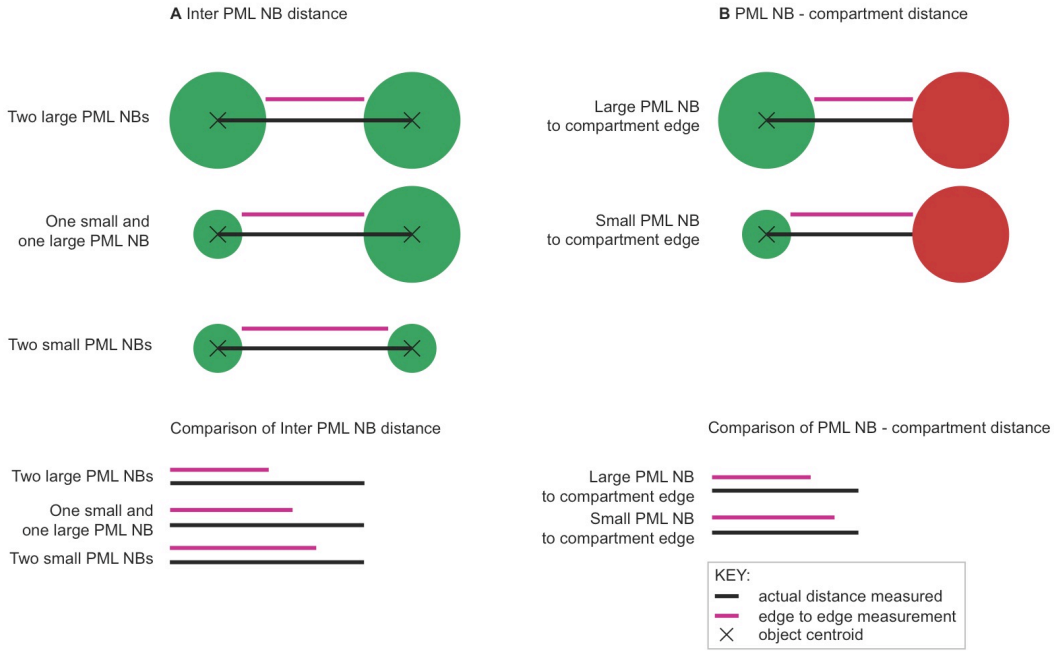


Figure 78 Measurement of inter-PML NB and PML NB - compartment distances

A) Inter-PML NB distances are measured between body centroids (marked by a cross). This can create differences between the measured and edge to edge distances for different sized PML NBs with identically spaced centroids. B) PML NB to functional compartment distances are measured from centroid to compartment edge. This can create differences between the measured and edge to edge distances for different sized PML NBs with identically distanced centroids from the functional compartment edge.

In A in all three cases the actual distance measured between the two PML NBs (be they small or large) is exactly the same, but if the measurement was taken between the edges of the bodies, they would actually be three different lengths. A potential solution is a correction made by subtracting the lengths of both PML NB radii from the distance between them, and using that as the distance measurement instead.

6.3.4 Statistical methodology issues

6.3.4.1 Sample size

The number of cells belonging to a sample can affect the results seen, especially if one looks at rare events. Therefore it is always better to gather as large a sample as one possibly can. However imaging single nuclei is time consuming and a major block to sample size. There is also some wastage of sample due to imaging artefacts leading to

poor segmentation. Therefore it is best to collect the cleanest, well stained data as possible or to over collect data (more cells than one needs), but ideally both! High throughput methods should help to increase the amount of data analysis possible (but at the cost of a higher wastage rate as nuclei are not chosen individually by the microscope operator) and improve the reliability of findings. Our SCT segmentation and statistical methods will lend themselves well to this high throughput data collection of large volumes of data. In this study whilst only the compartment data was determined from 50 cells in the dataset stained for that particular compartment in conjunction with PML NBs, the PML NB data could be pooled from all the different compartment datasets for that cell line or condition (as the green and red signal could be ignored) meaning there was about ten times the sample size for the PML NBs datasets. This is why the MRC5 PML NB subsets (G_1, G_0, S) possibly do not show as convincing trends as the larger PML datasets.

6.3.4.2 CSR analysis

6.3.4.2.1 Object number and size

The CSR approach does not work that well when there is very little of one compartment in comparison to the other (for instance the amount of PML versus the amount of CB). Despite observing in the IF (and according to (Grande et al., 1996; Sun et al., 2005)) that at least one PML NB within a nucleus is found to be adjacent to a Cajal body, PML NBs were not closer to Cajal bodies than expected under CSR in the majority of MRC5 VA and WI38 VA nuclei. This is because nearly all the PML NBs in a nucleus will have long minimum NNDs to the Cajal body (as there are so few) except for the PML NB that is adjacent to the Cajal body. Therefore single observations in cell biology will always remain a useful tool for initial investigations, which is complementary to quantification-based methods.

6.3.4.2.2 CSR: a useful model for PML NB organisation in the nucleus?

For the simulation of the spatial organisation of PML NBs it was assumed that they locate in the nucleus according to the spatial point pattern of complete spatial

randomness. However, it seems likely that these do not accurately represent the processes that govern PML NB spatial organisation, meaning that we may inappropriately accept or reject CSR to describe the organisation of PML NB in some cases. For instance PML NBs are most likely to reside within the ICD (Gorisch et al., 2004), which therefore excludes quite a large volume of the nucleus from them. Also, from the AMs we were able to visualise the regions of the nucleus that PML NBs seem to favour in their location. However, under CSR the assumption is made that PML NBs can be placed anywhere within the nucleus.

Despite these limitations, using CSR as a model for PML NB location within the nucleus has still allowed us to reveal positive associations between them and functional compartments. An excellent example of this is the close spatial relationship between PML NBs and telomeres in ALT positive cell lines, which has been strongly supported by the literature. We were clearly able to show that such an association exists within the MRC5 and WI38 VA cell lines (both of which are ALT positive), but was mostly absent in their asynchronous counterparts.

The inference that PML NB function relates to that of compartments with which it shows associations is useful when defining PML NB function, as exemplified by the many relationships described herein. Future application of such techniques to other nuclear compartments sharing undefined relationships with PML NBs may indeed help to highlight further functional relationships, or to discard less fruitful avenues of research. If there are indeed subtypes of PML NBs it will also be interesting to look at their spatial associations with each other, as this may provide more insight into the factors that underlie nuclear organization.

Fortunately, the information regarding the spatial preference of PML NBs gathered from the AMs can be used to inform future simulations of where PML NBs are likely to be found in the nucleus. This will allow us to create a more accurate model for where PML NBs reside that can faithfully mimic their true spatial preference.

6.3.4.3 AM limitations

A limitation of the aggregate maps was that where intensity was low (for example where a compartment had a low voxel count) there was not enough evidence to definitively categorise the compartment as belonging to a particular AM pattern group. Such compartments were labelled as diffuse. Whereas there are compartments that truly show a diffuse pattern (such as MRC5 VA ACHIS) there are others where it is less convincing (such as MRC5 VA TELO), and therefore it is essential to collect as many image stacks as possible to help reveal the patterns for such compartments.

6.4 Conclusions

We have shown that a systems approach encompassing cell biology, imaging and statistical analysis, and the novel image segmentation and statistical methods used herein are appropriate to reveal interrelationships between PML NBs and functional compartments within the mammalian nucleus. The tools developed will also be of benefit to the wider biological imaging and statistical communities, as they can be easily adapted to analyse data from other sources when looking to solve similar problems.

Our results show that there is clear evidence for meaningful organisation in the nucleus of normal fibroblasts, which becomes disrupted as a consequence of transformation or treatment with heat shock, interferon, or serum starvation to the advantage, and at the expense, of certain PML NB – functional compartment relationships.

Previous findings relating to the role of PML NBs in the nucleus have been confirmed; showing that they are likely to provide environments conducive to transcription, and play roles in the degradation of viral proteins, and in the ALT mechanism at telomeres. These functions are extremely diverse. It is therefore still unclear if there are subsets of PML NBs that each perform different roles, (and if so, how they are selected), or whether a particular PML NB can function in more than one role at the same time. An investigation using immunofluorescent staining of combinations of different compartments in addition to PML NBs within the same nucleus, and distance and spatial

analyses should be completed in the future to help determine if particular bodies can have more than one simultaneous role.

PML NB function may simply relate to where the bodies initially form within the nucleus and consequently which functional compartments they happen find as their neighbours. Alternatively they may recruit the partners they require for a particular role, or they themselves may be recruited to sites where they are needed.

7.1 Total sample sizes

Table 15 Success rates of SCT algorithm segmentation

Cell line and perturbation	Total number of cells collected	Sample size after segmentation (n)	Succes rate of SCT %
MRC5_ASYNC	500	435	87
MRC5_HS	500	438	87.6
MRC5_IFN	450	378	84
MRC5_SS	450	409	90.9
MRC5_VA	550	409	74.3
MRC5_BRDU	50	48	96
MRC5_G0	50	46	92
MRC5_G1	50	45	90
WI38_ASYNC	500	421	84.2
WI38_VA	500	376	75.2

Overall, the success rate for segmentation by the SCT algorithm ranged between 74 and 91% for the large sample sizes (n 376-438) and between 90 to 96% for the smaller sample sizes (n 45-48). In the future it seems that over collection of cells is needed if certain sample sizes are required.

It must be noted that for HS, the success rate is artificially high, as manual thresholding had to be employed in part due to the nature of the signal from the PML staining. However, on the whole the SCT algorithm consistently segments over three quarters of the sample population.

7.2 WB: PML and Ki67 protein levels in normal, treated and virally transformed MRC5 and WI38 cells

a) PML and actin in MRC5 ASYNC, IFN and HS total cell extracts

This control revealed the PML protein levels and content of MRC5 asynchronous (ASYNC) cells, and tested that the interferon and heat shock treatments used for the MRC5 IFN and HS datasets, respectively, had the appropriate effect upon PML protein levels within the cell (Figure 79). Cells were cultured and were either heat shocked or

treated with interferon beta. Total cell extracts were prepared, and western blotting was performed (all methods detailed in Section 2.6). The blot was incubated with rabbit anti PML and mouse anti actin.

The actin band (at 42kDa) showed that a similar amount of total cell extract was loaded for each of the samples. The band present at 50 kDa was a cross-reaction between the secondary antibody and the heavy chain. In the MRC5 ASYNC lane PML appeared as a ladder between 48 and 97 kDa (Jensen et al., 2001). This included various isoforms of PML and its SUMO modified forms. In the MRC5 IFN lane the PML protein levels were higher than those of MRC5 ASYNC cells, which showed that PML expression had been upregulated in these cells, as expected. In the MRC5 HS lane there was no difference between the PML protein levels in MRC5 ASYNC, showing that heat shock treatment had no effect on PML expression, which was also as expected.

b) PML and actin in MRC5 ASYNC and VA, and WI38 ASYNC and VA in total cell extracts

This control compared the PML protein levels and content of MRC5 and WI38 asynchronous (ASYNC) and virally transformed (VA) cells (Figure 79). Cells were cultured, total cell extracts were prepared, and western blotting was performed as above. The blot was incubated with rabbit anti PML and mouse anti actin.

The actin band (at 42kDa) showed that a similar amount of total cell extract was loaded for each of the samples. The band present at 50 kDa was a cross-reaction between the secondary antibody and the heavy chain. In the MRC5 ASYNC lane PML appeared as a ladder between 48 and 97 kDa (Jensen et al., 2001). The PML ladder for MRC5 VA and WI38 ASYNC were very similar to this, indicating that there was no difference in the PML expression of the three cell lines. In the WI38 VA lane the PML ladder appeared similar to that of the other lanes, but there was also a slightly larger band at just below 160 kDa, which may indicate a higher level of expression of a particularly modified PML protein.

c) PML, Ki67 proliferation marker, and actin in MRC5 ASYNC and SS nuclear and cytoplasmic protein extracts

This control compared the cytoplasmic and nuclear PML levels and content of MRC5 asynchronous ASYNC and serum starved (SS) cells (Figure 80). It also compared the Ki67 protein content of MRC5 ASYNC and SS cells. Cells were cultured and serum starved, nuclear and cytoplasmic extracts were prepared, and western blotting was performed as detailed in Section 2.6. The blot was incubated with rabbit anti PML, stripped, and then incubated with rabbit anti Ki67 proliferation marker, and mouse anti actin.

The actin band (at 42kDa) showed that a similar amount of total cell extract was loaded for each of the samples. The total amount of protein that could be added was only 20mg per lane, and therefore the signal was weak overall. The band present at 50 kDa was a cross-reaction between the secondary antibody and the heavy chain. PML protein appeared to be absent from the MRC5 ASYNC C (cytoplasmic extract) lane. In the MRC5 ASYNC N (nuclear extract) lane PML appeared as a weak ladder between 48 and 97 kDa (Jensen et al., 2001). PML protein was again absent from the MRC5 SS C (cytoplasmic extract) lane. In the MRC5 SS N (nuclear extract) lane PML also appeared as a weak ladder. There were no obvious differences in expression levels between PML in the MRC5 ASYNC N and MRC5 SS N lanes, although it was difficult to tell due to the weak staining overall.

On the Ki67 blot, Ki67 protein appeared to be absent from the MRC5 ASYNC C (cytoplasmic extract) lane. This is accounted for by the fact that Ki67 is an antigen that is only present in the nucleus. In the MRC5 ASYNC N (nuclear extract) lane Ki67 was present in a thick band above 250 kDa. Ki67 runs at molecular weights of 345 and 395 kDa and so partially ran off the top of the gel. Ki67 was absent from the MRC5 SS C (cytoplasmic extract) lane. In the MRC5 SS N (nuclear extract) lane Ki67 was also absent. This showed that serum starvation was successful as Ki67 is absent from quiescent cell populations. Some PML bands were visible on this blot because the antibodies used to detect both PML and Ki67 were raised in rabbit. Therefore there was some cross-reaction with the secondary antibody. However PML and Ki67 migrate at different heights so there could be no confusion between the two.

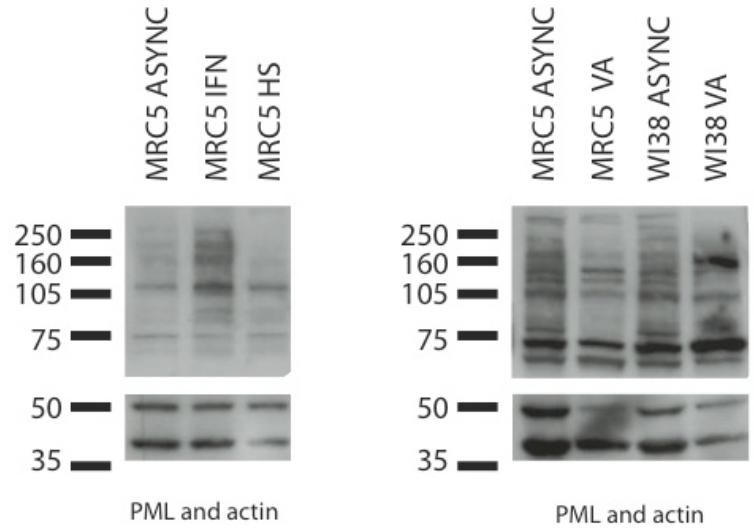


Figure 79 PML and actin blot for MRC5 ASYNC, IFN, HS and VA, and WI38 ASYNC and VA fibroblast total cell extracts

Left: PML bands in total cell protein extracts from MRC5 asynchronous, interferon treated, and heat shocked cell populations. Actin was used as a loading control. Right: PML in total cell protein extracts of MRC5 and WI38 ASYNC and VA cells.

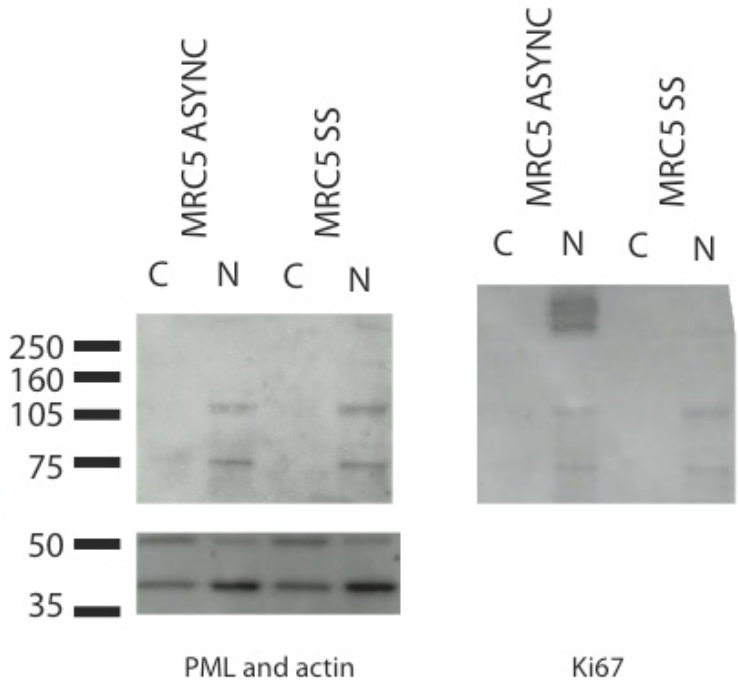


Figure 80 PML, Ki67, and actin blot for MRC5 ASYNC and SS cytoplasmic and nuclear extracts

Left: PML bands in nuclear, but not cytoplasmic protein extracts from MRC5 asynchronous and serum starved cell populations. Right: Ki67 in the nuclear protein extract of MRC5 ASYNC, but not the nuclear protein extract of MRC5 SS cells, or the cytoplasmic extracts of either MRC5 ASYNC or SS cells.

References

Alcalay, M., L. Tomassoni, E. Colombo, S. Stoldt, F. Grignani, M. Fagioli, L. Szekely, K. Helin, and P.G. Pelicci. 1998. The promyelocytic leukemia gene product (PML) forms stable complexes with the retinoblastoma protein. *Mol Cell Biol.* 18:1084-93.

Batty, E., K. Jensen, and P. Freemont. 2009. PML nuclear bodies and their spatial relationships in the mammalian cell nucleus. *Front Biosci.* 14:1182-96.

Berciano, M.T., M. Novell, N.T. Villagra, I. Casafont, R. Bengoechea, J.F. Val-Bernal, and M. Lafarga. 2007. Cajal body number and nucleolar size correlate with the cell body mass in human sensory ganglia neurons. *J Struct Biol.* 158:410-20.

Bernardi, R., and P.P. Pandolfi. 2007. Structure, dynamics and functions of promyelocytic leukaemia nuclear bodies. *Nat Rev Mol Cell Biol.* 8:1006-16.

Bernardi, R., P.P. Scaglioni, S. Bergmann, H.F. Horn, K.H. Vousden, and P.P. Pandolfi. 2004. PML regulates p53 stability by sequestering Mdm2 to the nucleolus. *Nat Cell Biol.* 6:665-72.

Bishop, C.L., M. Ramalho, N. Nadkarni, W. May Kong, C.F. Higgins, and N. Krauzewicz. 2006. Role for centromeric heterochromatin and PML nuclear bodies in the cellular response to foreign DNA. *Mol Cell Biol.* 26:2583-94.

Blasco, M.A. 2007. Telomere length, stem cells and aging. *Nat Chem Biol.* 3:640-9.

Boddy, M.N., K. Howe, L.D. Etkin, E. Solomon, and P.S. Freemont. 1996. PIC 1, a novel ubiquitin-like protein which interacts with the PML component of a multiprotein complex that is disrupted in acute promyelocytic leukaemia. *Oncogene.* 13:971-82.

Boe, S.O., M. Haave, A. Jul-Larsen, A. Grudic, R. Bjerkvig, and P.E. Lonning. 2006. Promyelocytic leukemia nuclear bodies are predetermined processing sites for damaged DNA. *J Cell Sci.* 119:3284-95.

Boisvert, F.M., M.J. Hendzel, and D.P. Bazett-Jones. 2000. Promyelocytic leukemia (PML) nuclear bodies are protein structures that do not accumulate RNA. *J Cell Biol.* 148:283-92.

Boisvert, F.M., M.J. Kruhlak, A.K. Box, M.J. Hendzel, and D.P. Bazett-Jones. 2001. The transcription coactivator CBP is a dynamic component of the promyelocytic leukemia nuclear body. *J Cell Biol.* 152:1099-106.

Bonilla, W.V., D.D. Pinschewer, P. Klenerman, V. Rousson, M. Gaboli, P.P. Pandolfi, R.M. Zinkernagel, M.S. Salvato, and H. Hengartner. 2002. Effects of promyelocytic leukemia protein on virus-host balance. *J Virol.* 76:3810-8.

Borden, K.L. 2002. Pondering the promyelocytic leukemia protein (PML) puzzle: possible functions for PML nuclear bodies. *Mol Cell Biol.* 22:5259-69.

Bridger, J.M., H. Herrmann, C. Munkel, and P. Lichter. 1998. Identification of an interchromosomal compartment by polymerization of nuclear-targeted vimentin. *J Cell Sci.* 111 (Pt 9):1241-53.

Brouwer, A.K., J. Schimmel, J.C. Wiegant, A.C. Vertegaal, H.J. Tanke, and R.W. Dirks. 2009. Telomeric DNA Mediates De Novo PML Body Formation. *Mol Biol Cell.*

Bryan, T.M., A. Englezou, L. Dalla-Pozza, M.A. Dunham, and R.R. Reddel. 1997. Evidence for an alternative mechanism for maintaining telomere length in human tumors and tumor-derived cell lines. *Nat Med.* 3:1271-4.

Carbone, R., M. Pearson, S. Minucci, and P.G. Pelicci. 2002. PML NBs associate with the hMre11 complex and p53 at sites of irradiation induced DNA damage. *Oncogene.* 21:1633-40.

Carvalho, T., J.S. Seeler, K. Ohman, P. Jordan, U. Pettersson, G. Akusjarvi, M. Carmo-Fonseca, and A. Dejean. 1995. Targeting of adenovirus E1A and E4-ORF3 proteins to nuclear matrix-associated PML bodies. *J Cell Biol.* 131:45-56.

Chelbi-Alix, M.K., L. Pelicano, F. Quignon, M.H. Koken, L. Venturini, M. Stadler, J. Pavlovic, L. Degos, and H. de The. 1995. Induction of the PML protein by interferons in normal and APL cells. *Leukemia.* 9:2027-33.

Chuang, T.C., S. Moshir, Y. Garini, A.Y. Chuang, I.T. Young, B. Vermolen, R. van den Doel, V. Mougey, M. Perrin, M. Braun, P.D. Kerr, T. Fest, P. Boukamp, and S. Mai. 2004. The three-dimensional organization of telomeres in the nucleus of mammalian cells. *BMC Biol.* 2:12.

Cohen, N., M. Sharma, A. Kentsis, J.M. Perez, S. Strudwick, and K.L. Borden. 2001. PML RING suppresses oncogenic transformation by reducing the affinity of eIF4E for mRNA. *Embo J.* 20:4547-59.

Condemine, W., Y. Takahashi, M. Le Bras, and H. de The. 2007. A nucleolar targeting signal in PML-I addresses PML to nucleolar caps in stressed or senescent cells. *J Cell Sci.* 120:3219-27.

Condemine, W., Y. Takahashi, J. Zhu, F. Puvion-Dutilleul, S. Guegan, A. Janin, and H. de The. 2006. Characterization of endogenous human promyelocytic leukemia isoforms. *Cancer Res.* 66:6192-8.

Culjkovic, B., I. Topisirovic, L. Skrabanek, M. Ruiz-Gutierrez, and K.L. Borden. 2005. eIF4E promotes nuclear export of cyclin D1 mRNAs via an element in the 3'UTR. *J Cell Biol.* 169:245-56.

Daniel, M.T., M. Koken, O. Romagne, S. Barbey, A. Bazarbachi, M. Stadler, M.C. Guillemin, L. Degos, C. Chomienne, and H. de The. 1993. PML protein expression in hematopoietic and acute promyelocytic leukemia cells. *Blood.* 82:1858-67.

de Lange, T. 1992. Human telomeres are attached to the nuclear matrix. *Embo J.* 11:717-24.

de The, H., C. Lavau, A. Marchio, C. Chomienne, L. Degos, and A. Dejean. 1991. The PML-RAR alpha fusion mRNA generated by the t(15;17) translocation in acute promyelocytic leukemia encodes a functionally altered RAR. *Cell.* 66:675-84.

Dellaire, G., and D.P. Bazett-Jones. 2004. PML nuclear bodies: dynamic sensors of DNA damage and cellular stress. *Bioessays.* 26:963-77.

Dellaire, G., R.W. Ching, K. Ahmed, F. Jalali, K.C. Tse, R.G. Bristow, and D.P. Bazett-Jones. 2006a. Promyelocytic leukemia nuclear bodies behave as DNA damage sensors whose response to DNA double-strand breaks is regulated by NBS1 and the kinases ATM, Chk2, and ATR. *J Cell Biol.* 175:55-66.

Dellaire, G., R.W. Ching, H. Dehghani, Y. Ren, and D.P. Bazett-Jones. 2006b. The number of PML nuclear bodies increases in early S phase by a fission mechanism. *J Cell Sci.* 119:1026-33.

Dellaire, G., C.H. Eskiw, H. Dehghani, R.W. Ching, and D.P. Bazett-Jones. 2006c. Mitotic accumulations of PML protein contribute to the re-establishment of PML nuclear bodies in G1. *J Cell Sci.* 119:1034-42.

Deniaud, E., and W.A. Bickmore. 2009. Transcription and the nuclear periphery: edge of darkness? *Curr Opin Genet Dev.* 19:187-91.

Diggle, P.J. 1983. Statistical Analysis of Spatial Point Patterns. Academic Press.

Dino Rockel, T., and A. von Mikecz. 2002. Proteasome-dependent processing of nuclear proteins is correlated with their subnuclear localization. *J Struct Biol.* 140:189-99.

Doucas, V., A.M. Ishov, A. Romo, H. Juguilon, M.D. Weitzman, R.M. Evans, and G.G. Maul. 1996. Adenovirus replication is coupled with the dynamic properties of the PML nuclear structure. *Genes Dev.* 10:196-207.

Draskovic, I., N. Arnoult, V. Steiner, S. Bacchetti, P. Lomonte, and A. Londono-Vallejo. 2009. Probing PML body function in ALT cells reveals spatiotemporal requirements for telomere recombination. *Proc Natl Acad Sci U S A.*

Dundr, M., and T. Misteli. 2001. Functional architecture in the cell nucleus. *Biochem J.* 356:297-310.

Dunham, M.A., A.A. Neumann, C.L. Fasching, and R.R. Reddel. 2000. Telomere maintenance by recombination in human cells. *Nat Genet.* 26:447-50.

Duprez, E., A.J. Saurin, J.M. Desterro, V. Lallemand-Breitenbach, K. Howe, M.N. Boddy, E. Solomon, H. de The, R.T. Hay, and P.S. Freemont. 1999. SUMO-1 modification of the acute promyelocytic leukaemia protein PML: implications for nuclear localisation. *J Cell Sci.* 112 (Pt 3):381-93.

Dyck, J.A., G.G. Maul, W.H. Miller, Jr., J.D. Chen, A. Kakizuka, and R.M. Evans. 1994. A novel macromolecular structure is a target of the promyelocyte-retinoic acid receptor oncoprotein. *Cell.* 76:333-43.

Eskiw, C.H., G. Dellaire, J.S. Mymryk, and D.P. Bazett-Jones. 2003. Size, position and dynamic behavior of PML nuclear bodies following cell stress as a paradigm for supramolecular trafficking and assembly. *J Cell Sci.* 116:4455-66.

Everett, R.D. 2006. Interactions between DNA viruses, ND10 and the DNA damage response. *Cell Microbiol.* 8:365-74.

Everett, R.D., and M.K. Chelbi-Alix. 2007. PML and PML nuclear bodies: implications in antiviral defence. *Biochimie.* 89:819-30.

Everett, R.D., W.C. Earnshaw, A.F. Pluta, T. Sternsdorf, A.M. Ainsztein, M. Carmena, S. Ruchaud, W.L. Hsu, and A. Orr. 1999a. A dynamic connection between centromeres and ND10 proteins. *J Cell Sci.* 112 (Pt 20):3443-54.

Everett, R.D., P. Lomonte, T. Sternsdorf, R. van Driel, and A. Orr. 1999b. Cell cycle regulation of PML modification and ND10 composition. *J Cell Sci.* 112 (Pt 24):4581-8.

Everett, R.D., S. Rechter, P. Papior, N. Tavalai, T. Stamminger, and A. Orr. 2006. PML contributes to a cellular mechanism of repression of herpes simplex virus type 1 infection that is inactivated by ICP0. *J Virol.* 80:7995-8005.

Fabunmi, R.P., W.C. Wigley, P.J. Thomas, and G.N. DeMartino. 2001. Interferon gamma regulates accumulation of the proteasome activator PA28 and immunoproteasomes at nuclear PML bodies. *J Cell Sci.* 114:29-36.

Fay, F.S., K.L. Taneja, S. Shenoy, L. Lifshitz, and R.H. Singer. 1997. Quantitative digital analysis of diffuse and concentrated nuclear distributions of nascent transcripts, SC35 and poly(A). *Exp Cell Res.* 231:27-37.

Ferguson, B.J., C.L. Dovey, K. Lilley, A.H. Wyllie, and T. Rich. 2007. Nuclear phospholipase C gamma: punctate distribution and association with the promyelocytic leukemia protein. *J Proteome Res.* 6:2027-32.

Fogal, V., M. Gostissa, P. Sandy, P. Zacchi, T. Sternsdorf, K. Jensen, P.P. Pandolfi, H. Will, C. Schneider, and G. Del Sal. 2000. Regulation of p53 activity in nuclear bodies by a specific PML isoform. *Embo J.* 19:6185-95.

Fuchsova, B., P. Novak, J. Kafkova, and P. Hozak. 2002. Nuclear DNA helicase II is recruited to IFN-alpha-activated transcription sites at PML nuclear bodies. *J Cell Biol.* 158:463-73.

Gilson, E., and V. Geli. 2007. How telomeres are replicated. *Nat Rev Mol Cell Biol.* 8:825-38.

Goddard, A.D., J. Borrow, P.S. Freemont, and E. Solomon. 1991. Characterization of a zinc finger gene disrupted by the t(15;17) in acute promyelocytic leukemia. *Science.* 254:1371-4.

Gorisch, S.M., M. Wachsmuth, C. Ittrich, C.P. Bacher, K. Rippe, and P. Lichter. 2004. Nuclear body movement is determined by chromatin accessibility and dynamics. *Proc Natl Acad Sci U S A.* 101:13221-6.

Grande, M.A., I. van der Kraan, B. van Steensel, W. Schul, H. de The, H.T. van der Voort, L. de Jong, and R. van Driel. 1996. PML-containing nuclear bodies: their spatial distribution in relation to other nuclear components. *J Cell Biochem.* 63:280-91.

Guillot, P.V., S.Q. Xie, M. Hollinshead, and A. Pombo. 2004. Fixation-induced redistribution of hyperphosphorylated RNA polymerase II in the nucleus of human cells. *Exp Cell Res.* 295:460-8.

Hancock, R. 2004. Internal organisation of the nucleus: assembly of compartments by macromolecular crowding and the nuclear matrix model. *Biol Cell.* 96:595-601.

Hayakawa, F., A. Abe, I. Kitabayashi, P.P. Pandolfi, and T. Naoe. 2008. Acetylation of PML is involved in histone deacetylase inhibitor-mediated apoptosis. *J Biol Chem.* 283:24420-5.

Hayakawa, F., and M.L. Privalsky. 2004. Phosphorylation of PML by mitogen-activated protein kinases plays a key role in arsenic trioxide-mediated apoptosis. *Cancer Cell.* 5:389-401.

Henson, J.D., A.A. Neumann, T.R. Yeager, and R.R. Reddel. 2002. Alternative lengthening of telomeres in mammalian cells. *Oncogene.* 21:598-610.

Huang, M.E., Y.C. Ye, S.R. Chen, J.R. Chai, J.X. Lu, L. Zhoa, L.J. Gu, and Z.Y. Wang. 1988. Use of all-trans retinoic acid in the treatment of acute promyelocytic leukemia. *Blood.* 72:567-72.

Ishov, A.M., and G.G. Maul. 1996. The periphery of nuclear domain 10 (ND10) as site of DNA virus deposition. *J Cell Biol.* 134:815-26.

Ishov, A.M., A.G. Sotnikov, D. Negorev, O.V. Vladimirova, N. Neff, T. Kamitani, E.T. Yeh, J.F. Strauss, 3rd, and G.G. Maul. 1999. PML is critical for ND10 formation and recruits the PML-interacting protein daxx to this nuclear structure when modified by SUMO-1. *J Cell Biol.* 147:221-34.

Ishov, A.M., R.M. Stenberg, and G.G. Maul. 1997. Human cytomegalovirus immediate early interaction with host nuclear structures: definition of an immediate transcript environment. *J Cell Biol.* 138:5-16.

Janderova-Rossmeislova, L., Z. Novakova, J. Vlasakova, V. Philimonenko, P. Hozak, and Z. Hodny. 2007. PML protein association with specific nucleolar structures differs in normal, tumor and senescent human cells. *J Struct Biol.* 159:56-70.

Jensen, K., C. Shiels, and P.S. Freemont. 2001. PML protein isoforms and the RBCC/TRIM motif. *Oncogene.* 20:7223-33.

Jiang, G., F. Yang, C. Sanchez, and M. Ehrlich. 2004. Histone modification in constitutive heterochromatin versus unexpressed euchromatin in human cells. *J Cell Biochem.* 93:286-300.

Kakizuka, A., W.H. Miller, Jr., K. Umesono, R.P. Warrell, Jr., S.R. Frankel, V.V. Murty, E. Dmitrovsky, and R.M. Evans. 1991. Chromosomal translocation t(15;17) in

human acute promyelocytic leukemia fuses RAR alpha with a novel putative transcription factor, PML. *Cell.* 66:663-74.

Kamitani, T., K. Kito, H.P. Nguyen, H. Wada, T. Fukuda-Kamitani, and E.T. Yeh. 1998. Identification of three major sentrinization sites in PML. *J Biol Chem.* 273:26675-82.

Kiesslich, A., A. von Mikecz, and P. Hemmerich. 2002. Cell cycle-dependent association of PML bodies with sites of active transcription in nuclei of mammalian cells. *J Struct Biol.* 140:167-79.

Koken, M.H., G. Linares-Cruz, F. Quignon, A. Viron, M.K. Chelbi-Alix, J. Sobczak-Thepot, L. Juhlin, L. Degos, F. Calvo, and H. de The. 1995. The PML growth-suppressor has an altered expression in human oncogenesis. *Oncogene.* 10:1315-24.

Koken, M.H., F. Puvion-Dutilleul, M.C. Guillemin, A. Viron, G. Linares-Cruz, N. Stuurman, L. de Jong, C. Szostecki, F. Calvo, C. Chomienne, and et al. 1994. The t(15;17) translocation alters a nuclear body in a retinoic acid-reversible fashion. *Embo J.* 13:1073-83.

Koken, M.H., A. Reid, F. Quignon, M.K. Chelbi-Alix, J.M. Davies, J.H. Kabarowski, J. Zhu, S. Dong, S. Chen, Z. Chen, C.C. Tan, J. Licht, S. Waxman, H. de The, and A. Zelent. 1997. Leukemia-associated retinoic acid receptor alpha fusion partners, PML and PLZF, heterodimerize and colocalize to nuclear bodies. *Proc Natl Acad Sci U S A.* 94:10255-60.

Kumar, P.P., O. Bischof, P.K. Purbey, D. Notani, H. Urlaub, A. Dejean, and S. Galande. 2007. Functional interaction between PML and SATB1 regulates chromatin-loop architecture and transcription of the MHC class I locus. *Nat Cell Biol.* 9:45-56.

Lachner, M., R.J. O'Sullivan, and T. Jenuwein. 2003. An epigenetic road map for histone lysine methylation. *J Cell Sci.* 116:2117-24.

Lafarga, M., M.T. Berciano, E. Pena, I. Mayo, J.G. Castano, D. Bohmann, J.P. Rodrigues, J.P. Tavanez, and M. Carmo-Fonseca. 2002. Clastosome: a subtype of nuclear body enriched in 19S and 20S proteasomes, ubiquitin, and protein substrates of proteasome. *Mol Biol Cell.* 13:2771-82.

Lallemand-Breitenbach, V., M. Jeanne, S. Benhenda, R. Nasr, M. Lei, L. Peres, J. Zhou, J. Zhu, B. Raught, and H. de The. 2008. Arsenic degrades PML or PML-RARalpha through a SUMO-triggered RNF4/ubiquitin-mediated pathway. *Nat Cell Biol.* 10:547-55.

Lallemand-Breitenbach, V., J. Zhu, F. Puvion, M. Koken, N. Honore, A. Doubeikovsky, E. Duprez, P.P. Pandolfi, E. Puvion, P. Freemont, and H. de The. 2001. Role of promyelocytic leukemia (PML) sumolation in nuclear body formation, 11S proteasome recruitment, and As2O3-induced PML or PML/retinoic acid receptor alpha degradation. *J Exp Med.* 193:1361-71.

Lamond, A.I., and D.L. Spector. 2003. Nuclear speckles: a model for nuclear organelles. *Nat Rev Mol Cell Biol.* 4:605-12.

LaMorte, V.J., J.A. Dyck, R.L. Ochs, and R.M. Evans. 1998. Localization of nascent RNA and CREB binding protein with the PML-containing nuclear body. *Proc Natl Acad Sci U S A.* 95:4991-6.

Lanctot, C., T. Cheutin, M. Cremer, G. Cavalli, and T. Cremer. 2007. Dynamic genome architecture in the nuclear space: regulation of gene expression in three dimensions. *Nat Rev Genet.* 8:104-15.

Lavau, C., A. Marchio, M. Fagioli, J. Jansen, B. Falini, P. Lebon, F. Grosveld, P.P. Pandolfi, P.G. Pelicci, and A. Dejean. 1995. The acute promyelocytic leukaemia-associated PML gene is induced by interferon. *Oncogene.* 11:871-6.

Lazaris-Karatzas, A., K.S. Montine, and N. Sonenberg. 1990. Malignant transformation by a eukaryotic initiation factor subunit that binds to mRNA 5' cap. *Nature.* 345:544-7.

Lehming, N., A. Le Saux, J. Schuller, and M. Ptashne. 1998. Chromatin components as part of a putative transcriptional repressing complex. *Proc Natl Acad Sci U S A.* 95:7322-6.

Li, H., C. Leo, J. Zhu, X. Wu, J. O'Neil, E.J. Park, and J.D. Chen. 2000. Sequestration and inhibition of Daxx-mediated transcriptional repression by PML. *Mol Cell Biol.* 20:1784-96.

Lin, H.K., S. Bergmann, and P.P. Pandolfi. 2004. Cytoplasmic PML function in TGF-beta signalling. *Nature.* 431:205-11.

Luciani, J.J., D. Depetris, Y. Usson, C. Metzler-Guillemain, C. Mignon-Ravix, M.J. Mitchell, A. Megarbane, P. Sarda, H. Sirma, A. Moncla, J. Feunteun, and M.G. Mattei. 2006. PML nuclear bodies are highly organised DNA-protein structures with a function in heterochromatin remodelling at the G2 phase. *J Cell Sci.* 119:2518-31.

Luderus, M.E., B. van Steensel, L. Chong, O.C. Sibon, F.F. Cremers, and T. de Lange. 1996. Structure, subnuclear distribution, and nuclear matrix association of the mammalian telomeric complex. *J Cell Biol.* 135:867-81.

Maul, G.G., A.M. Ishov, and R.D. Everett. 1996. Nuclear domain 10 as preexisting potential replication start sites of herpes simplex virus type-1. *Virology.* 217:67-75.

McManus, K.J., and M.J. Hendzel. 2001. CBP, a transcriptional coactivator and acetyltransferase. *Biochem Cell Biol.* 79:253-66.

Misteli, T. 2001. The concept of self-organization in cellular architecture. *J Cell Biol.* 155:181-5.

Mitchell, J.A., and P. Fraser. 2008. Transcription factories are nuclear subcompartments that remain in the absence of transcription. *Genes Dev.* 22:20-5.

Muller, S., M.J. Matunis, and A. Dejean. 1998. Conjugation with the ubiquitin-related modifier SUMO-1 regulates the partitioning of PML within the nucleus. *Embo J.* 17:61-70.

Murata, S., H. Yashiroda, and K. Tanaka. 2009. Molecular mechanisms of proteasome assembly. *Nat Rev Mol Cell Biol.* 10:104-15.

Muratani, M., D. Gerlich, S.M. Janicki, M. Gebhard, R. Eils, and D.L. Spector. 2002. Metabolic-energy-dependent movement of PML bodies within the mammalian cell nucleus. *Nat Cell Biol.* 4:106-10.

Negorev, D., and G.G. Maul. 2001. Cellular proteins localized at and interacting within ND10/PML nuclear bodies/PODs suggest functions of a nuclear depot. *Oncogene.* 20:7234-42.

Nichol, J.N., L.A. Petruccelli, and W.H. Miller, Jr. 2009. Expanding PML's functional repertoire through post-translational mechanisms. *Front Biosci.* 14:2293-306.

olympusconfocal.com. 2009. http://www.olympusconfocal.com/theory/glossary.html

Pandolfi, P.P., F. Grignani, M. Alcalay, A. Mencarelli, A. Biondi, F. LoCoco, F. Grignani, and P.G. Pelicci. 1991. Structure and origin of the acute promyelocytic leukemia myl/RAR alpha cDNA and characterization of its retinoid-binding and transactivation properties. *Oncogene.* 6:1285-92.

Parada, L.A., S. Sotiriou, and T. Misteli. 2004. Spatial genome organization. *Exp Cell Res.* 296:64-70.

Potts, P.R., and H. Yu. 2007. The SMC5/6 complex maintains telomere length in ALT cancer cells through SUMOylation of telomere-binding proteins. *Nat Struct Mol Biol.* 14:581-90.

R. http://www.r-project.org/

Ramirez, M.J., and J. Surralles. 2008. Laser confocal microscopy analysis of human interphase nuclei by three-dimensional FISH reveals dynamic perinucleolar clustering of telomeres. *Cytogenet Genome Res.* 122:237-42.

Rechsteiner, M., C. Realini, and V. Ustrell. 2000. The proteasome activator 11 S REG (PA28) and class I antigen presentation. *Biochem J.* 345 Pt 1:1-15.

Regad, T., and M.K. Chelbi-Alix. 2001. Role and fate of PML nuclear bodies in response to interferon and viral infections. *Oncogene.* 20:7274-86.

Rockel, T.D., D. Stuhlmann, and A. von Mikecz. 2005. Proteasomes degrade proteins in focal subdomains of the human cell nucleus. *J Cell Sci.* 118:5231-42.

Russell, R.A., N.M. Adams, D.A. Stephens, E. Batty, K. Jensen, and P.S. Freemont. 2009. Segmentation of fluorescence microscopy images for quantitative analysis of cell nuclear architecture. *Biophys J.* 96:3379-89.

Ruthardt, M., A. Orleth, L. Tomassoni, E. Puccetti, D. Riganelli, M. Alcalay, R. Mannucci, I. Nicoletti, F. Grignani, M. Fagioli, and P.G. Pelicci. 1998. The acute promyelocytic leukaemia specific PML and PLZF proteins localize to adjacent and functionally distinct nuclear bodies. *Oncogene.* 16:1945-53.

Salomoni, P., and C. Bellodi. 2007. New insights into the cytoplasmic function of PML. *Histol Histopathol.* 22:937-46.

Salomoni, P., and P.P. Pandolfi. 2002. The role of PML in tumor suppression. *Cell.* 108:165-70.

Salsman, J., N. Zimmerman, T. Chen, M. Domagala, and L. Frappier. 2008. Genome-wide screen of three herpesviruses for protein subcellular localization and alteration of PML nuclear bodies. *PLoS Pathog.* 4:e1000100.

Scaglioni, P.P., T.M. Yung, L.F. Cai, H. Erdjument-Bromage, A.J. Kaufman, B. Singh, J. Teruya-Feldstein, P. Tempst, and P.P. Pandolfi. 2006. A CK2-dependent mechanism for degradation of the PML tumor suppressor. *Cell.* 126:269-83.

Seeler, J.S., A. Marchio, D. Sitterlin, C. Transy, and A. Dejean. 1998. Interaction of SP100 with HP1 proteins: a link between the promyelocytic leukemia-associated nuclear bodies and the chromatin compartment. *Proc Natl Acad Sci U S A.* 95:7316-21.

Shen, T.H., H.K. Lin, P.P. Scaglioni, T.M. Yung, and P.P. Pandolfi. 2006. The mechanisms of PML-nuclear body formation. *Mol Cell.* 24:331-9.

Shiels, C., S.A. Islam, R. Vatcheva, P. Sasieni, M.J. Sternberg, P.S. Freemont, and D. Sheer. 2001. PML bodies associate specifically with the MHC gene cluster in interphase nuclei. *J Cell Sci.* 114:3705-16.

Solovei, I., L. Schermelleh, K. During, A. Engelhardt, S. Stein, C. Cremer, and T. Cremer. 2004. Differences in centromere positioning of cycling and postmitotic human cell types. *Chromosoma.* 112:410-23.

Sternsdorf, T., K. Jensen, B. Reich, and H. Will. 1999. The nuclear dot protein sp100, characterization of domains necessary for dimerization, subcellular localization, and modification by small ubiquitin-like modifiers. *J Biol Chem.* 274:12555-66.

Sternsdorf, T., K. Jensen, and H. Will. 1997. Evidence for covalent modification of the nuclear dot-associated proteins PML and Sp100 by PIC1/SUMO-1. *J Cell Biol.* 139:1621-34.

Strudwick, S., and K.L. Borden. 2002. The emerging roles of translation factor eIF4E in the nucleus. *Differentiation.* 70:10-22.

Stuurman, N., A. de Graaf, A. Floore, A. Josso, B. Humbel, L. de Jong, and R. van Driel. 1992. A monoclonal antibody recognizing nuclear matrix-associated nuclear bodies. *J Cell Sci.* 101 (Pt 4):773-84.

Sun, J., H. Xu, S.H. Subramony, and M.D. Hebert. 2005. Interactions between coilin and PIASy partially link Cajal bodies to PML bodies. *J Cell Sci.* 118:4995-5003.

Szostecki, C., H.H. Guldner, H.J. Netter, and H. Will. 1990. Isolation and characterization of cDNA encoding a human nuclear antigen predominantly recognized by autoantibodies from patients with primary biliary cirrhosis. *J Immunol.* 145:4338-47.

Szostecki, C., H. Krippner, E. Penner, and F.A. Bautz. 1987. Autoimmune sera recognize a 100 kD nuclear protein antigen (sp-100). *Clin Exp Immunol.* 68:108-16.

Takahashi, Y., V. Lallemand-Breitenbach, J. Zhu, and H. de The. 2004. PML nuclear bodies and apoptosis. *Oncogene.* 23:2819-24.

Tatham, M.H., M.C. Geoffroy, L. Shen, A. Plechanovova, N. Hattersley, E.G. Jaffray, J.J. Palvimo, and R.T. Hay. 2008. RNF4 is a poly-SUMO-specific E3 ubiquitin ligase required for arsenic-induced PML degradation. *Nat Cell Biol.* 10:538-46.

Towbin, B.D., P. Meister, and S.M. Gasser. 2009. The nuclear envelope--a scaffold for silencing? *Curr Opin Genet Dev.* 19:180-6.

Tsukamoto, T., N. Hashiguchi, S.M. Janicki, T. Tumbar, A.S. Belmont, and D.L. Spector. 2000. Visualization of gene activity in living cells. *Nat Cell Biol.* 2:871-8.

Vannucchi, S., Z.A. Percario, M.V. Chiantore, P. Matarrese, M.K. Chelbi-Alix, M. Fagioli, P.G. Pelicci, W. Malorni, G. Fiorucci, G. Romeo, and E. Affabris. 2000. Interferon-beta induces S phase slowing via up-regulated expression of PML in squamous carcinoma cells. *Oncogene.* 19:5041-53.

Varadaraj, A., C.L. Dovey, L. Laredj, B. Ferguson, C.E. Alexander, N. Lubben, A.H. Wyllie, and T. Rich. 2007. Evidence for the receipt of DNA damage stimuli by PML nuclear domains. *J Pathol.* 211:471-80.

von Mikecz, A. 2006. The nuclear ubiquitin-proteasome system. *J Cell Sci.* 119:1977-84.

von Mikecz, A., S. Zhang, M. Montminy, E.M. Tan, and P. Hemmerich. 2000. CREB-binding protein (CBP)/p300 and RNA polymerase II colocalize in transcriptionally active domains in the nucleus. *J Cell Biol.* 150:265-73.

Wang, J., C. Shiels, P. Sasieni, P.J. Wu, S.A. Islam, P.S. Freemont, and D. Sheer. 2004. Promyelocytic leukemia nuclear bodies associate with transcriptionally active genomic regions. *J Cell Biol.* 164:515-26.

Wang, Z.G., L. Delva, M. Gaboli, R. Rivi, M. Giorgio, C. Cordon-Cardo, F. Grosveld, and P.P. Pandolfi. 1998. Role of PML in cell growth and the retinoic acid pathway. *Science.* 279:1547-51.

Weis, K., S. Rambaud, C. Lavau, J. Jansen, T. Carvalho, M. Carmo-Fonseca, A. Lamond, and A. Dejean. 1994. Retinoic acid regulates aberrant nuclear localization of PML-RAR alpha in acute promyelocytic leukemia cells. *Cell.* 76:345-56.

Weisshaar, S.R., K. Keusekotten, A. Krause, C. Horst, H.M. Springer, K. Gottsche, R.J. Dohmen, and G.J. Praefcke. 2008. Arsenic trioxide stimulates SUMO-2/3 modification leading to RNF4-dependent proteolytic targeting of PML. *FEBS Lett.* 582:3174-8.

Wojcik, C., and G.N. DeMartino. 2003. Intracellular localization of proteasomes. *Int J Biochem Cell Biol.* 35:579-89.

Xie, S.Q., and A. Pombo. 2006. Distribution of different phosphorylated forms of RNA polymerase II in relation to Cajal and PML bodies in human cells: an ultrastructural study. *Histochem Cell Biol.* 125:21-31.

Yang, S., C. Kuo, J.E. Bisi, and M.K. Kim. 2002. PML-dependent apoptosis after DNA damage is regulated by the checkpoint kinase hCds1/Chk2. *Nat Cell Biol.* 4:865-70.

Yeager, T.R., A.A. Neumann, A. Englezou, L.I. Huschtscha, J.R. Noble, and R.R. Reddel. 1999. Telomerase-negative immortalized human cells contain a novel type of promyelocytic leukemia (PML) body. *Cancer Res.* 59:4175-9.

zeiss.de 2009. http://www.zeiss.de/c12567be0045acf1/Contents-Frame/3d7a40584d71593841256a71004cb2d4

Zhao, R., M.S. Bodnar, and D.L. Spector. 2009. Nuclear neighborhoods and gene expression. *Curr Opin Genet Dev.* 19:172-9.

Zhong, S., S. Muller, S. Ronchetti, P.S. Freemont, A. Dejean, and P.P. Pandolfi. 2000a. Role of SUMO-1-modified PML in nuclear body formation. *Blood.* 95:2748-52.

Zhong, S., P. Salomoni, and P.P. Pandolfi. 2000b. The transcriptional role of PML and the nuclear body. *Nat Cell Biol.* 2:E85-90.